

1989

Theoretical and experimental studies on flame propagation and quenching of powdered fuels

Se-Won Kim

Iowa State University

Follow this and additional works at: <https://lib.dr.iastate.edu/rtd>

 Part of the [Mechanical Engineering Commons](#)

Recommended Citation

Kim, Se-Won, "Theoretical and experimental studies on flame propagation and quenching of powdered fuels " (1989). *Retrospective Theses and Dissertations*. 9058.

<https://lib.dr.iastate.edu/rtd/9058>

This Dissertation is brought to you for free and open access by the Iowa State University Capstones, Theses and Dissertations at Iowa State University Digital Repository. It has been accepted for inclusion in Retrospective Theses and Dissertations by an authorized administrator of Iowa State University Digital Repository. For more information, please contact digirep@iastate.edu.

INFORMATION TO USERS

The most advanced technology has been used to photograph and reproduce this manuscript from the microfilm master. UMI films the text directly from the original or copy submitted. Thus, some thesis and dissertation copies are in typewriter face, while others may be from any type of computer printer.

The quality of this reproduction is dependent upon the quality of the copy submitted. Broken or indistinct print, colored or poor quality illustrations and photographs, print bleedthrough, substandard margins, and improper alignment can adversely affect reproduction.

In the unlikely event that the author did not send UMI a complete manuscript and there are missing pages, these will be noted. Also, if unauthorized copyright material had to be removed, a note will indicate the deletion.

Oversize materials (e.g., maps, drawings, charts) are reproduced by sectioning the original, beginning at the upper left-hand corner and continuing from left to right in equal sections with small overlaps. Each original is also photographed in one exposure and is included in reduced form at the back of the book. These are also available as one exposure on a standard 35mm slide or as a 17" x 23" black and white photographic print for an additional charge.

Photographs included in the original manuscript have been reproduced xerographically in this copy. Higher quality 6" x 9" black and white photographic prints are available for any photograph or illustration appearing in this copy for an additional charge. Contact UMI directly to order.

U·M·I

University Microfilms International
A Bell & Howell Information Company
300 North Zeeb Road, Ann Arbor, MI 48106-1346 USA
313/761-4700 800/521-0600

Order Number 9003538

**Theoretical and experimental studies on flame propagation and
quenching of powdered fuels**

Kim, Se-Won, Ph.D.

Iowa State University, 1989

U·M·I
300 N. Zeeb Rd.
Ann Arbor, MI 48106

**Theoretical and experimental studies on flame
propagation and quenching of powdered fuels**

by

Se-Won Kim

A Dissertation Submitted to the
Graduate Faculty in Partial Fulfillment of the
Requirements for the Degree of
DOCTOR OF PHILOSOPHY

Major: Mechanical Engineering

Approved:

Signature was redacted for privacy.

In Charge of Major Work

Signature was redacted for privacy.

For the Major Department

Signature was redacted for privacy.

For the Graduate College

Iowa State University
Ames, Iowa
1989

TABLE OF CONTENTS

NOMENCLATURE		xxiii
1 INTRODUCTION		1
1.1 Present Study		1
1.2 Relevance of Study		2
1.3 Literature Review		3
1.3.1 Electrostatic suspension of particles		3
1.3.2 Mathematical model of reactive flow		7
1.3.3 Flammability limits		14
1.3.4 Flame quenching		15
1.3.5 Aluminum combustion		38
1.3.6 Coal combustion		43
2 A NEW METHOD FOR EVALUATION OF THE BURNING VELOCITY OF POWDERED FUELS		56
2.1 Experimental Design		56
2.2 Electrostatic Suspension Theory (Open System)		57
2.3 Test Procedure		59
2.4 Preliminary Results		60

2.5	First Modified Design of Combustor	61
2.6	Second Modified Design of Combustor	63
2.7	Results and Discussions	65
3	EXPERIMENTAL DESIGN AND CALIBRATION	71
3.1	Experimental Design	71
3.1.1	Electrostatic suspension (closed system)	71
3.1.2	Needle electrode	74
3.1.3	Glass container	74
3.1.4	Upper and adjusting plate electrode	79
3.2	Overall Experimental Setup	80
3.3	Particle Preparation	90
3.4	Calibration	93
3.4.1	Particle concentration	93
3.4.2	Capacitor	103
4	FLAME PROPAGATION AND QUENCHING OF ALUMINUM PARTICLES	109
4.1	Experimental Technique and Procedure	109
4.2	Quenching of Methane-air Flame	111
4.3	Quenching of Aluminum-air Flame	114
4.3.1	Effect of particle concentration	118
4.3.2	Effect of particle size and shape	132
4.3.3	Effect of size distribution	141
4.3.4	Effect of moisture content	144

4.3.5	Effect of an ignition energy	144
4.4	Burning Velocity of Aluminum-air Flame	148
4.4.1	Flame propagation behavior	150
4.4.2	Effect of particle concentration	151
4.4.3	Effect of particle size	151
4.5	Conclusion	158
5	FLAME PROPAGATION AND QUENCHING OF COAL PAR-	
	TICLES	160
5.1	Experimental Technique and Procedure	160
5.2	Quenching of Coal-air Flame	162
5.2.1	Effect of particle concentration	162
5.2.2	Effect of particle size	180
5.2.3	Effect of volatile content	187
5.3	Burning Velocity of Coal-air Flames	196
5.4	Observation of Flame Propagation of Coal	196
5.5	Conclusion	199
6	CORRELATIONS OF QUENCHING DISTANCE	202
6.1	Quenching Distance Correlation of Aluminum Powder	202
6.2	Quenching Distance Correlation of Coal Powders	205
6.3	Conclusion	210
7	COMPUTER SIMULATION OF ALUMINUM COMBUSTION	213
7.1	Formulation	213

7.2	Governing Equations	215
7.3	Formulation of Reaction Mechanism	217
7.4	Transformations	220
7.5	Transport Properties	221
7.6	Transformation of Energy Equation	222
7.6.1	Adiabatic transformation	224
7.6.2	Lagrangian transformation	224
7.7	Formulation of Parameters	226
7.7.1	Temperature	226
7.7.2	Density	226
7.7.3	Radial coordinate	226
7.7.4	Mixture velocity	226
7.7.5	Pressure	227
7.7.6	Total mass	227
7.8	Burning Velocity	228
7.9	Boundary and Initial Conditions	228
7.10	Finite Difference Method	229
7.11	Trapezoidal Method	230
7.12	Results and Discussions	230
7.13	List of Computer Program	238
8	MODEL OF FLAME PROPAGATION AND QUENCHING	
	OF COAL-AIR FLAME	271
8.1	Introduction	271

8.2	Model Assumptions and Advantages	272
8.3	Governing Equations	273
8.4	Flame Velocity	276
8.5	Transformation	276
8.6	Auxiliary Equations	277
8.7	Solution Technique	282
	8.7.1 Initial and boundary conditions	282
	8.7.2 Finite difference formulation	283
8.8	Results and Discussions	284
9	CONCLUSIONS AND RECOMMENDATIONS	292
10	ACKNOWLEDGEMENT	298
11	BIBLIOGRAPHY	300
12	APPENDIX A: ERROR ANALYSIS	312
	12.1 Particle Diameter	313
	12.1.1 Particle diameter of aluminum particle	313
	12.1.2 Particle diameter of coal particle	314
	12.2 Breakdown Voltage	314
	12.3 Capacitance	315
	12.4 External Voltage	315
	12.5 Particle Concentration	316
	12.5.1 Particle concentration of aluminum particle	316
	12.5.2 Particle concentration of coal particles	317

12.6	Quenching Distance	318
13	APPENDIX B: THEORETICAL ANALYSIS OF QUENCHING	320
13.1	Energy Conservation Method	320
13.1.1	Radiative heat flux	320
13.1.2	Flame quenching	323
13.2	Ignition Criteria Method	326
13.2.1	Mass transfer number	326
13.2.2	Criterion for successful ignition	327
13.2.3	Quenching of powdered fuels	328
13.2.4	Quenching distance	329
14	APPENDIX C: EXPERIMENTAL DATA	331

LIST OF TABLES

Table 3.1:	Capacitances of the external capacitors	85
Table 3.2:	Mean diameter of aluminum particles	91
Table 3.3:	Proximate analysis of five types of coal powders	94
Table 3.4:	Ultimate analysis of Penn. Seam coal	95
Table 3.5:	Mean diameter of coal particles	96
Table 4.1:	Comparison of minimum quenching distances of methane-air flames	115
Table 6.1:	Regression coefficients and analysis of variance of spherical aluminum	204
Table 6.2:	Regression coefficients and analysis of variance of spherical aluminum	209
Table 7.1:	Numerical values of the parameters	223
Table 14.1:	Quenching distance vs. methane concentration in air, $P = 1$ atm., $T =$ room temperature	332
Table 14.2:	Quenching distance vs. methane concentration in air, $P = 1$ atm., $T =$ room temperature	333

Table 14.3:	Quenching distance vs. methane concentration in air, $P = 1$ atm., $T =$ room temperature	334
Table 14.4:	Quenching distance vs. particle concentration for a $10 - 15\mu\text{m}$ aluminum particle	335
Table 14.5:	Quenching distance vs. particle concentration for a $10 - 15\mu\text{m}$ aluminum particle	336
Table 14.6:	Quenching distance vs. particle concentration for a $15 - 20\mu\text{m}$ aluminum particle	337
Table 14.7:	Quenching distance vs. particle concentration for a $15 - 20\mu\text{m}$ aluminum particle	338
Table 14.8:	Quenching distance vs. particle concentration for a $20 - 25\mu\text{m}$ aluminum particle	339
Table 14.9:	Quenching distance vs. particle concentration for a $20 - 25\mu\text{m}$ aluminum particle	340
Table 14.10:	Quenching distance vs. particle concentration for a $25 - 30\mu\text{m}$ aluminum particle	341
Table 14.11:	Quenching distance vs. particle concentration for a $25 - 30\mu\text{m}$ aluminum particle	342
Table 14.12:	Quenching distance vs. particle concentration for a $25 - 30\mu\text{m}$ aluminum particle	343
Table 14.13:	Quenching distance vs. particle concentration for a $30 - 38\mu\text{m}$ spherical aluminum particle	344

Table 14.14: Quenching distance vs. particle concentration for a 30 – 38 μm spherical aluminum particle	345
Table 14.15: Quenching distance vs. particle concentration for a 38 – 45 μm spherical aluminum particle	346
Table 14.16: Quenching distance vs. particle concentration for a 38 – 45 μm spherical aluminum particle	347
Table 14.17: Quenching distance vs. particle concentration for a batch spher- ical aluminum particle	348
Table 14.18: Quenching distance vs. particle concentration for a batch spher- ical aluminum particle	349
Table 14.19: Quenching distance vs. particle concentration for a 15 – 20 μm irregular aluminum particle	350
Table 14.20: Quenching distance vs. particle concentration for a 15 – 20 μm irregular aluminum particle	351
Table 14.21: Quenching distance vs. particle concentration for a 25 – 30 μm irregular aluminum particle	352
Table 14.22: Quenching distance vs. particle concentration for a 25 – 30 μm irregular aluminum particle	353
Table 14.23: Quenching distance vs. particle concentration for a 30 – 38 μm irregular aluminum particle	354
Table 14.24: Quenching distance vs. particle concentration for a 30 – 38 μm irregular aluminum particle	355

Table 14.25: Quenching distance vs. particle concentration for a 38 – 45 μm irregular aluminum particle	356
Table 14.26: Quenching distance vs. particle concentration for a batch irregular aluminum particle	357
Table 14.27: Quenching distance vs. particle concentration for a batch irregular aluminum particle	358
Table 14.28: Quenching distance vs. particle concentration for a 16.7 μm Adaville No. 11 coal particle	359
Table 14.29: Quenching distance vs. particle concentration for a 16.7 μm Adaville No. 11 coal particle	360
Table 14.30: Quenching distance vs. particle concentration for a 25.5 μm Adaville No. 11 coal particle	361
Table 14.31: Quenching distance vs. particle concentration for a 25.5 μm Adaville No. 11 coal particle	362
Table 14.32: Quenching distance vs. particle concentration for a 36.6 μm Adaville No. 11 coal particle	363
Table 14.33: Quenching distance vs. particle concentration for a 36.6 μm Adaville No. 11 coal particle	364
Table 14.34: Quenching distance vs. particle concentration for a 16.7 μm Hanna No. 80 coal particle	365
Table 14.35: Quenching distance vs. particle concentration for a 16.7 μm Hanna No. 80 coal particle	366

Table 14.36: Quenching distance vs. particle concentration for a 25.5 μm Hanna No. 80 coal particle	367
Table 14.37: Quenching distance vs. particle concentration for a 25.5 μm Hanna No. 80 coal particle	368
Table 14.38: Quenching distance vs. particle concentration for a 36.6 μm Hanna No. 80 coal particle	369
Table 14.39: Quenching distance vs. particle concentration for a 36.6 μm Hanna No. 80 coal particle	370
Table 14.40: Quenching distance vs. particle concentration for a 16.7 μm Illinois No. 6 coal particle	371
Table 14.41: Quenching distance vs. particle concentration for a 16.7 μm Illinois No. 6 coal particle	372
Table 14.42: Quenching distance vs. particle concentration for a 25.5 μm Illinois No. 6 coal particle	373
Table 14.43: Quenching distance vs. particle concentration for a 25.5 μm Illinois No. 6 coal particle	374
Table 14.44: Quenching distance vs. particle concentration for a 36.6 μm Illinois No. 6 coal particle	375
Table 14.45: Quenching distance vs. particle concentration for a 36.6 μm Illinois No. 6 coal particle	376
Table 14.46: Quenching distance vs. particle concentration for a 16.7 μm Lower Kittaining coal particle	377

Table 14.47: Quenching distance vs. particle concentration for a 25.5 μm Illinois No. 6 coal particle	378
Table 14.48: Quenching distance vs. particle concentration for a 25.5 μm Illinois No. 6 coal particle	379
Table 14.49: Quenching distance vs. particle concentration for a 36.6 μm Illinois No. 6 coal particle	380
Table 14.50: Quenching distance vs. particle concentration for a 36.6 μm Illinois No. 6 coal particle	381
Table 14.51: Quenching distance vs. particle concentration for a 9.1 μm Penn. Seam coal particle	382
Table 14.52: Quenching distance vs. particle concentration for a 9.1 μm Penn. Seam coal particle	383
Table 14.53: Quenching distance vs. particle concentration for a 16.7 μm Penn. Seam coal particle	384
Table 14.54: Quenching distance vs. particle concentration for a 16.7 μm Penn. Seam coal particle	385
Table 14.55: Quenching distance vs. particle concentration for a 25.5 μm Penn. Seam coal particle	386
Table 14.56: Quenching distance vs. particle concentration for a 25.5 μm Penn. Seam coal particle	387
Table 14.57: Quenching distance vs. particle concentration for a 36.6 μm Penn. Seam coal particle	388

Table 14.58: Quenching distance vs. particle concentration for a $36.6\mu\text{m}$

Penn. Seam coal particle 389

LIST OF FIGURES

Figure 1.1:	Schematics of the particle behavior in the electric field	5
Figure 1.2:	Temperature distribution in a flame	30
Figure 1.3:	Schematics of wall loss quenching of a flame propagating in a tube (Modified from Hertzberg [1980b])	35
Figure 2.1:	Layout of an experimental setup	58
Figure 2.2:	Sintered glass test tube	62
Figure 2.3:	Second modified experimental setup	64
Figure 2.4:	DPDT switch and circuit breaker	66
Figure 2.5:	Cylinders and screens	67
Figure 2.6:	Voltage versus piston moving speed	68
Figure 2.7:	Burning velocity of Penn. Seam coal	70
Figure 3.1:	Closed systems for coal and aluminum tests	73
Figure 3.2:	Needle electrode and adjusting system	75
Figure 3.3:	Schematics of the particle fall in a flame propagation system	77
Figure 3.4:	Schematics of upper and adjusting plate	81
Figure 3.5:	Schematics of overall experimental setup	82
Figure 3.6:	Photograph of overall experimental setup	83

Figure 3.7:	Flowmeter calibration, Gilmont A3114	87
Figure 3.8:	Flowmeter calibration, Gilmont B5463	88
Figure 3.9:	Flowmeter calibration, Gilmont D2321	89
Figure 3.10:	SEM pictures of spherical and irregular aluminum particles .	92
Figure 3.11:	Size distribution of 9.1 μm mean diameter coal particles . . .	97
Figure 3.12:	Size distribution of 16.7 μm mean diameter coal particles . .	98
Figure 3.13:	Size distribution of 25.5 μm mean diameter coal particles . .	99
Figure 3.14:	Size distribution of 36.6 μm mean diameter coal particles . .	100
Figure 3.15:	Calibration of weighted method of particle calibration	102
Figure 3.16:	Schematics of light scattering method of particle concentration measurement	104
Figure 3.17:	Calibration of particle concentration of aluminum particle . .	105
Figure 3.18:	External circuit for a capacitor calibration	106
Figure 3.19:	Calibration of a capacitor	108
Figure 4.1:	Experimental setup for methane-air flame quenching	112
Figure 4.2:	Quenching distance vs. fuel/air ratio of methane-air flame . .	113
Figure 4.3:	Spark ignition energy vs. particle concentration of 22.5 μm spherical aluminum particle	116
Figure 4.4:	Photograph of a spark ignition of aluminum particles	119
Figure 4.5:	Quenching distance vs. particle concentration of 12.5 μm spher- ical aluminum particle	120
Figure 4.6:	Quenching distance vs. particle concentration of 17.5 μm spher- ical aluminum particle	121

Figure 4.7:	Quenching distance vs. particle concentration of 22.5 μm spherical aluminum particle	122
Figure 4.8:	Quenching distance vs. particle concentration of 27.5 μm spherical aluminum particle	123
Figure 4.9:	Quenching distance vs. particle concentration of 34.0 μm spherical aluminum particle	124
Figure 4.10:	Quenching distance vs. particle concentration of 41.5 μm spherical aluminum particle	126
Figure 4.11:	Quenching distance vs. particle concentration of 20.0 μm irregular aluminum particle	128
Figure 4.12:	Quenching distance vs. particle concentration of 27.5 μm irregular aluminum particle	129
Figure 4.13:	Quenching distance vs. particle concentration of 34.0 μm irregular aluminum particle	130
Figure 4.14:	Quenching distance vs. particle concentration of 41.5 μm irregular aluminum particle	131
Figure 4.15:	Quenching distance vs. particle concentration of spherical aluminum particles of various particle sizes	134
Figure 4.16:	Minimum quenching distance vs. particle diameter of spherical aluminum particles	135
Figure 4.17:	Quenching distance vs. particle concentration of irregular aluminum particles of various particle sizes	136

Figure 4.18: Minimum quenching distance vs. particle concentration irregular aluminum particles	137
Figure 4.19: Quenching distance vs. particle concentration of spherical and irregular aluminum particles of $27.5 \mu m$ in diameter	138
Figure 4.20: Quenching distance vs. particle concentration of spherical and irregular aluminum particles of $34.0 \mu m$ in diameter	139
Figure 4.21: Minimum quenching distance vs. particle diameter of spherical and irregular aluminum particles	140
Figure 4.22: Quenching distance vs. particle concentration of spherical batch aluminum particles	142
Figure 4.23: Quenching distance vs. particle concentration of irregular batch aluminum particles	143
Figure 4.24: Size distribution of spherical batch aluminum particles	145
Figure 4.25: Size distribution of irregular batch aluminum particles	146
Figure 4.26: Effect of relative humidity on quenching distance of $41.5 \mu m$ spherical aluminum particles	147
Figure 4.27: Effect of ignition energy on quenching distance of $22.5 \mu m$ spherical aluminum particles	149
Figure 4.28: Photographs of flame propagation of $27.5 \mu m$ spherical aluminum powder	152
Figure 4.29: Distance of flame front with time	153
Figure 4.30: Burning velocity vs. time of three aluminum powders	154

Figure 4.31: Burning velocity vs. particle concentration of 12.5 μm aluminum particle	155
Figure 4.32: Burning velocity vs. particle concentration of 17.5 μm aluminum particle	156
Figure 4.33: Burning velocity vs. particle concentration of 22.5 μm aluminum particle	157
Figure 4.34: Burning velocity vs. particle concentration of three particle sizes	159
Figure 5.1: Quenching distance vs. particle concentration of 16.7 μm Lower Kittaining coal	165
Figure 5.2: Quenching distance vs. particle concentration of 25.5 μm Lower Kittaining coal	166
Figure 5.3: Quenching distance vs. particle concentration of 36.6 μm Lower Kittaining coal	167
Figure 5.4: Quenching distance vs. particle concentration of 16.7 μm Illinois # 6 coal	168
Figure 5.5: Quenching distance vs. particle concentration of 25.5 μm Illinois # 6 coal	169
Figure 5.6: Quenching distance vs. particle concentration of 36.6 μm Illinois # 6 coal	170
Figure 5.7: Quenching distance vs. particle concentration of 9.1 μm Penn. Seam coal	172
Figure 5.8: Quenching distance vs. particle concentration of 16.7 μm Penn. Seam coal	173

Figure 5.9: Quenching distance vs. particle concentration of 25.5 μm Penn. Seam coal	174
Figure 5.10: Quenching distance vs. particle concentration of 36.6 μm Penn. Seam coal	175
Figure 5.11: Quenching distance vs. particle concentration of 16.7 μm Adaville no. 11 coal	177
Figure 5.12: Quenching distance vs. particle concentration of 25.5 μm Adaville no. 11 coal	178
Figure 5.13: Quenching distance vs. particle concentration of 36.6 μm Adaville no. 11 coal	179
Figure 5.14: Quenching distance vs. particle concentration of 16.7 μm Hanna # 80 coal	181
Figure 5.15: Quenching distance vs. particle concentration of 25.5 μm Hanna # 80 coal	182
Figure 5.16: Quenching distance vs. particle concentration of 36.6 μm Hanna # 80 coal	183
Figure 5.17: Quenching distance vs. particle concentration of Lower Kit- taing coal of each particle sizes	184
Figure 5.18: Quenching distance vs. particle concentration of Illinois # 6 coal of each particle sizes	185
Figure 5.19: Quenching distance vs. particle concentration of Penn. Seam coal of each particle sizes	186

Figure 5.20: Quenching distance vs. particle concentration of Adaville # 11 coal for various particle sizes	188
Figure 5.21: Quenching distance vs. particle concentration of Hanna # 80 coal of each particle sizes	189
Figure 5.22: Minimum quenching distance vs. particle diameter for each type of coal	190
Figure 5.23: Quenching distance vs. particle concentration of 16.7 μm coal for different volatile content	192
Figure 5.24: Quenching distance vs. particle concentration of 25.5 μm coal for different volatile content	193
Figure 5.25: Quenching distance vs. particle concentration of 36.6 μm coal of for different volatile content	194
Figure 5.26: Minimum quenching distance vs. volatile content of each sizes of coal	195
Figure 5.27: Position of flame front with time of Adaville no. 11 coal . . .	197
Figure 5.28: Burning velocity vs. time of Adaville no. 11 coal	198
Figure 5.29: Burning velocity vs. particle concentration of 16.7 μm Penn. Seam coal	200
Figure 5.30: Burning velocity vs. particle concentration of 25.5 μm Penn. Seam coal	201
Figure 6.1: Predicted vs. observed data of regression of aluminum powders	206
Figure 6.2: Residual vs. predicted values of regression of aluminum powders	207
Figure 6.3: Predicted vs. observed data of regression of coal powders . .	211

Figure 6.4:	Residual vs. predicted values of regression of coal powders . .	212
Figure 7.1:	Schematics of a dust explosion in a cylindrical test section . .	214
Figure 7.2:	Schematics of a burning aluminum droplet (Markstein [1966])	218
Figure 7.3:	Predicted temperature profile	232
Figure 7.4:	Predicted profile of mass fractions of reactants and product .	233
Figure 7.5:	Predicted pressure history	234
Figure 7.6:	Predicted burning velocities	235
Figure 7.7:	Predicted quenching distance vs. particle concentration of 12.5 μm spherical aluminum	237
Figure 8.1:	Schematics of flame region	274
Figure 8.2:	Schematics of coal flame model.	279
Figure 8.3:	Coal particle constituents and reaction rates (Smoot and Hor- ton [1977])	280
Figure 8.4:	Predicted flame velocity vs. particle concentration	286
Figure 8.5:	Predicted species profile variation with distance	287
Figure 8.6:	Predicted particle and gas temperature variation with distance	288
Figure 8.7:	Predicted flame velocity vs. particle diameter	289
Figure 8.8:	Predicted flame velocity vs. volatile content	290
Figure 8.9:	Predicted quenching distance vs. particle concentration of Penn. Seam coal	291
Figure 13.1:	Schematics of flame quenching in parallel plates	322

NOMENCLATURE

A	area, m^2
a	absorption coefficient, $1/m$
B	mass transfer number
B_b	Boltzmann number
C	capacitance, Farad
C_m	particle concentration, g/m^3
C_p	specific heat at constant pressure, $J/(Kg K)$
C_v	specific heat at constant volume, $J/(Kg K)$
c	fuel concentration
D	diameter of a test section, cm
D_i	diffusion coefficient
D_m	mass diffusivity, m^2/sec
D_q	quenching distance, mm
D_{20}	surface area mean diameter, μm
D_{30}	volume mean diameter, μm
d_p	particle diameter, μm
d_q	quenching distance, mm
E	activation energy, $J/mole$

E	electric field strength, V/m
E_b	blackbody emissive power, W
e	coefficient of restitution
e	extinction coefficient
F	geometric view factor
f	swelling factor
f	geometric constant
g	gravitational acceleration, m/s^2
H	plate separation distance, mm
H_i^0	enthalpy of formation of specie i
h	heat transfer coefficient $W/(m^2K)$
I	intensity of light with particles, W
I_o	intensity of light without particles, W
J	current flux
K_p	Plank mean absorption coefficient
k	rate coefficient
k	thermal conductivity, W/mK
Le	Lewis number, α/D_m
L	latent heat of vaporization, J/Kg
l	dead space thickness, mm
l	path length of light, cm
m	mass, g
\dot{m}	mass flow rate, Kg/sec

Nu	Nusselt number, hL/k
n	particle number density, $1/m^3$
P	pressure, N/m^2
Pr	Prantle number, $c_p\mu/k$
Pe	Peclet number, $S_u D/\alpha$
P_b	Plank number, $4\sigma DT_b^3/\lambda$
Q	heat of reaction, J/Kg
Q	charge, Coulomb
q	heat flux, W/m^2
q	fuel to air ratio
R	radius of a test section, cm
R	resistance, Ω
R_g	universal gas constant
R_w	radiation number
r''	homogeneous reaction rate, $mole/sec - m^2$
r'''	heterogeneous reaction rate, $mole/sec - m^2$
Re	Reynolds number, VL/ν
R.H.	relative humidity
r	radial coordinate, m
S	surface area, m^2
S_v	specific surface area, $1/m$
S_u	burning velocity, cm/sec
s	stoichiometric coefficient on a mass basis

T	temperature, K
T_o	initial flame temperature, K
T_a	adiabatic flame temperature, K
T_b	burned flame temperature, K
T_f	flame temperature, K
T_i	initial flame temperature, K
T_u	unburned mixture temperature, K
t	time, sec
t_q	quenching time, sec
t_e	evaporation (evolution) time, sec
t_c	chemical reaction time, sec
t_f	particle free fall time, sec
t_p	flame propagation time, sec
U_A	uncertainty of a variable A
V	volume of a test section, m^3
V	particle oscillation velocity, m/sec
V	electric potential, V
V_o	bed feed velocity, m/sec
V.C.	volatile content of coal
v	velocity, m/sec
W	molecular weight, g/mole
w	chemical reaction rate, mole/sec m^2
x	distance, m

Y_i	mass fraction of specie i
Z	function of flame propagation

Greek

α	thermal diffusivity, m^2/sec
β	extinction coefficient
γ	ratio of specific heats
Γ	$(1-\gamma)/\gamma$
δ	boundary layer thickness, mm
ϵ	emissivity
ε	eddy diffusivity
η	weighted non-grayness
θ	dimensionless temperature
λ	thermal conductivity, W/mK
μ	viscosity, Kg/m·sec
ν	kinematic viscosity, m^2/sec
ρ	density, Kg/m^3
σ	scattering coefficient
τ	time constant, 1/sec
τ	optical thickness, mm
ϕ	variable of an adiabatic transformation
ϕ	volatile content

ω	Rosseland Albedo
Ω	collision integral

Subscript

avg	average
b	burned state
e	electric
f	fluid
g	gas
i	specie i
i	initial
i	spatial step
m	mixture
min	minimum
max	maximum
n	time step
p	particle
r	radiation
stoi	stoichiometric condition
t	turbulence
u	unburned state
w	wall

1 INTRODUCTION

1.1 Present Study

The goal of the present study is to investigate the burning velocity and the quenching distance characteristics of an aluminum-air and coal-air flames of various particle sizes, shapes, types, and concentrations at atmospheric pressure and at room temperature confined by a parallel plate electrodes and a glass cylinder.

A unique electrostatically controlled sparking system was perfected that generates a uniform particulate cloud also facilitates the measurement of the particle concentrations. This system overcomes the conventional problems of spatial variations and local transients in the particle concentration often encountered with unsteady or gravity fed dispersion systems.

The following fundamental subjects have been identified for detailed study:

1. The effects of particle size, concentration, and particle shape on quenching distance and burning velocity of aluminum-air mixtures.
2. The effects of particle size, concentration, and volatile content on quenching distance and burning velocity of coal-air mixtures.
3. Mathematical modeling of flame propagation and quenching of powdered fuels.

4. Developing correlation equations of the experimental data.
5. Design of practical size small scale flat flame burner for a powdered fuels and the investigation of the effect of electric field on the particle transport and the burning velocity.

These studies relate to problems in particle technology that are both of recent scientific interest and of practical importance in industry.

1.2 Relevance of Study

It is generally known that many solid materials are combustible. Finely dispersed solid particles may be readily ignited and will burn in air. As the size of the particle decreases, dust clouds can ignite very rapidly and present a serious explosion hazard in many industrial situations. Palmer [1973], Field [1982], and Nagy and Verakis [1983] reviewed various types of incidents of dust explosions.

From the scientific point of view, the factors controlling quenching can reveal various aspects of the combustion mechanisms. As an example, quenching distance measurements have been used to study the inhibition of premixed flames. From the practical point of view, quenching behavior is important in understanding flame-holding phenomena, in the design of flame traps and in the assessment of explosion hazards in the flow of combustible mixtures in industrial processes and is also relevant to the general evaluation of explosion hazards. In addition, quenching distances, burning velocities, and flammability limits are fundamental properties of gaseous or powdered fuel combustion systems and should, therefore, aid in the development of models for dust explosion.

The study of flame propagation and quenching has major applications in the following areas; optimum design of furnaces and coal-fired power generators, analysis of combustion phenomena in internal combustion engines, development of a new fuel efficient engines while satisfying emission constraints by reducing the amount of hydrocarbons emission in internal combustion engine exhaust caused primarily by the flame wall quenching within the engine, control of combustion processes in industry and propulsion, problem of safety and prevention of a serious explosion hazards in many industrial situations.

1.3 Literature Review

1.3.1 Electrostatic suspension of particles

1.3.1.1 Dynamics of an electric suspension The charging process occurs as a result of the “capacitance” effect of the particle itself while in electrical contact with the wall. During the time of charging the particle becomes part of a large capacitor, the wall, and therefore charges to the same sign and potential. If the externally applied electric field E remains unchanged in sign, forces of the type $F_e = QE$ will tend to drive particles away from the wall. Image forces of the kind $F_i = Q^2/(4\pi\epsilon)r^2$ will attract particles toward the wall. A particle confined between two parallel plates and possessing sufficiently large charge will continue in motion indefinitely once set in motion, oscillating between the parallel plates, sustained by the DC electric field. A unique charge thus exists on the particle for any electric field strength and given variables.

Body forces such as gravity, inelastic collisions with the walls, and viscous air drag

serve to limit the maximum possible velocity of the particle. The natural independent variable controlling the motion is the externally applied electric field.

Any particle-wall-gas properties which affect the dynamics discharging process at the walls such as surface conductivity, dielectric constant, relative humidity, and geometry will limit the maximum charge transfer to the particle. The schematics of the particle behavior in the electric field is shown in Figure 1.1.

The motion of a particle oscillating between parallel electrodes responding to the influence of an electric field of strength E can be described by

$$\frac{d^2 x_p}{dt^2} = \frac{QE}{m} \pm g \quad (1.1)$$

From the above equation, Colver [1976] derived the average velocity of the particle oscillating between the parallel plates, V , and magnitude of charge, Q ,

$$V = \left[\frac{1}{8}(1 + e) \right]^{1/2} \left(\left[\frac{QE}{m} \frac{1}{1 - e^2} + \frac{g}{1 + e^2} \right]^{1/2} + \left[\frac{QE}{m} \frac{1}{1 - e^2} - \frac{g}{1 + e^2} \right]^{1/2} \right) \quad (1.2)$$

where e is the coefficient of restitution and g is the gravitational acceleration.

Colver [1976] showed numerically that the magnitude of a charge of a spherical conducting aluminum particle can be calculated from the equation of the form,

$$Q = 4\pi\epsilon a^2 EK \quad (1.3)$$

He confirmed K value equal to 1.64 theoretically and experimentally for conducting particle possessing equilibrium charge. The theoretical equilibrium force required to lift a single conducting sphere from a plane in a uniform electric field is,

$$F_e = \pi\epsilon_0 D^2 E^2 \quad (1.4)$$

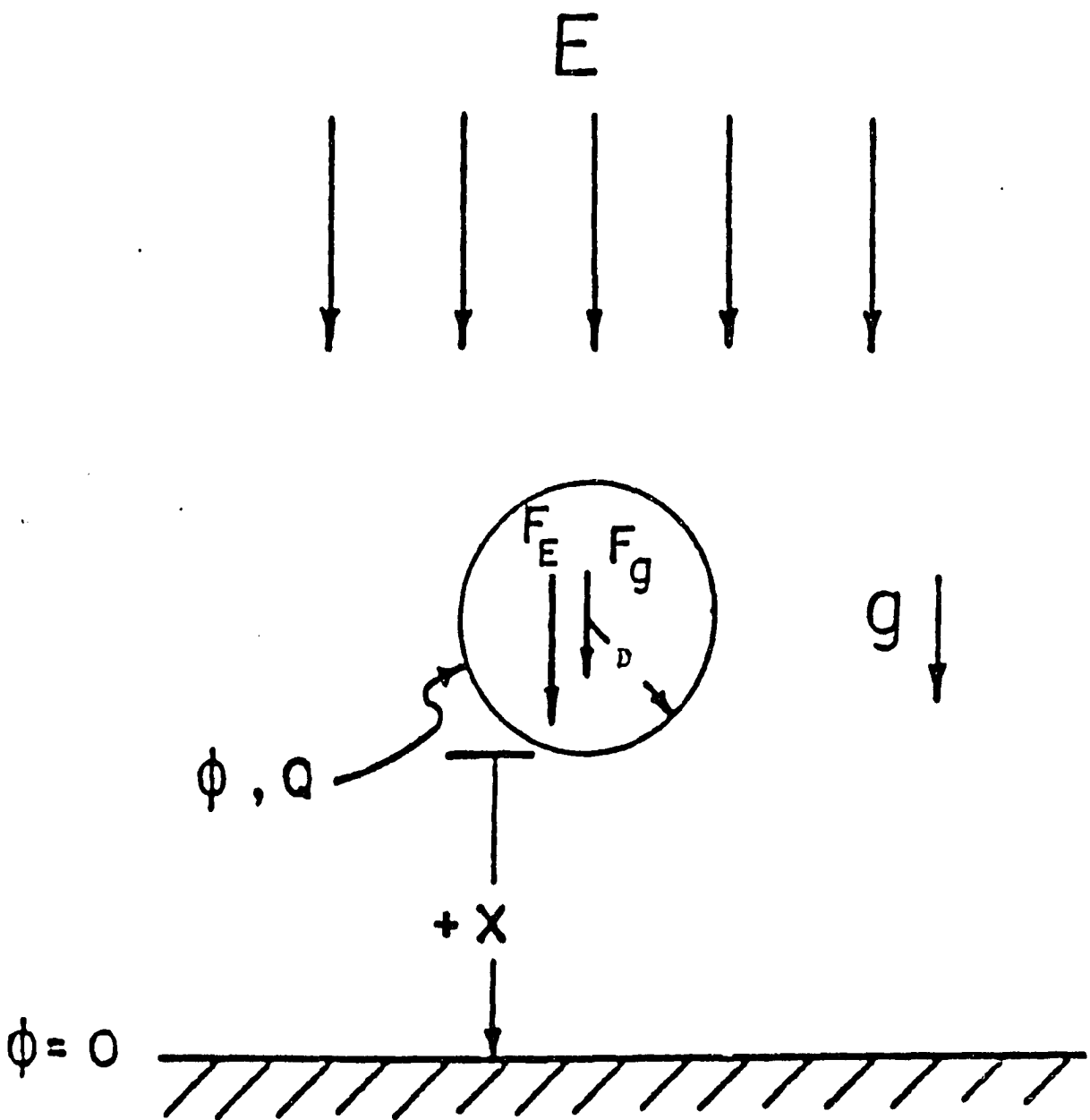


Figure 1.1: Schematics of the particle behavior in the electric field

1.3.1.2 Dynamic and stationary charging Colver [1976] conducted an experiment on dynamic charging of metallic particles against a conducting wall by a DC electric field. Metallic particles as small as $29 \mu m$ in diameter were electrically charged while in dynamic and stationary contact with either wall of a charged parallel plate capacitor. He showed that the particle charge distribution tends to remove particles away from the wall. The forces from the interaction of the induced charge and the externally applied electric field tended to move the particles away from the plate overcoming the image attraction. Continuous cyclic motion resulted as a particle impacts, discharges, and recharges with each electrodes. He found that particles in clouds in the presence of gravity and standard atmospheric air also demonstrate a continuous motion between the parallel plates.

He determined the dynamic and stationary charged particle motions theoretically and experimentally by considering the particles as capacitors in themselves. Inelastic particle-wall collisions and a conservative body force such as gravity give a critical lower limit electric field strength for sustained particle motion. It followed that in the absence of contact effects, the applied electric field is entirely responsible for the resulting lifting force on a particle since it alone determines the electric strength E and also controls the amount of charge Q accumulated on the particle.

1.3.1.3 Particle diffusion Colver and Howell [1980] measured particle number densities experimentally by three independent methods; by electrical current density, by laser beam attenuation, and by direct count. It was shown that in an electric suspension the diffusion process is significant and furthermore can be isolated experimentally in the absence of any fluid dynamic driving force.

Also, they traced the origin of electric suspension diffusion to one or more of the following processes; (1) particle concentration gradients in the electric field strength along the plate as a consequence of spatial variations in net charge concentration, (2) random particle motion due to particle-particle collisions or particle-wall collisions. The minimum electric field strength for sustained particle motion was given by Colver [1976] as

$$E_{L.L.} = \left[\left[\frac{1 - e^2}{1 + e^2} mg + F_D \right] \frac{6}{\pi^3} \epsilon_0 D^2 \right]^{1/2} \quad (1.5)$$

F_D is a drag force per particle which is,

$$F_D = 3\pi\mu dV [1 + 3D\rho V/16\mu]^{1/2} \quad (1.6)$$

where the above equation is valid for particle Reynolds number below 100, and d , μ , and ρ are the particle diameter, viscosity and density respectively.

Multiparticles are expected to be suspended similarly but with interparticle collisions considered. Cotroneo and Colver [1978] developed an equation for vertical current flux, J ,

$$J = fnQV [e^{-n\sigma l\alpha} + \gamma(1 - e^{-n\sigma l\alpha})] \quad (1.7)$$

where the first term in the brackets accounts for particles moving a distance l without collision and the second term accounts for the remaining fraction undergoing collisions. The parameters f , α , and γ are suggested to account for particle history effects, randomization as a result of collisions, irregular bounces, or particle rotation.

1.3.2 Mathematical model of reactive flow

Combustion processes occur in many power developing systems such as the internal combustion engine. Moreover such power system have important applications

in various industrial processes and are likely to continue playing an important role for many years to come.

A combustion characteristic of interest in many cases is the determination of the burning velocity as well as the flame structure. Regarding the development of the laminar flame theory, Mallard and Le Chatelier were the first to present a phenomenological theory based on an energy balance. Later, considerable effort was spent in devising models and theories to determine the burning velocity and flame structure. Most of these theories were strictly concerned with the case of an adiabatic one dimensional flame. They may be divided into three groups depending on the mechanism postulated for flame propagation. These are; first, thermal theories, in which the diffusion of heat ahead of the flame is considered the major cause of flame propagation; second, diffusional theories, in which the diffusion of the radicals and atoms ahead of the flame is significant; third, comprehensive theories, in which both the diffusion of energy and matter is taken into consideration.

In general terms, the adiabatic one-dimensional flame theory consists of applying the equations of conservation of mass and energy to a one-dimensional flow of a combustible mixture which is unburned at the cold boundary and approaches an equilibrium state at the hot boundary. The velocity of the flow at the cold boundary, which is the laminar burning velocity, is solved as the eigenvalue of the system of conservation equations. It is assumed that the flow can be considered as that of a continuum, that chemical kinetics provide the necessary expressions for the quantities entering into the conservation equations due to chemical changes and, finally, that the transport phenomena are determined by the knowledge of the heat transfer coefficient

and the law of diffusion. The momentum equation is usually taken care of by the assumption that pressure variations in the flame can be neglected.

Several approaches have been employed to solve the conservation equations. These range from the approximate analytical methods to the numerical integration of the ordinary differential equations modeling the system. However, all the adiabatic one-dimensional theories did not account for the existence of flame quenching and flammability limits. Flame quenching is related to the linear scale of the apparatus in which the flame propagates and the flammability limits are related to the mixture composition and pressure.

The laminar flame problem is the earliest combustion problem to be studied theoretically which required the simultaneous consideration of both chemical kinetics and fluid mechanics for its solution. The problem of determining the burning velocity of a deflagration wave was first studied by Mallard and Le Chatelier in 1883. Since then there have been many analytical attempts to study simple steady flames with varying degrees of complexity and approximations. Some of these have been summarized by Williams [1985].

After the work of Mallard and Le Chatelier who considered gas phase conduction of primary importance and the chemical reaction rate to be secondary, Taffanel concluded that the burning velocity was proportional to the square root of the product of reaction rate and thermal conductivity/heat capacity ratio (Lewis and von Elbe [1961]). The following results for a steady, adiabatic stationary flame is obtained:

$$v_o \sim \frac{1}{\rho} \left(\frac{kr}{C_p} \right)^{1/2} \quad (1.8)$$

Taffanel further extended his theory for ideal gases:

$$v_o \sim p^{0.5n-1} \exp(-E/2RT_f) \quad (1.9)$$

This simple treatment was followed by a series of more rigorous models of propagating gas phase flames during the 1950s. These models generally treated only a single overall reaction rate, together with additional assumptions that permitted either an approximate analytical solution or a simple numerical solution. Predictions were generally directed towards burning velocity, with little emphasis on detailed chemical structure.

Klein [1957] investigated flame structure as well as burning velocity in his numerical model. Hirschfelder et al. [1949] formulated the unsteady flame problem as a system of three-dimensional nonlinear partial differential equations and solved the one-dimensional steady flame as a two point boundary value problem. They used approximate methods to estimate the mass flow rate which is the eigenvalue of the two-point boundary value problem and then used a numerical shooting method to obtain the temperature and species profiles. Although the first problem they studied involved only single step kinetics, they later applied the same solution procedure to study flames for which the kinetics involved chain reaction [1952].

In 1956, Spalding [1956] applied a time-dependent system of nonlinear partial differential equations using explicit finite-difference techniques to study hydrazine flames. He assumed initial profiles for the temperature and species concentrations and obtained the steady state burning velocity by carrying out the computations till it reaches a steady state. This procedure avoids many of the difficulties associated with steady state solutions, and also uses a transformation that limits the dimension-

less flame thickness to the fixed interval between 0 and 1. Spalding's method was subsequently used by Adams and Cook [1960] to study the effect of pressure on the reaction mechanism and speed of hydrazine flames, and by Dixon-Lewis [1967, 1970] to study rich hydrogen-oxygen flames. Dixon-Lewis [1967] used a set of fourteen reaction and detailed model of transport properties to describe hydrogen-oxygen kinetics, but assumed a steady state approximation for the radical distribution in the flame (Dixon-Lewis [1984]). He studied the flame structure and flame reaction kinetics of hydrogen-oxygen-nitrogen flames using detailed expressions for the diffusive transport coefficients in multi-component systems. Dixon-Lewis and Shepherd [1974] also used this time-dependent numerical model to study ignition by localized sources.

The work of Dixon-Lewis and co-workers described above proved the one-dimensional unsteady flame with complex chemistry and detailed diffusive transport coefficients could be solved using numerical methods. Spalding et al. [1971] presented an implicit-finite difference method in which the unsteady flame equations were transformed to a form which could be solved by a numerical method developed by Patankar and Spalding [1970] for two dimensional boundary layer equations. They used simplified transport properties and a four step chain reaction mechanism to study the propagation of hydrogen-bromine flames. However this method requires careful ordering of the solution of the equations, and a certain manner of linearizing the source terms. Same numerical procedure was adopted later by Tsatsaronis [1978] to study unsteady flame propagation in methane, oxygen, nitrogen mixtures using very detailed chemical kinetics mechanisms and transport properties.

Work has been extended to hydrocarbon-air flames as more complex reaction

sequences have been postulated and evaluated. Brown et al. [1968] used general conservation equations to formulate a one-dimensional, steady state, propagating flame model which predicted the temperature and concentration profiles of acetylene-oxygen flames. Recently, Eraslan and Brown [1988] solved one-dimensional, laminar, premixed equations to simulate the ionic structure of rich acetylene flame using 205 reaction equations. They transformed the governing equations then used the method of lines to solve the resulting equations.

The work of Smoot et al. [1976] treats a general gaseous system using the general approach of Spalding et al. [1971], but with a different numerical solution technique for the set of stiff parabolic equations. This treatment provides a generalized solution of the one-dimensional unsteady equations for gaseous flames. They used a mixed explicit-implicit finite difference technique. The diffusive transport terms were solved explicitly and the kinetic terms were solved using linearized implicit techniques. Bledgian [1973] employed a method of lines technique where the nonlinear parabolic initial-boundary value problem is reduced to a set of nonlinear first order initial value problems. Sophisticated methods of initial value problem integrators were used to solve the resulting ordinary differential equations system instead of using finite difference approximations in his method of lines approach. Westbrook and Dryer [1979,1980] have deduced a comprehensive reaction mechanism for methanol oxidation algorithm developed by Lund [1978] to solve the unsteady flame equations. They used simplified expressions for the diffusive transport coefficients which were adjusted to give good laminar flame speed prediction for methane-air flames.

Dixon-Lewis [1979] has more recently used a composite flux method to study a

variety of problems like the kinetic mechanism, structure and propagation of flames in hydrogen-oxygen-nitrogen flames and flame inhibition by organic halogen compounds. He discusses the ranges of applicability of the partial equilibrium and quasi-steady assumptions in relation to the distribution of radical populations in the flames.

Warnatz [1981] has extensively studied both freely propagating and burner stabilized flames in a variety of premixed gases. He linearized the chemical reaction terms and solved the time-dependent equations implicitly with assumed initial guesses for the temperature and species profiles. He also used a simplified transport model which agrees well with the complete multi-component formulation of diffusion and thermal conduction. In his recent study of the concentration, pressure and temperature dependence of the flame velocity in hydrogen-oxygen-nitrogen mixtures he concludes that at the present state of knowledge, predictions of laminar premixed flame propagation should be as reliable as experimental results.

Coffee and Heimerl [1981] examined various methods of approximating multi-species transport phenomena using a method of lines in their model of premixed, laminar, steady-state flames. They concluded that the selection of the input values for the individual species transport properties is more important than the selection of the approximation method.

There have also been a number of approaches which solve a steady state formulation of the flame equations. These include the works of Dixon-Lewis [1968], Wilde [1972], and Smooke [1982]. The advantages and the difficulties in using steady state solution procedures have been discussed by Smooke [1982]. These methods are good for obtaining burning velocities and steady state profiles, but cannot provide

information on the ignition and development of flames.

1.3.3 Flammability limits

A fuel is usually considered to be flammable if external ignition results in the formation of a flame which can propagate through the mixture. It has been found empirically that a flame propagating in hydrocarbon-air mixtures is quenched if its temperature is lowered to about 1000 - 1200 C and the propagation velocity at the moment of extinction has a finite value of a few centimeters per seconds. The existence of flammability limits is a result of heat loss to the surroundings. When a certain relationship exists between the heat loss rate and the heat release rate is satisfied within the flame front, the flame ceases to propagate and dies out.

The first attempt to analyze the problem of flammability limits theoretically was made by Zeldovich [1944] over 45 years ago. First, Zeldovich related the occurrence of flammability limits to the phenomenon of heat transfer from the preheat zone or chemical reaction zone to the surrounding walls and formulated appropriate equations. Second, he showed that all flammable mixtures should have limit compositions, below which flame propagation is impossible, due to heat loss from the flame to the surroundings. Third, he draws attention to the influence of diffusion, particularly in cases in which Lewis number differs from unity (Zeldovich and Barenblatt [1959]). Later, Spalding [1957], Williams [1964], and Mayer [1957] proposed a simplified, one-dimensional model of the extinction mechanism based on thermal theory of heat from the flame to the surrounding.

Among the various other theories which were put forward have been several based

on assumptions such as flame quenching is due to the effects of convection (Hertzberg [1980a]), chemical kinetics (Macek [1966]), flame stretch as a result of the existence of a velocity gradients (Lewis and von Elbe [1961]), preferential diffusion of one of the reactants of the flame (Bregeon [1978a,b]), or the action of factors bringing about instability (Kydd and Foss [1964]). It follows that the mechanism of flame quenching is probably a combination of more than one factor, depending on the particular flame.

There are considerable problems associated with carrying out fundamental research on flammability limits of dust-air mixtures because it is extremely difficult to make the experimental conditions reproducible as a result of the differences in physical and chemical properties of different coal dusts, differences in the design of the experimental apparatus, the use of different ignition energies, etc. Under such circumstances a better standardization of the experimental conditions is one of the most urgent requirements for the research.

1.3.4 Flame quenching

1.3.4.1 Experimental studies on quenching The study of flame quenching was initiated by sir Humphry Davy in 1815 when he became interested in devising ways to prevent explosions in coal mines. He was able to design the well known Davy safety lamp, which depends on the principle that explosions in methane will not pass through small apertures or tubes.

Payman and Wheeler [1923] conducted an experiment on the propagation of methane-air and coal gas-air flames through tubes of small diameter. They carried out their experiments by recording the flame speed with the tube diameter for various

mixtures to demonstrate the cooling effect of the walls as the tube diameter was decreased. They noted the effect of flame speed on the ability of the flame to pass through tubes or holes of small diameter, and they established the fact that flames having higher propagation velocities are more difficult to quench.

Holm [1932] provided a quantitative measure of flame quenching by the burner method. The principle of this technique is to determine whether a flame stabilized on a burner will flash back or be quenched when the flow of the combustible mixture is interrupted. Holm carried out his experiments on methane-air and coal gas-air mixtures at various concentrations. He also studied the effect of material of the wall and concluded that while the thermal properties of the gaseous mixture certainly affected the flame quenching, the thermal conductivity of the wall material was comparatively unimportant. This led him to hypothesize that flame extinction occurs due to the cooling effect of the unburned gas in contact with its external surface.

Another method, known as the flanged electrode method, to determine the quenching distance was introduced by Blanc et al. [1947], and by Lewis and von Elbe [1961]. In this method, two spark electrodes were flanged with glass plates and a series of experiments were conducted to obtain the relation between the minimum ignition energy versus the distance separating the electrodes. When the electrodes spacing approached to within a critical distance the curve took a rather sharp vertical turn, meaning that the glass plates suppressed the development of a self-sustaining flame. This distance was considered to be the quenching distance. Using this method, these authors measured the quenching distance for methane, propane and hydrogen-air mixtures as a function of pressure, fuel and diluent concentration. Lewis and

co-workers also measured the quenching of methane and propane with oxygen and nitrogen mixtures flames in cylindrical tubes and between parallel plates by determining the limits of flammability for downward propagation at atmospheric pressure.

Friedman [1949] generated quenching data for hydrogen-oxygen flames and studied the effect of the nature of the surface on quenching. Some tests were carried out in which platinum foil, an efficient catalyst for atomic hydrogen recombination, was glued over the surfaces of the quenching gap. Virtually no effect was found on the critical gap width. In a later paper, Friedman and Johnston [1950] extended the quenching data of the propane-air system by studying the effect of pressure, initial temperature, nature of the surface and mixture strength on quenching distance.

Having some quenching measurements for the propane-air flame did not prevent other investigators from carrying out experiments for this system to ascertain the various trends associated with the phenomenon of quenching. Simon et al. [1954] used the tube method to determine the relation between the pressure flammability limits and quenching distance for propane, ethylene and tri-methylpentane flames at various mixtures. Generally in the tube method, a glass tube is filled with the combustible mixture and the mixture is ignited by a spark at one end of the tube, which is enlarged and open to the atmosphere or to a large plenum in order to maintain constant pressure combustion. Then, the diameter of the tube that makes a flame fails to propagate is determined. It is common practice in this method to keep the diameter fixed while varying the pressure until the limiting pressure is obtained. The procedure is repeated for various tube diameters.

Potter and Berlad contributed a great deal of work in the area of laminar flame

quenching. Berlad and Potter [1956] designed a variable width rectangular channel burner to study the effect of oxygen and inert diluent concentration on propane-air quenching. Potter and Berlad [1951] carried out experiments on propane-air quenching as a function of fuel-air ratio and pressure to test the derived equations. Satisfactory agreement was obtained.

Potter and Berlad [1956] also explored the effect of type of fuel on flame quenching using eight fuels of three groups: saturated, unsaturated, and aromatic hydrocarbons as well as hydrogen. For lean mixtures they found that the quenching distance increased as the carbon chain is lengthened or branched, while for rich mixtures it depended on the molecular weight of the fuel with a calculated exponent of - 0.3 and - 0.5, for equivalence ratios equal to 1.5 and 1.7 respectively. In addition, the pressure dependence of the quenching distance for various fuels was presented; an expression was established relating the pressure exponent of quenching distance to the overall reaction order, the pressure dependence of flame temperature and the flame activation energy.

Potter and Berlad [1956] found that quenching distance of a flame, in the same mixture, was different depending on whether the flame propagated upward or downward. They found that for channel distances longer than 9 mm the limits for both upward and downward propagation were the same as in the standard tube. According to theory, complete independence of the limits from the dimensions of the tube is possible only for channels or tubes of very large size.

In order to assess the relative importance of heat and mass transfer in the quenching of hydrocarbon flames, Potter and Berlad [1955] studied the effect of inert gas on

quenching distance by replacing helium by argon in the propane-oxygen mixture. The idea of the study was that such replacement would affect the thermal conductivity and diffusion coefficient of the mixture differently. Thus, its effect on any flame property could be used to distinguish between the thermal and diffusional mechanisms. The observed effect of the above replacement on flame quenching was compared with that predicted by a thermal theory and a diffusional theory. Predictions of the thermal theory agreed well with the experimental results while those of the diffusional theory did not. This supported the widely accepted view that a thermal mechanism was responsible for flame quenching. Furthermore, Berlad and Potter [1956] made use of the quenching data to empirically establish a relation between burning velocity, the boundary velocity gradient and quenching distance. Massey and Lindley [1958] reviewed the subject of flame quenching with some emphasis on its application in flame arrestor.

The influence of various flow parameters; pressure, velocity and turbulence on quenching distance was investigated by Ballal and Lefebvre [1976, 1977]. They conducted a series of tests on flowing combustible mixtures at various mixture compositions. They proposed that thermal diffusion processes are important even at very high flow velocities. They found that quenching distance increases with an increase in turbulence intensity and decreases with an increase in pressure, but, they did not find any appreciable effect of turbulence scale or flow velocity on quenching distance.

Ballal [1980,1983a,b], and Ballal and Lefebvre [1976,1977,1978a,b,1979,1980a,b] measured a quenching distance and minimum ignition energy of various mist and solid dust clouds by using a zero-gravity test apparatus. Ballal obtained quenching

data at various particle concentrations and sizes of liquid and powdered fuels. He ascertained that heat conduction, radiation, and diffusion are dominant factors in flame quenching.

Recently, Jarosinski et al. [1986] measured the quenching distance of three different powdered fuels in air; cornstarch, aluminum, and coal dusts. They put a grid of steel quenching plate in the middle of their test apparatus and measured a quenching distance by observing whether the fully developed flame propagates through the grid or not. They measured higher quenching distances than Ballal [1983a]. The reason is the quenching distance determined by Ballal is the minimum diameter that a flame can propagate which is initiated by a spark, and the one measured by Jarosinski et al. [1986] is the maximum spacing between the walls for which heat outflow to the wall is able to quench the fully developed freely propagating flame.

1.3.4.2 Theoretical studies on quenching The quenching distance (or quenching diameter) can be defined as the minimum distance between parallel plates (or tube diameter) which will allow the passage of a flame. Generally, four methods of measuring quenching distance or diameter can be distinguished. These are;

1. the burner method; determination of whether a flame stabilized on a burner will flash back or be quenched when flow to the burner is interrupted.
2. the tube method; determination of the critical tube diameter for the propagation of a flame in a quiescent mixture.
3. the parallel electrode method; determination of the critical separation distance for the ignition and propagation of flame.

4. extrapolation of blow off-flash back stability diagrams to the quenching points.

These various methods were used to determine the quenching distance and its relation to the other parameters of the problem. But no measurements were made of the flame structure at or near the quenching limit.

There is somewhat general consensus among most of the research workers that a flame quenches mainly because of the heat transfer by conduction to the containing wall in the direction normal to that of flame propagation. Thus it is apparent that models other than the adiabatic ones must be invoked to predict the observed phenomenon of flame quenching.

Mathematically, two distinct wall quenching configurations can be identified, side-on and head-on quenching. Side-on quenching occurs when the flame propagates along a cold surface with only a single contact point between the flame and the cold wall, while head-on wall quenching refers to the situation in which a propagating flame encounters a cold obstacle in its path. Side-on quenching has been described in terms of a two-dimensional boundary layer problem by von Karman and Millan [1952] and Fendell [1977], while head-on flame quenching has been modeled as a one-dimensional, non-steady process by Kurkov and Mirsky [1968], Adamczyk and Lavoie [1978], Carrier et al. [1979], and Westbrook et al. [1981]. Ishikawa [1978] and Ishikawa and Branch [1978] analyzed a flame quenching process in a spark ignition engine and proposed a simple model of quenching. In these descriptions of quenching processes, either a simple heat release or one step chemical kinetics was used to describe the characteristics of the propagating flame structure. One significant aspect of these head-on quenching models is that they were unable to account for the high levels

of hydrocarbons observed in the engine experiments. The suggestions were made by Adamczyk and Lavoie [1978] and Lavoie [1978] that improved agreement might be obtained with the use of detailed chemical kinetics in these models.

Lack of understanding of complicated flow characteristics has blocked detailed analysis on wall flame quenching. Ferguson and Keck [1977] assumed that wall flame quenching may not be influenced by the existing turbulence and proposed their laminar quenching theory for application to a spark ignition engine. Their reasoning is based on Daniel's experimental results, that is, the quench layer thickness is of the same order of magnitude as the quenching distances of laminar flame quenching devices.

The theoretical analysis on flame quenching may be categorized into two classes: those beginning with an arbitrary assumption concerning the conditions required for flame propagation, and those which involve direct solution of the conservation equations. The first class employs assumption for the flame quenching criteria in which either thermal diffusion processes, Friedman [1949], or mass diffusion processes, Simon et al. [1954], dominate the phenomenon. This methods can not predict the flame structure or burning velocity near or at the quenching limit, but, it has been used to obtain correlations for the quenching distance. The second class normally utilizes numerical solutions and provides a better phenomenological description. The second class provides a flame structure along with a burning velocity at or near the limit. The work of von Karman and Millan [1952], and of Kurkov and Mursky [1968] are typical descriptions of the problem.

Without exception, previous non-adiabatic theories accounted for the conductive heat loss to the wall by assuming a volumetric heat loss term in the energy equation. The heat transfer coefficients were determined from the solution of the energy equation for the equivalent non-reactive laminar flow. This approach, though not very adequate, has principally been adopted to make the mathematical solution tractable, through handling a system of one-dimensional ordinary differential equations.

Nevertheless, the solutions derived from the simple analysis are useful in discussing the effect of fluid dynamics although they provide an intuitive understanding at best. The quenching distance in this method is determined by setting up a criteria at which either the rate of heat loss or the rate of destruction of radical species due to the wall effect is equated to their respective rates of generations in the reaction zone of the flame.

Friedman [1949] adopted the first approach in an attempt to develop a simplified model for flame quenching on a thermal basis, which considers the loss of heat from the flame to the surroundings to be the primary cause of its extinction. The quenching criterion he postulated was that quenching occurs when the rate of heat generation by the flame is equal to the rate of heat loss to the wall. After some simplifying assumptions and making use of Mallard-Le Chatelier equation for flame thickness, Friedman showed that the quenching distance, adiabatic burning velocity, and thermal diffusivity of the unburned gas were related as follows:

$$\frac{DqSu}{\alpha} = \frac{2}{f} \left(\frac{T_a - T_i}{T_i - T_0} \right)^{1/2} \quad (1.10)$$

where f is a geometric constant.

Based on a diffusional mechanism, which suggests that flames extinguish in small tubes mainly due to the destruction of chain carriers at the wall rather than the heat loss to the surrounding, Simon et al. [1954] established a short-cut theory to predict the quenching distance. As a criterion for flame quenching, they assumed that the number of effective collisions per unit volume initiated by the active particles while diffusing to the wall and before being destroyed must be equal to or greater than the total number of effective collisions per unit volume necessary for the flame to propagate. The following expression for the quenching distance was obtained.

$$D_q = \left[\frac{fAP}{N_f} \sum \frac{p_i k_i}{D_i} \right]^{1/2} \quad (1.11)$$

where f is a geometrical constant, A is an empirical constant which represents the fraction of molecules which must react for the flame to propagate, k_i is the specific rate constant, D_i is a diffusion coefficient, and N_f is the number density of fuel.

Though the above expression gives values of quenching distance that agreed satisfactorily with the experimental data, entirely ignoring the heat transfer to the wall was unacceptable to most researchers. This led Potter and Berlad [1955] to derive a thermal analog to the above equation, according to which the flame was quenched if the heat loss to the wall exceeded a critical fraction of the heat produced by the flame. The final form of the equation determining the quenching distance was

$$D_q = \left[\frac{Fg\alpha c}{w} \right]^{1/2} \quad (1.12)$$

where, F is an empirical constant which represents the fraction of the heat generated which must be retained by the flame to propagate, c is the fuel concentration, and w is the average flame reaction rate. In the above equation, the dependence of the quenching distance on the burning velocity appears through the reaction rate term.

The second approach in quenching analysis, solving the appropriate conservation equations, was adopted by many investigators. Daniel [1956] presented an analysis for the non-adiabatic one-dimensional energy equation of laminar flame with heat losses for cases of uniform and non-uniform cooling. In both cases, he found that for small heat losses, two burning velocities existed; however, the smaller one was physically unreal since it increased with the increase in cooling. Furthermore, he showed that there is a maximum value of heat loss beyond which there could be no solution for the energy equation. Since the effect of decreasing the tube diameter is to increase the heat loss to the wall, Daniel deduced that there should be a minimum diameter, that is the quenching diameter, and a corresponding minimum velocity below which flame propagation is impossible. The theory did not make possible the quantitative prediction of this limiting diameter.

Lewis and von Elbe [1961] numerically solved the energy equation in the wave and dead space zones separately using a constant reaction rate. Two solutions, relating the variations of maximum temperature with the distance from the wall, were obtained; one corresponded to a hot flame and the other to a cool flame, which was not of physical importance. As the tube diameter was decreased, the two solution curves came closer together and finally merged at a critical tube diameter.

A clearer analysis than the previous one is presented by von Karman and Millan [1952] by analytically solving the one-dimensional energy equation with volumetric heat loss included. The non-dimensional mass burning rate was obtained as a function of certain heat loss parameter and ignition temperature. The model retained the feature of having two solutions approaching each other until they coincided at the

maximum heat loss rate, beyond which no solution could be obtained. It is worthwhile to note that the above feature of having two solutions converging to one at the extinction limit is generally exhibited by all non-adiabatic flame models.

Mayer [1957] provided simplified thermal theory based on the application of the macroscopic energy conservation equation between a plane in the unburned gas and another located where the peak temperature occurs. He used an Arrhenius-Semenov type expression for the burning velocity and obtained an equation relating the actual flame temperature T_f to the adiabatic flame temperature T_a and a heat loss parameter β as follows:

$$\rho C_p (T_a - T_f) B e^{-E/2RT_f} = q(\beta, T_f) \quad (1.13)$$

where, B is an empirical constant, and q is the heat loss rate to the surrounding. From the above equation, real flame temperature is only possible for limited ranges of adiabatic flame temperature and β depending on whether the heat loss mechanism was radiative, conductive, or both.

Using a rather rigorous formulation, Spalding [1957] devised a theory by solving the conservation equations of mass and energy. The volumetric heat loss to the surrounding and power law form of the reaction rate was used. He assumed that the heat loss occurs only in the post reaction zone, which was separated from the reaction region by an artificial catalyst plug. After some approximations, Spalding developed an analytical expression which related a heat loss parameter, the maximum flame temperature and the temperature dependence of both the reaction and heat loss rates. From this relation, the flame extinction limit could be deduced provided that the reaction rate dependence on temperature was steeper than that of heat loss rate.

Berlad and Yang [1960] developed an approximate mathematical model that predicts extinction limits with conductive and radiative losses distributed all over the flame. The combination of energy and mass conservation equations along with the boundary conditions resulted in an expression for the maximum flame temperature in terms of two integrals for the reaction and heat loss rate with respect to the space coordinate. In order to carry out the integrations, they assumed a Gaussian error function with two undetermined parameters to represent the temperature distribution inside the wave. They obtained the limiting values of tube diameter, mixture composition and pressure by trial and error.

Many researchers extended Spalding's original analysis by considering the heat losses upstream and downstream from the flame zone. They used the thin flame approximation and power law kinetics, approximately solving the one-dimensional energy equation with a volumetric heat loss term. The solution showed that neglecting either upstream or downstream heat losses caused an overestimate of the critical heat loss parameter by a factor of about two.

Berlad and Yang [1960] numerically integrated the one-dimensional non-adiabatic flame equations employing Arrhenius kinetics to obtain the burning velocity and the structure of a simulated propane-air mixture near extinction limits. Conductive and radiative heat losses were included and solutions were obtained for different Lewis numbers. Moreover, the existence of two burning velocities was verified numerically. Gerstein and Stine [1973] solved the one-dimensional flame equations using a more realistic model for the radiative loss to obtain the non-adiabatic burning velocity, lean flammability limit and quenching diameter for a methane-air mixture.

Buckmaster [1976,1977] analyzed the quenching of deflagration waves. He presented an asymptotic analysis for the one-dimensional mass and energy conservation equations, using Arrhenius kinetics, in the limit of infinite activation energy. The model agreed well with all the previous work in predicting fast and slow waves that converge to a single value at the extinction limit. The limiting flame speed was found to be about 0.61 times of the adiabatic value whereas that of maximum flame temperature at extinction was slightly smaller than the adiabatic one.

Unfortunately, despite the present degree of development of computer techniques, no multi-dimensional theory of flame quenching has yet been developed. The only two-dimensional theory of a laminar flame with a heat losses to the wall, established by von Karman and Millan [1952], can only be used to a very limited extent for the estimates of the structure of a flame in contact with the wall. Also, this method can not be used to determine the limit conditions of a flame, in view of the assumption that the limiting burning velocity is a known value determined on the grounds of one-dimensional theory.

These limitations were eliminated in the method of Aly et al. [1979], and Aly and Hermance [1981]. Unfortunately, their assumption of a plane flame propagating freely between parallel plates at a speed equal to the burning velocity is unrealistic. Experiments shows that the displacement of a plane flame in a quenching channel is possible only in a very narrow range of conditions approaching the limit conditions within the remaining range of conditions the flame is curved and propagates at a velocity which is higher than the burning velocity. They solved the laminar steady two dimensional conservation equations by assuming the flow is in the direction of the

flame and the temperature is two dimensional to calculate the quenching distance of the propane-air flame between parallel plates. They found their quenching distance to be over twice the experimentally determined value. A possible reason is that diffusion of the reactants perpendicular to the duct walls was neglected arbitrarily in their formulation. Later, Carrier et al. [1984] extended the previous authors' work by numerically integrating the governing equations using quasi-linearization and alternating direction implicit finite difference techniques with a Shvab-Zeldovich type formulation and Oseen linearization of the convective terms including the diffusion of the reactants perpendicular to the walls.

1.3.4.3 One-dimensional quenching model Williams [1985] developed a one-dimensional model of flame quenching. It can be used to determine the limit conditions of existence of a flame and the characteristic points on the temperature curve for the limit flame. The temperature profile is shown in Figure 1.2. The one-dimensional energy equation with heat loss,

$$\frac{d}{dx}\left(\lambda \frac{dT}{dx}\right) - \rho C_p u L \frac{dT}{dx} + Qw - L = 0 \quad (1.14)$$

where, L is the rate of heat loss per unit volume and time, and w is the chemical reaction rate. To minimize the deviations from the one-dimensional model, consider the analysis of a limiting flame propagating downwards in a narrow channel between two infinite parallel plain walls. Williams [1985] assumed the following:

1. Lewis number equals to one.
2. w equals 0 for $x < 0$, w_m for $0 \leq x \leq b$, and 0 for $x > b$.

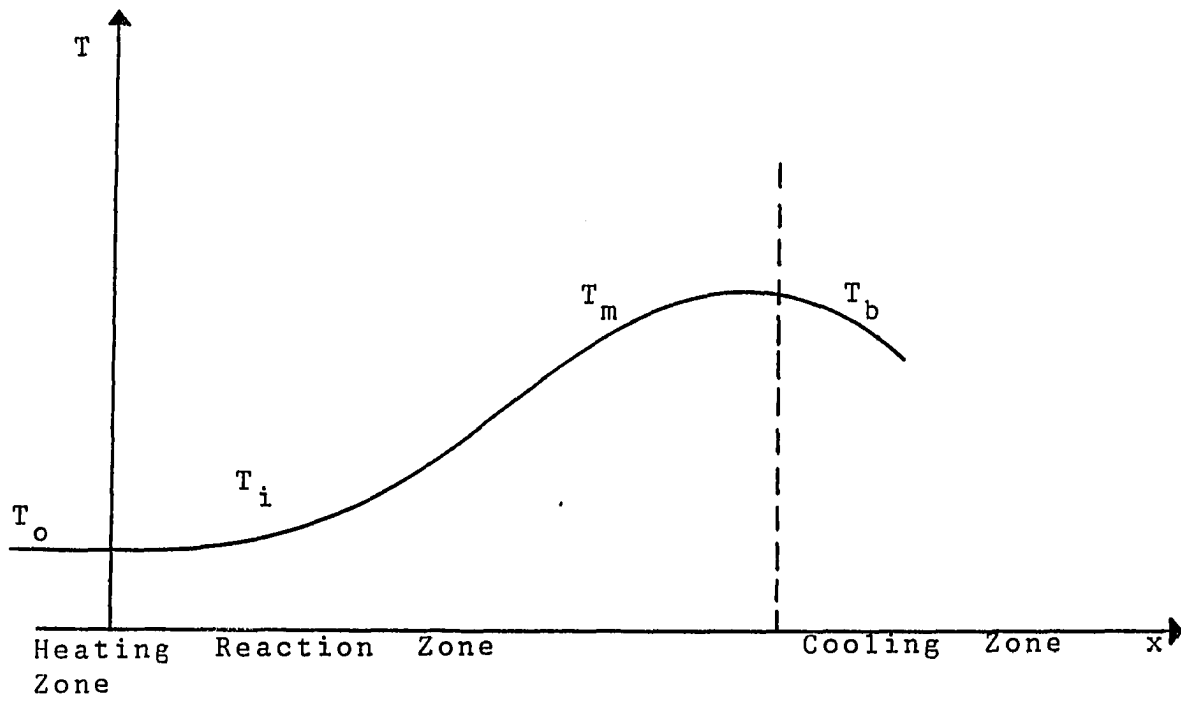


Figure 1.2: Temperature distribution in a flame

3. λ and C_p are constants.

The width b of the combustion zone is determined from the relationship,

$$Qw_m b = C_p(T_a - T_o)\rho u_L \quad (1.15)$$

where, T_a and T_o are adiabatic and initial flame temperature, respectively. The specific heat loss rate from the flame to the wall is expressed as

$$L = k(T - T_o) \quad (1.16)$$

Introducing the following dimensionless coordinates,

$$dX = \frac{C_p \rho u_L}{\lambda} dx \quad (1.17)$$

$$\tau = \frac{T - T_o}{T_a - T_o} \quad (1.18)$$

Then the energy equation is reduced to the following form.

$$\frac{d^2 \tau}{dX^2} - \frac{d\tau}{dX} - \psi \tau = -\varphi \quad (1.19)$$

where,

$$\varphi = \frac{\lambda_m Q w_m}{(T_a - T_o) C_p^2 \rho^2 u_L^2} \quad (1.20)$$

$$\psi = \frac{\lambda_m k}{C_p^2 \rho^2 u_L^2} \quad (1.21)$$

Thus, the solution of the differential equation is,

$$\tau = \frac{\varphi}{\psi} + A e^{\alpha_1 X} + B e^{\alpha_2 X} \quad (1.22)$$

where,

$$\alpha_{1,2} = \frac{1}{2}(1 \pm \sqrt{1 + 4\psi}) \quad (1.23)$$

The thickness of the reaction zone as expressed in terms of the dimensionless coordinate X is $(C_p \rho u_L / \lambda_m) b$. From the continuity condition of the temperature τ and the temperature gradient $d\tau/dX$ across the boundaries between zones at the points $X = 0$ and $X = s$, we can find the unknown coefficients A and B by performing some algebraic manipulations. The temperature at the beginning of the reaction zone is,

$$\tau_i = -\frac{\varphi}{\psi} \frac{\alpha_2}{\alpha_1 - \alpha_2} (1 - e^{\alpha_1 s}) \quad (1.24)$$

and, the temperature at the end of the chemical reaction is,

$$\tau_b = -\frac{\varphi}{\psi} \frac{\alpha_1}{\alpha_1 - \alpha_2} (1 - e^{\alpha_2 s}) \quad (1.25)$$

The maximum temperature can be determined by equating the first derivative of the temperature to zero;

$$\tau_m = -\frac{\varphi}{\psi} (1 - e^{(\frac{\alpha_1 \alpha_2}{\alpha_1 - \alpha_2}) s}) \quad (1.26)$$

$$X_m = \frac{\alpha_1}{\alpha_1 - \alpha_2} s \quad (1.27)$$

A fundamental criterion which determines the conditions for flame quenching by a channel wall is the Peclet number.

$$Pe = \frac{\rho C_p u_L D_q}{\lambda} \quad (1.28)$$

where D_q is the quenching distance.

The heat transfer between the flame and the wall in a channel is expressed by the Nusselt number defined as

$$Nu = \frac{h D_q}{\lambda_m} \quad (1.29)$$

where h is the heat transfer coefficient. If the distance between the channels approaches the quenching distance D_q , the following expression is obtained.

$$k = \frac{2h}{D_q} = \frac{2\lambda_m Nu}{D_q^2} \quad (1.30)$$

There exist rigorous relationship between the quenching distance and the flame thickness, δ . Andrews and Bradley [1972] and Jarosinski [1984] found that the quenching distance is equal to two times of the flame thickness. Jarosinski [1983] experimentally evaluated the Peclet number equal to 40. Also, he measured the limit temperature of the flame to be $\tau_b = 0.8 - 0.85$.

1.3.4.4 Quenching mechanism; wall heat loss Various competing processes can dissipate power from a combustion wave and thus quench its propagation at some characteristically low limit velocity. The processes are

1. Heat losses due to free radicals near the wall
2. Free, buoyant convection
3. Conductive and convective wall losses
4. Radiation losses
5. Selective, diffusional demixing
6. Flame stretch

For upward propagation, extinction is caused by the ascendance of the buoyancy force operating through the mechanism of flame stretch.

Flames propagating through tubes of finite dimensions will lose combustion energy to their surroundings by heat conduction through the tube walls because the walls are initially colder than the burned gas. This loss process generates steep temperature gradients in the gas near the wall and in the quenched boundary layer, as shown in Figure 1.3.

For large plate separation distances, the quenched boundary layer is far removed from the central regions and does not significantly influence the actual burning velocity. However, as the separation distance is diminished, the temperature gradients in the quenched boundary layer converge and soon begin to influence the bulk propagation rate. Eventually propagation is quenched at some finite gap distance, referred to as the quenching distance. The non-adiabatic loss processes involve the heat flow vectors perpendicular to the propagation direction. As indicated in Figure 1.3, the losses are not only in the rim regions where flame zone contracts the wall but also from the unburned regions just behind the flame zone (Hertzberg [1980b]).

The governing equation can be obtained by an elementary derivation. Assume a flat, laminar, flame front that is propagating in steady state. The heat convected is given by,

$$Q_{conv} = \rho C_p S_u (T_b - T_u) \pi r_o^2 \quad (1.31)$$

where S_u is the burning velocity, r_o is the tube radius, and T_b and T_u are the temperature of the burned and unburned gas, respectively. This convected heat is approximately equal to the rate of heat generated by the combustion reaction.

The heat loss through the wall is given by

$$Q_{loss} = \frac{\lambda}{r_o} (T_b - T_u) Nu 2\pi \beta \delta \Delta x \quad (1.32)$$

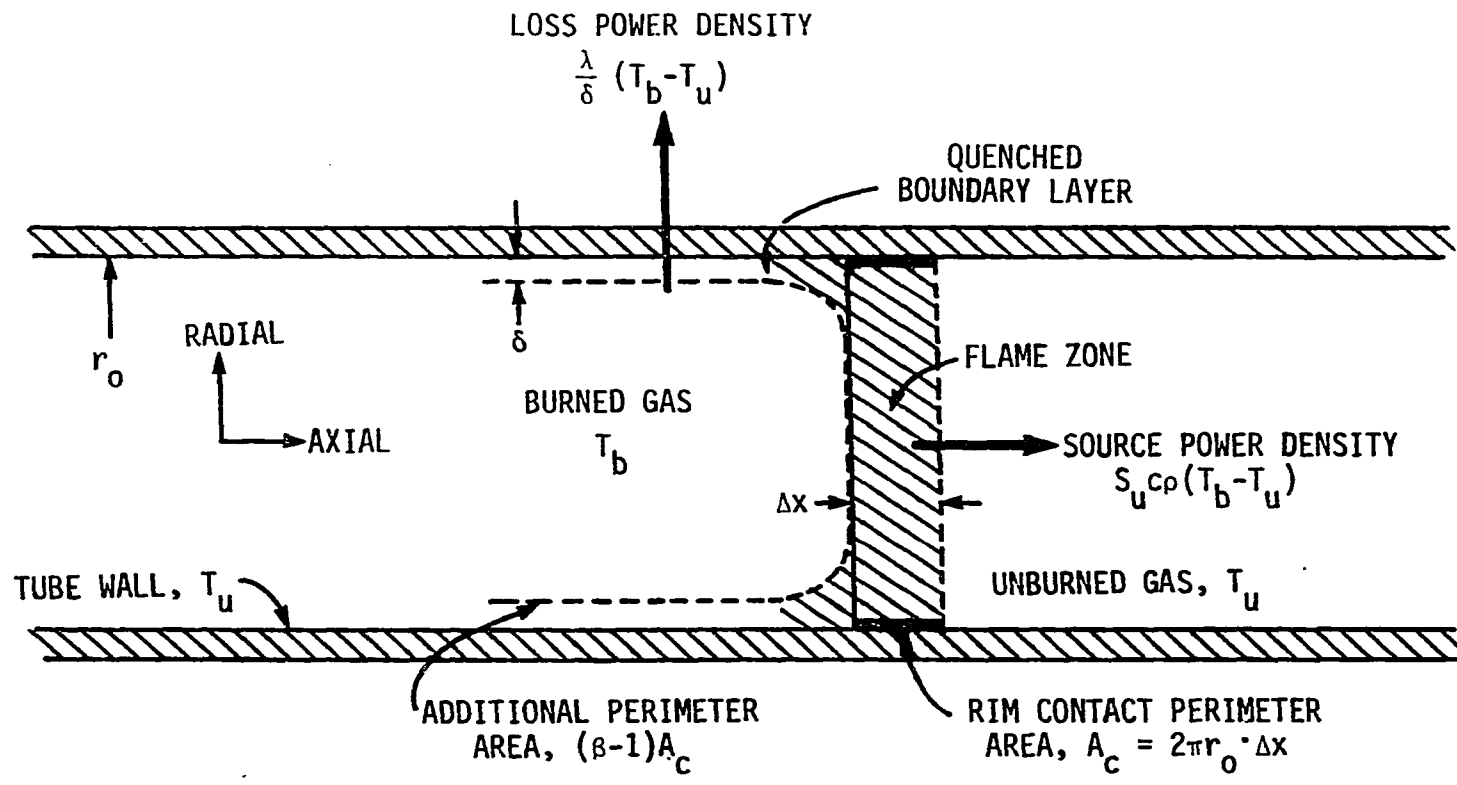


Figure 1.3: Schematics of wall loss quenching of a flame propagating in a tube (Modified from Hertzberg [1980b])

where β is a dimensionless geometric wall loss factor, λ is the effective thermal conductivity, and δ is the boundary layer thickness for radial conduction losses to a cold boundary wall. The limiting case is obtained when the convected heat rate is dissipated as heat loss. Setting the above equations equal and using the following relationship,

$$\alpha = \frac{\lambda}{\rho C_p}, \quad \Delta x = \alpha / S_u \quad (1.33)$$

the final equation is obtained in the following form.

$$Pe = \frac{S_u d q}{\alpha} = 2(2\beta Nu)^{1/2} \quad (1.34)$$

Thus, the Peclet number, Pe , is a useful dimensionless parameter that correlates the measured quenching distance data with the combustion and transport properties. For plates, the ratio of loss area to flame area for the gas is half that for tubes, and hence the critical Peclet constant should be 0.71 times as large.

The present research will also involve the development of an analytical model of quenching for a propagating flame between two parallel plates. The Peclet number is a useful parameter for both modeling and handling of the experimental data.

1.3.4.5 Quenching of coal dust flame To date, relatively little data are known for coal powder in regard to its quenching distance. This is in sharp contrast to gaseous combustibles where quenching distance data have been well documented.

Pioneering work on the behavior of coal dust-air mixtures has been carried out at the Pittsburgh Mining and Safety Research Center. As part of a broad program aimed at reducing underground mine explosions, studies of ignition, flammability

limits, quenching, and inhibition of propagation through tubes have been made on coal dust-methane-air and coal dust-air mixtures.

Those investigations, while giving useful clues as to quenching behavior, have not systematically explored the quenching of pure coal dust-air mixtures. The following is a summary of these studies:

1. The study by Litchfield [1981] suggest a minimum quenching distance of about 1 cm for the coal dust tested. However, the situation surrounding the spark ignition within the confines of the parallel electrodes is complex, and it may not be possible in such a circumstance to separate ignition, pyrolysis, and quenching effects.
2. The quenching diameter studies by Singer et al. [1966] involved only mixtures of coal dust and methane. They apparently found it impossible to initiate a propagating pure coal dust-air flame at the entrance of a 7.9 cm^2 quenching apparatus. Several ranks of coal were examined.
3. In the case of the studies of the propagation of coal dust-air explosions through fixed diameter vertical explosion tubes, no systematic studies of quenching diameters were made. However, a number of observation have been made that bear on the question of quenching diameters in heterogeneous systems like coal dust-air. For example, Grumer et al. [1974] observed marked effects of wall temperature on the ability to propagate an explosion through a 15 cm in diameter tube filled with two sizes of Pittsburgh seam coal. Powell [1962] has reported that a coal dust-air flame would not propagate through tubes less than 14 cm in diameter.

4. Recently, Jarosinski et al. [1986] reported the minimum quenching distance of 25.0 mm for less than 5 μm bituminous coal of 32.1 percent volatile content.

The above observations and results point to considerable uncertainty as to the quenching distance to be expected for coal dust-air mixtures. In particular, the effects of powder dispersal, coal type, coal fineness, mixture strength, method of ignition, and test section geometry need to be studied in a unified program. Research is needed in this area along with the development of a calibration device for determining quenching distance of powders. To this end, an important objective of the present research is to develop a new testing device for measuring the quenching distance of coal-air mixtures and of powders in general.

1.3.5 Aluminum combustion

The development of a mechanism for aluminum combustion requires a clear understanding of the physical and chemical processes involved in both the single particle and the dust cloud phase.

1.3.5.1 Chemical kinetics of aluminum combustion Few experimental studies on the chemical equilibria of the aluminum-air combustion system have been conducted. This is due to the fact that extremely high temperatures must be maintained for the combustion. Brewer and Searcy [1951] studied the chemical equilibrium of the aluminum combustion in air. From subsequent thermodynamic calculations, they argued that aluminum monoxide (AlO) and aluminum suboxide (Al_2O) were the only gaseous oxides of aluminum present. Porter et al. [1955] and Drowart et al. [1960] identified the presence of Al , O , AlO , Al_2O , and Al_2O_2 in the gas phase

by spectrometry. The most abundant aluminum oxide was Al_2O followed by AlO . Therefore, a mechanism for the aluminum combustion must account for the presence of Al , O , AlO , Al_2O , and Al_2O_2 in the gas phase. The relative importance of any of these species is dependent on the initial fuel concentration. Ogle [1986] proposed a aluminum combustion mechanism based on the above observations. He found the activation energy not by experiment but by fitting his experimental data of rate of pressure rise into the Arrhenius type equation of reaction rate.

1.3.5.2 Heterogeneous kinetics A sequence of physical and chemical steps are involved in converting the reactants into products. Rosner [1972] identified vaporization of the particle, dissolution of gaseous reactant, deposition of a solid product, etc., during the course of multiphase reactions. The description of the system as a whole is greatly clarified by the concept of the rate-controlling step: the rate of each physical or chemical process can be no faster than the slowest rate.

Markstein [1966] formulated a criterion for metal combustion for identifying conditions at which heterogeneous reactions become the rate controlling step. Markstein estimated that metal combustion is surface reaction controlled when the particle diameter is roughly 40 mean free paths or smaller. Markstein's criterion is the only general guideline for differentiating between kinetic versus diffusion control. For simpler geometries susceptible to classical boundary layer analysis, other transport limitations such as exothermicity, diffusion-induced convection or complex kinetics can be easily analyzed by the method of Rosner [1966]. There is no general method which allows a distinction between diffusion or kinetic control during particulate combustion.

1.3.5.3 Single particle combustion of aluminum There has been considerable interest in aluminum particle combustion due to its use as an additive in various solid propellant and high explosive formulations. A recent review on solid propellant application is given by Price [1983].

In a numerical modeling study of aluminum combustion in a $CO_2 - N_2$ environment, King [1978] found that finite kinetics could cause significant departures from the diffusion flame limit for both the predicted burning times and flame standoff distances. The numerous complexities which finite kinetics introduces into particle combustion behavior are virtually unexplored.

1.3.5.4 Combustion of an aluminum dust cloud The investigation of multiparticle aluminum combustion has been studied most frequently at either constant pressure or constant volume. The constant pressure experiment involves the attainment of a steady flame using an apparatus similar to a Bunsen burner, such as the one used by Cassel [1964]. This configuration allows for the measurement of laminar burning velocity, blowoff and flashback velocities, and average flame temperature as a function of particle concentration and size. A prototype cutting torch based on a similar design was reported by Grosse and Conway [1958]. Using a premixed flame of aluminum and pure oxygen, they reported cutting a three inch hole into a thirty inch thick concrete slab at a rate of more than one inch per minute. This is an impressive demonstration of the exothermicity of aluminum combustion.

The constant pressure aluminum dust flame has been extensively studied at the U.S. Bureau of Mines, Cassel et al. [1949], Cassel [1964], Cassel and Liebman [1959]. The results of these studies yield valuable qualitative information about dust flame

behavior: the laminar burning velocity increases with either increasing dust concentration or decreasing particle size. These studies also established the importance of thermal radiation as the dominant transport process in flame propagation and demonstrated that all combustion parameters were dependent on the dust cloud size.

Aluminum dust explosibility tests have been conducted by Jacobson et al. [1964] in a constant volume combustion chamber. Their results reflect the same qualitative trends found in the steady dust flame work: explosion intensity increases as either dust concentration increases or particle size decreases. They also reported a significant increase of explosibility due to particle shape. Also, both the burning velocity and explosion intensity tend to first increase and then pass through a maximum as dust concentration increases.

Kim [1986] studied the effects of particle size, concentration on minimum ignition energy and lean flammability limit of aluminum dust flames in air. He also investigated the effect of particle size distribution and reported that a mono-sized aluminum powder requires less energy to ignite comparing to batch particles of the same mean diameter.

The mathematical analysis of aluminum dust combustion has been restricted thus far to simple thermal theories (Cassel et al. [1949], Ogle [1986]) for constant pressure combustion. Some very good work with reactive two phase flow models for coal combustion have been presented by Smoot and Smith [1985], Krazinski et al. [1979], and Slezak et al. [1985], but the analytical methodologies of these studies have not become standard practice in the general field of particulate combustion.

1.3.5.5 Mathematical modeling of a dust explosion Nagy and Verakis [1983] and Bartknecht [1981] extensively reviewed a history of dust explosion testing and its major concepts. Much of the analysis on dust explosion has been concerned with simulating the pressure history within a spherical bomb with central ignition. In principle these models can be used in conjunction with experimental data to extract the burning velocity value. This type of parameter estimation is very approximate, however, because it ignores the complex dependence of the burning velocity on turbulence and chemical kinetics. The matter is further complicated by the fact that the explosion pressure history is very sensitive to the experimental conditions.

Dust explosion models can be classified as either integral balance, gas dynamic or transport models. The integral balance models are usually based on a transient global mass balance written for the unburnt mixture, Nagy and Verakis [1983]. The gas dynamic models are obtained by writing the equations for balance of mass, momentum and energy with transport processes neglected, Takeno and Iijima [1981]. The transport models are derived by writing down the equations for mass, momentum, and energy with transport phenomena included, Ramos [1983a,b], Aggarwal and Sirignano [1984,1985]. Much of the modeling schemes for gas explosions also applies to dust explosions. This is because the mathematical form of the governing equations for a homogeneous multiphase model for dust explosion dynamics is identical to the mathematical form of the governing equation for gas explosion dynamics. The major difference is that the mixture properties for a multiphase system can be quite different from the gas phase properties.

1.3.6 Coal combustion

The combustion of coal is very complicated process, requiring the knowledge of fluid dynamics, heat transfer, and chemical kinetics. Although much research has been directed towards understanding the mechanism of the coal combustion, the complexities involved have made its quantitative description extremely difficult. The various composition of different types of coals further makes it more difficult to analyze the problem.

Initially, the interest in coal combustion arose because of its importance in coal mine explosion prevention. The use of pulverized coal as a fuel in power plants has further drawn the attention of many researchers. The recent interest in alternative energy sources has attracted additional research in the use of coal for gasification and fluidized bed systems. Each of these applications would benefit from sound understanding of coal dust combustion.

The coal particles burn in a very complicated manner. The combustion process includes heterogeneous surface reactions, devolatilization and subsequent reaction of the volatiles, swelling, cracking, and other physiochemical changes to the particles. In addition, coal particles do not always burn simply as shrinking spheres, but can burn internally and form hollow spheres as well. Thus, the coal particles, rather than undergoing external reaction at their outer surface, are capable of reacting internally as well. The composition of volatiles released, and the combustion itself therefore makes analytical description of the process extremely difficult.

Additional complications arise in describing the structure of coal particles because of their shape and variable density. Coal particles are not spherical in shape,

but are highly irregular and porous. Also, the coal particle density decreases during combustion.

1.3.6.1 Properties of coal Coal is a complex material whose precise composition is difficult to determine. Coals are usually classified either by ultimate analysis or by proximate analysis. The ultimate analysis of coal is a chemical determination of the six basic components; carbon, hydrogen, oxygen, nitrogen, sulfur, and ash. Most coals contain by weight from 65 to 90 % carbon, 2 to 7 % hydrogen, up to 25 % oxygen, 1 to 2 % nitrogen, and up to 10 % sulfur. Ash consists mainly of silicon dioxide, as well as various amounts of aluminum, iron, and calcium. The ash content of coal is generally below 30 %.

The proximate analysis is a less complicated test which the coal composition is classified into four constituents; fixed carbon, volatile matter, moisture, and ash. The proximate analysis of the coals tested in this research is listed in Chapter 4. The proximate analysis is performed by the method recommended by the American Society for Testing Materials (ASTM). This involves first heating the coal to about 380 K to evaporate water. Another sample is heated 7 minutes in an evacuated container at 1230 K to evaporate the volatile matter and moisture without igniting the fixed carbon. Then heating of another sample of coal in oxygen to about 1000 K will burn off all the combustible matter in coal leaving only the ash behind.

An important parameter used in the classification of coal is the coal rank. In general, coals of high rank contain greater percentages of fixed carbon and less volatile matter. The major ranks of coal are: 1. Lignite: 2. Subbituminous: 3. Bituminous: 4. Semi-anthracite: 5. Anthracite.

Vast differences in the composition of the various coals make generalizations difficult.

1.3.6.2 Heterogeneous combustion of coal When coal particles burn, the combustion process involves both homogeneous, gas phase reactions and heterogeneous reaction at the solid surface.

The heterogeneous reaction of a coal particle proceeds in several stages. First, oxygen molecules must diffuse through the surrounding boundary layer to the particle surface. Once at the surface, the oxygen molecule must be absorbed into the solid particle so that reaction can occur. The resultant products then are desorbed from the particle and diffuse through the boundary layer into the surrounding gas. Overall reaction will be controlled by the slowest step in this sequence. Essenhigh [1976] proposed that for temperatures below 2000 K, the heterogeneous reaction is diffusion controlled for particles greater than about 100 μm in diameter. For temperatures greater than 2000 K, the reaction can be diffusion controlled even for particles in the 10 μm range.

Calculation by Howard and Essenhigh [1966] based on the analysis of their experimental data have suggested a shift in the rate controlling mechanism throughout the flame. This shift in activation energy was interpreted as being a result of devolatilization. In the initial region of the flame, the efflux of volatiles from the coal particle surface reaches its maximum. If the devolatilization rate is high enough, the volatiles being ejected can effectively screen the surface from oxygen attack. Making the oxygen molecules difficult to reach the surface and to be absorbed into it. Then the overall heterogeneous reaction will be absorption controlled. In the tail of the

flame where devolatilization is no longer significant, the oxygen molecules can readily be absorbed onto the surface and the reaction then becomes controlled by desorption. In either case, the rate was found to be controlled by surface processes rather than by diffusion.

Aside from the influence of volatiles on the heterogeneous reaction rate, the activation energy decreases with rising temperature. Field [1970] proposed that the activation energy should be taken as a decreasing function of temperature.

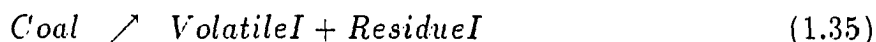
As far as the reaction order is concerned, it is generally agreed that the heterogeneous reaction is of order unity with respect to the oxygen concentration, even though Gray et al. [1974] raised questions as to the validity of this generalization.

Finally, the difficulty in identifying the nature of the products of the heterogeneous reaction arises. There are two basic paths that the reaction can follow. One possibility is the direct reaction of carbon with oxygen to form carbon dioxide, CO_2 , which then diffuses into the surrounding gas. In this case, the heat of reaction is liberated directly on the particle surface. Another possible mechanism is the reaction of carbon and oxygen to form carbon monoxide, CO , which then diffuses into the gas and is subsequently oxidized to produce carbon dioxide. In this case some of the heat liberated by reaction is released on the coal particle surface, while the remainder is released in the gas phase.

1.3.6.3 Coal pyrolysis Coal particles release volatile matter which then reacts in the gas phase, in addition to heterogeneous combustion. Devolatilization is difficult to analyze, both because of the variety of compounds which are released during pyrolysis and because of the influence of the heating rate on the results.

Coal particles, first of all, should not be thought of containing well-defined amounts of fixed carbon and volatile matter. Gray et al. [1974] showed that the coal undergoes a re-arrangement of its chemical bonds which split the original organic components into a volatile fraction and a solid matrix of fixed carbon.

Kobayashi et al. [1976], and Ubhayakar et al. [1976] proposed one elementary model of the devolatilization process. It is developed by considering the coal to degrade into a residue and a volatile component via two competing reactions:



The first reaction is assumed to dominate at relatively low temperatures and yields certain volatiles. The second reaction, which has a higher activation energy than the first, becomes more important at higher temperatures. The second reaction also results in higher volatile yields than the first. Thus the model accounts for the increase in volatile yields with increasing temperature. A more comprehensive pyrolysis model would have to describe the formation of volatile components in the coal, the transport of volatiles out of the particle, and the subsequent loss of certain volatiles because of secondary, char formation reactions.

The devolatilization process cannot always be considered separately from the heterogeneous reaction of the fixed carbon. The efflux of volatiles from a coal particle can be large enough to reduce the rate of carbon consumption at the surface. If the rate of volatiles evolution is slow, then oxygen will readily reach the particle surface to react, but if the rates of devolatilization is high, the gaseous volatiles will effectively screen the coal particle from oxygen attack. The volatiles are ejected from the surface

and subsequently burn via a diffusion flame which surrounds the particle. As the devolatilization rate decreases, the flame front recedes towards the solid surface and eventually stabilizes there, allowing both heterogeneous and homogeneous reactions to occur simultaneously. For a given coal particle, the efflux rate of the volatiles has been found to vary with particle size. Howard and Essenhigh [1966] found that particles larger than about $65 \mu m$ did not react heterogeneously during the period of rapid devolatilization.

The pyrolysis of coal is a very complicated process, as explained previously. The uncertainties in the mechanisms discussed above point out the need for additional research on coal pyrolysis mechanism.

1.3.6.4 Experimental studies on coal combustion: burning velocity

Most of the available knowledge on coal combustion has been obtained with various burners producing standing flames. A common feature of the burner is the use of some sort of flame-stabilizing device to generate a standing flame. Hattori [1956] used an acetylene pilot flame to ignite a mixture of pulverized coal and air being discharged into the atmosphere. Flame velocities were calculated from measured flow rates and the angle of the flame front. To some extent, the combustion was non-adiabatic because of the radiative heat loss to the surroundings by the gas and particles. Also, there was undoubtedly some heat interchange with the pilot flame.

Ghosh et al. [1956] used a burner whose coal-air flame was ignited and sustained by preheating the burner walls to around 1200 K. Since this was closer to the flame temperature, there would have been less radiant heat exchange with the surroundings. Flame velocities were calculated as the volumetric feed rate divided by the cross

section of the burner tube. Burgoyne and Long [1958] used an annular pilot flame of methane, coal and air to sustain an inner flame of coal dust. Flame velocities were calculated from flow rates and geometry of the flame front, and were subject to the usual non-adiabatic uncertainties.

Marshall et al. [1964] used a brass ring as a flame holder. It was suspended over the mouth of the burner port which ejected the coal enriched air mixture into the atmosphere. Flame velocities were determined from the measured feed rate and the angle of the flame front. As before, radiant heat loss to the surroundings probably affected the results.

Howard and Essenhigh [1966] used a set of metal tubes as a flame holder to anchor a turbulent coal flame in a furnace. Smoot and Horton [1977] performed an extensive series of tests with atmospheric coal flames in the air. The flames were enclosed in a cylindrical steel burner and stabilized on a set of wire screens. Flame velocities were calculated from the volumetric flow rate and the cross section of the burner. The experimental results were probably perturbed by conductive and radiative heat transfer from the flame to the burner walls and flame holder.

Common to all of the techniques is the possible importance of heat losses. This factor, negligible in gas flames, results from the high concentration of hot particulates in a gas whose optical length is the same order as the burner diameter. Thus, the hot particles generates a radiative heat that can be expected to escape from the flame. Only burners having very large diameters or walls having temperature and emissivity profiles matching the flame would avoid this problem. Such ideal devices have not yet been used. Therefore, all of the data thus far obtained are dependent on the

individual experimental technique and apparatus.

The burning velocities of the coal changes with a change of particle concentration. From the lean flammability limit where the burning velocity is zero, the burning velocity increases to a maximum that occurs at a concentration near stoichiometric. Thereafter, the burning velocity decreases slowly with increasing concentration. As compared to gaseous flames, extremely rich coal-air composition will support a flame. Generally, it is believed that the rich flammability of solid fuels does not exist or requires extremely rich concentration.

Many investigators have concentrated on compositions near stoichiometric, since that is the practical concentration in furnaces. However, information available for the richer flames where a peak burning velocity is observed shows the peak velocities ranging from 5 to 35 cm/sec. The peak velocity is inversely related to particle size, and can be correlated with the specific surface area of the coal particle.

Considerably more information is available to show how burning velocity changes if other parameters are varied while concentration is constant. Horton et al. [1977] reported that on the lean side of the particle concentration, burning velocity increases with decreasing particle size. Also increasing volatile matter in the coal particles increases the burning velocity. Smoot and Horton [1977] studied the effect of particle size range on the burning velocity of the coal flame. They showed that peak burning velocities are related to the specific surface area of the mixture. They proposed that the smaller particles are more important in establishing burning velocity.

Surprisingly large differences in burning velocities are observed by various investigators. Hattori [1956] reported a burning velocity of 8 cm/sec for the 74-149 μm

coal, contrary to 112 cm/sec reported by Ghosh et al. [1956] for less than 74 μm particles. After allowance is made for particle size, oxygen concentration etc., it appears that increasingly higher burning velocities were measured in the following order by the various researchers: Marshall et al. [1964], Burgoyne and Long [1958], Smoot and Horton [1977], Hattori [1956], and Ghosh et al. [1956]. At least part of the differences are likely due to the fact that fine coals tend to agglomerate. Ghosh et al. [1956] reported that one type of coal particles less than 40 μm could not be burned due to the poor dispersing characteristics. The agglomeration of coal particles effectively create larger particles which burn with low burning velocities. Thus agglomeration may be a factor in any coal particles containing small particles if no fluidizing agent is used. In addition, the method of flame stabilization has a large influence on burning velocity. The heat transfer from the flame holder to the incoming mixture may affect the burning velocity. Intermediate velocities were measured by Hattori [1956] who used pilot flames of various sorts. The fastest burning velocities were measured by Ghosh et al. [1956] in a furnace with preheated walls.

From the above investigations, the following general assumptions can be made.

1. Burning velocities are dependent on the experimental technique and apparatus.
2. Peak atmospheric burning velocities vary from 5 to 112 cm/sec, depending on test apparatus, coal size, and type.
3. Peak burning velocities occur at particle concentration higher than the stoichiometric concentration.
4. The rich flammability limit, if it exists, occurs at very high particle concentra-

tions comparing to gaseous fuels.

5. A smaller particle size increases burning velocity on the lean side but may decrease it on the rich side. Also, smaller particles shift the peak to a leaner concentration.
6. Increasing volatile content of the coal increases burning velocity.
7. C/H ratios of pyrolysis products vary with a position in the flame.
8. Irregular coal particles soften, become rounded and filled with blow holes in the course of combustion.
9. A considerable amount of volatile matters remain unreacted, and the amount is a function of particle concentration.
10. The extent of coal devolatilization is dependent on the specific coal type and is especially related to coal concentration.

1.3.6.5 Theoretical studies on coal combustion In gaseous flames, gas conduction and species diffusion counter to the flow, and chemical reaction are important processes. Heat losses can also be important. In practical gaseous flames such as methane-air, as many as 20 different species can be present, thus complicating the description of diffusion and reaction processes greatly. In particulate flames, such as coal-air systems, additional processes add to the complexity. Particulate and gaseous radiation, conduction between the gaseous and particulate phases, heat-up of particles, devolatilization processes, oxidizer diffusion from the bulk gas to the coal or char particles, heterogeneous oxidation of the char, volatiles combustion in the

gas phase, velocity drag and thermal lag between gases and solids are several of the complicating factors in these heterogeneous flames.

Gaseous flames were considered to be dominated by competing effects of chemical reaction and upstream conduction, while upstream radiation was considered to be the rate-controlling step in coal-air flames. More recent work has emphasized the importance of molecular processes, especially diffusion effects, in coal-air flames. Thus many aspects of gas phase combustion in particulate systems are similar to those encountered in gaseous flames. Many of the features of gaseous flames, such as species diffusion and gas phase chemical reaction are also found in coal-air flames. Therefore, the theoretical development of premixed gaseous flames will aid the theoretical modeling of the coal-air flame.

While gaseous flame propagation models developed from consideration of conduction and chemical reaction, early treatments of propagation in coal flames were based on radiation.

Cassel et al. [1949] have modified the gas phase Mallard-Le Chatelier burning velocity equation to include radiation. The resultant equation is similar to that of Essenhigh and Csaba [1962], but with effects of conduction added.

$$v_o = [k(T_f - T_i)/\delta + \delta\rho_p\epsilon F\alpha\sigma(T_f^4 - T^4)]/(\rho_p r_p)/(\rho C_p + \rho_p C_{p,p})(T_i - T) \quad (1.37)$$

where ϵ is the emissivity of the particle, α is a correction factor which accounts for radiation of glowing combustion products, F is a view factor, and ρ_p is a density of the particle.

Further refinement to the radiation theory was presented by Essenhigh and Csaba [1966]. They accounted for temperature differences between particles and gas and

added a finite pre-ignition zone. This treatment was intended to be most applicable to thick flames. They assumed negligible combustion in the pre-ignition zone, a fixed ignition temperature, no particle lag, particulate radiation from a grey body flame, and negligible upstream thermal conduction in the gas. The burning velocity takes the following form:

$$v_o = I_f(1 - e^{-mt_i}) / [(T_i - T_0)(\rho C_p + \rho_p C_{p,p})(T_i - T)] \quad (1.38)$$

where m is a cloud attenuation coefficient which is equal to $3\rho_p v_0 / 4r_p \rho_s$, and t_i is the ignition time, and I_f is the intensity of radiation from the flame at the point of ignition.

Bhaduri and Bandyopadhyay [1971] further modified the basic radiative approach by incorporating heat generation due to chemical reaction for a single coal particle size assuming thermal equilibrium between the gas and particle. They neglected heat conduction and included only heterogeneous oxidation of the carbon in low volatile coal to carbon dioxide.

Marshall et al. [1964] developed a simple theory which included the radiative effects, conductive effects, and coal devolatilization. They postulated that devolatilization of the coal, particulate radiation and gaseous conduction were the important rate limiting processes. Their work also suggests that burning velocity should vary inversely as the square root of the particle diameter.

Krier and Krazinski [1974] formulated general one-dimensional model equations for coal flame propagation including particle-gas velocity drag and temperature lag effects, coal particle devolatilization, char oxidation, and volatiles combustion and molecular diffusion, in addition to radiative and conductive heat transfer effects. They

solved a non-linear set of steady state conservation equations for a dilute, particle-gas mixture assuming negligible body forces, gas radiation, and radiative heat transfer among particles. Krazinski et al. [1979] have reported additional work on a model of coal-air flame propagation. They solved a series of stiff differential equations numerically using a predictor-corrector finite difference method.

Actually, coal combustion phenomena is turbulent rather than laminar, as observed by many researchers. Recently, Smith et al. [1987] developed a two-dimensional steady state model for coal combustion. They included turbulence effects, radiation from gases, walls, and particles using flux method. Multistep devolatilization and heterogeneous reaction schemes are included in their model. They also modeled major gas phase reactions assuming local equilibrium, thus the reaction rates are limited by the turbulent rate of mixing.

2 A NEW METHOD FOR EVALUATION OF THE BURNING VELOCITY OF POWDERED FUELS

A new electrostatic concept in testing and controlling the burning rate of powdered fuels such as coal and aluminum was evaluated experimentally and theoretically (for the electrostatics) using a flat flame burner.

However, experimental difficulties were found in establishing a stable flame and with carbon buildup on the burner such that this method was abandoned after considerable effort was made in redesigning and testing. Some of the successful aspects of this study will be reported here.

In this method an electrostatic powder dispersion method was utilized to provide accurate control for the generation of a steady state particulate cloud.

2.1 Experimental Design

The combustible powder is put into a large reservoir having an auger feed that delivers the particles to the test section. The auger is driven by a Dayton AC-DC series motor through a 40 to 1 gear box to reduce the speed. The speed of the motor was controlled by using a Variac voltage transformer. A speaker driver was added to make an acoustic exciter to break up the cohesive powder such as coal. To provide a uniform electric field, it is vital that the charging electrode plates be parallel. This is

accompanied by connecting the micrometer heads to two of the supporting insulators. The distance between the plates can be adjusted by using a screw feed to move the upper plate. A Hipotronics high voltage power supply (0 - 50 kV) is used to generate the electric field to the plates. Figure 2.1 shows the schematic of the experimental setup.

2.2 Electrostatic Suspension Theory (Open System)

Colver [1980] identified the naturally occurring and electrically induced particle cohesive forces and parameters and their inhibiting effects on the formation of an electric suspension. He successfully produced an electrically driven coal dust suspension in an acoustically excited fixed bed. Also, he developed a theory for the particle mechanics and electrodynamics of a one-dimensional electric suspension including charge relaxation at the bed interface (which becomes significant as bed resistivity is increased).

The particle cloud behavior is described by the following equation:

$$\frac{dV}{dt} = \frac{QE}{m} - \frac{V}{\tau} - g_0 \quad (2.1)$$

In the present experiment, the particle Reynold's number $Re_p = \rho Vd/\mu < 20$ is maintained. Steady mass and current flux are;

$$\dot{m} = mnV \quad (2.2)$$

$$J = QnV \quad (2.3)$$

Also, from the Gauss's law (one-dimensional);

$$\frac{dE}{dx} = \frac{Qn}{\epsilon_0} \quad (2.4)$$

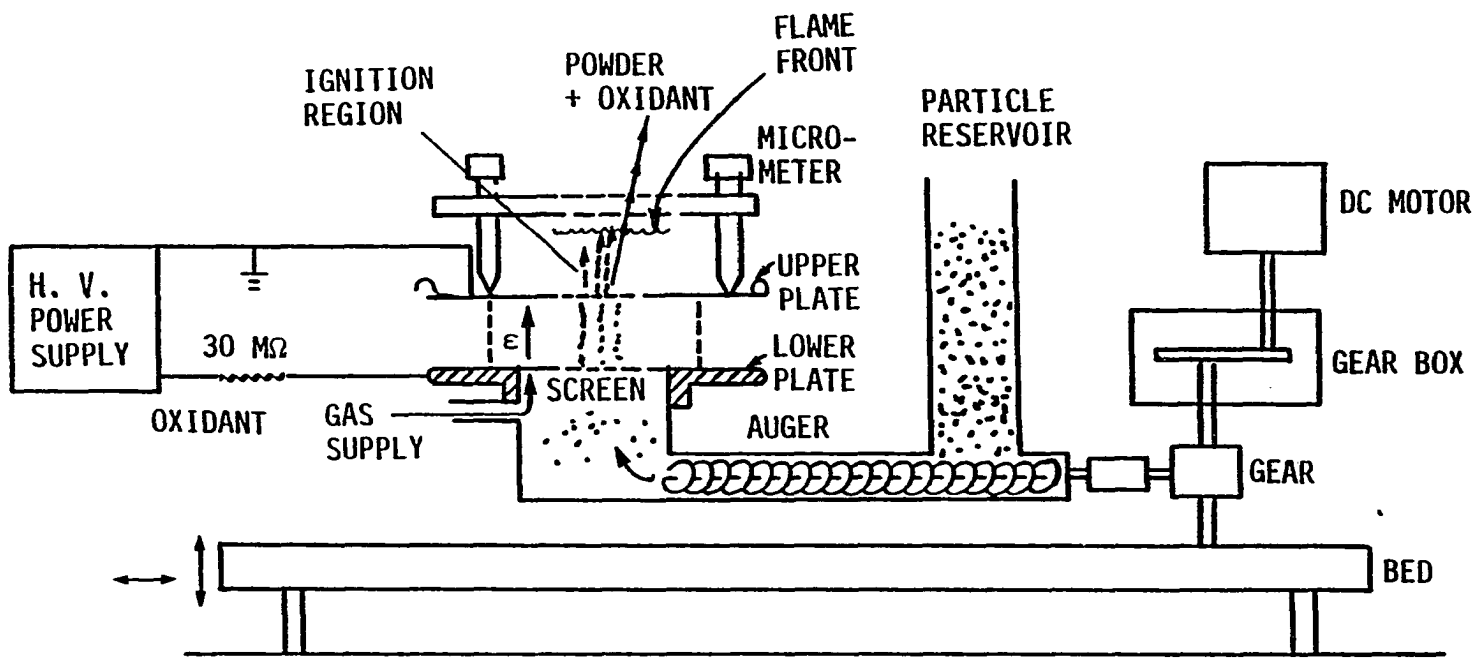


Figure 2.1: Layout of an experimental setup

and the time constant τ is expressed as follows in case particle Reynold's number Re_p is less than 100;

$$\tau = \tau_0[1 + 3Re_p/16]^{-1/2} \quad (2.5)$$

where, $\tau_0 = m/3\pi\mu d_p$. Using the above relations, the solution of the governing equations is;

$$E - E_0 = Jt/\epsilon_0 \quad (2.6)$$

and,

$$V = \left(\frac{QE_s\bar{\tau}}{m}\right)\left[1 - \frac{J\bar{\tau}}{\epsilon_0 E_s} - \frac{mg}{QE_s}\right][1 - e^{-t/\tau}] + \left(\frac{QJ\bar{\tau}}{m\epsilon_0}t\right) + V_0 e^{-t/\tau} \quad (2.7)$$

where, V_0 is the bed feed velocity, and a velocity-average time constant $\bar{\tau}$ is given by

$$\bar{\tau} = \left[\int_0^V \tau dV\right]/V \quad (2.8)$$

$$X = \bar{\tau}V(1 - e^{-t/\bar{\tau}}) + AB\bar{\tau}[t/\bar{\tau} - (1 - e^{-t/\bar{\tau}})] + Ct^2/2 \quad (2.9)$$

where X is a distance above the bed.

2.3 Test Procedure

The procedure of testing for measuring the burning velocity of a powder is as follows;

1. Feed the particles to the reservoir below the lower electrode using an auger and motor delivery system.
2. Set the upper electrode parallel to the lower electrode and adjust the gap distance.

3. Apply the electric field.
4. Ignite the particles above the upper plate using a pilot propane flame.
5. Test for flash-back or stable burning.

2.4 Preliminary Results

The preliminary results for this experiment are as follows.

1. ALCOA 2068 spherical atomized aluminum (85.8 % AL, 9.52 % Ce, 4.4 Mn, balance others) powder was sieved for various mesh sizes and tested. All sizes below 30 μm gave a very bright flame. The extension of the flame varied with different fuel to air ratios, and either "flashback" or a flame was observed that lasted for few seconds.
2. ALCOA 6002 spherical atomized aluminum (99 % AL, balance others) was tested with and without sieving. With this powder, no stable flame was observed.
3. Ampal 601 irregular aluminum (99.5 % AL) was tested. Delivering this powder through the auger proved to be very difficult. The irregular shape of this powder contributed to this difficulty. Reducing the diameter of auger made it possible to deliver a limited amount of powder. No stable flame was observed with this aluminum powder.
4. With Loucia coal (50 - 80 mesh) a flashback was readily obtained.

5. Putting the various sizes of glass cylinders on the tops of the upper electrode to reduce air dilution of the fuel mixture concentration did not help much in this experiment.

A propane and air flame was then introduced as an ignition source instead of a pilot (torch) flame in order to release larger amounts of heat. However, flashback into the electric field region of the electrostatic driver shorted the high voltage electrode because of the conductivity of the flame. Thus, improvements in the design of the experiment were sought.

Although the preliminary results noted above were encouraging, an analysis of the fundamental method being used here suggested to us that we should consider an alternative approach that emphasized the pneumatic transport of the particles, with the electric field being used for augmentation of the particle motion rather than for its primary source of motion. This led to the design of another combustor device shown in Figure 2.2.

2.5 First Modified Design of Combustor

At the heart of the problem previously mentioned in stabilizing a powder flame are the experimental difficulties in separating powders into a uniform cloud and then transporting them at controlled rates through a delivery system at very low velocities near that of the burning velocity.

The burning velocity measured by the United States Bureau of Mines using a Hartmann tube tester had a value of 7.01 cm/sec for the case of atomized aluminum powder. This burning velocity is quite low by a factor of about 10 compared to typical

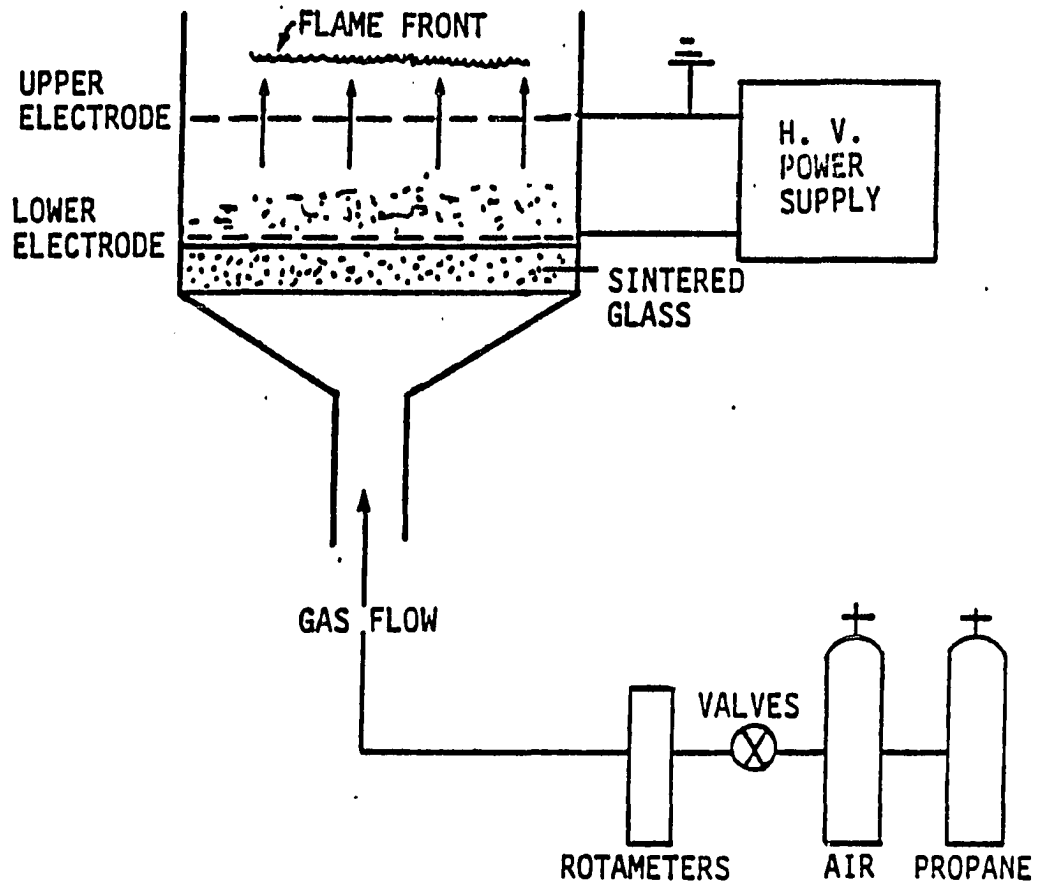


Figure 2.2: Sintered glass test tube

combustible gases. The relative particle velocity V , which is the velocity of the particle relative to the gas, should not exceed the burning velocity, which explains our previous difficulties in stabilizing a flame since the electric field can generate particle speed up to 100 cm/sec. The above ideas show that the dominant factor in this test should not be the electric field transport; rather it should be the pneumatic transport of the powder using oxidant flow augmented by the electric field. That is, the electric field should be applied so as to control the relative particle velocity and to aid in moving heavy particles, but not to dominate the particle motion.

Using a new testing device, a steady-state flame was obtained for the first time in this test without applying the electric field by using the spherical aluminum particles. Big Ben coal also produced a flame.

2.6 Second Modified Design of Combustor

A finally modified setup is shown in Figure 2.3. A DC motor-actuator is used to move the piston so that the transport of the particles above the lower screen is achieved. The upper screen is made to rotate to keep the screen from being clogged with burned particles which prevents the fresh particles from being transported above the upper screen.

A DPDT switch and circuit breaker as shown in Figure 2.4 are used to control the motion of the piston. The circuit breaker is positioned to be hit by an actuator screw when the top of the piston touches the hinge, so that the motor can be stopped. An on-off switch is connected between the DPDT switch and the circuit breaker to change the direction of the piston. The piston and connecting bar are made of plexiglass.

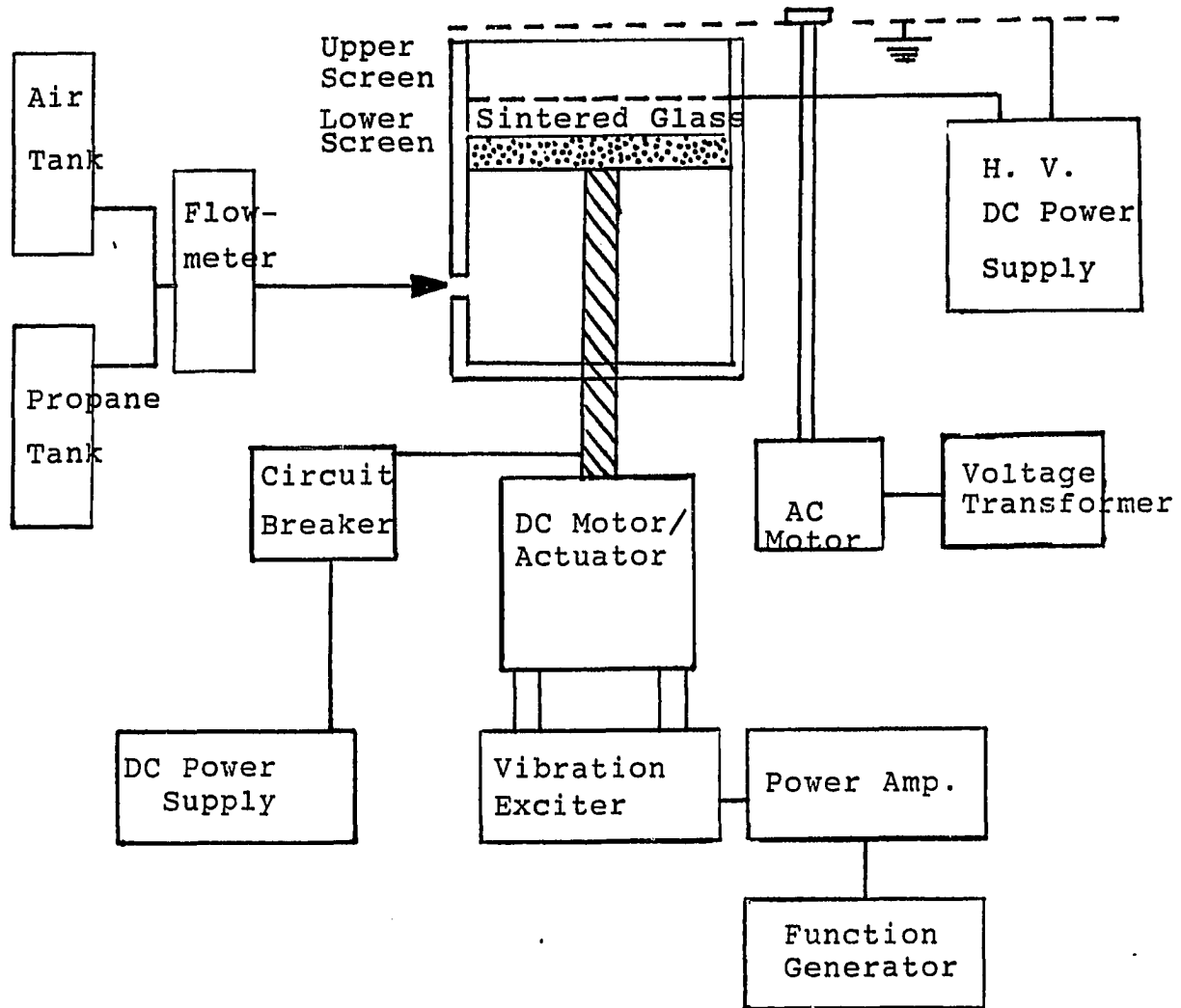


Figure 2.3: Second modified experimental setup

The piston has a diameter of 77.5 mm and an O-ring seal keeps the particles from falling down the piston. A 60 mm diameter sintered glass is mounted on the top of the piston. The cylinder is made of teflon with vacuum grease is used to lubricate the contact surface between the inside wall of the cylinder and the piston. A connecting bar with a diameter of 16 mm and a hole on the top portion of the connecting bar is used to distribute a uniform air flow to the sintered glass.

A vibration exciter (Bruel & Kjaer type 4808) along with a power amplifier (Bruel & Kjaer type 2712) and a function generator (B + K Precision model 3020) are used to break up a cohesive particles such as coal particles.

A 2.4 by 2.4 mm^2 wire screen is used for the the upper and lower screens as shown at Figure 2.5. The piston speed is calibrated from the output voltage of DC motor to calculate the mass flow rate of the particles. Their calibration is plotted in Figure 2.6.

2.7 Results and Discussions

It was possible to get a cone-shaped flame above the upper electrode for all sizes of the spherical aluminum powder. Also, it was possible to get a flat flame stabilized above the upper screen, but it was inconsistent. The main reason for this problem is that the particle transport through the lower electrode is not steady and the flame behavior is strongly affected by a small fluctuation in the particle transport pattern.

A medium volatile bituminous coal (Penn. Seam) was used first without the electric field. A stabilized flat flame was observed which was sustained for few seconds. Otherwise, a cone-shaped flame could be obtained which sustained for more than 20

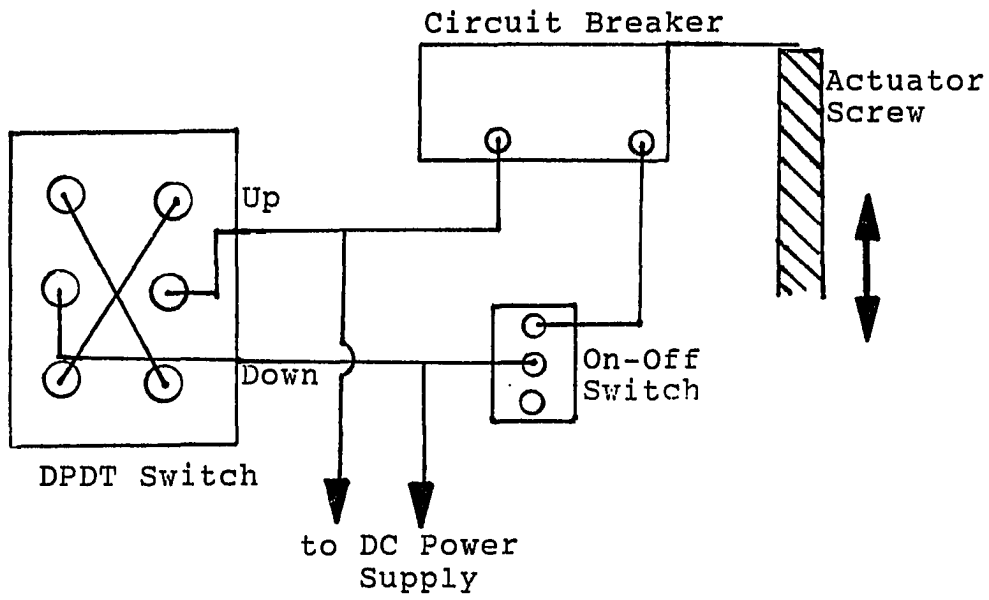


Figure 2.4: DPDT switch and circuit breaker

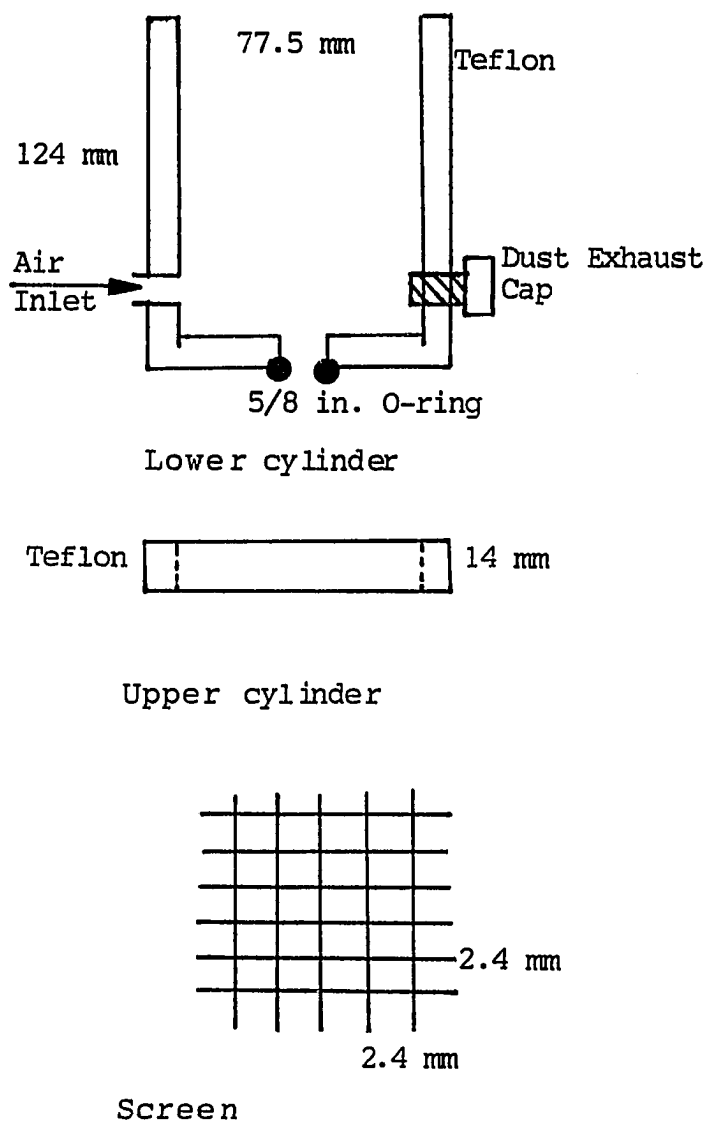


Figure 2.5: Cylinders and screens

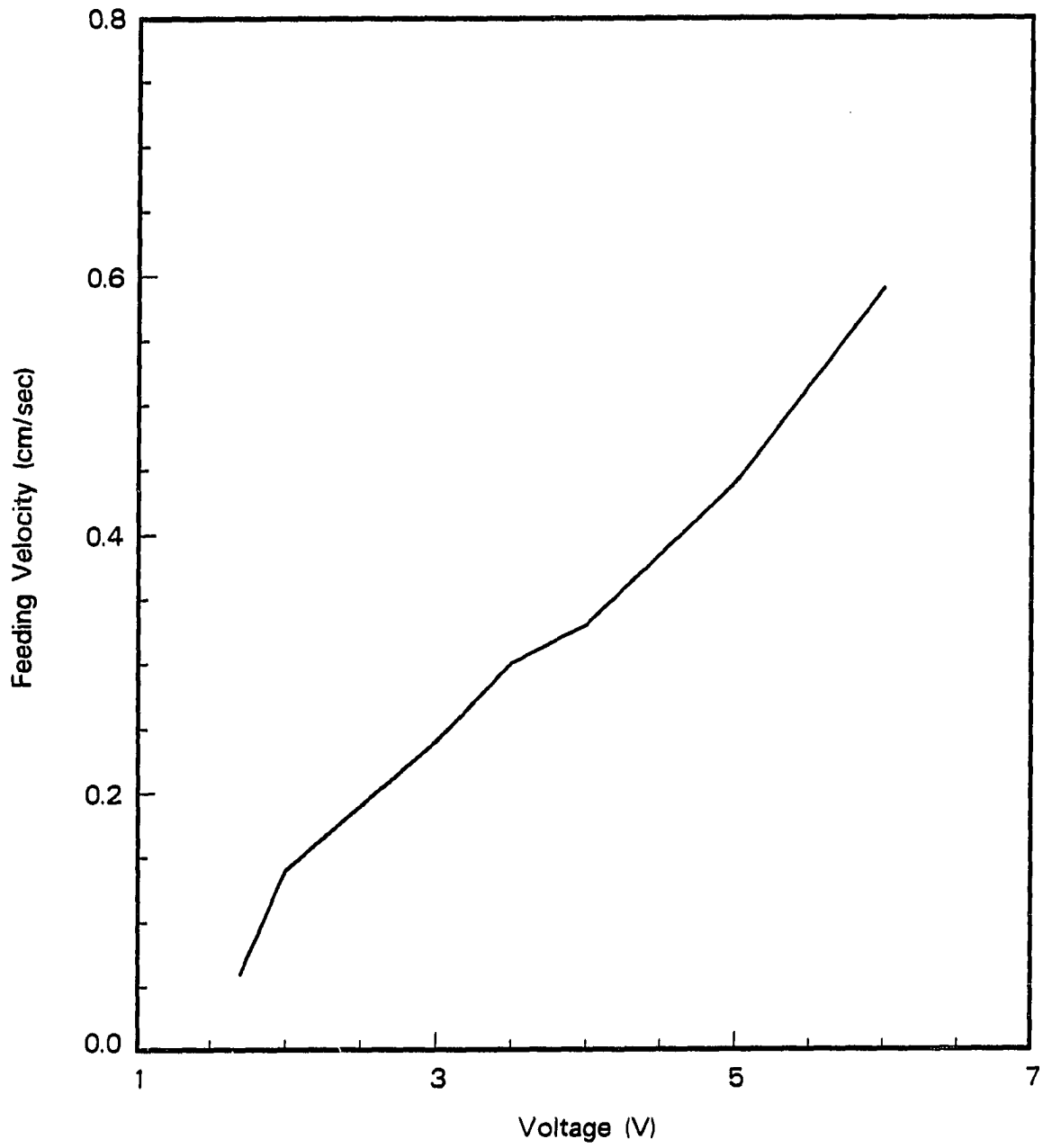


Figure 2.6: Voltage versus piston moving speed

seconds. With the electric field ranges 1.5 - 3.0 kV/cm, the flame was lifted few millimeters above the upper screen. For higher electric fields, the flame was either impossible to be generated or was blown away.

The above results show that the ability to control the pneumatic transport of particles precisely is essential in getting a stabilized flat flame so that a burning velocity can be obtained. A refinement on the particle delivery system are also desired.

For the Penn Seam coal, the burning velocity was measured when a flat flame could be observed. The flame velocity is determined by dividing the flow rate by the burner mouth area. Figure 2.7 shows the effect of particle concentration on burning velocity for this coal.

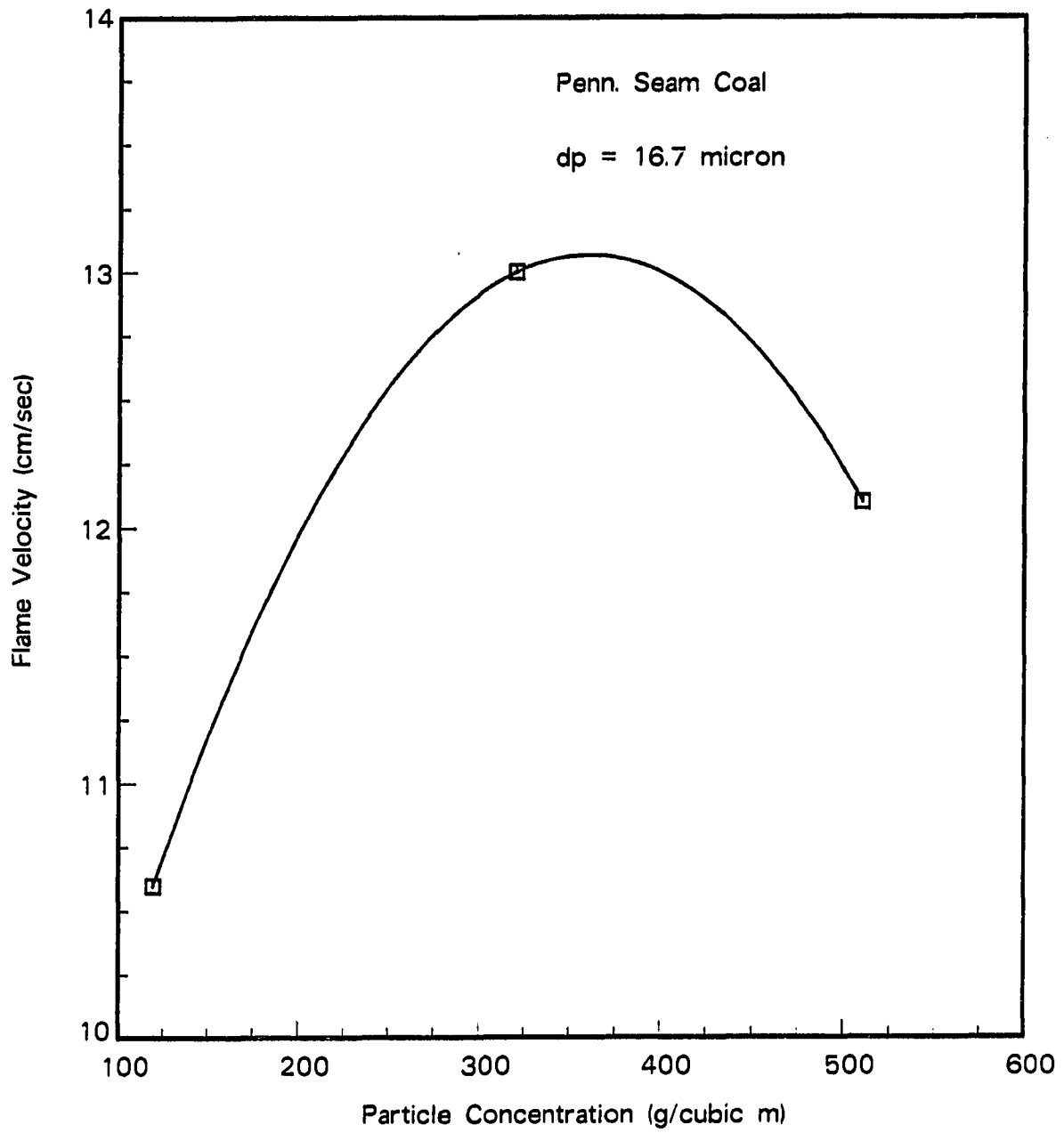


Figure 2.7: Burning velocity of Penn. Seam coal

3 EXPERIMENTAL DESIGN AND CALIBRATION

An important consideration in the present study was the production of a particulate cloud of uniform number density for use in investigating electrical discharge phenomena. Various pneumatic methods have been used to achieve particle dispersion for spark testing (see Hartman et al. [1954]). However, such methods can produce dispersion of particles exhibiting locally nonuniform and unsteady behavior which can often lead to difficulties in controlling and measuring the particle concentration. The electrostatic method of generating a particulate suspension, which was developed by Colver [1976], has been shown to generate a very uniform and steady particulate clouds for which the particle number density could be measured accurately and also be simply controlled in time. A means of initiating and localizing a spark was perfected using an adjustable needle electrode.

3.1 Experimental Design

3.1.1 Electrostatic suspension (closed system)

In the same manner as the particle oscillates between two parallel charged electrodes, multiple particles may also be suspended. Calculations showed that a single spherical aluminum particle of 25 μm diameter moves at the speed faster than 1.4

m/sec and possesses a charge of 2.71×10^{-14} C if it is exposed to a field of 20 KV/cm electric field strength. The following equation summarizes the motion of a single particle. The particle velocity oscillating between the plate electrodes is;

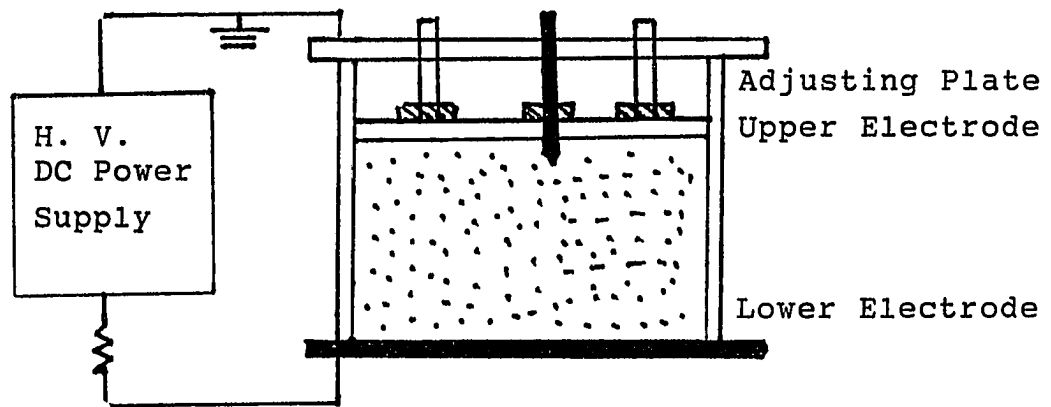
$$V = \left[\frac{1}{8}(1 + e) \right]^{1/2} \left(\left[\frac{QE}{m} \frac{1}{1 - e^2} + \frac{g}{1 + e^2} \right]^{1/2} + \left[\frac{QE}{m} \frac{1}{1 - e^2} - \frac{g}{1 + e^2} \right]^{1/2} \right) \quad (3.1)$$

where e is the coefficient of restitution and g is the gravitational acceleration. And the charge per particle is;

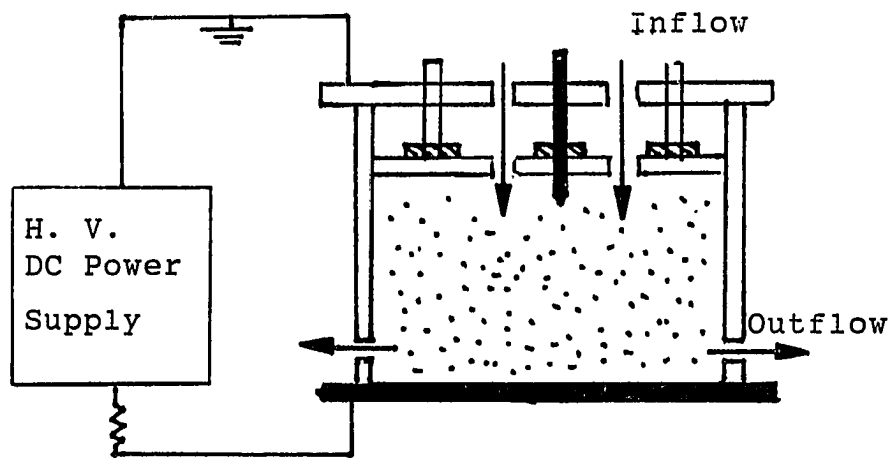
$$Q = 4\pi\epsilon a^2 E(1.64) \quad (3.2)$$

In order to maintain a uniform suspension, a closed system was developed using an insulating glass cylinder between the electrodes to confine the particulate cloud which otherwise diffuse away as a result of particle-particle and particle-electrode collisions. The system is sketched in Figure 3.1. Following preliminary tests on the above system, it was found that coal particles sticking at the glass cylinder blocked the path of the laser beam making it impossible to calculate the particle concentration. Thus, a 1.5 mm diameter hole was placed 5mm above the bottom electrode along the center of the test section to let the laser beam pass. This small hole minimized the amount of coal particles escaping through the hole. Also, at the top electrode, four air inlet holes 7 mm in diameter served to aid the suspension of the coal particulate clouds in addition to the vibration exciter. The experimental setup is sketched in Figure 3.1.

The particle concentration is measured either by a weighing method or by light scattering. The particle concentration could be easily controlled by changing the total quantity of particles inside the glass container.



Closed system for Aluminum



Closed system for coal

Figure 3.1: Closed systems for coal and aluminum tests

3.1.2 Needle electrode

First, a high-power pulse laser (YAG : 2 J max.; Ruby : 5 Joules max.) was tested as an ignition source. A laser beam has an advantage of not disturbing the particle motion. However, it proved inapplicable in this research for the following reasons: first, the two lasers were not powerful enough to ignite the particulate clouds; second, the crystal window which was mounted at the center of the upper electrode to let the laser beam pass through became coated with hot burning particles. It became impossible for the laser beam to pass through the window after a few tests. The above difficulties lead to the development of the needle electrode system for a spark ignition. A previous moving needle electrode system (Kim [1986]) has an advantage of minimizing the electric field disturbance in the suspension system but proved impractical because the alignment of the needle electrode at the center of the system was very difficult because of the vibration of the test section and the restriction of adjusting the needle penetration depth whenever the plate separation distance changes. The needle electrode is mounted on the upper electrode and screwed onto it so that the needle penetration depth can be adjusted according to the electrode separation distance. Needle electrode shape and its dimensions are sketched in Figure 3.2.

3.1.3 Glass container

First a small cylinder is used which is 79.2 mm in diameter. To resist the pressure due to the ignition, a 5 mm thick heavy glass is used. However, the small cylinder volume of the cylinder caused some difficulties in varying the particle concentrations,

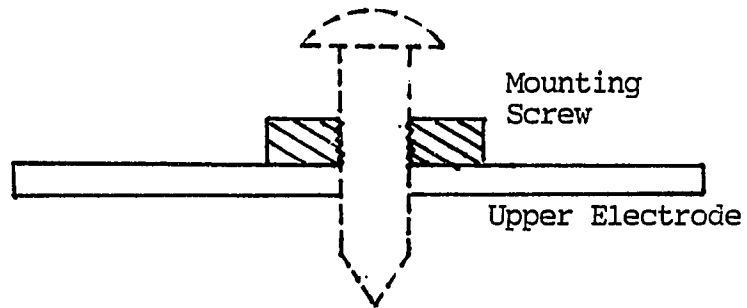
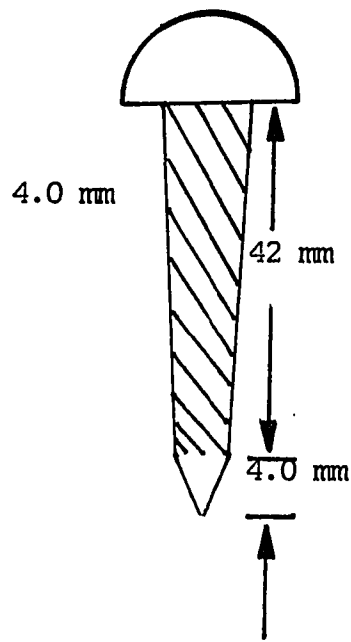


Figure 3.2: Needle electrode and adjusting system

since a small change in the weight of the powder leads to a large change in the particle concentration. Also, a small cylinder diameter causes more wall effects and increases radiation losses.

The above disadvantages led to the design of a bigger cylinder which has a diameter of 142.4 mm. There, however, are practical limitations on the size of the cylinder. When the spark is generated at the center of the electrode, the electric field collapse causing the suspended particles to fall down freely to the lower electrode. It follows that the diameter of the cylinder should be small enough so that the flame can propagate from the needle electrode to the cylinder wall (i.e., a travel distance of radius of the cylinder) before the particles can fall down to the lower electrode.

Ideally, an upper electrode would be divided into several sections with each one having its own power supply, this would exclude design limitation on the length. But, physically it is impossible to make such an electrode because of the corona discharges that would occur between adjacent sections of the electrode.

To determine the maximum cylinder size, the following calculations are conducted. Consider the free falling particle as shown in Figure 3.3. From Newton's second law,

$$(m_p - m_b)g - 3\pi\mu d_p v = m_p \frac{dv}{dt} \quad (3.3)$$

where, m_p is the mass of the particle, m_b is the mass of the air taken by the particle, μ is the viscosity, d_p is the diameter of the particle, and v is the velocity of the particle.

And,

$$m_p = \rho_p \frac{\pi}{6} d_p^3 \quad (3.4)$$

$$m_b = \rho_f \frac{\pi}{6} d_p^3 \quad (3.5)$$

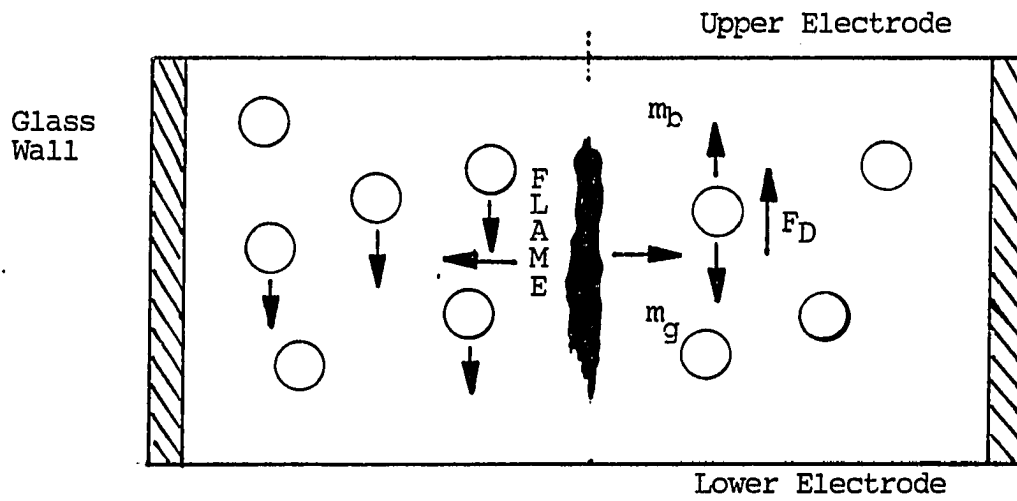


Figure 3.3: Schematics of the particle fall in a flame propagation system

where, ρ_p is a density of particle, and ρ_f is a density of a fluid. The governing equation takes the following form.

$$\frac{dv}{dt} + \frac{18\mu}{\rho_p d_p^2} v = \left(1 - \frac{\rho_f}{\rho_p}\right)g \quad (3.6)$$

Initially the particle velocity is zero. Solving the above equation with the initial condition gives;

$$v = g\tau\left(1 - \frac{\rho_f}{\rho_p}\right)(1 - e^{-t/\tau}) \quad (3.7)$$

where, τ is a time constant, equal to

$$\tau = \frac{\rho_p d_p^2}{18\mu} \quad (3.8)$$

Integrating the expression for the velocity one more time, with an initial condition of $x = 0$ at $t = 0$, gives an expression for a falling distance;

$$x = g\tau\left[t - \tau\left(1 - \frac{\rho_f}{\rho_p}\right)(1 - e^{-t/\tau})\right] \quad (3.9)$$

Now, the time for the propagation of the flame from the center to the cylinder wall, t_p , is;

$$t_p = \frac{D_c/2}{v} \quad (3.10)$$

where, D_c is the diameter of the cylinder.

The time for the fall of a particle to the lower plate, t_f , can be obtained by replacing x with the plate separation distance H in equation 3.7.

$$H = g\tau\left[t_f - \tau\left(1 - \frac{\rho_f}{\rho_p}\right)(1 - e^{-t_f/\tau})\right] \quad (3.11)$$

The criterion is that the flame should propagate to the end of the test section before the particles fall down to the lower electrode. That is,

$$t_f > t_p \quad (3.12)$$

Now, let's evaluate a maximum cylinder diameter satisfying the above condition for the case of aluminum powder. The parameters for this calculation are obtained for the case of aluminum powder of 20 μm in diameter in a plate separation distance of 10 mm. The burning velocity v is chosen from the measurements in this research to be around 50 cm/sec.

Now, t_p is,

$$t_p = \frac{D_c}{sv} = 1.25 D_c \quad (3.13)$$

The time constant τ is calculated to be equal to 0.00325 sec^{-1} . Calculating t_f from equation 3.9 by trial and error gives

$$t_f = 0.3167 \text{ sec.} \quad (3.14)$$

Applying these values to the criterion for flame propagation, the maximum permissible cylinder size is obtained.

$$D_c < 25.34 \text{ cm.} \quad (3.15)$$

So the glass cylinder diameter should be smaller than 25.34 cm. In the present studies a glass cylinder of 14.24 cm in diameter was chosen taking into account the fact that gap separation distance can be smaller than 10 mm.

3.1.4 Upper and adjusting plate electrode

The upper electrode was 14.20 mm in diameter and fabricated from 1/8 inch thick copper plate. The three flat head bolts, 1/4 inch in diameter and 3 1/2 inches long each, were soldered on the top of the copper plate in a triangle to position the plate electrode parallel to the lower electrode. A teflon plate 1/4 inch in thickness

was fit on the top of the upper electrode and an O-ring was inserted to seal the test section. The teflon plate was screwed down tightly on the copper plate with 3 nuts. An adjusting plate electrode was made of plexiglass having a groove at the outer edge of the plate so that it was sit tightly on the top of the glass container. The upper plate was connected to the adjusting plate with the bolts. The upper plate electrode serves two purposes. First, it supports the upper plate so that it can be kept in position. Second, it allowed for the upper and lower electrode separation distance to be adjusted. A schematic of upper electrode and adjusting plate is shown in Figure 3.4.

3.2 Overall Experimental Setup

The schematic of the overall experimental setup is shown in Figure 3.5. Figure 3.6 shows the picture of test section and overall experimental setup. At the halfway point from the center of the lower plate, four copper-constantan thermocouples are inserted in parallel and connected to an X-Y plotter and an oscilloscope through the reference junction. As the flame propagates, the temperature rise is recorded. A flame propagated more than half the radius of the test section is accepted as a propagated flame. A vibration exciter (Bruel & Kjaer Type 4808) along with power amplifier (Bruel & Kjaer Type 2712) and function generator (B+K Precision Model 3020) are used to break up the cohesive particles such as coal. By trial, it was found that the best results are obtained at the frequency of 750 Hz. It is believed that this frequency is the natural frequency of this system or multiple of it, because at this frequency a good suspension of the particle clouds are observed with a noisy sound.

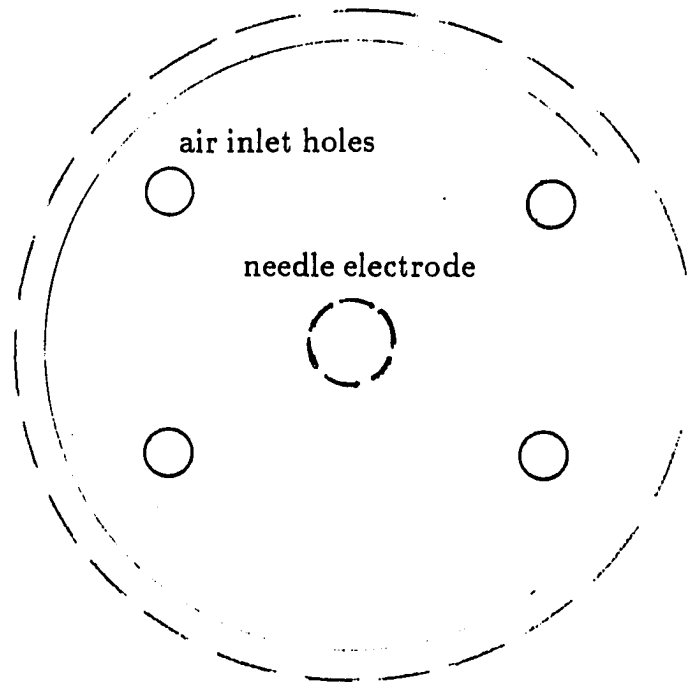
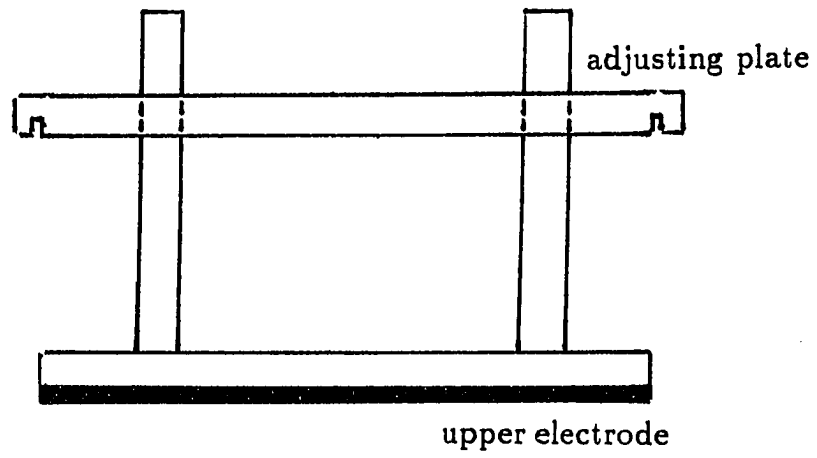


Figure 3.4: Schematics of upper and adjusting plate

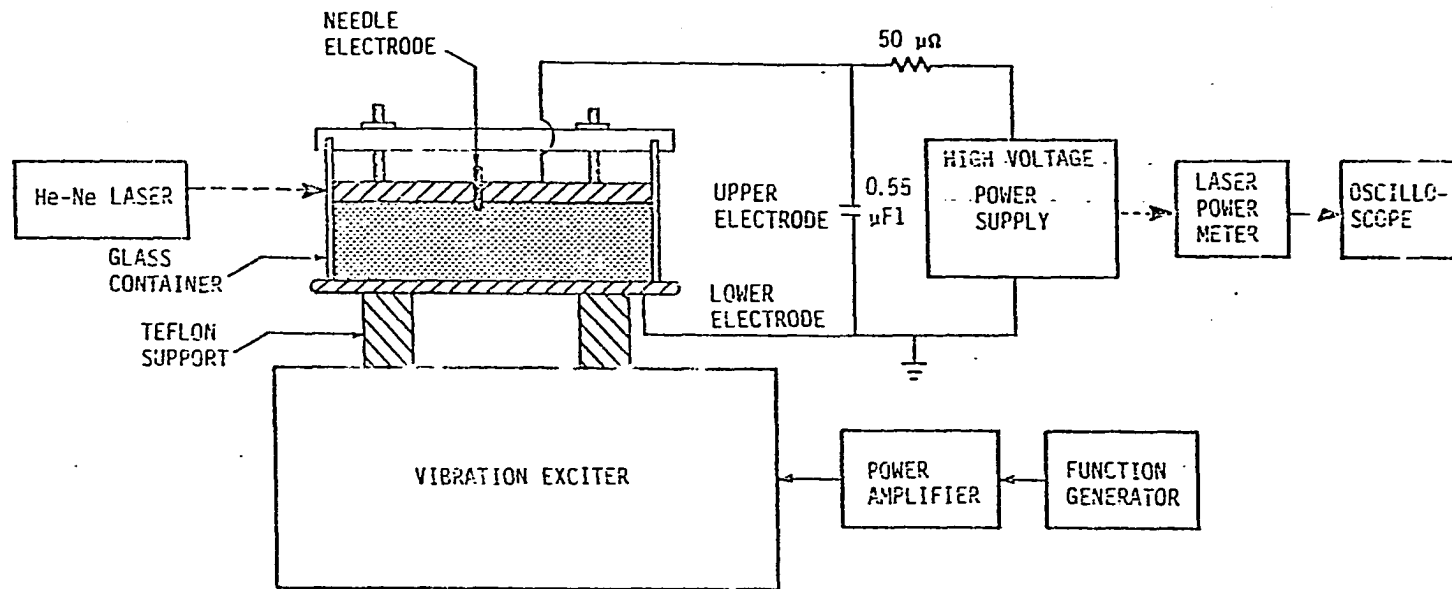


Figure 3.5: Schematics of overall experimental setup

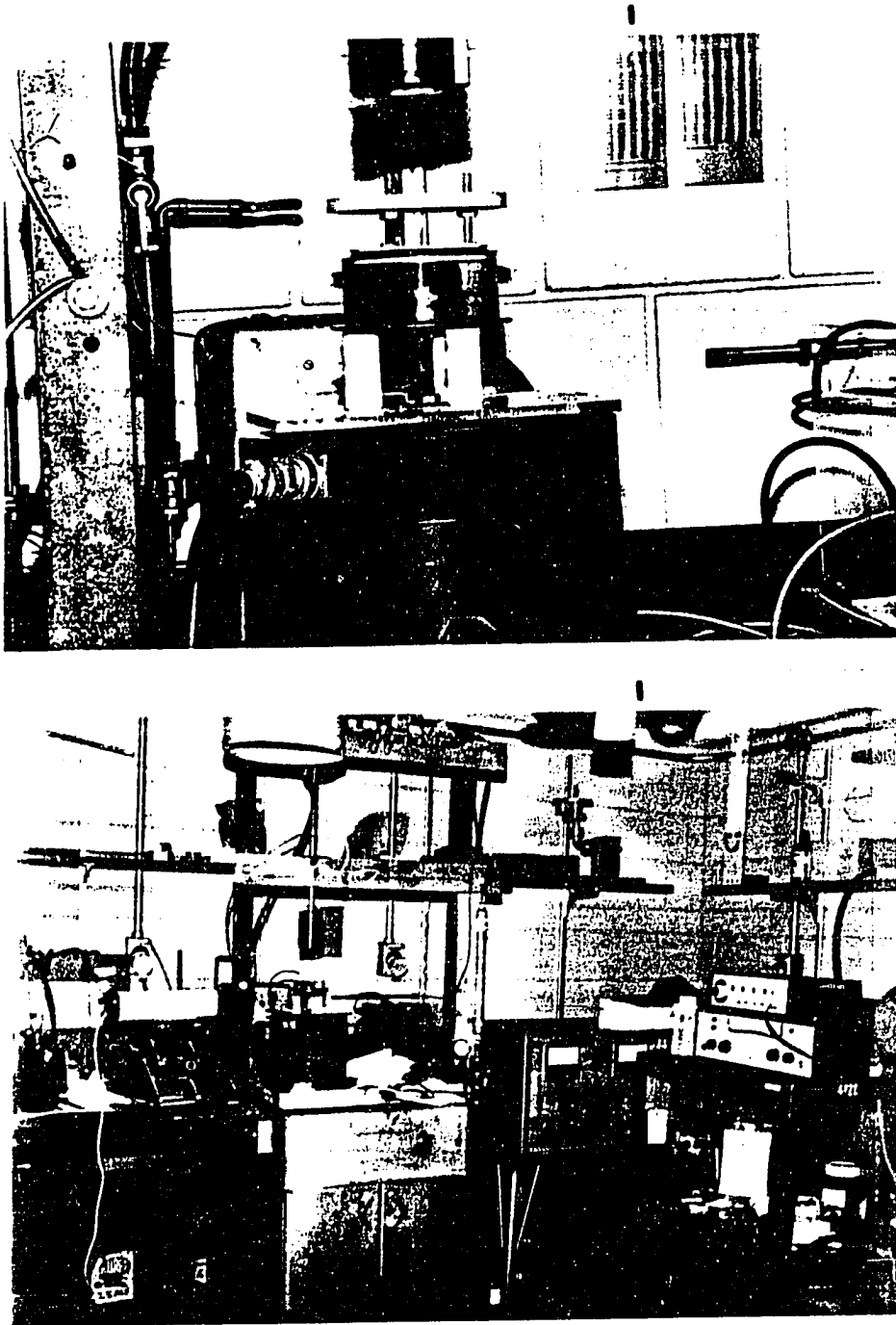


Figure 3.6: Photograph of overall experimental setup

The high voltage side of a high voltage DC power supply (Hipotronics Model 850B) is connected to the upper electrode through a large series resistor of $50\text{ M}\Omega$. For this power supply, three DC voltage ranges are available, 0-10/25/50 kV, with a maximum allowable current of 5 mA at less than 2 % rms ripple. The high voltage is measured with the electrostatic voltmeter Model ESH manufactured by Electrical Instrument Service. This voltmeter has a maximum error of less than 1 %, and multirange 0-5/15/30/50 kV measurement can be obtained.

A He-Ne laser (Metrologic Model ML801-K) was used not only to monitor the suspension behavior of particulate clouds but also to measure the particle concentration. The laser power meter (Metrologic Model 45-540) has a photo-diode sensor and it is used to measure the laser beam intensity for the particle concentration calculation. The laser power meter has four ranges, 0-20 mw/2 mw/200 μ w/20 μ w. The photo-diode of the laser meter is aligned with a pin hole so that the scattered and fringe light is not be detected by this photo-diode. This laser power meter is also connected to a storage oscilloscope (Tektronix 434) to monitor the intensity of the beam continuously. This oscilloscope has amplitude scales from 5 v to 1 mv per division and is calibrated before the measurement. This oscilloscope is especially useful when the fluctuations of the beam is high so the read-out of the laser power meter is difficult to monitor.

Four external high voltage capacitors are used to store the charge and are connected in parallel with the main electrodes. The capacitance values are given in Table 3.1. The plate capacitor consists of four plates which could be plugged in so that the total capacitance can be varied from 1,400 pF to 19,300 pF. For this research, all

Table 3.1: Capacitances of the external capacitors

Capacitor	Capacitance (pF)
Plate 1	1,400
Plate 2	2,500
Plate 3	5,400
Plate 4	10,000
Cylinder 1	5,000
Cylinder 2	10,000
Cylinder 3	20,000
Total	54,300

four plates are used. Three other cylindrical capacitors was commercially made for high voltage application with a maximum allowable voltage of 30 KV DC (Plastic Capacitors, Inc.). The total capacitance of these external capacitors is 54,300 pF.

Three flow meters (Gilmont A3114, B5463, D2321) was calibrated and used to measure the flow rate of gases. The Gilmont A3114 flow meter has a range of 0-260 mL/min and was used for the flow rate measurement of methane gas. The Gilmont B5463 flow meter has a range of 0-1900 mL/min and was used for the flow rate measurement of air. The Gilmont D2321 flow meter has a range of 0-36,000 mL/min and was used to measure the flow rate of air going into the upper plate of the test section which was used to stir up the coal particles. The flow rate of the air going into the upper plate was kept as small as possible so that the coal particles could barely escape through the holes at the wall of the glass cylinder. The calibration chart for the flow meters are shown at Figures 3.7, 3.8, and 3.9, respectively.

To measure the burning velocity of powders a high speed camera (16 mm, Red Lake Model Hycam) and a video camera (Panasonic WV3170) were used. The high speed camera was set at 1/1,000 shutter speed. Eastman Ektachrom Video News Film 7240 was used. The film is run at the speed of 400 frames/second, which is about 17 times faster than a video camera. The 16 mm films were played back and the starting and finishing frames were obtained so that the burning velocity of the flame front could be obtained by dividing the flame travelling distance by time it took to travel the distance. Also slide film were made using 16 mm film to measure the position of the flame front at each time step. Also a video camera was used to take pictures of flame propagation of aluminum and coal powder. The video camera has a

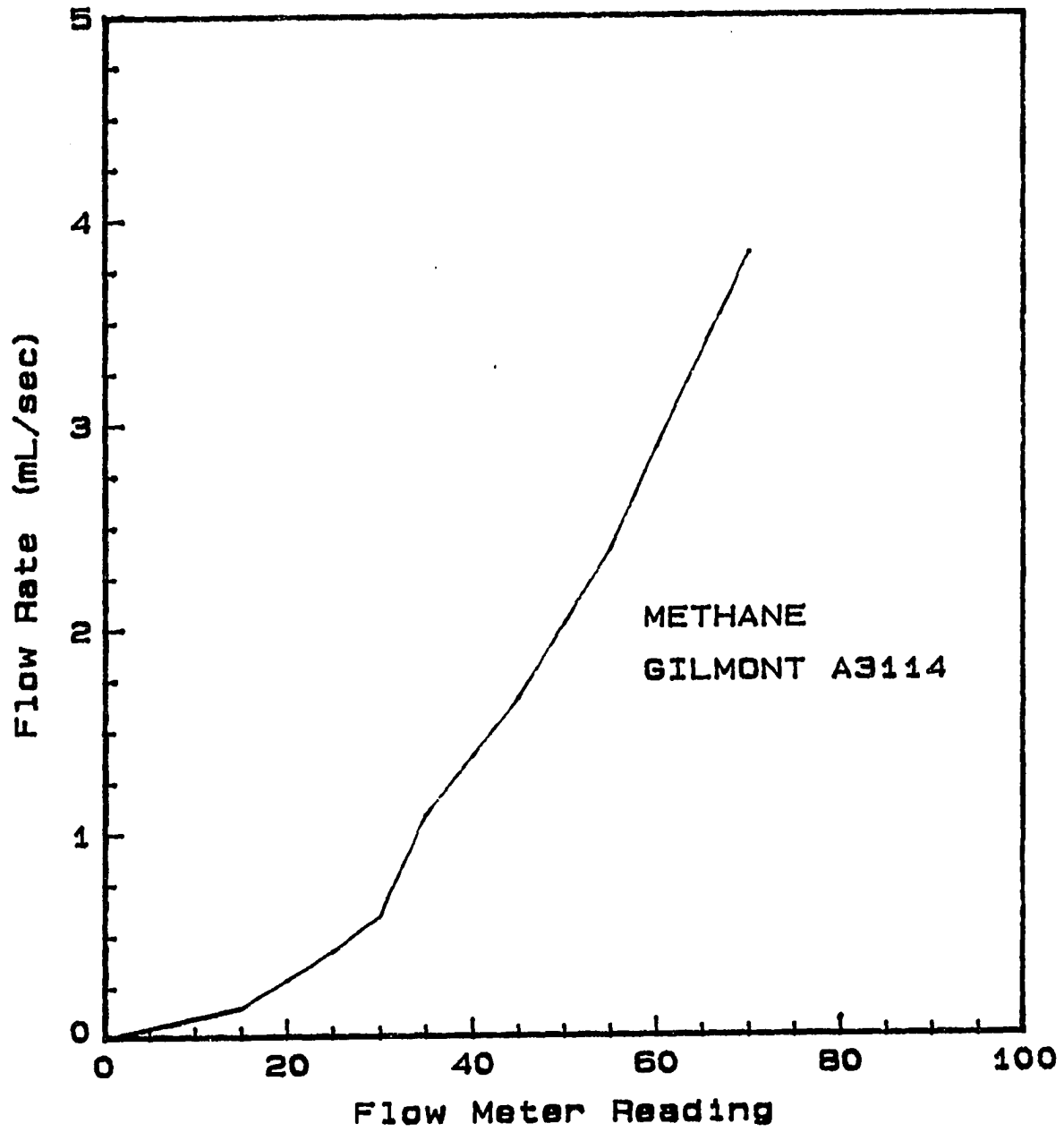


Figure 3.7: Flowmeter calibration, Gilmont A3114

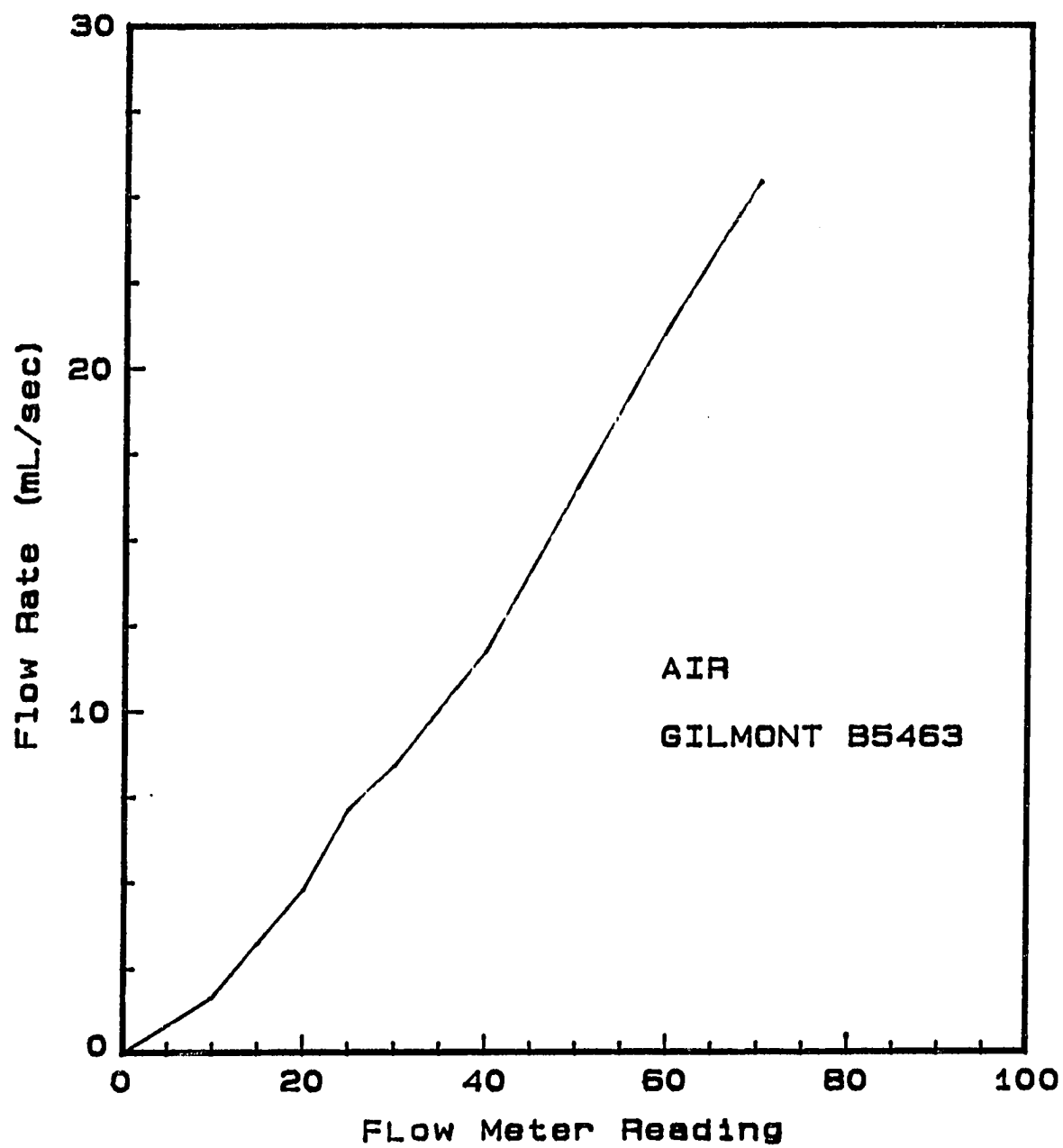


Figure 3.8: Flowmeter calibration, Gilmont B5463

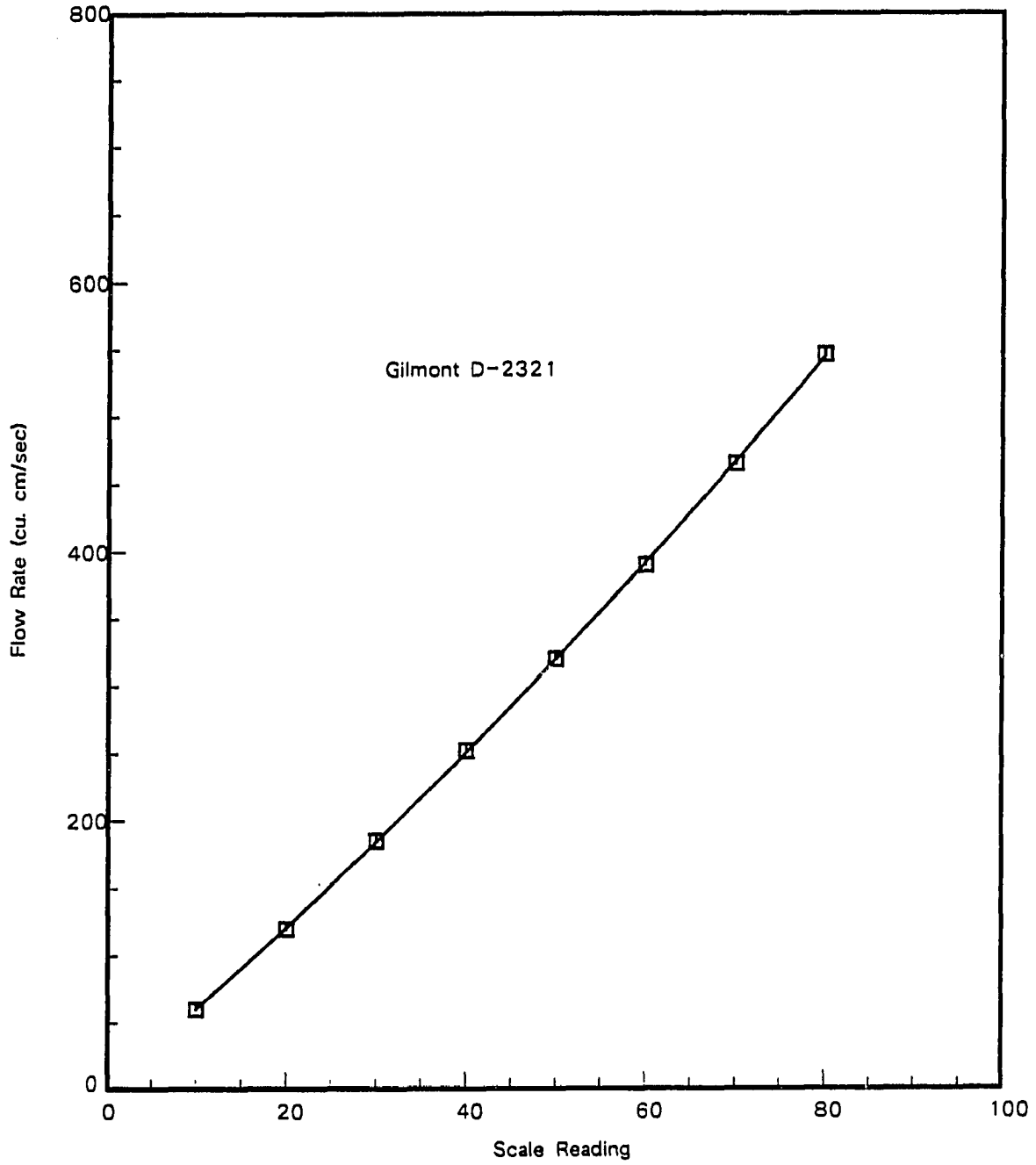


Figure 3.9: Flowmeter calibration, Gilmont D2321

built-in stop watch making it easier to measure the travelled time. The IRIS control of the video camera was nearly closed to reduce the intense amount of light liberated by the flame. Without using the IRIS control, the exposed picture were almost white making it impossible to find the flame front.

3.3 Particle Preparation

For this research, two type of aluminum powders and five types of coal powders have been tested. For aluminum, spherical and irregular atomized aluminum powder were used. Both powders was sifted to a sieve size ranges in a sonic sifter (ATM model L3P). Each range particles are tested for size analysis through a particle size analyzer (HIAC/ROYCO Model 4300) and a mean particle sizes were obtained for each of the particle ranges. The results are listed in Table 3.2. The result shows that the particles sieved through the sonic sifter are very accurate and the mean diameter obtained from the particle size analyzer is close to the arithmetic mean of the sieve ranges. The scanning electron microscopic pictures, Figure 3.10, shows the difference in shape between the spherical aluminum and the irregular aluminum. The SEM picture reveals the fact that the spherical aluminum particles are not exactly spherical in shape, but the irregular aluminum particles are very irregular in shape as expected.

The five different types of coal particles selected for test had a volatile contents from 16.9 % up to 44.4 %. The proximate analysis of each type of coal powders was carried out by Coal Research Associates, Star City, West Virginia, and the results are listed in Table 3.3. Also, an ultimate analysis is performed (Penn-Rillton Company)

Table 3.2: Mean diameter of aluminum particles

Sieve Ranges	Mean Diameter (μm)
10-15	11.8
15-20	17.1
20-25	22.0
25-30	26.9
30-38	33.7
38-45	41.3

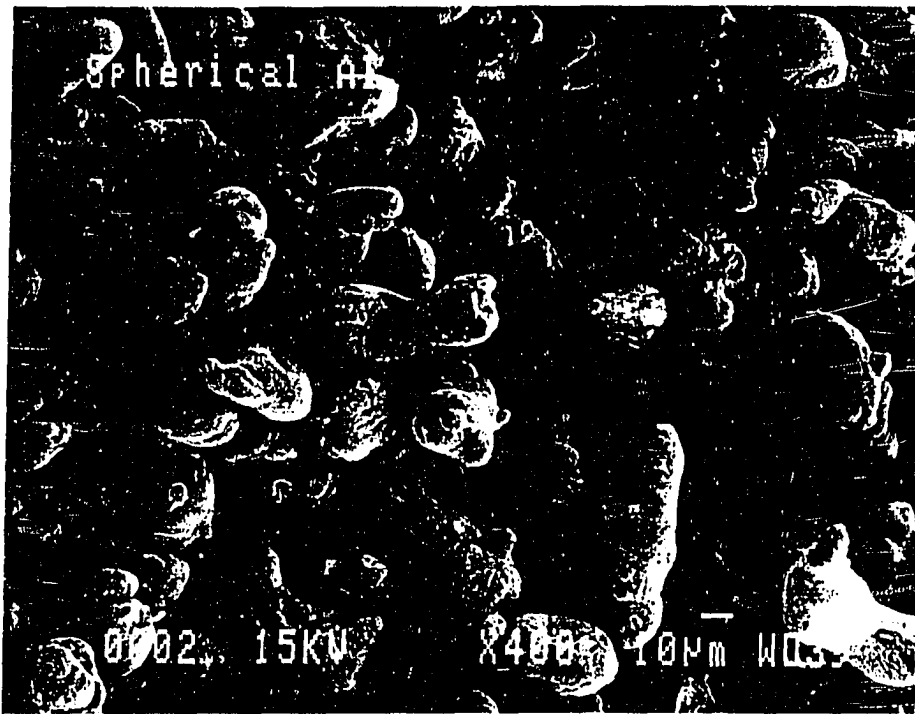


Figure 3.10: SEM pictures of spherical and irregular aluminum particles

for Penn. Seam coal and listed in Table 3.4.

Each of the five types of coal powders were sieved in four sieve ranges, 0-37/44/53/74 μ m. Each size range of coal was tested for the particle size distribution using a scanning electron microscope. The results show that the actual particle sizes are smaller than the sieve ranges. One explanation is that the coal particles are cohesive and agglomerate during sieving. The sieve ranges and mean particle diameter were obtained from SEM analysis and are listed in Table 3.5. The size distribution analysis of each particle sizes are shown Figures 3.11, 3.12, 3.13, and 3.14 for each size ranges of coal powder.

3.4 Calibration

The calibration of the apparatus and variables is a very important procedure in the course of the experiments. In this study, the calibrations are performed on the particle concentration and the external capacitor. Also, the balance is calibrated every time before using it by using the built-in calibrator.

3.4.1 Particle concentration

If the total mass m_p of particles of diameter d_p is suspended uniformly in a container of diameter D and plate separation distance H , then the particle concentration can be calculated by dividing the mass of total particles by the volume of the container,

$$C_m = \frac{4m_p}{\pi D^2 H} \quad (3.16)$$

The weighted method is calibrated by measuring the actually suspended parti-

Table 3.3: Proximate analysis of five types of coal powders

Coal Type	Ash	Fixed Carbon	Volatile
Lower Kitt.	13.9	69.2	16.9
Ill. No. 6	10.2	61.9	27.9
Penn. Seam	7.2	58.4	34.4
Adaville	7.8	50.4	41.8
Hanna	10.5	45.1	44.4

Table 3.4: Ultimate analysis of Penn. Seam coal

Composition	Mass Fraction
H2	5.6
C	78.3
N2	9.2
S	1.5
Ash	5.2

Table 3.5: Mean diameter of coal particles

Sieve Range	Mean Diameter (μm)
0-37	9.1
37-44	16.7
44-53	25.5
53-74	36.6

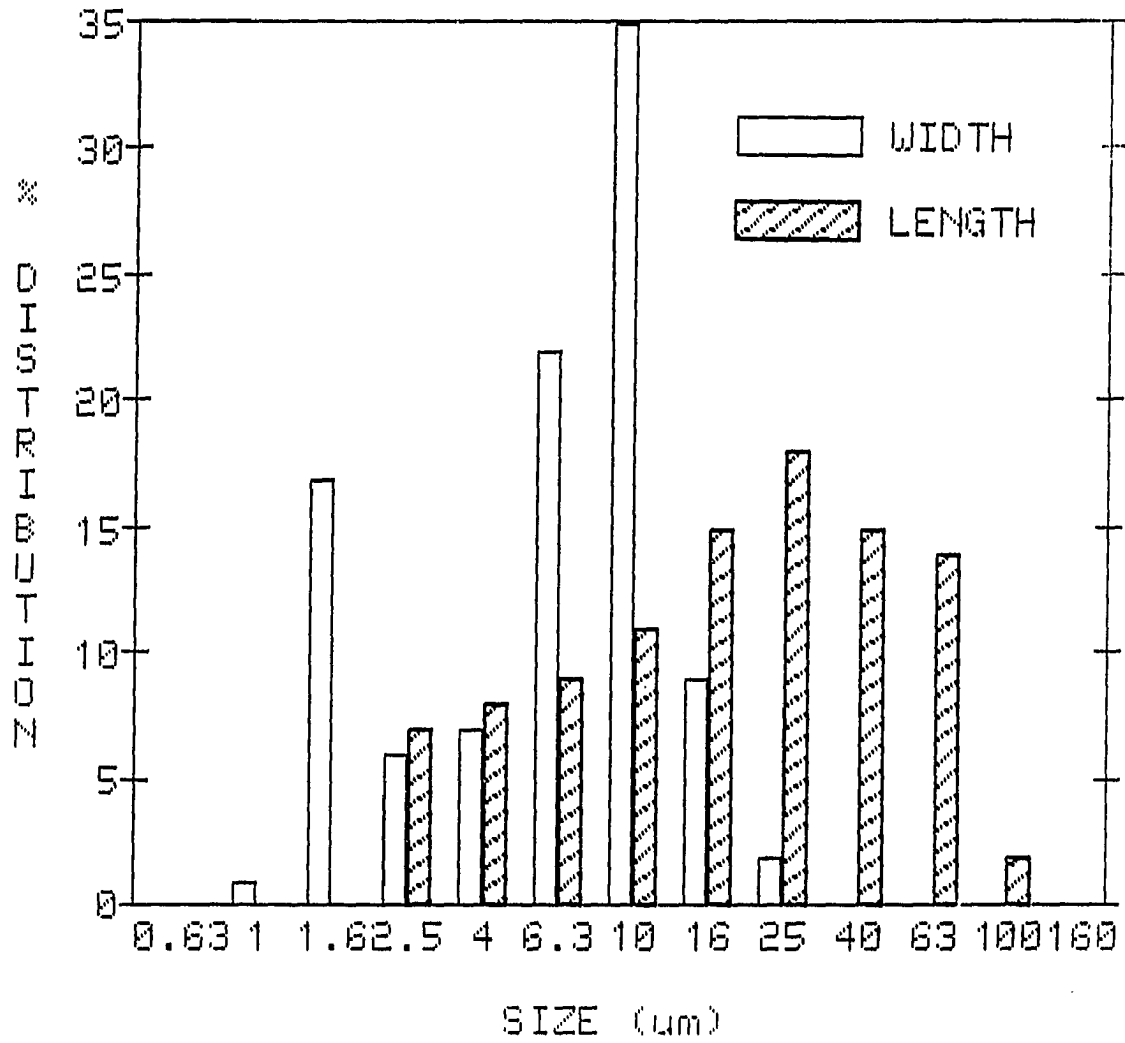


Figure 3.11: Size distribution of 9.1 μm mean diameter coal particles

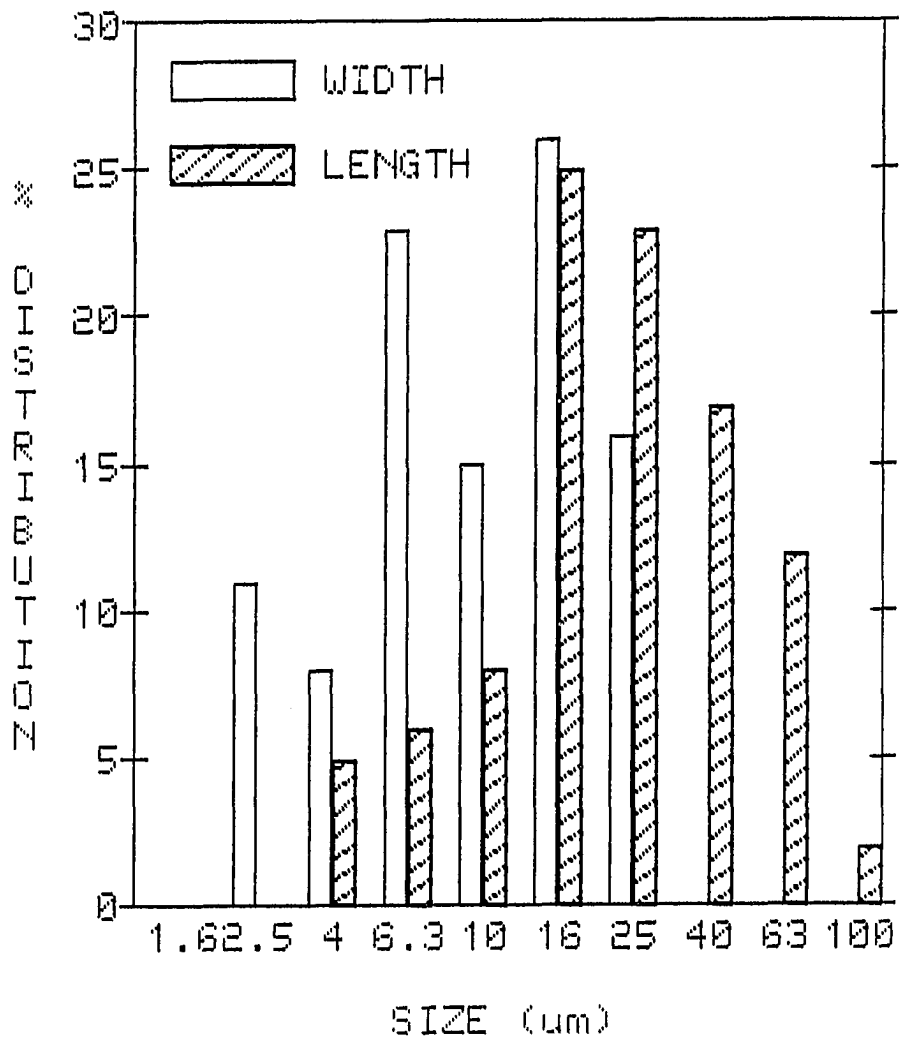


Figure 3.12: Size distribution of 16.7 μm mean diameter coal particles

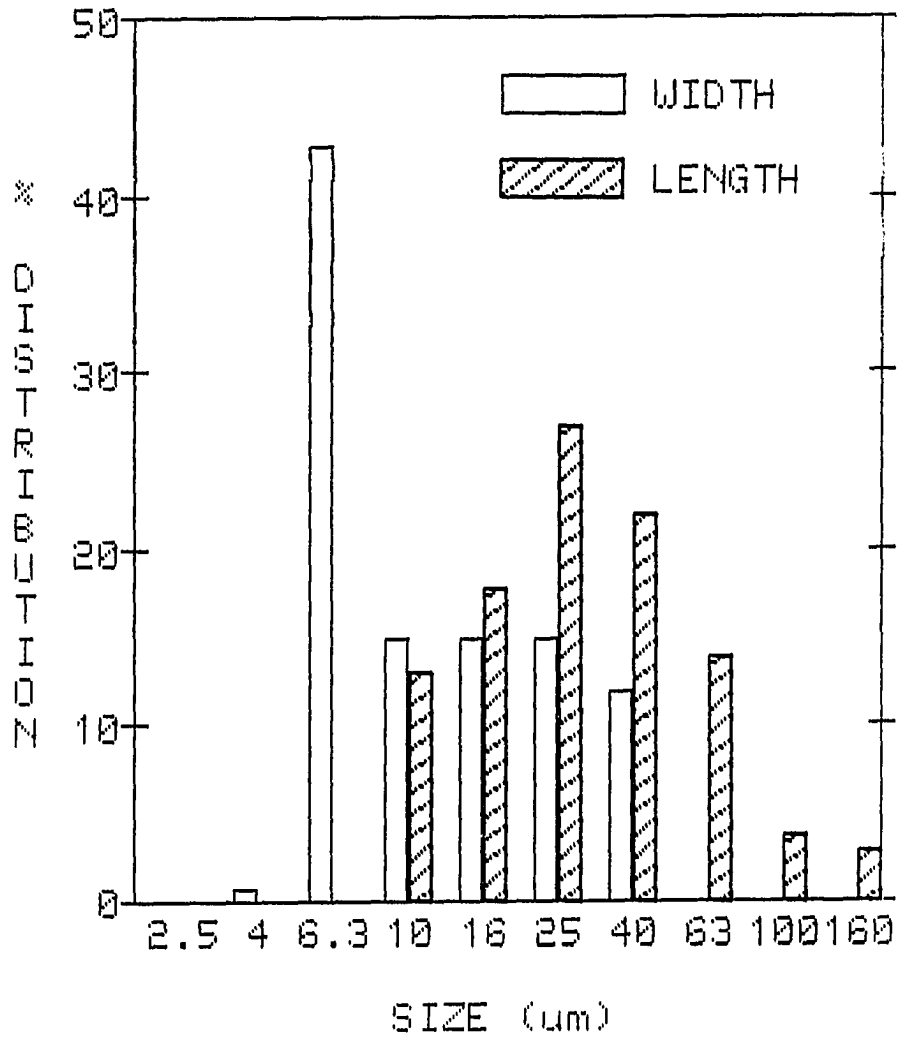


Figure 3.13: Size distribution of 25.5 μm mean diameter coal particles

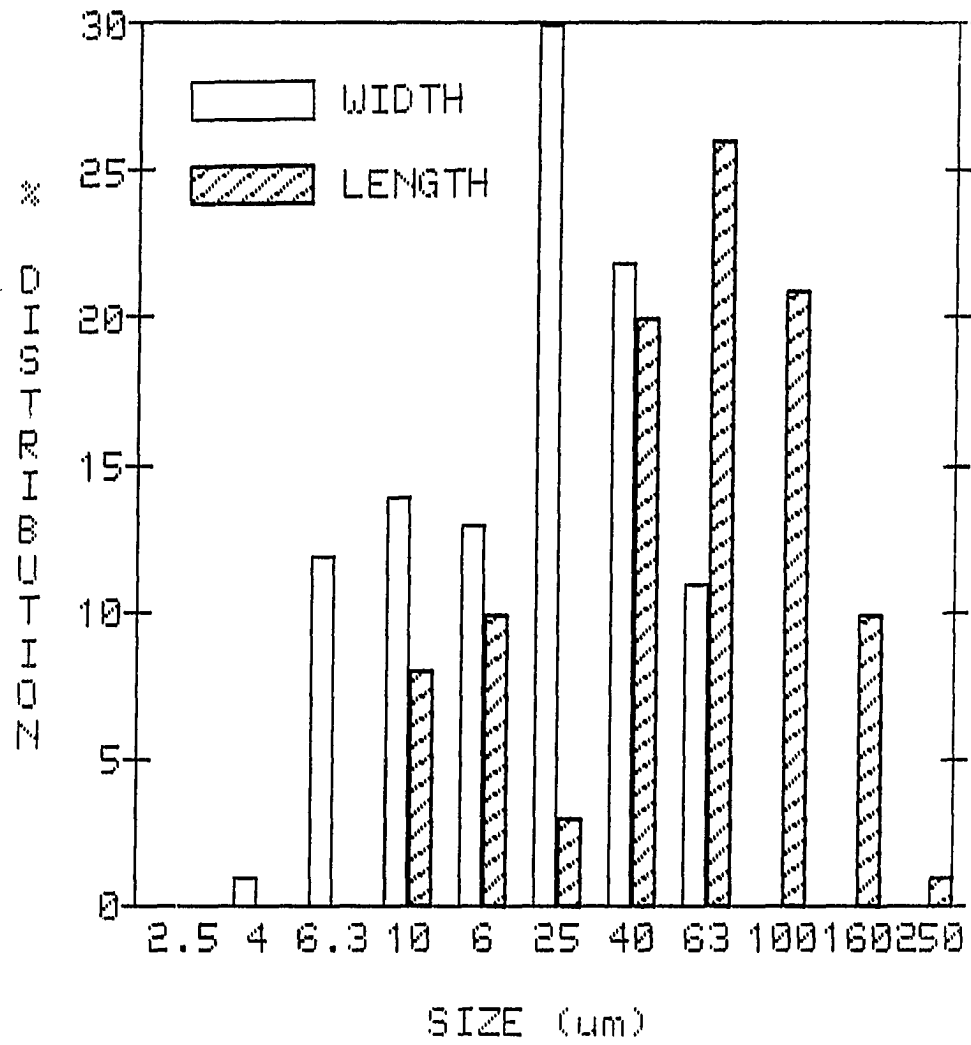


Figure 3.14: Size distribution of 36.6 μm mean diameter coal particles

cles only. That is, the amount of powders sitting in the bottom electrode after the suspension is collected and weighed for the particle concentration calculation. The result is shown in Figure 3.15. It is found that as the particle size decreases, less amount of powder is suspended. About 7.0 % of particles are not suspended for the particles below 20 μm in diameter, and about 4.0 % of particles are not suspended for particles above 20 μm .

The light scattering method is used to measure particle concentration of coal powder. The Beer-Lambert law for the transmission of lights through a homogeneously dispersed mixture of uniform spherical particles is

$$\frac{I}{I_0} = \exp(-eAnl) \quad (3.17)$$

and, in terms of particle concentration;

$$\frac{I}{I_0} = \exp\left(-\frac{3}{2}eC_m l / \rho_p d_p\right) \quad (3.18)$$

where, e is an extinction coefficient, l is a path length, ρ_p is a density of a particle, and d_p is a particle diameter. Thus,

$$C_m = \frac{2\rho_p d_p}{3el} \ln\left(\frac{I_0}{I}\right) \quad (3.19)$$

The extinction coefficient e includes loss of light due to both absorption and scattering. Theoretical values of e were calculated from Mie theory based on the wavelength of light, the complex refractive index of dust, and various size distributions of dusts. In case when the particle diameter is much longer than the wave length of the beam, which is 633 nm for this laser, the extinction coefficient asymptotically approaches a value of 2.0. These calculations are for the ideal, perfectly collimated

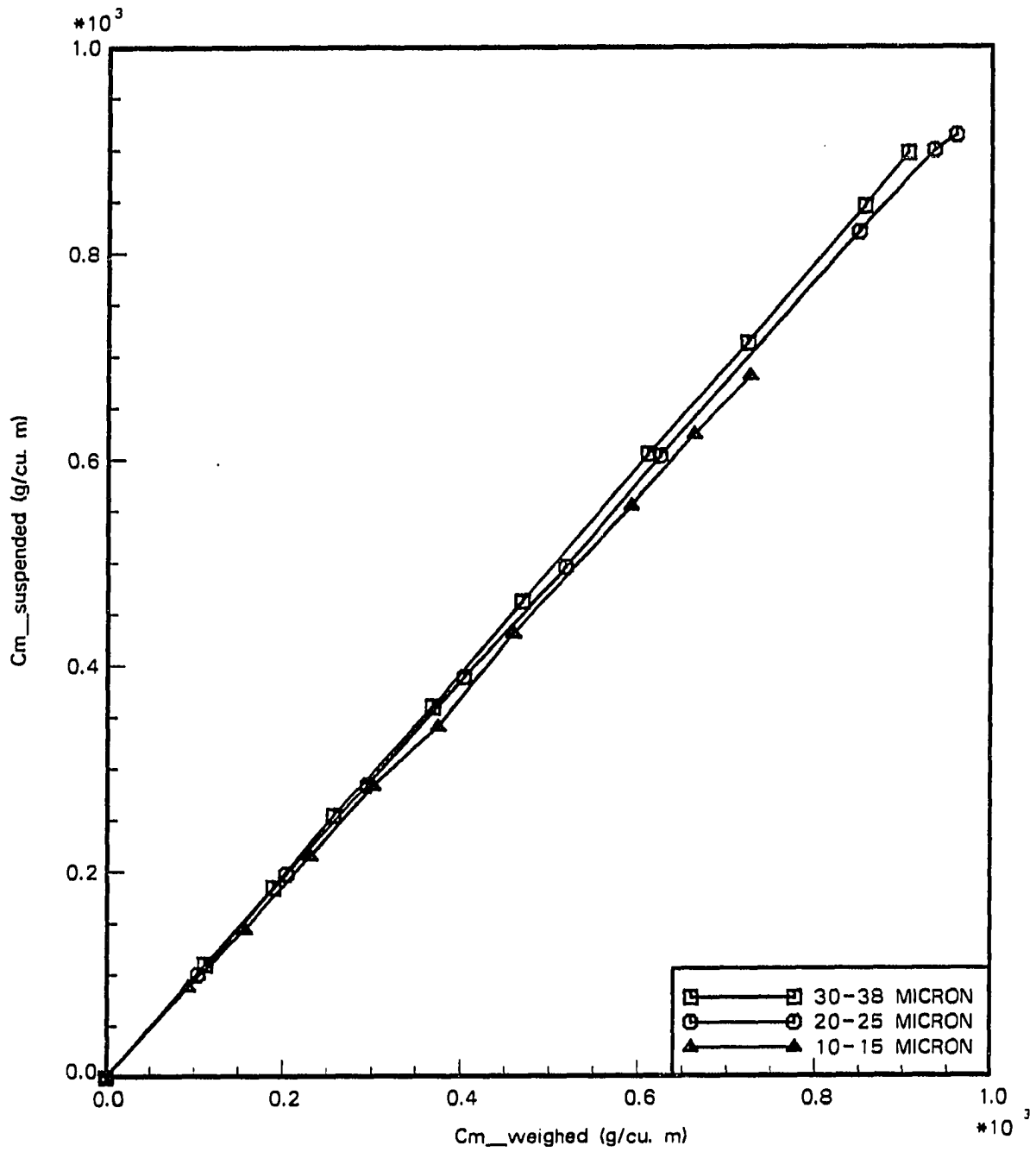


Figure 3.15: Calibration of weighted method of particle calibration

case such as a laser light source and a far field detector which does not collect any of the scattered light, which is exactly the case of this experiment. Figure 3.16 shows the schematics of the setup for the particle concentration measurement, and Figure 3.17 shows the calibrated plot for the aluminum of 12.5 μm in mean diameter. The result shows that the particle concentration versus intensity ratio curve is almost a straight line in a semi-log graph paper. The extinction coefficient can be calculated from the slope of this line.

For coal particles, the weighted method can not be used because not all the coal particles are suspended in a test section, and for a given amount of coal the suspended amount of coal particles depend not only on the electric field strength but also on the frequency and amplitude of acoustic wave of vibration exciter and on the air flow rate from the upper electrode. So the calibration chart for the aluminum in Figure 3.17 is used for particle concentration measurement of coal powders. The output from the laser power meter is connected to the storage oscilloscope for more precise reading.

3.4.2 Capacitor

A current i is defined as a charge passage per unit time. So the capacitor charge Q over time t is,

$$Q = \int_0^t i dt \quad (3.20)$$

For calibration of a capacitor, the integral of the above equation is performed graphically. In previous research (Kim [1986]), the author calibrated the capacitors by using the external circuit as shown in Figure 3.18. With a voltage drop V_R across

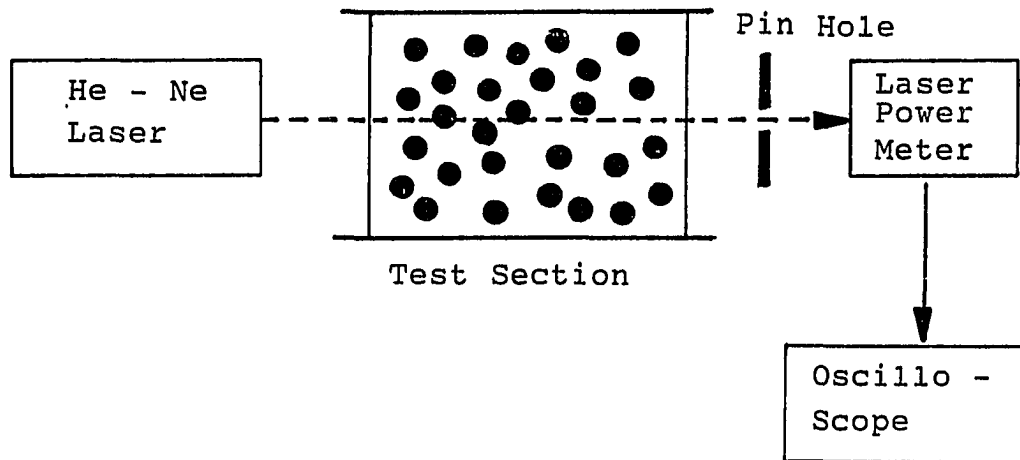


Figure 3.16: Schematics of light scattering method of particle concentration measurement

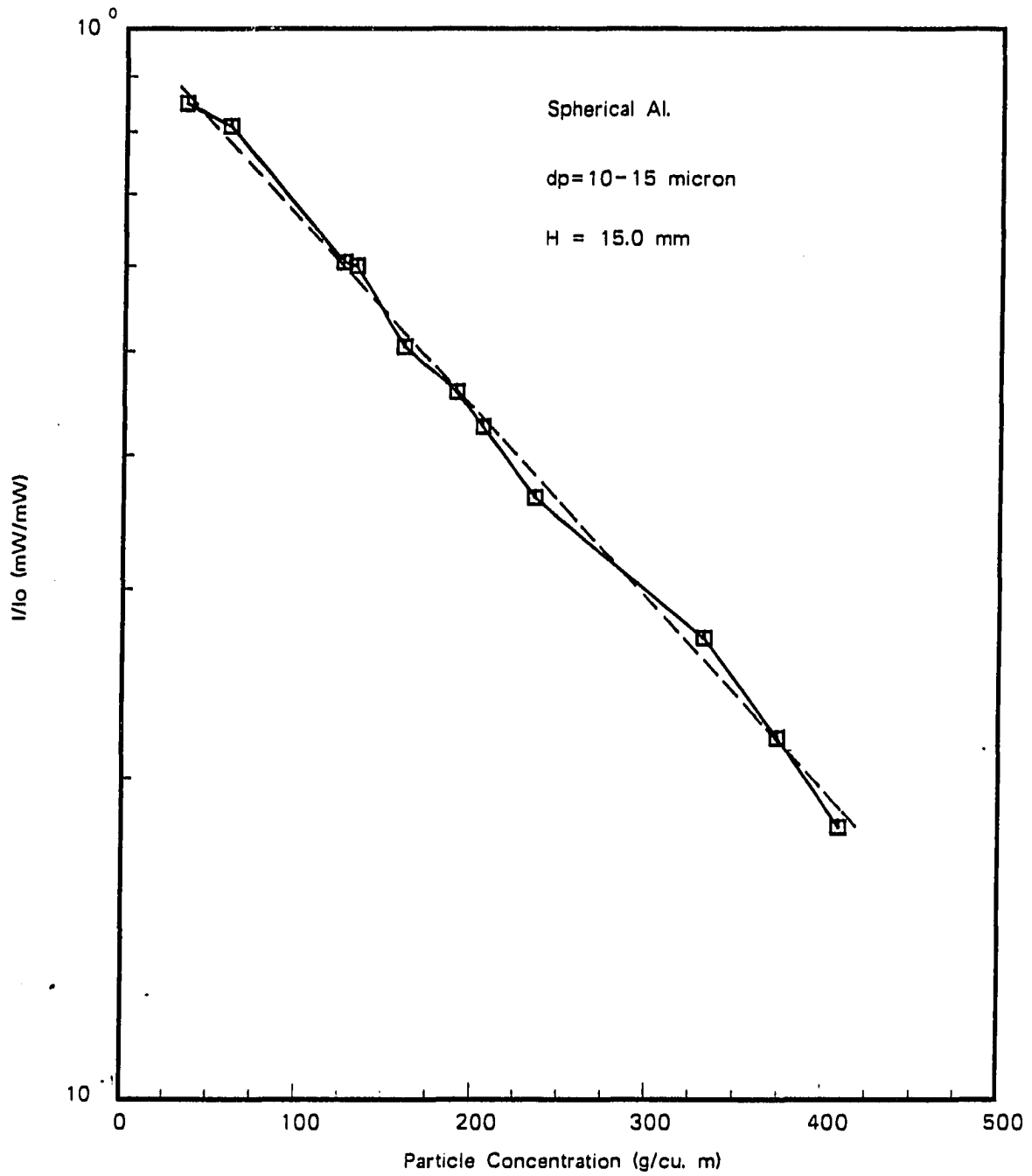


Figure 3.17: Calibration of particle concentration of aluminum particle

C1 : Fixed capacitor
C2 : Variable capacitor
R = 4000 Ω

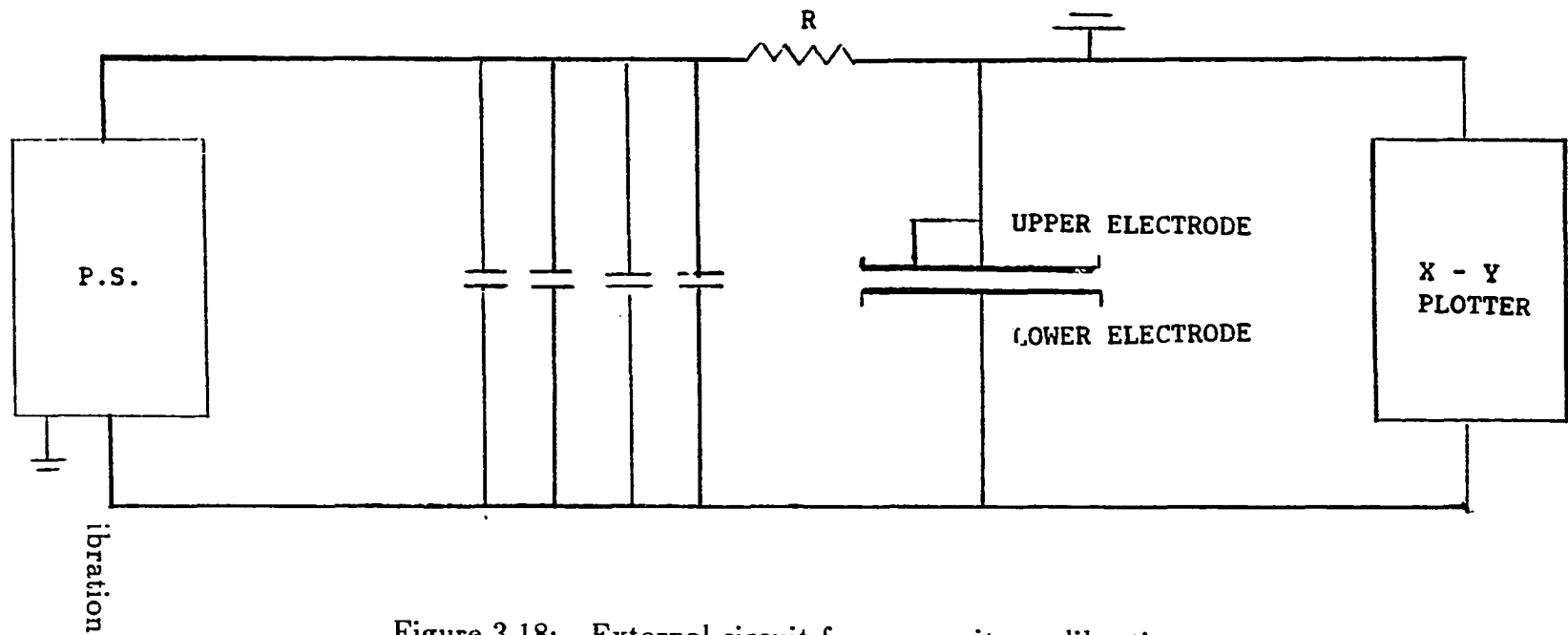


Figure 3.18: External circuit for a capacitor calibration

the resistor R , the charge Q is;

$$Q = \int_0^t \frac{V_R}{R} dt \quad (3.21)$$

R is constant, thus;

$$Q = \frac{1}{R} \int_0^t V_R dt \quad (3.22)$$

He used Hewlett Packard 7046A X-Y recorder to get a curve of V_R versus time, then the area under the curve is measured graphically. Also, from the definition of capacitance;

$$Q = CV \quad (3.23)$$

where, V is an applied voltage. The calibrated result, Figure 3.19, showed that the measured capacitance value is accurate enough that the calibration plot need not be used.

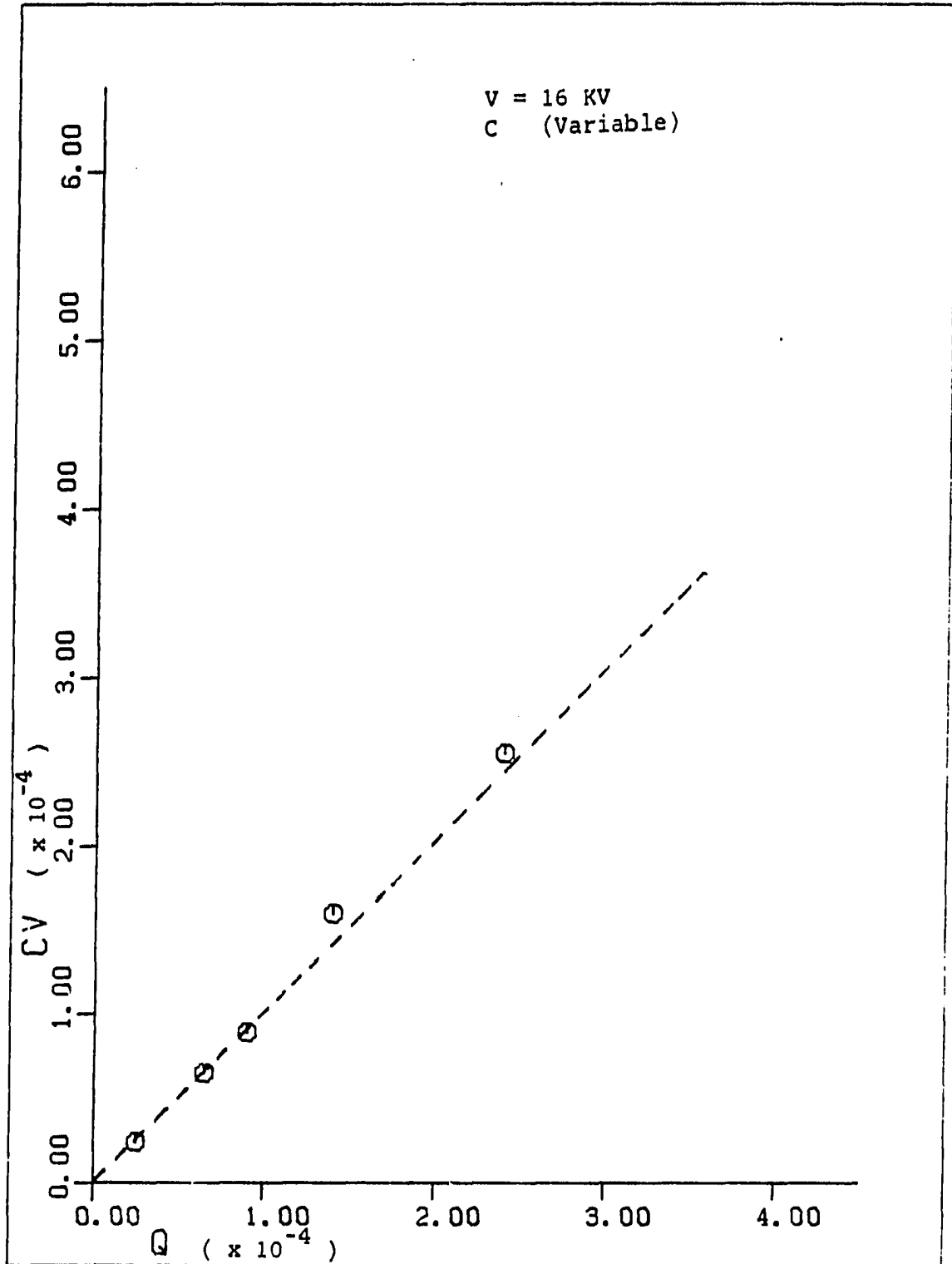


Figure 3.19: Calibration of a capacitor

4 FLAME PROPAGATION AND QUENCHING OF ALUMINUM PARTICLES

4.1 Experimental Technique and Procedure

As a preliminary test, a small glass cylinder 7.92 cm in diameter by 4.0 cm in height was used. A successful particle suspension test with spark ignition was accomplished. Then a larger cylinder 14.7 cm in diameter by 6.0 cm in height was used which improved the observation of the particle suspension and the spark ignition process. Also the larger cylinder required larger powder samples, which improved the measurements of lean particle concentrations. Finally, bigger cylinder was found to greatly improve the measurement of the burning velocity by providing a longer flame travelling distance.

The glass cylinder was polished with a fine sand paper (# 500) to remove the pits around the lips of the glass container. Also, the copper electrodes were polished with a very fine sand paper (# 700) to smooth the surface and to round the outer edges to prevent the glass container from being scratched by the sharp edges.

The experimental procedure for the quenching test was as follows.

1. Set the electrode gap distance large enough distance for ignition, around 20 - 30 mm.

2. Adjust the needle electrode penetrating distance so that the needle does not affect the particle motion but is to initiate a spark when the uniform suspension of particle clouds are present.
3. Weigh out the mass of aluminum powder accurately up to ± 0.0001 gram using the Torsional balance starting from a lesser amount.
4. Put the aluminum powder on the lower electrode inside the glass cylinder, and distribute the powders evenly all over the surface of the lower electrode.
5. Turn on the He-Ne laser and align the suspension monitoring system so that laser beam passes through the center of the test section.
6. Apply the electric field between the electrodes to obtain a uniform suspension of particles.
7. Increase the electric field to initiate a spark.
8. Observe the flame and record whether the flame is propagated or quenched.
9. Increase or decrease the particle concentration and repeat the above procedure for the whole range of particle concentrations until the lean and/or rich flammability limits are obtained.
10. Decrease the electrode gap distance and repeat the above procedure.
11. When no flame propagation is observed for the whole range of particle concentrations at some fixed electrode gap distance, stop the experiment. That electrode gap distance is the minimum quenching distance.

The experimental procedure for the flame propagation is the same as above except that the electrode gap distance is maintained at a large enough distance so that the effect of quenching can be neglected. The burning velocity was recorded with a varying particle concentrations at a fixed electrode gap distance. The particle concentration was started from above the lean flammability limit as obtained from the quenching data.

4.2 Quenching of Methane-air Flame

Quenching data of gaseous fuels such as methane are well established and the data obtained by various researchers are very consistent. To justify the experimental technique and apparatus of this research, a quenching distance of methane in air at various fuel-to-air ratios was obtained and the results were compared with the data of different researchers. A commercial 99.5 % pure methane (Air Products, Inc.) was used for this experiment. The methane and air flowed into the test section through the openings in the upper plate and escaped through the holes at the wall of the glass cylinder as shown in Figure 4.1.

For a given methane concentration, the methane-air mixture is kept flowing through the test section until the test section is filled with a uniform mixture of methane-air gas. The flame arrestor is mounted before the test section to prevent the methane flame from propagating back to the fuel line. The flame arrestor is made of brass cylinder filled with glass beads so that the distance between the glass beads is much smaller than the minimum quenching distance of the methane-air flame (Figure 4.1).

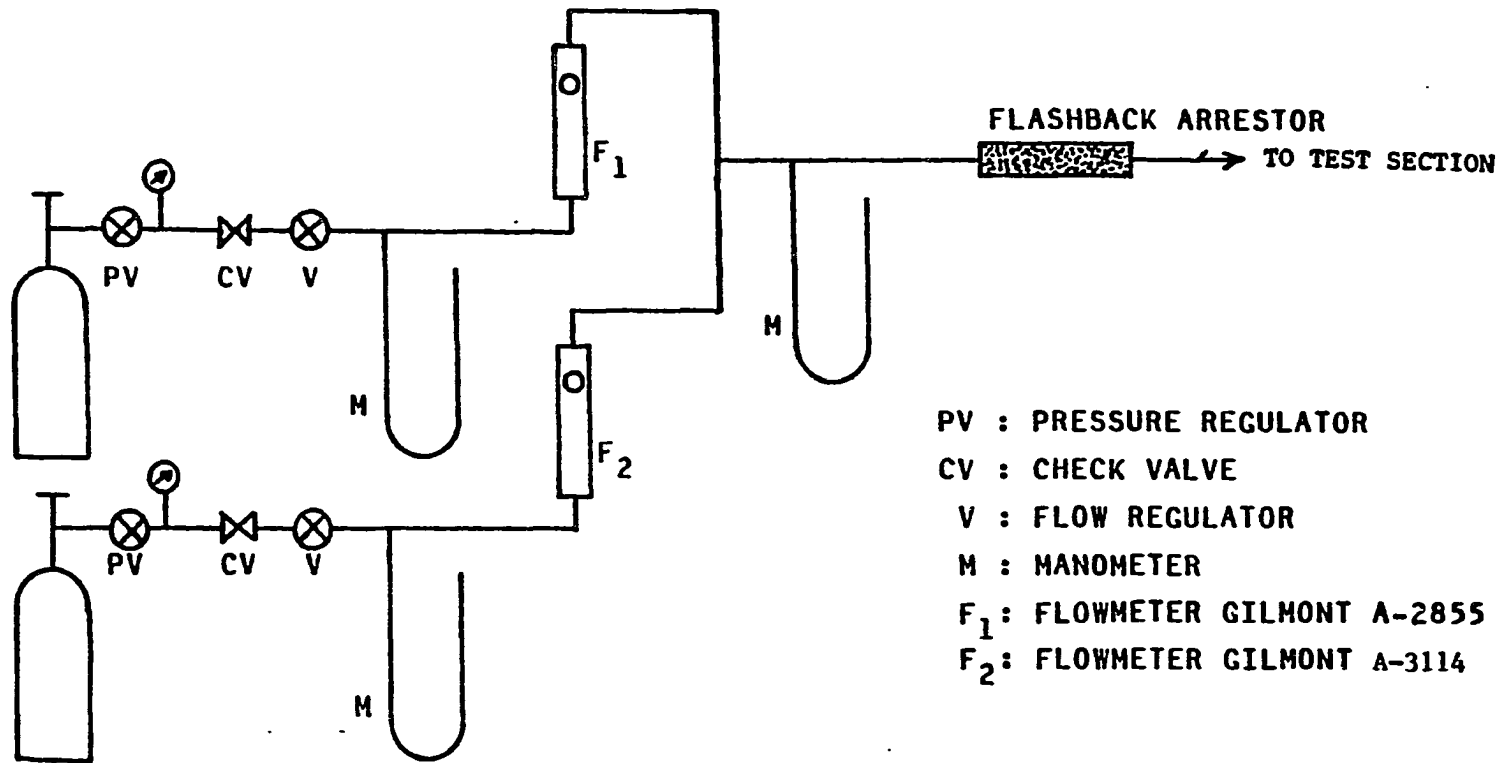


Figure 4.1: Experimental setup for methane-air flame quenching

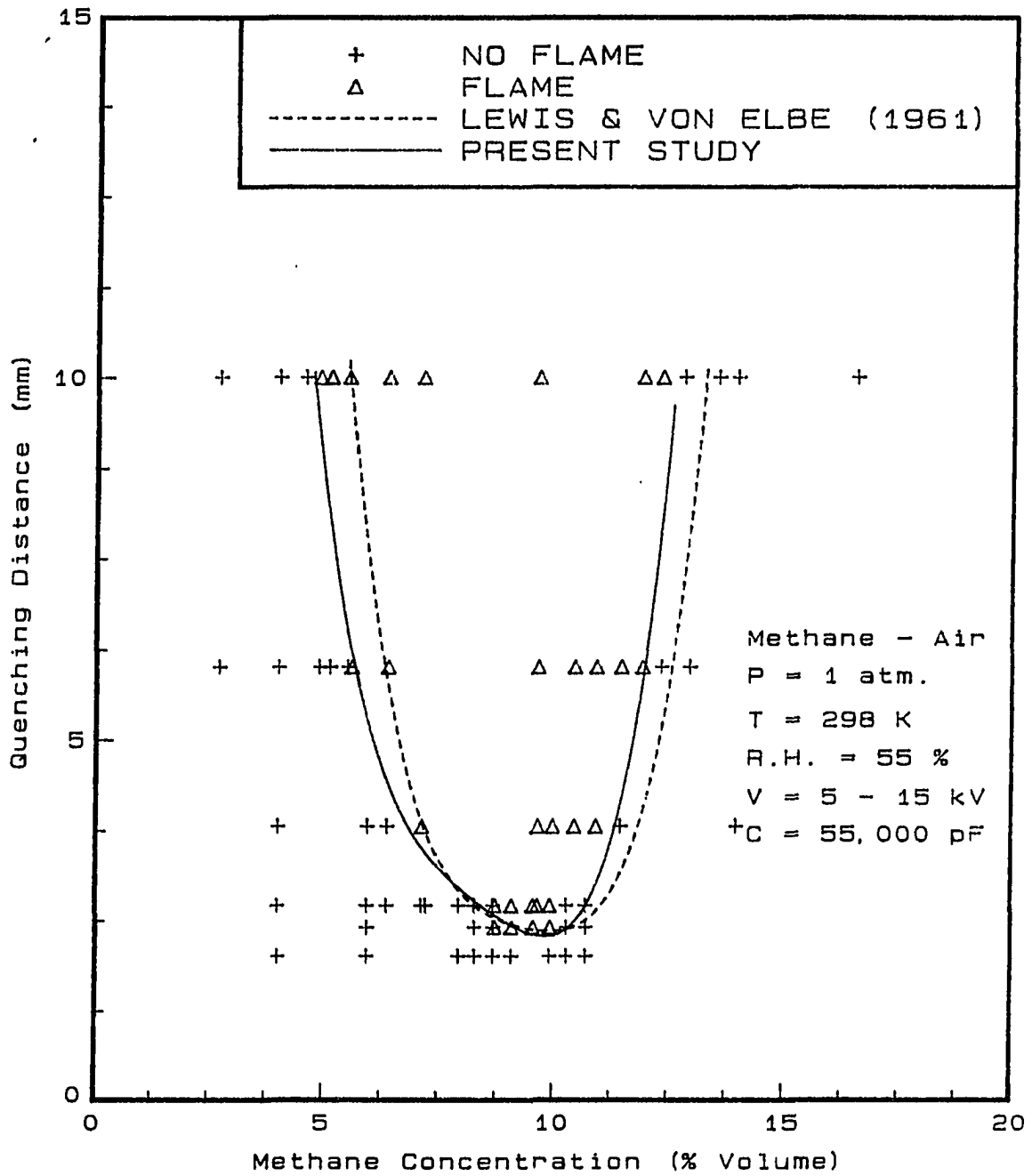


Figure 4.2: Quenching distance vs. fuel/air ratio of methane-air flame

The quenching results for methane are shown in Figure 4.2. The results confirm that the quenching data obtained in this apparatus are consistent with other researcher's data. Lewis and von Elbe [1961] obtained a minimum quenching distance of 2.16 mm which is very close to 2.1 mm obtained in this research. Also the lower and upper flammability limits, 4.9 and 12.7 % respectively, are close to those of Lewis and von Elbe's [1961] 5.3 and 15.0 %, respectively. Also the minimum quenching distance is near the stoichiometric concentration. The quenching distances of methane-air flames of various researchers were compared in Table 4.1.

From this agreement between experiments on the quenching of methane-air flame, the present experimental approach appears to be reliable.

4.3 Quenching of Aluminum-air Flame

Four important parameters in combustion research are,

1. Flammability limits
2. Minimum ignition energy
3. Quenching distance
4. Burning velocity

In his previous research work, Kim [1986] investigated the effect of particle size and concentration on the flammability limits and the minimum ignition energy of aluminum powder. Figure 4.3 shows the relationship between the minimum ignition energy and particle concentration of 27.5 μm aluminum powder. The result showed that the minimum ignition energy decreases until it reaches a minimum value, which

Table 4.1: Comparison of minimum quenching distances of methane-air flames

Min. Quenching Distance (mm)	Researcher
2.10	Kim [1986]
2.50	Holm [1932]
2.40	Harris et al. [1949]
2.16	Lewis and von Elbe [1961]
2.00	Jarosinski [1983]

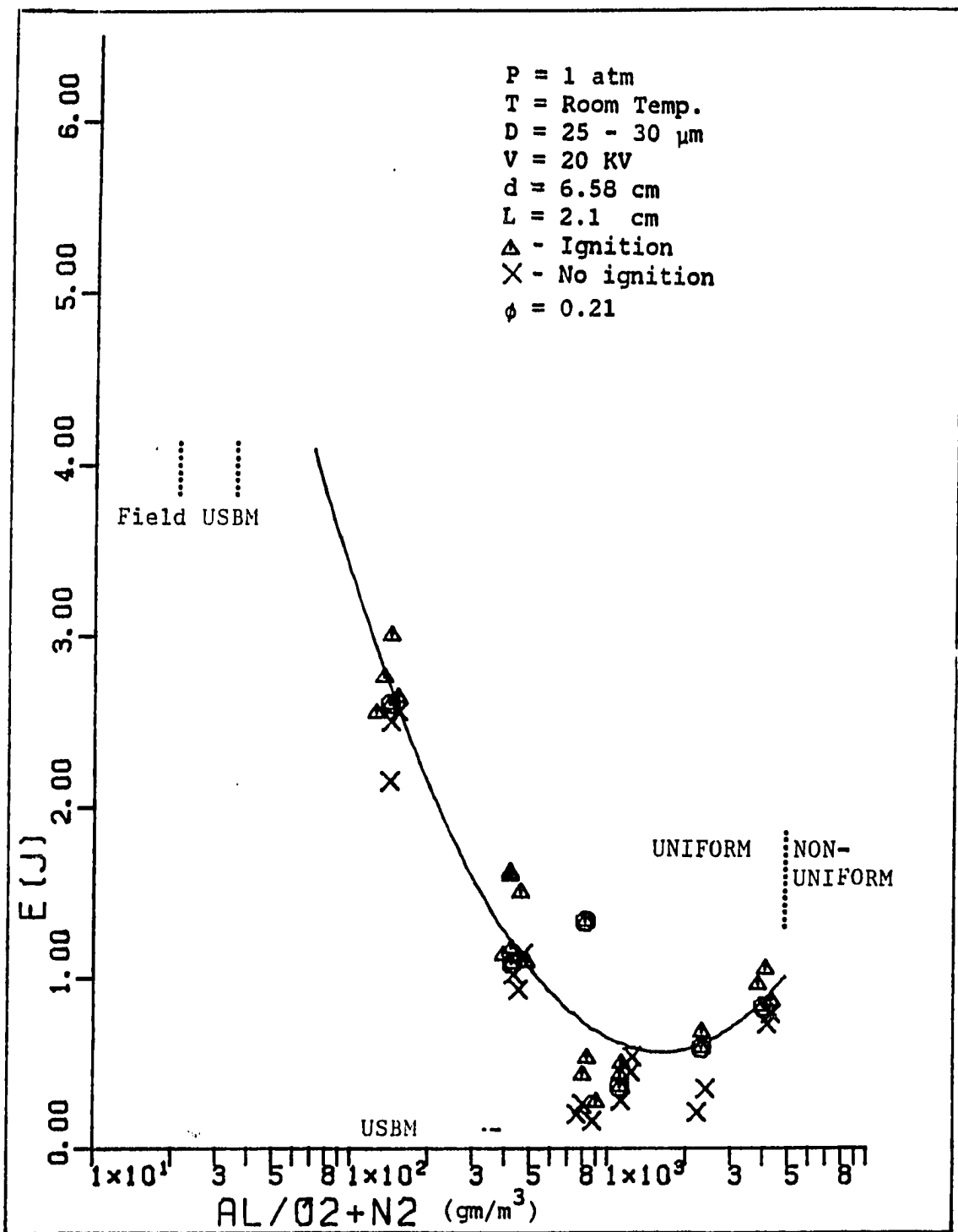


Figure 4.3: Spark ignition energy vs. particle concentration of 22.5 μm spherical aluminum particle

then increases as the particle concentration increases. In this research, the quenching distance and burning velocity of aluminum particles were studied, along with flammability limits.

Quenching distance is defined as the minimum plate spacing to prevent flame propagation. The lean flammability limit is the limiting fuel concentration below which a flame can not propagate, and the rich flammability limit is the limiting fuel concentration above which a flame can not propagate. Since the electrical spark ignition process is a random event, the conditions for 50 percent probability of ignition of the mixture is regarded as successful ignition. Figure 4.4 shows a typical photograph of a spark ignition of uniform particulate cloud at room temperature and atmospheric pressure for 25 - 30 μm aluminum powder. Up to now, a very limited amount of work has done on the quenching of powdered fuels. Jarosinski et al. [1986] reported the minimum quenching distance of 10.4 mm for spherical atomized aluminum. But Ballal [1983b] reported the value of 4.0 mm. In the present work and in Ballal's work, the quenching distance is defined as the minimum distance (diameter) through which a flame can propagate initiated by a spark. Jarosinski defined the quenching distance to be the maximum spacing between the walls for which heat outflow to the walls is able to quench the fully developed freely propagating flame. It follows that the discrepancies in the quenching distance of aluminum powder between the two researchers can be explained by the difference in the definition of the quenching distance. Ballal [1983a] used a vertical tube filled with suspended particles with the flame initiated by spark as the tube fell freely under the influence of Earth's gravity. Thus, he eliminated the influence of buoyancy and the settling of fuel powders on the propagating

flame. Jarosinski et al. [1986] measured a quenching distance for a flame propagating upward from the open to the closed end of the tube which was 1.88 m long and 0.190 m inside diameter. He put a grid of steel quenching plates in the middle of the test apparatus. He determined the quenching distance as the maximum grid spacing that propagates the fully developed flame.

4.3.1 Effect of particle concentration

4.3.1.1 Effect of particle concentration of spherical aluminum Six different sizes of aluminum powder were used for the tests, 12.5, 17.5, 22.5, 27.5, 34.0, 41.5 μm in diameter. Figures 4.5 to 4.10 shows the relationship between quenching distance and aluminum concentration for each particle size. The figures show that the quenching distance decreases until it reaches a minimum value, which is a minimum quenching distance, then increases as the particle concentration increases. And there is a specific concentration for minimum quenching distance which is higher than stoichiometric concentration. Also a lean flammability limit exists. However, rich flammability limits proved impossible to achieve whether or not there exists rich flammability limit. Because a mono-layer limit exists for this method, it is impossible to generate an uniform suspension of aluminum clouds above the particle concentration of 3,000 - 4,000 g/m^3 .

For 12.5 μm particle, the minimum quenching distance was 3.50 mm at the particle concentration of 1145.0 g/m^3 which was about 3.7 times higher than the stoichiometric concentration (306.2 g/m^3). The lean flammability limit was 90 g/m^3 which is higher than the limit obtained in previous research on minimum ignition



Figure 4.4: Photograph of a spark ignition of aluminum particles

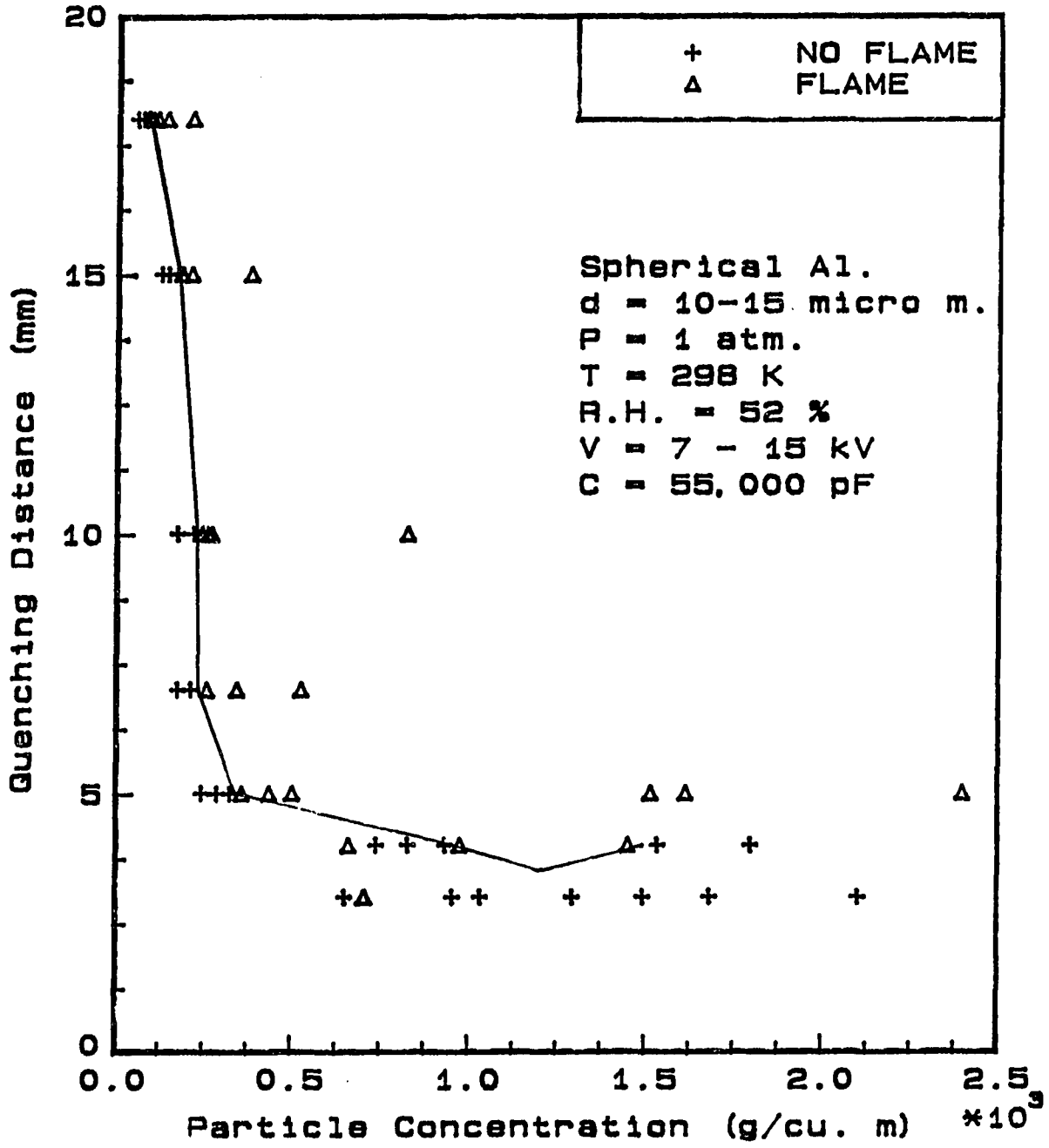


Figure 4.5: Quenching distance vs. particle concentration of 12.5 μm spherical aluminum particle

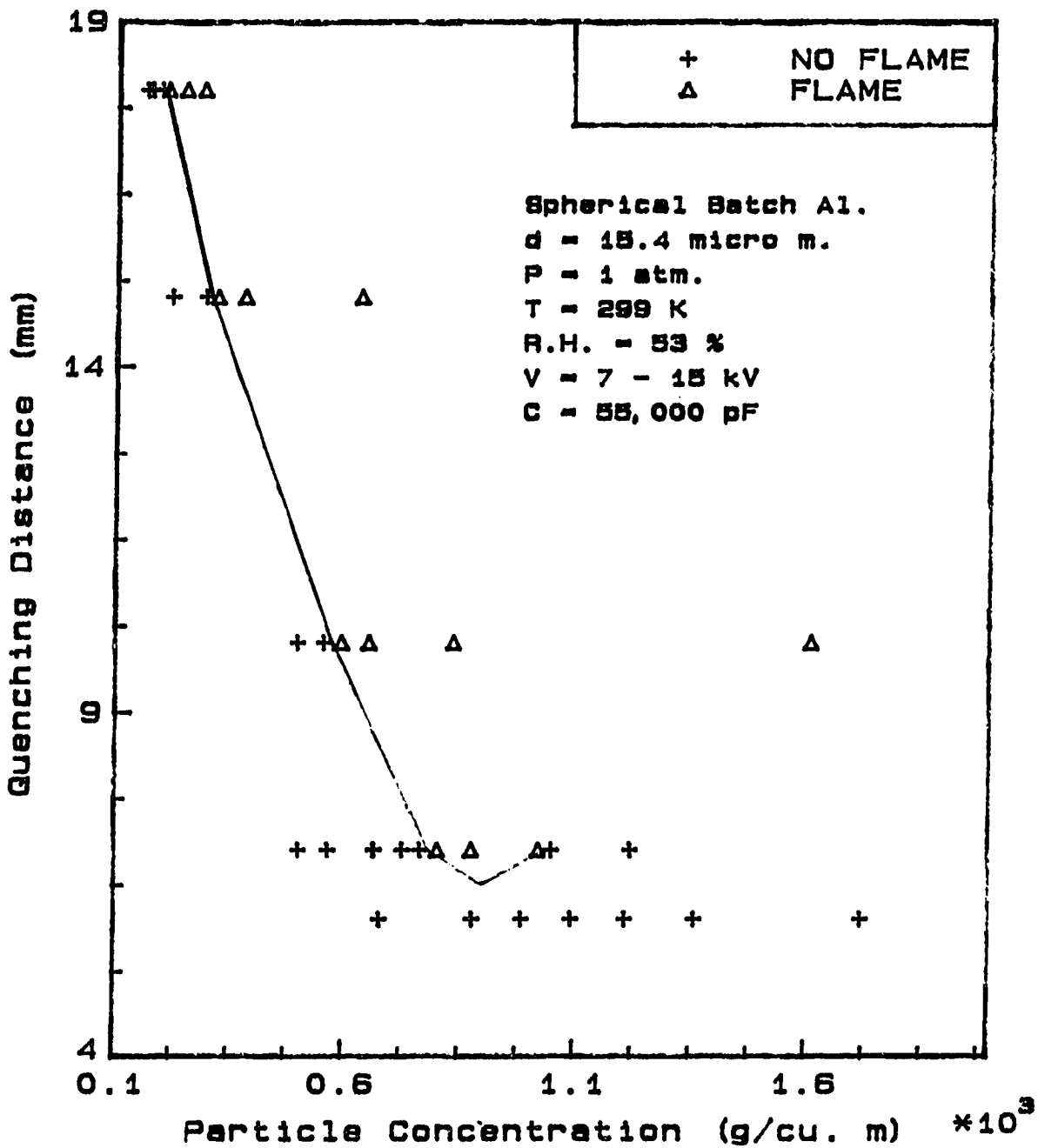


Figure 4.6: Quenching distance vs. particle concentration of 17.5 μm spherical aluminum particle

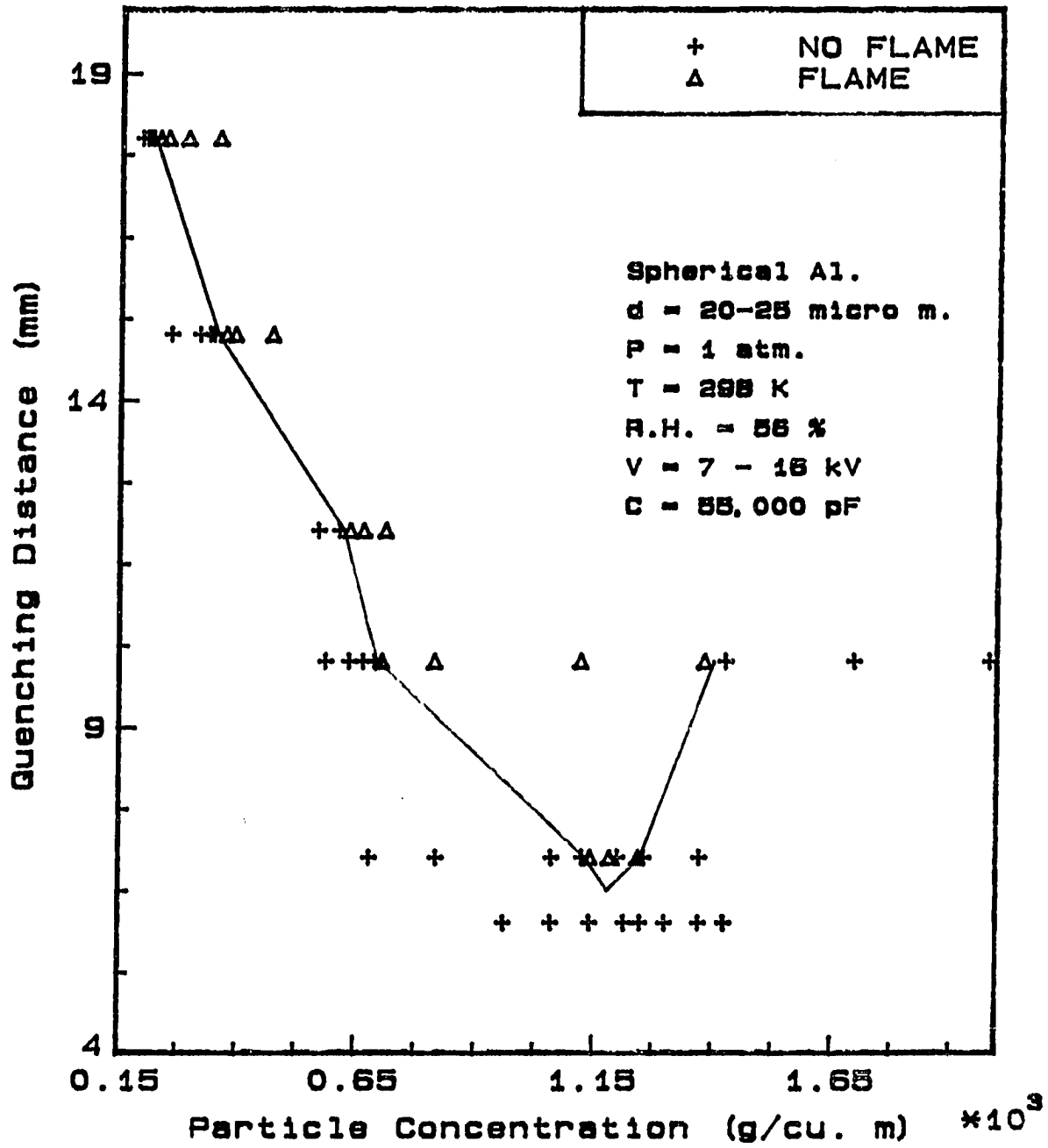


Figure 4.7: Quenching distance vs. particle concentration of 22.5 μm spherical aluminum particle

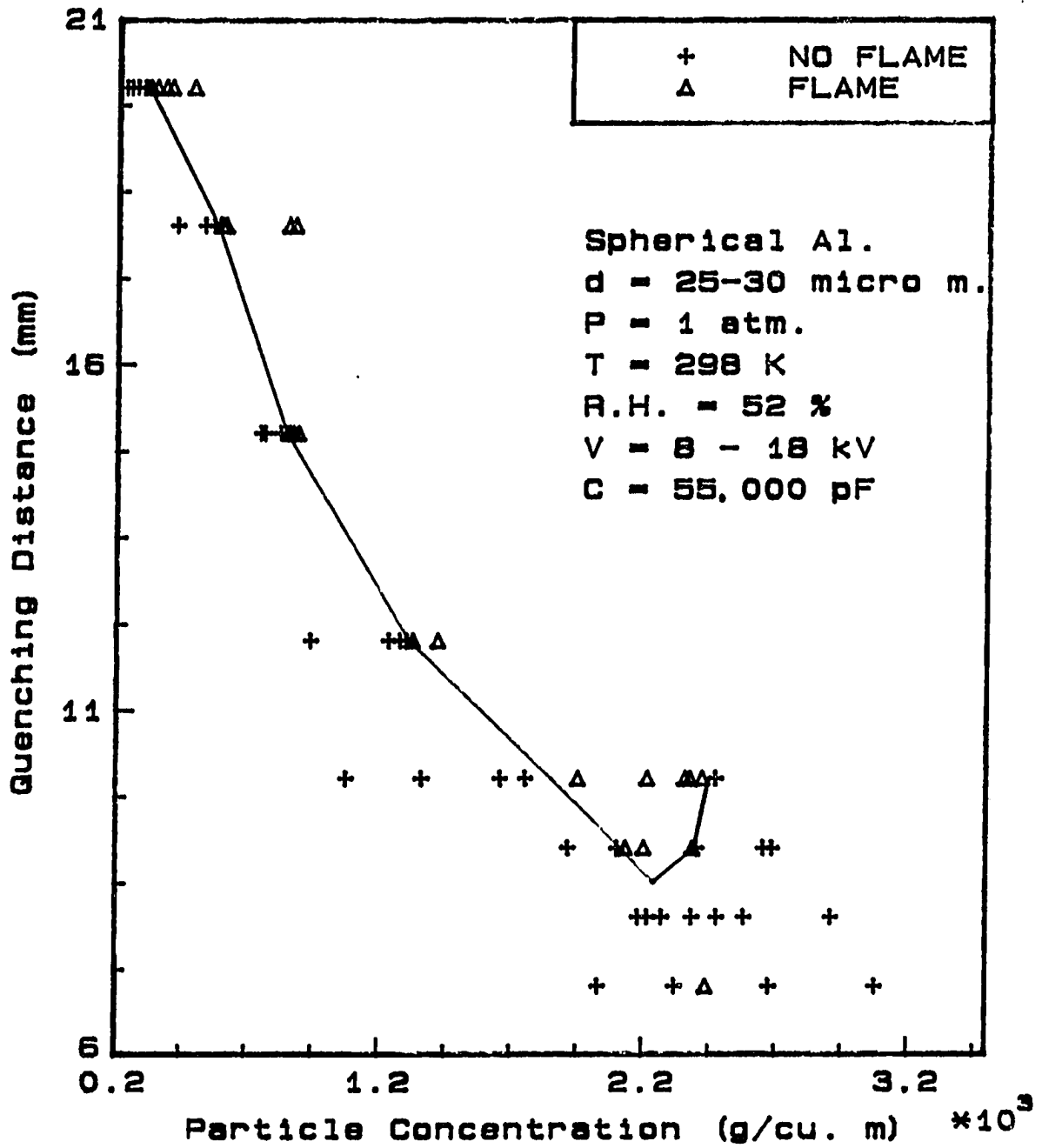


Figure 4.8: Quenching distance vs. particle concentration of $27.5 \mu\text{m}$ spherical aluminum particle

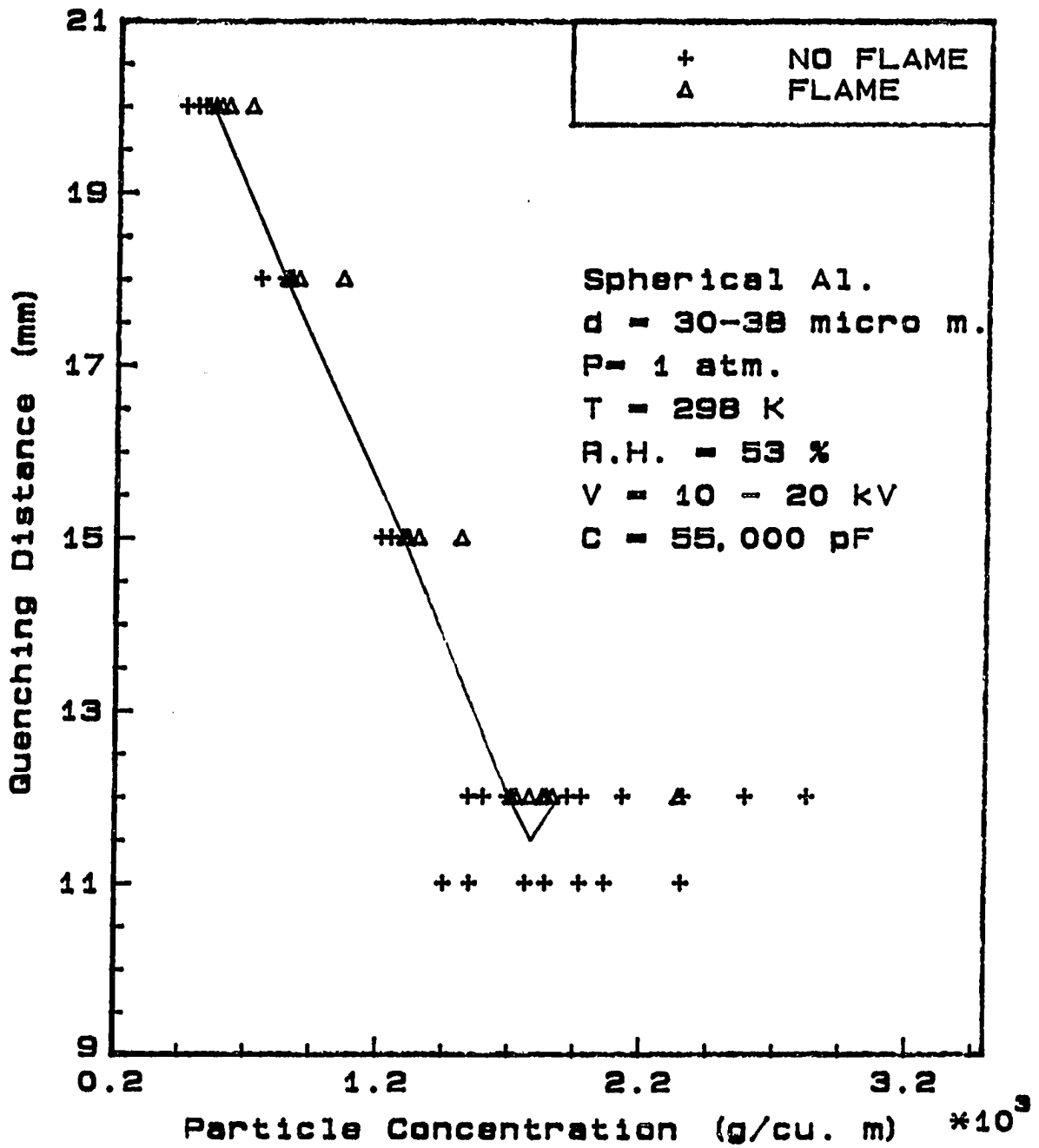


Figure 4.9: Quenching distance vs. particle concentration of 34.0 μm spherical aluminum particle

energy which is 60 g/m^3 and about double of the data obtained by Jacobson et al. [1964]. The lean flammability limits obtained by Kim [1986] and Jacobson et al. [1964] are the values obtained at the optimum ignition energy, but the value for this research work was obtained at the maximum ignition energy. Thus the discrepancies of lean flammability limits are probably due to the difference in the test condition. One particular characteristic of this size aluminum was that the quenching distance is much more sensitive to the particle concentration around the minimum quenching distance range than any other aluminum powder.

The minimum quenching distance for $17.5 \mu\text{m}$ particle was 5.50 mm at the particle concentration of 840.0 g/m^3 which is 2.7 times higher than the stoichiometric concentration. This particle concentration was the lowest one among all sizes of aluminum powder. The lean flammability limit was 115.0 g/m^3 .

For $22.5 \mu\text{m}$ particles, the minimum quenching distance was 6.80 mm of the concentration of 1170.0 g/m^3 which is 3.8 times higher than the stoichiometric concentration. The lean flammability limit was 180.0 g/m^3 which is higher than that of previous work on minimum ignition energy, 70 g/m^3 . The rich flammability limit was relatively well defined in this case, about 1600.0 g/m^3 .

For $27.5 \mu\text{m}$ aluminum powder, the minimum quenching distance was 8.70 mm at the particle concentration of 2240.0 g/m^3 which is 7.3 times higher than the stoichiometric concentration. This particle concentration was the highest among all sizes of aluminum powder tested. The lean flammability limit was 230.0 g/m^3 which is higher than that of previous work, 90 g/m^3 .

The minimum quenching distances for 34, $41.5 \mu\text{m}$ aluminum particles were 12.0

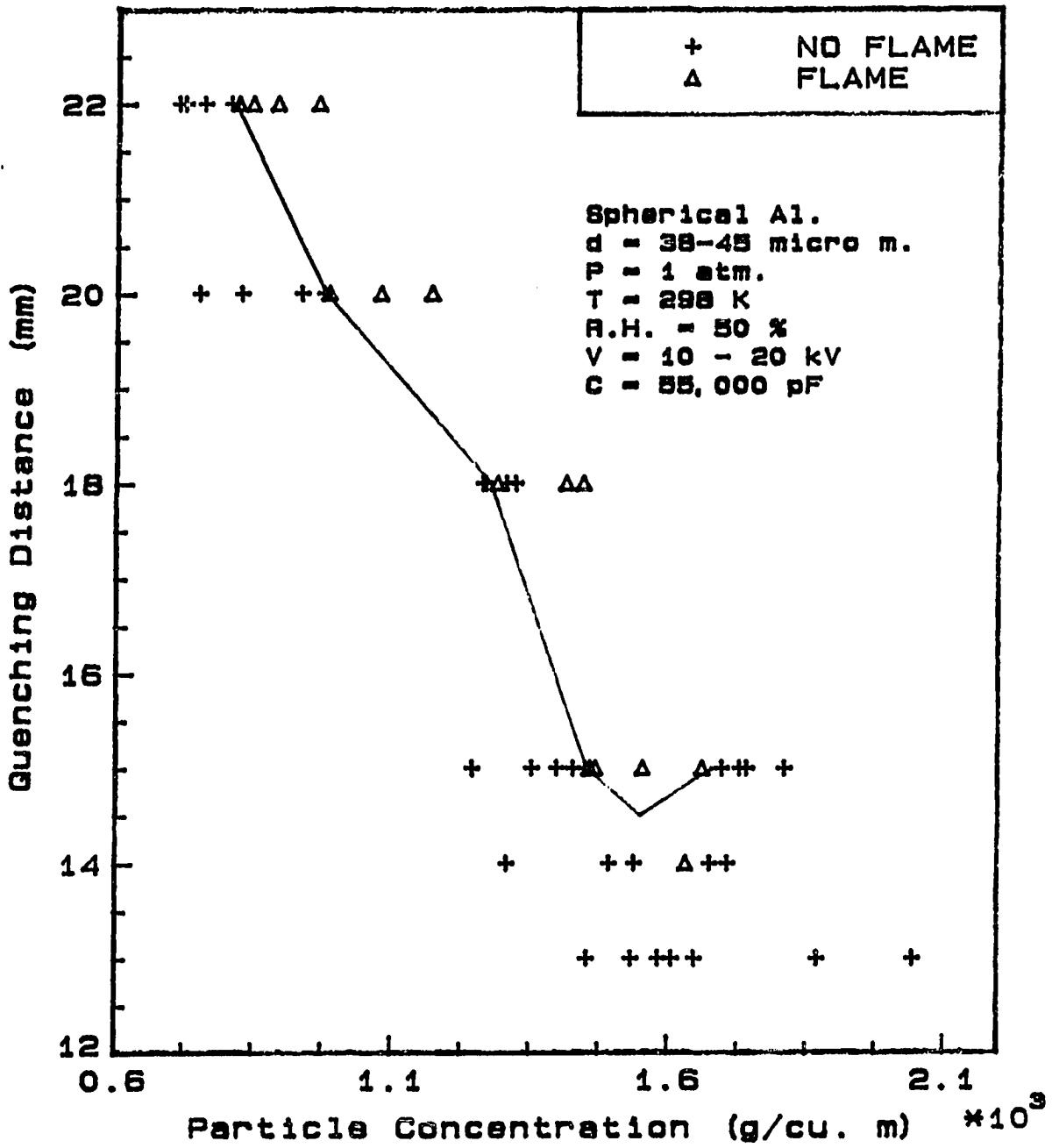


Figure 4.10: Quenching distance vs. particle concentration of $41.5 \mu\text{m}$ spherical aluminum particle

and 14.5 mm, respectively. Corresponding particle concentrations were 1680.0 and 1540.0 g/cm^3 , respectively. For 34 μm particles, the quenching distance changed almost linearly with a particle concentration at the lean concentration range.

4.3.1.2 Effect of particle concentration of irregular shaped aluminum

Irregular shaped aluminum powder were tested in four different particles sizes, 20.0, 27.5, 34.0, 41.5 μm . The particle diameter should be calculated from the equivalent diameter formulation because the particles are not spherical in shape at all. Equivalent diameter D_{eq} is $((4 \times SurfaceArea)/Perimeter)$, but the different shape of each of the particles makes it very difficult to determine the equivalent diameter. Thus, the mean sieve range was used as the mean diameter of the particle.

Figures 4.11 to 4.14 shows the quenching distance variation with the change of particle concentration. For 20 μm irregular aluminum particles, the minimum quenching distance was 4.50 mm at the particle concentration of 730.0 g/m^3 as shown in Figure 4.11. The lean flammability limit was 200 g/m^3 . For 27.5 μm irregular aluminum powder, the minimum quenching distance was 6.50 mm at the particle concentration of 750 g/m^3 as shown Figure 4.12. This distance of 6.50 mm was less than the case of spherical aluminum powder of the same size which is 8.70 mm. The lean flammability limit was 290.0 g/m^3 . The minimum quenching distances of these two particle sizes occurred at very close concentrations.

As will be discussed later, irregular aluminum has a greater surface area than spherical aluminum for the same mean diameter, so irregular aluminum has a more complete chemical reaction with the available oxygen at the surface. The quenching distance of these two sizes of irregular aluminum are lower than those of spherical

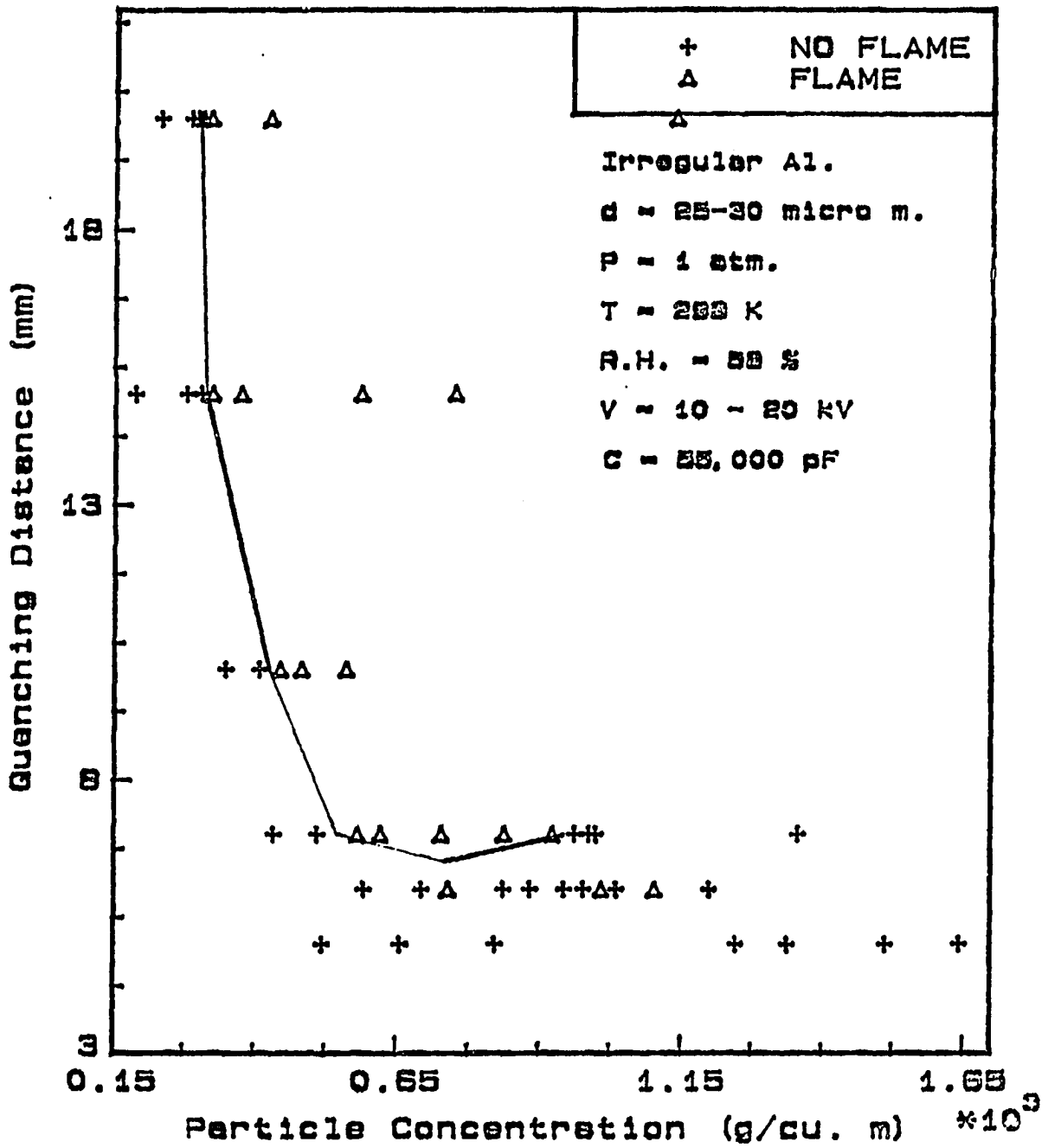


Figure 4.12: Quenching distance vs. particle concentration of 27.5 μm irregular aluminum particle

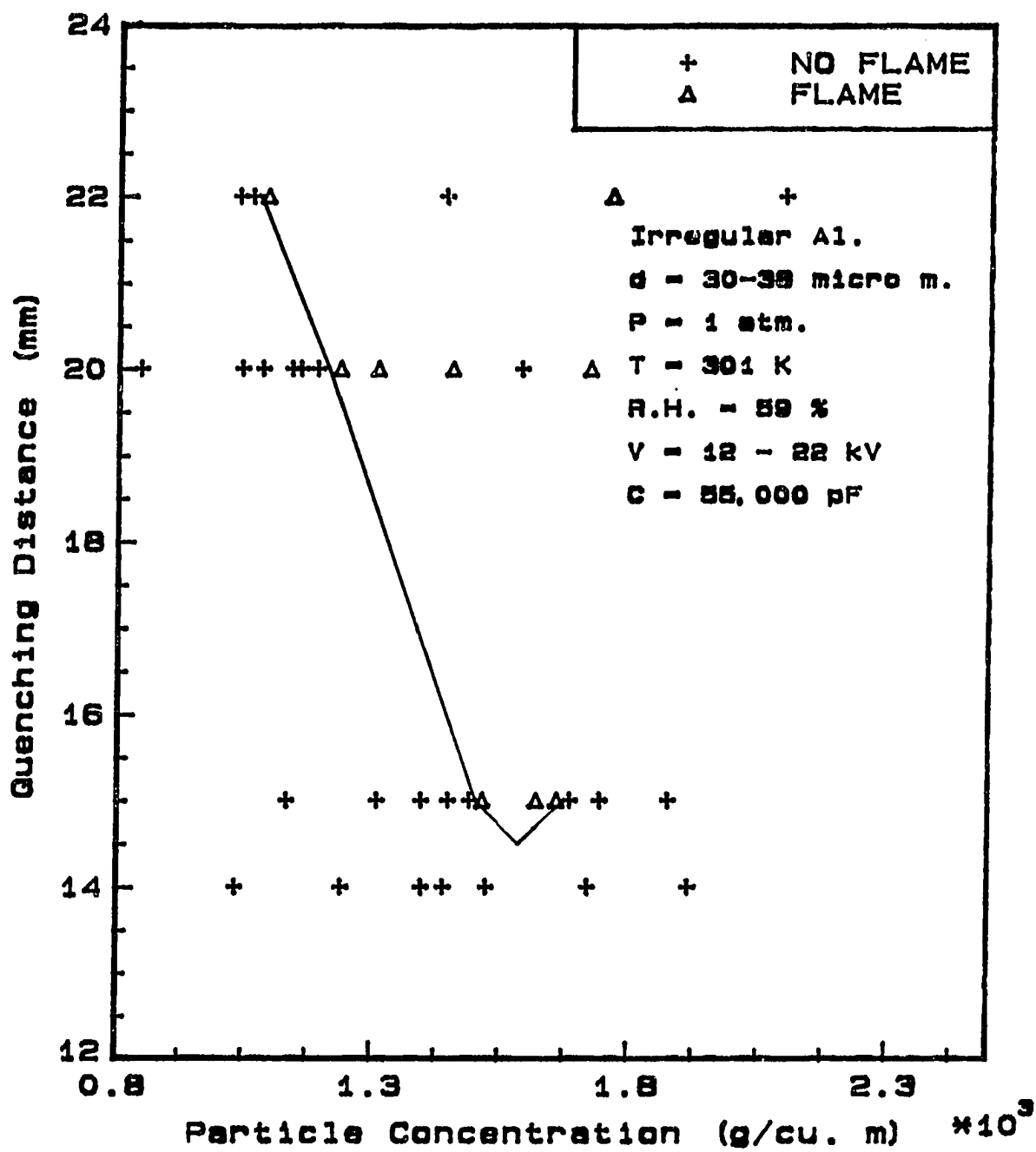


Figure 4.13: Quenching distance vs. particle concentration of 34.0 μm irregular aluminum particle

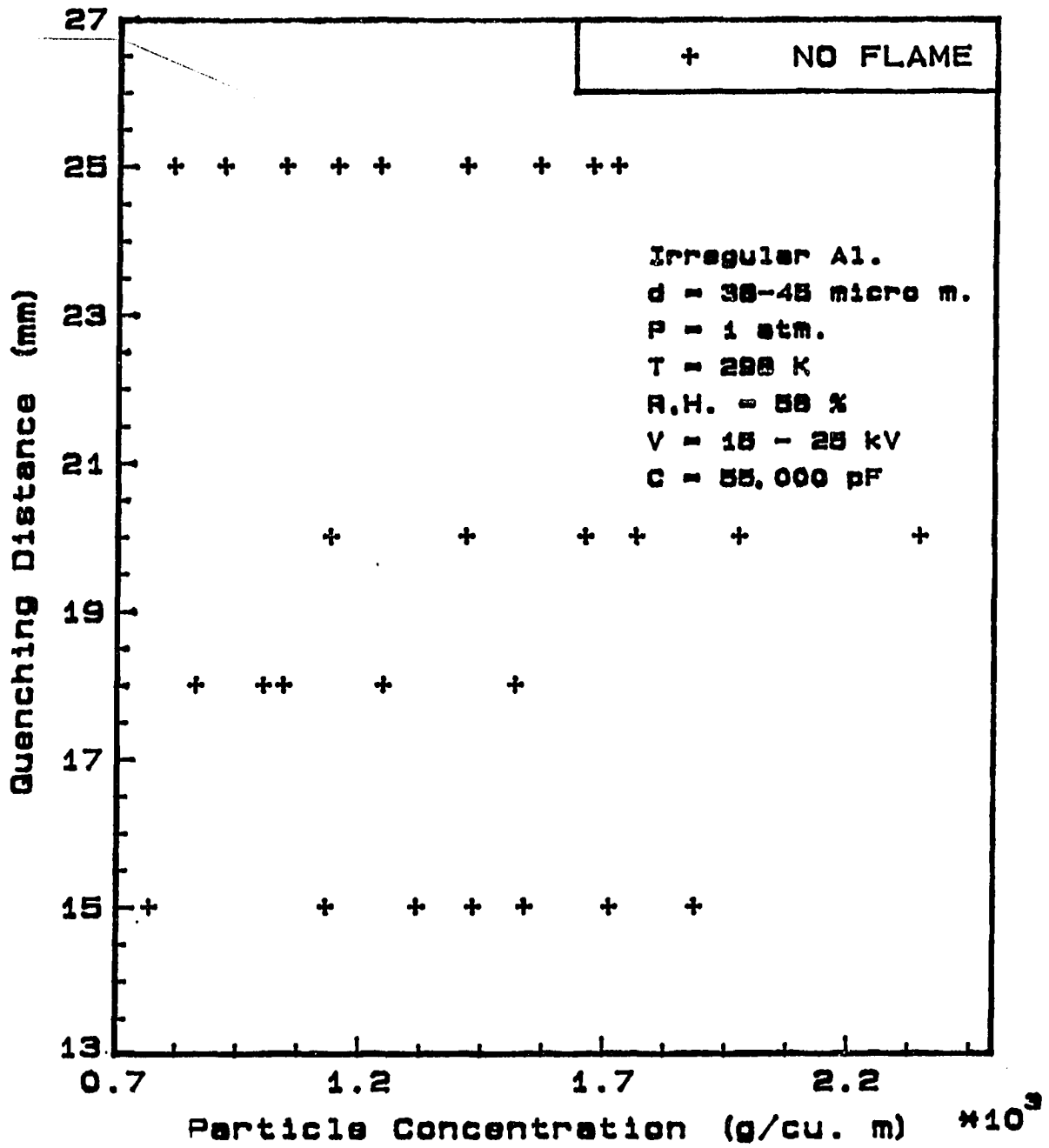


Figure 4.14: Quenching distance vs. particle concentration of 41.5 μm irregular aluminum particle

aluminum of the same mean diameter.

Figure 4.13 shows that the minimum quenching distance of $34.0 \mu\text{m}$ irregular aluminum is 14.70 mm at the particle concentration of 1580.0 g/m^3 , and the lean flammability limit is 850.0 g/m^3 . Comparing to the spherical aluminum of the same size, this aluminum had higher minimum quenching distance, also higher lean flammability limit. It is believed that the irregular aluminums bigger than $25 \mu\text{m}$ has a longer reaction time than spherical aluminum, thus experiencing more heat loss and making it more difficult to ignite.

It was impossible to ignite the $41.5 \mu\text{m}$ irregular aluminum at any particle concentration ranges and at any plate separation distances. Thus, the minimum quenching distance of $41.5 \mu\text{m}$ irregular aluminum should be much higher than 25.0 mm .

4.3.2 Effect of particle size and shape

Particle size and shape are very important factors in flame propagation and quenching process of a dust explosion.

Figure 4.15 shows the effect of particle size on quenching distance for various particle concentrations for spherical aluminum particles. For a given particle concentration, the quenching distance increases as the particle size increases. Also the lean flammability limit increases as the particle size increases. The lean flammability limit increases slowly for particles sizes below $25 \mu\text{m}$ but it increases rapidly above $25 \mu\text{m}$. The minimum quenching distance increases steadily as the particle size increases as shown in Figure 4.16.

The reaction between the oxygen and a dust particle is controlled by diffusion

of oxygen and, consequently, is dependent on surface area. In case of a spherical aluminum, the finer the particle size, the greater the surface area/volume, and the greater the specific surface area, the higher the reaction rate.

For irregular particles, the same particle size dependence was observed. But in this case, the quenching distance and lean flammability limit increased rapidly above $30\ \mu\text{m}$ in diameter. And for $41.5\ \mu\text{m}$ size, the quenching distance was above 30.0 mm, and did not ignite in this test apparatus. They are shown in Figures 4.17 and 4.18.

The irregular shaped aluminum has greater specific surface area than spherical aluminum for the same equivalent diameter. As explained in previous section, the irregular aluminum have more complete chemical reaction with the available oxygen around the surface. But as the particle size increases above $30\ \mu\text{m}$ in diameter, irregular aluminum has a longer reaction time experiencing more heat loss during that time.

Figure 4.19 shows the effect of particle shape on quenching distance for $27.5\ \mu\text{m}$ in diameter particles. The minimum quenching distance for irregular aluminum, 6.50 mm, was much smaller than that of spherical aluminum, 8.70 mm. But the lean flammability limit was almost same.

The reverse was true for $34.0\ \mu\text{m}$ particles as shown in Figure 4.20. The quenching distance for irregular aluminum, 14.70 mm, was much bigger than that of a spherical aluminum, 11.80 mm. The lean flammability limit also showed the same trends.

Another difference in the behavior of the two particles were, the irregular alu-

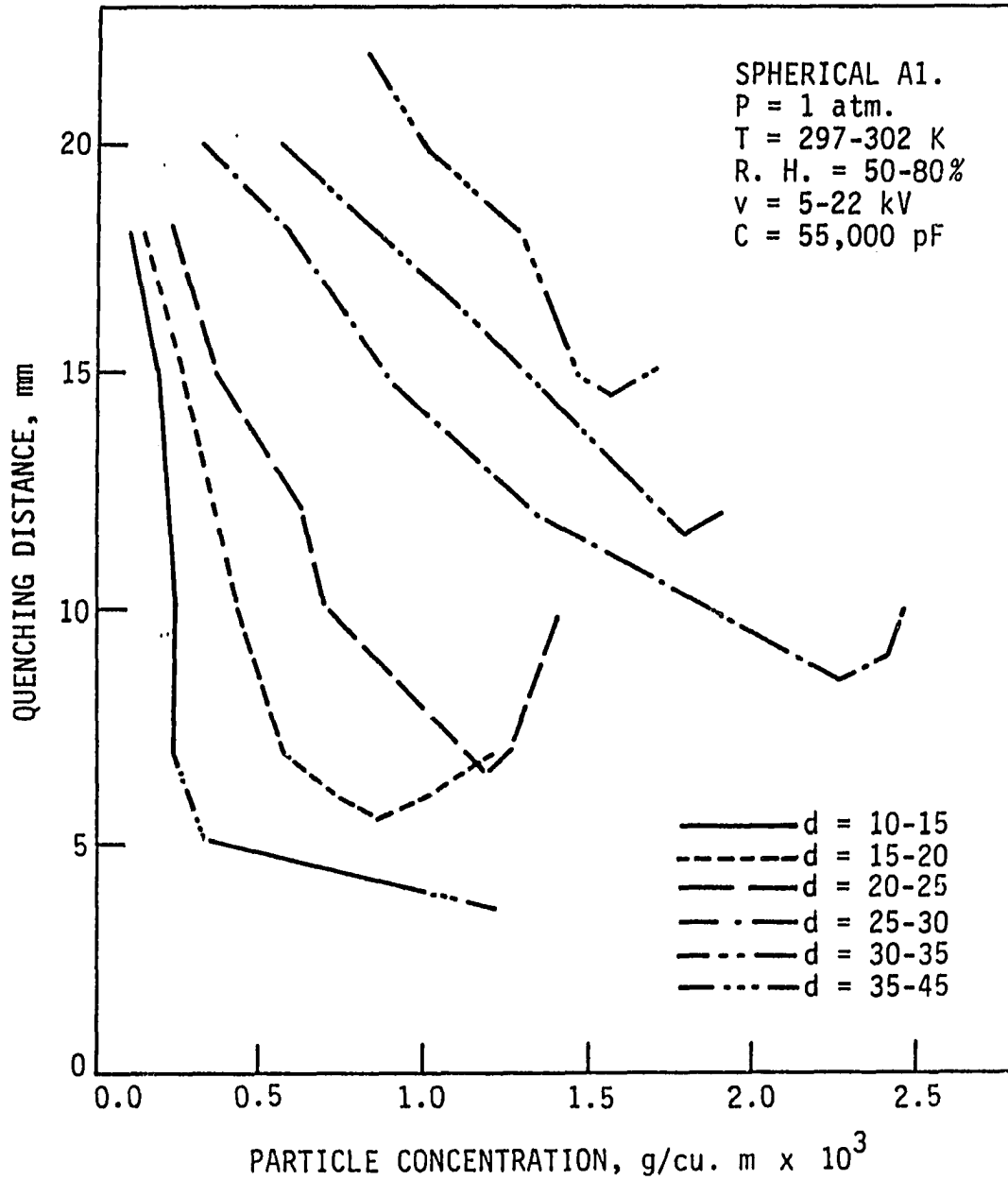


Figure 4.15: Quenching distance vs. particle concentration of spherical aluminum particles of various particle sizes

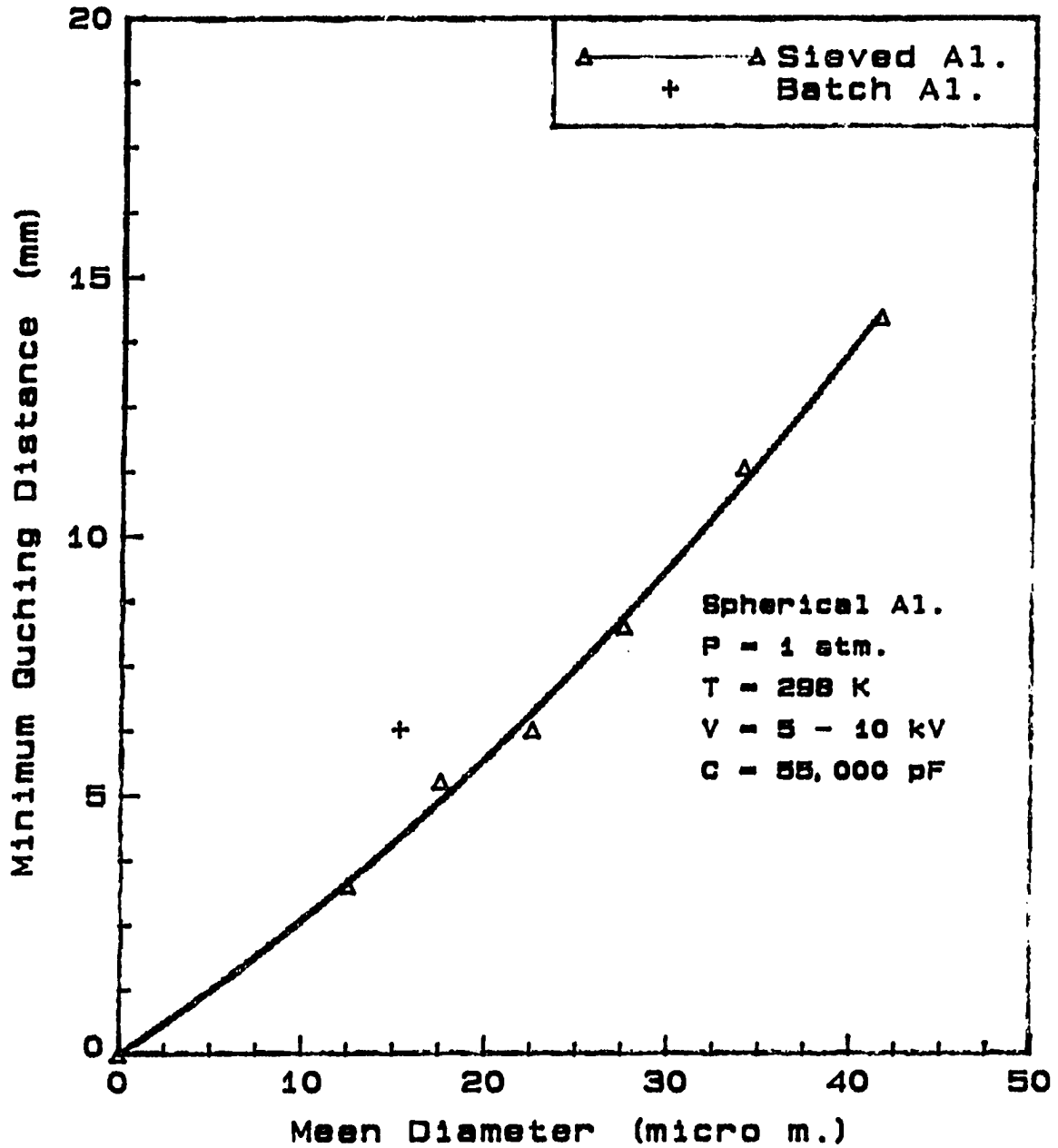


Figure 4.16: Minimum quenching distance vs. particle diameter of spherical aluminum particles

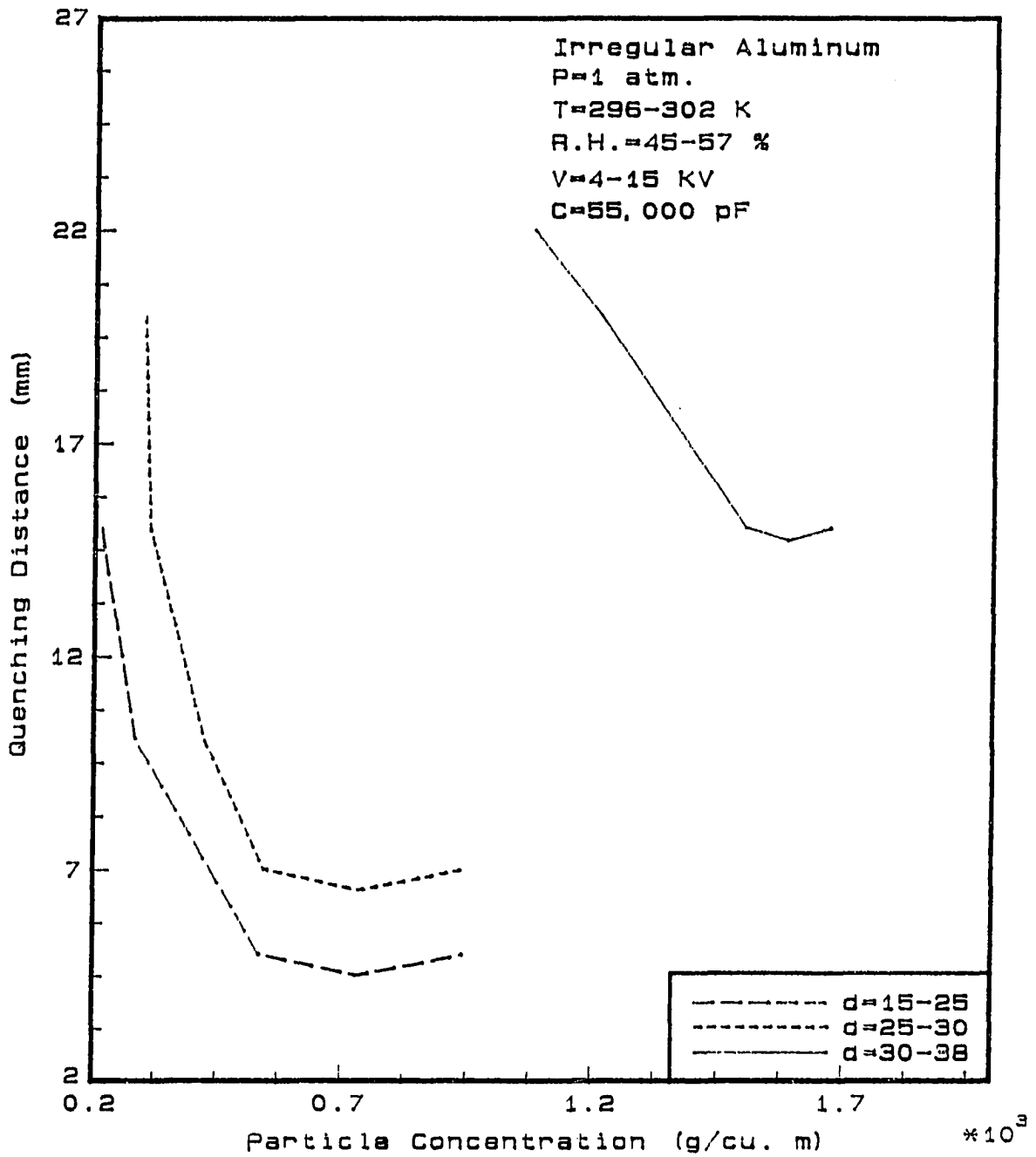


Figure 4.17: Quenching distance vs. particle concentration of irregular aluminum particles of various particle sizes

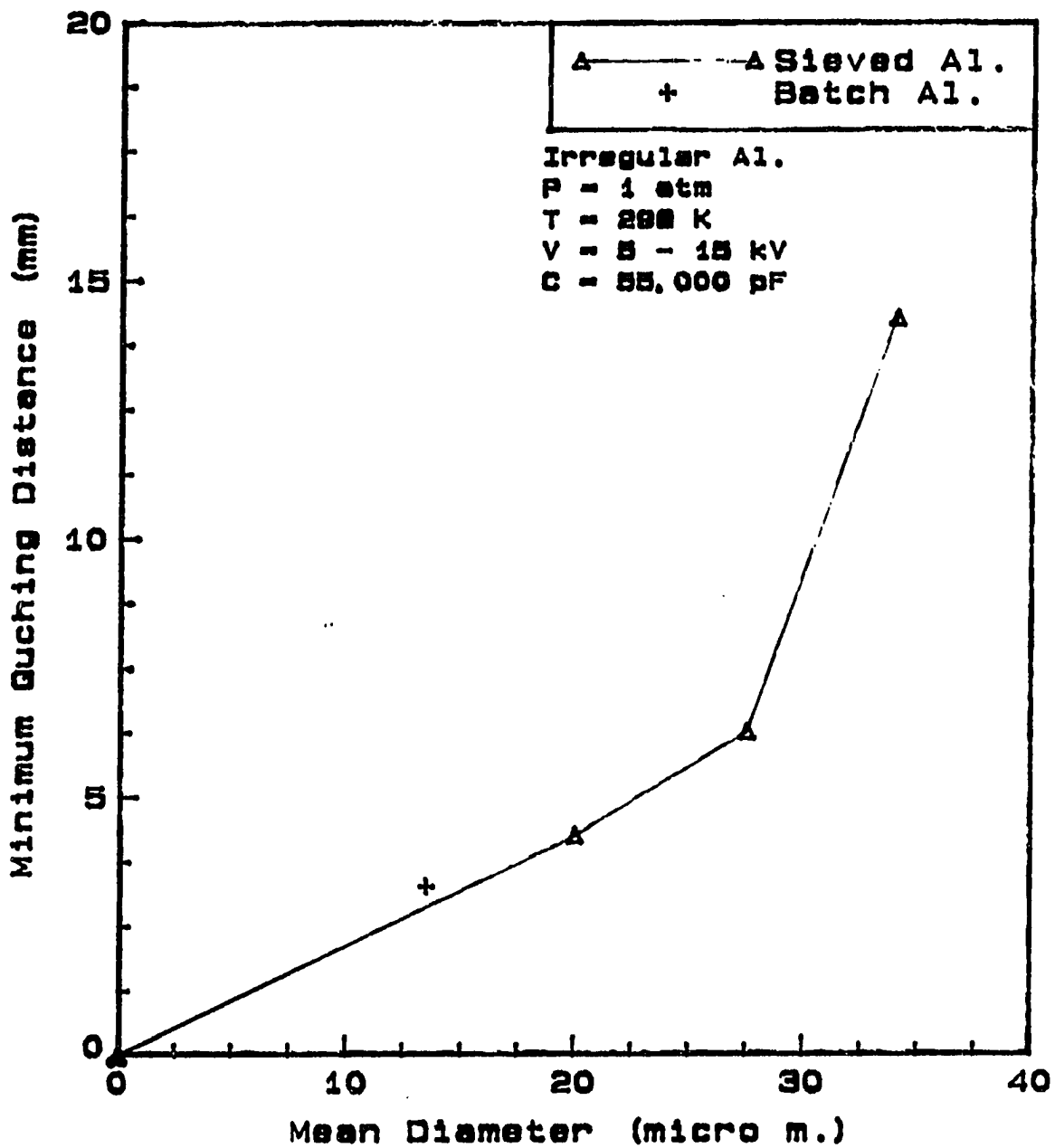


Figure 4.18: Minimum quenching distance vs. particle concentration irregular aluminum particles

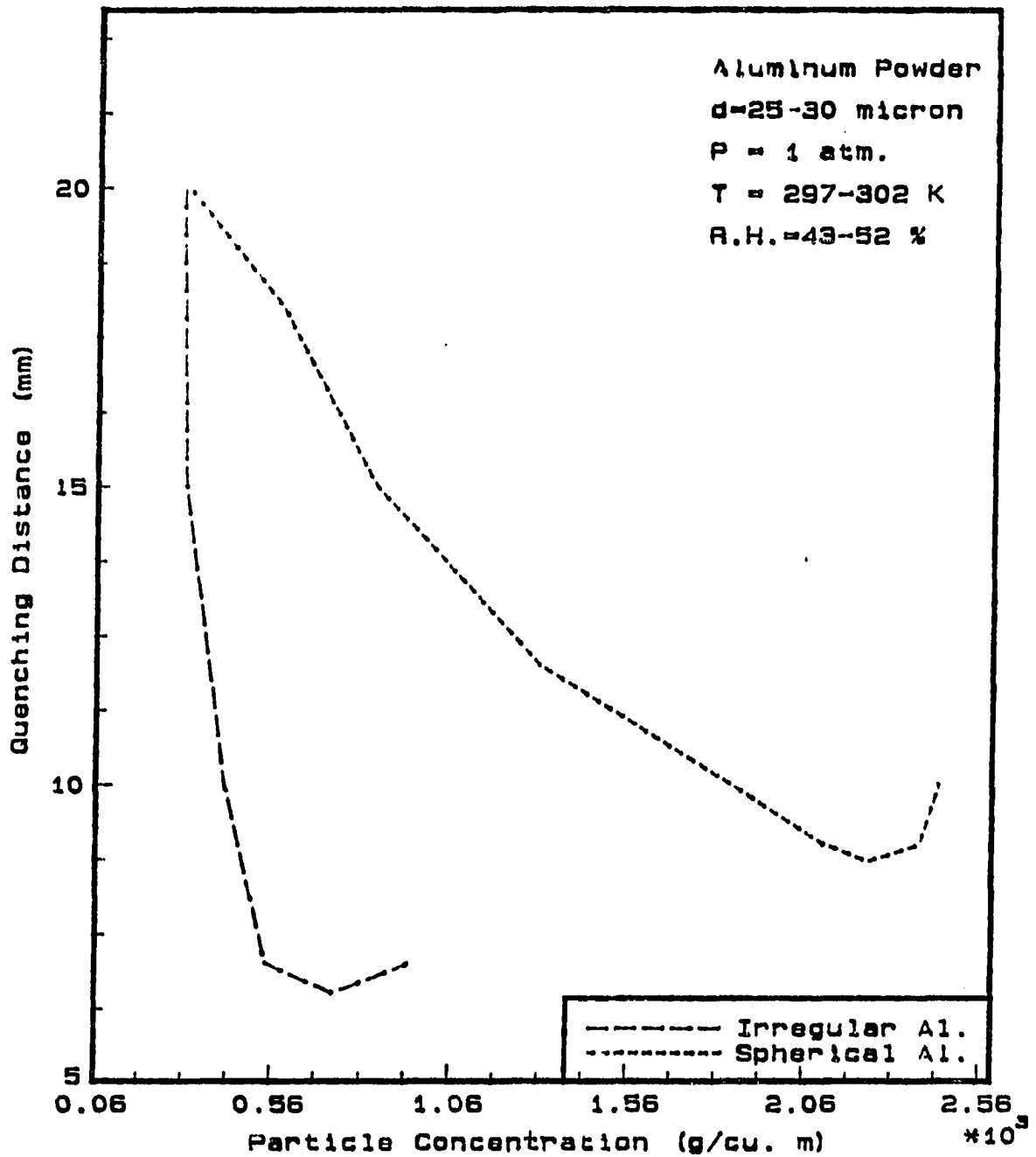


Figure 4.19: Quenching distance vs. particle concentration of spherical and irregular aluminum particles of $27.5 \mu m$ in diameter

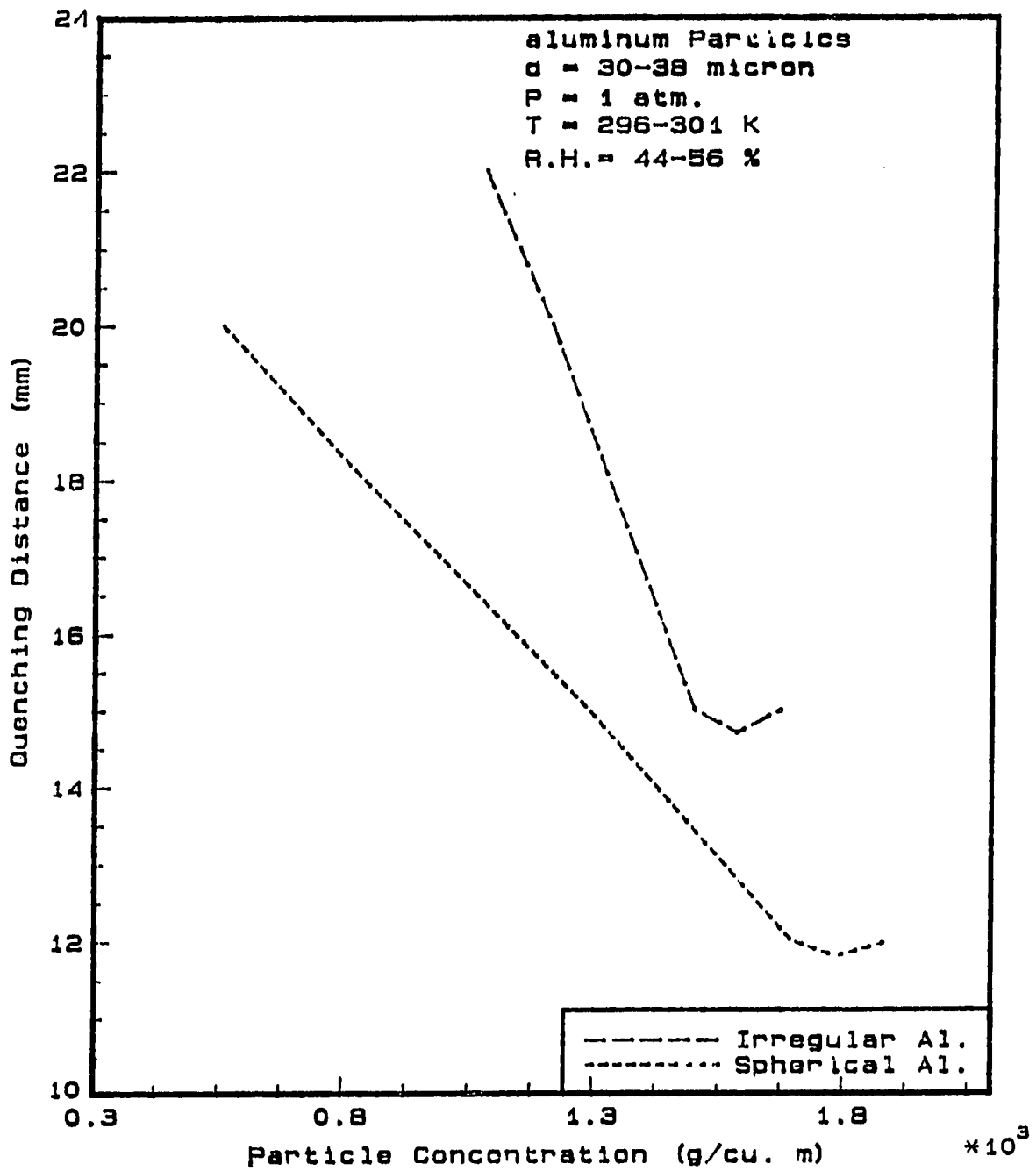


Figure 4.20: Quenching distance vs. particle concentration of spherical and irregular aluminum particles of $34.0 \mu\text{m}$ in diameter

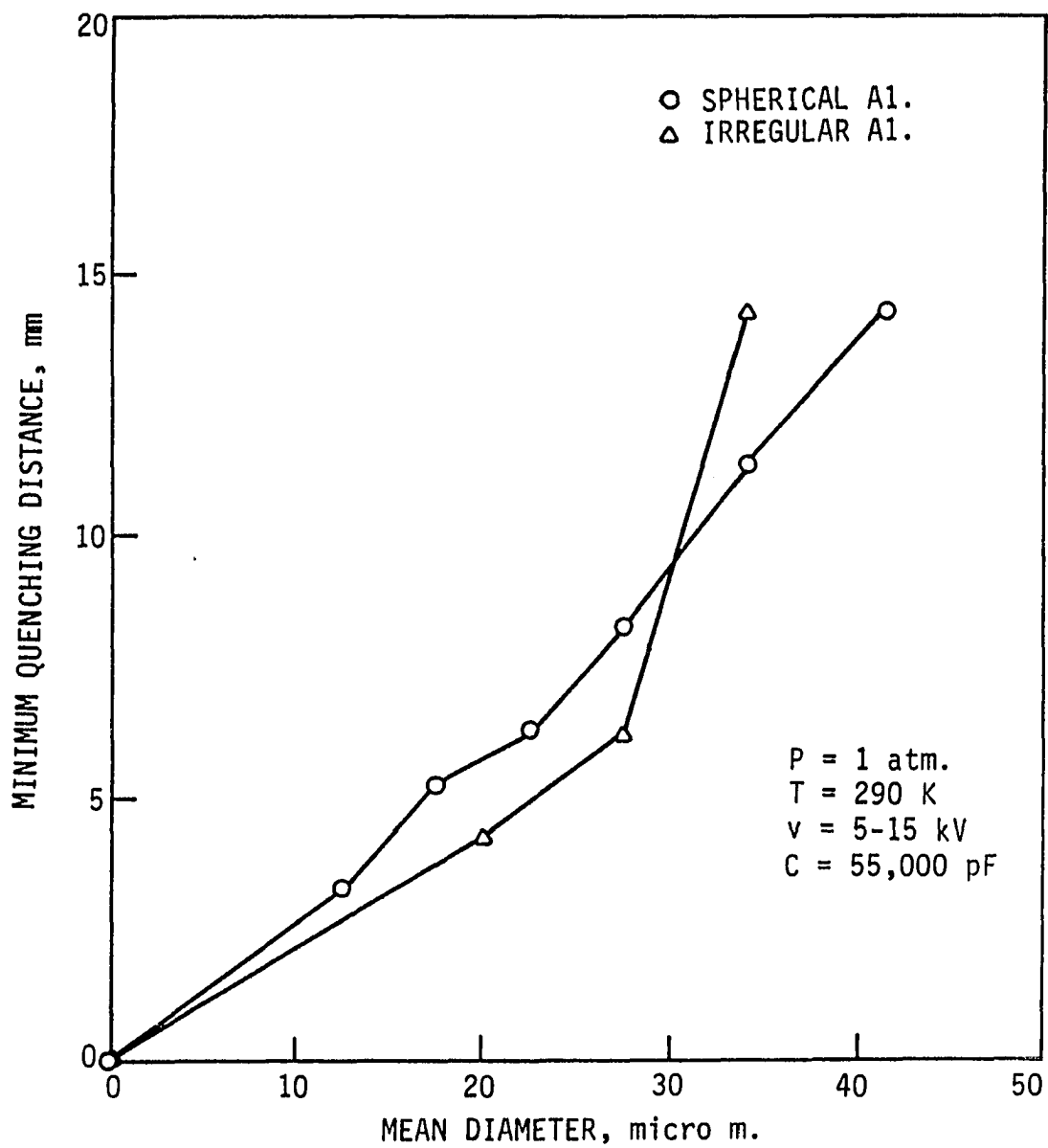


Figure 4.21: Minimum quenching distance vs. particle diameter of spherical and irregular aluminum particles

minimum showed a much stiffer slope than the spherical aluminum at the lean particle concentration ranges. That means, the quenching distance of irregular aluminum changed more rapidly than that of spherical aluminum due to the change of the particle concentration. Figure 4.21 shows the effects of particle size and shape on minimum quenching distance clearly.

4.3.3 Effect of size distribution

Each of the batch samples of irregular and spherical aluminum powders were tested from the can. Spherical batch powder had a mean diameter of $15.4 \mu m$ and irregular batch powder had a mean diameter of $13.4 \mu m$. The size distribution of the batch particles are shown in Figures 4.22 and 4.23.

Figure 4.24 shows the quenching distance of spherical batch powders. The minimum quenching distance for this batch particle was 6.50 mm comparing to 5.60 mm for the mono-sized particle of $17.5 \mu m$ in diameter. That is, batch powder was more difficult to ignite than the mono-sized powder of the same mean diameter.

Figure 4.25 shows the same effect for the irregular batch powders, the batch powder of $13.4 \mu m$ mean diameter had a minimum quenching distance of 3.40 mm which is smaller than the extrapolated quenching distance of 2.90 mm for the mono-sized particle of same mean diameter. But the lean flammability limit was in agreement with the mono-sized particles. Figures 4.16 and 4.18 in previous section also shows the effect of size distributed powders on minimum quenching distance.

The particle motion of batch sampled particles displayed a more turbulent motion of the particles which is thought to have a significant effect on the flame propagation

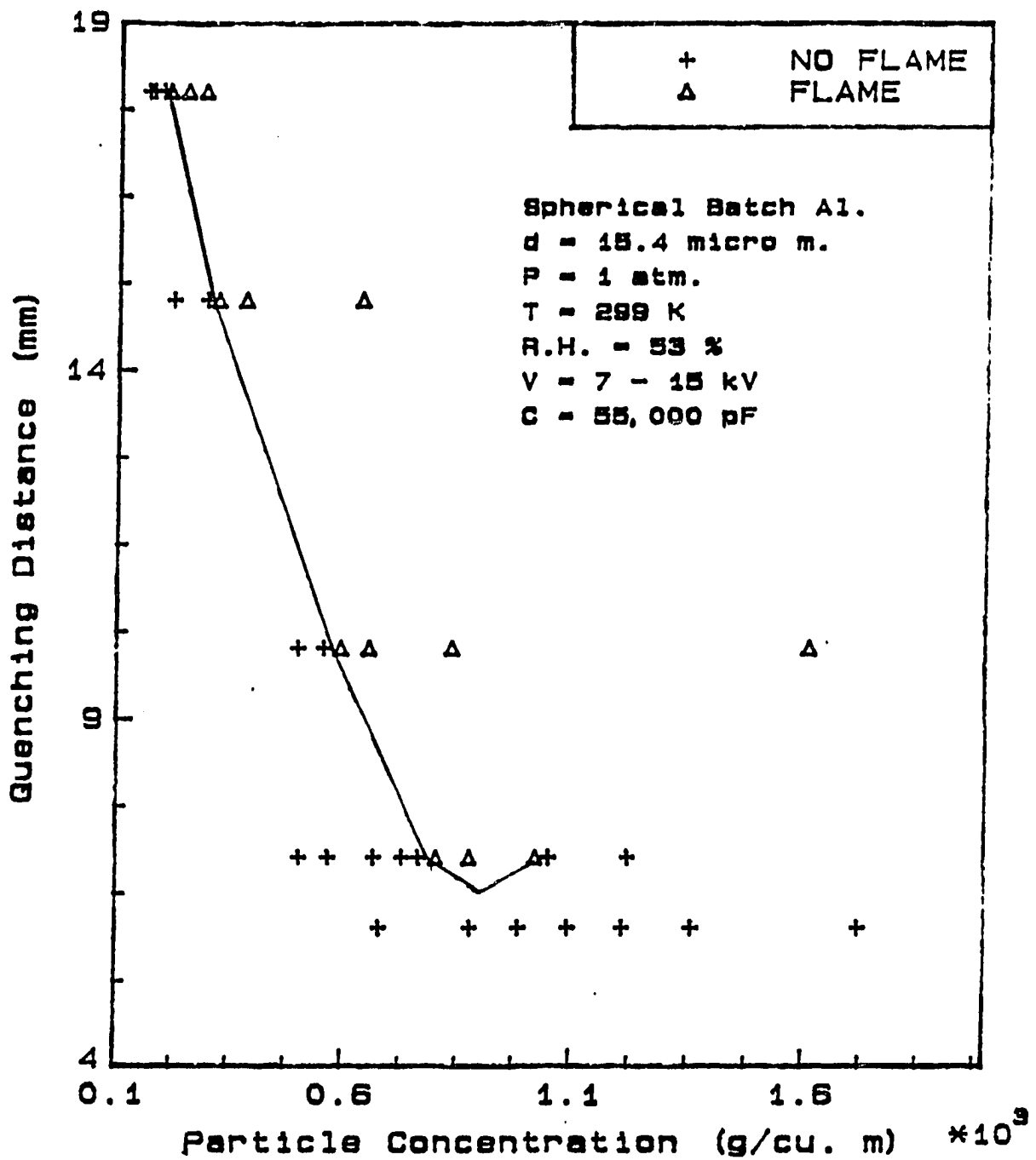


Figure 4.22: Quenching distance vs. particle concentration of spherical batch aluminum particles

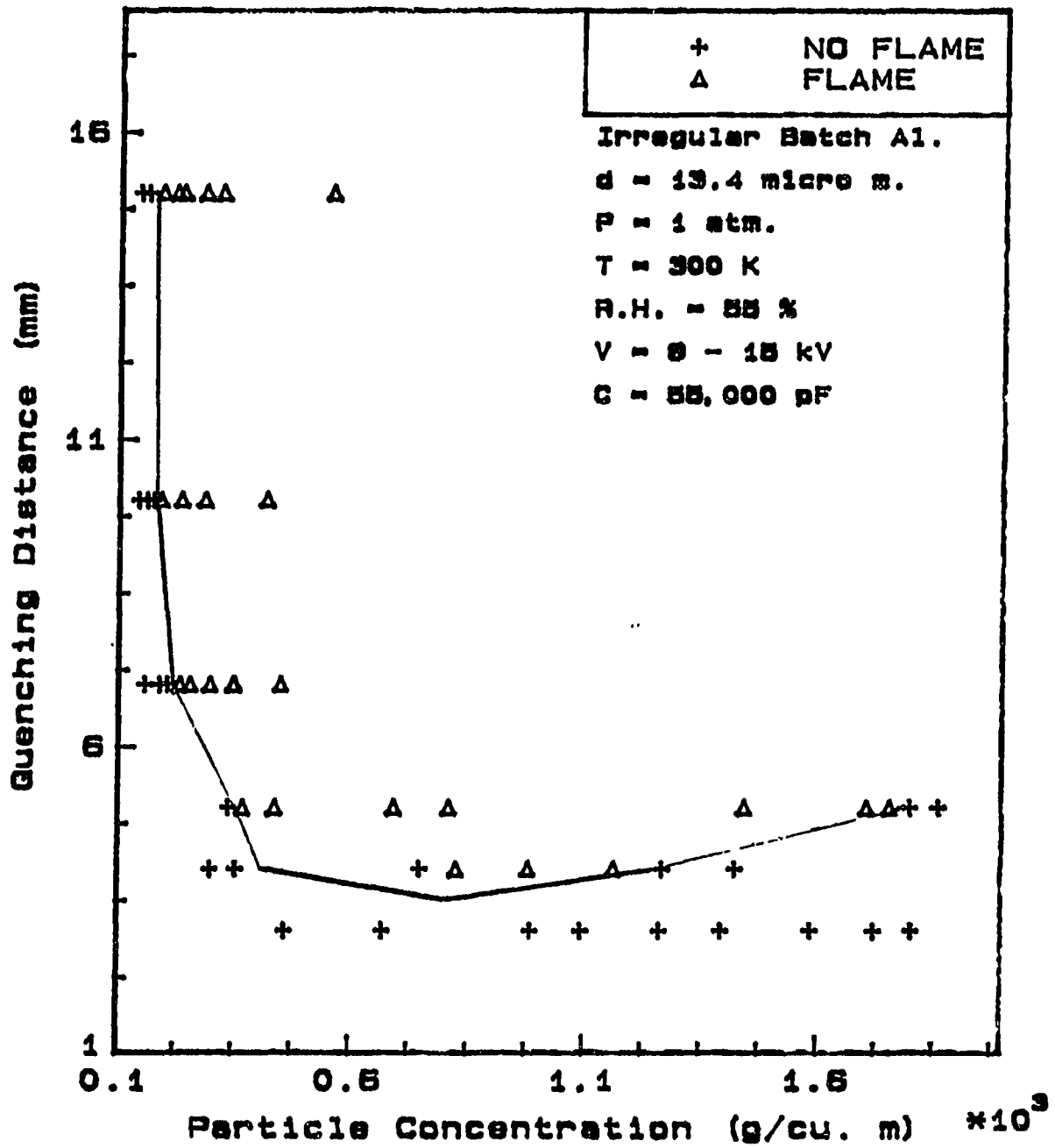


Figure 4.23: Quenching distance vs. particle concentration of irregular batch aluminum particles

behavior. This turbulence can help explain the above result where at high concentrations the bigger sized particles play a dominant role acting as a heat sink, and make the mixture of particles more difficult to ignite.

4.3.4 Effect of moisture content

As the moisture content in the air increases, it is more difficult to ignite the dust clouds. Nagy and Verakis [1983] showed in their work at U.S. Bureau of Mines that the ignition temperature and spark ignition energy increases as the amount of admixed water is increased.

A spherical aluminum of $41.5 \mu\text{m}$ in diameter were tested at various relative humidity ranges, 37 to 60 %. Figure 4.26 shows that as the relative humidity of air increases it requires more particle concentration to ignite the mixture for the fixed quenching distance. For example, for a fixed quenching distance of 18.0 mm, it required 1275.0 g/m^3 for the flame propagation to be observed at the relative humidity of 37 %, but it required 1305.0 g/m^3 at the relative humidity of 60 %. In other words, the quenching distance increased as the relative humidity of air increased for a given particle concentration.

4.3.5 Effect of an ignition energy

Theoretically, when the spark ignition energy is high enough it should not affect the quenching distance data by the change of the ignition energy. The spherical aluminum of $22.5 \mu\text{m}$ in diameter was tested at various external voltages as shown in Figure 4.27. As the voltage increased, the quenching distance decreased. But the

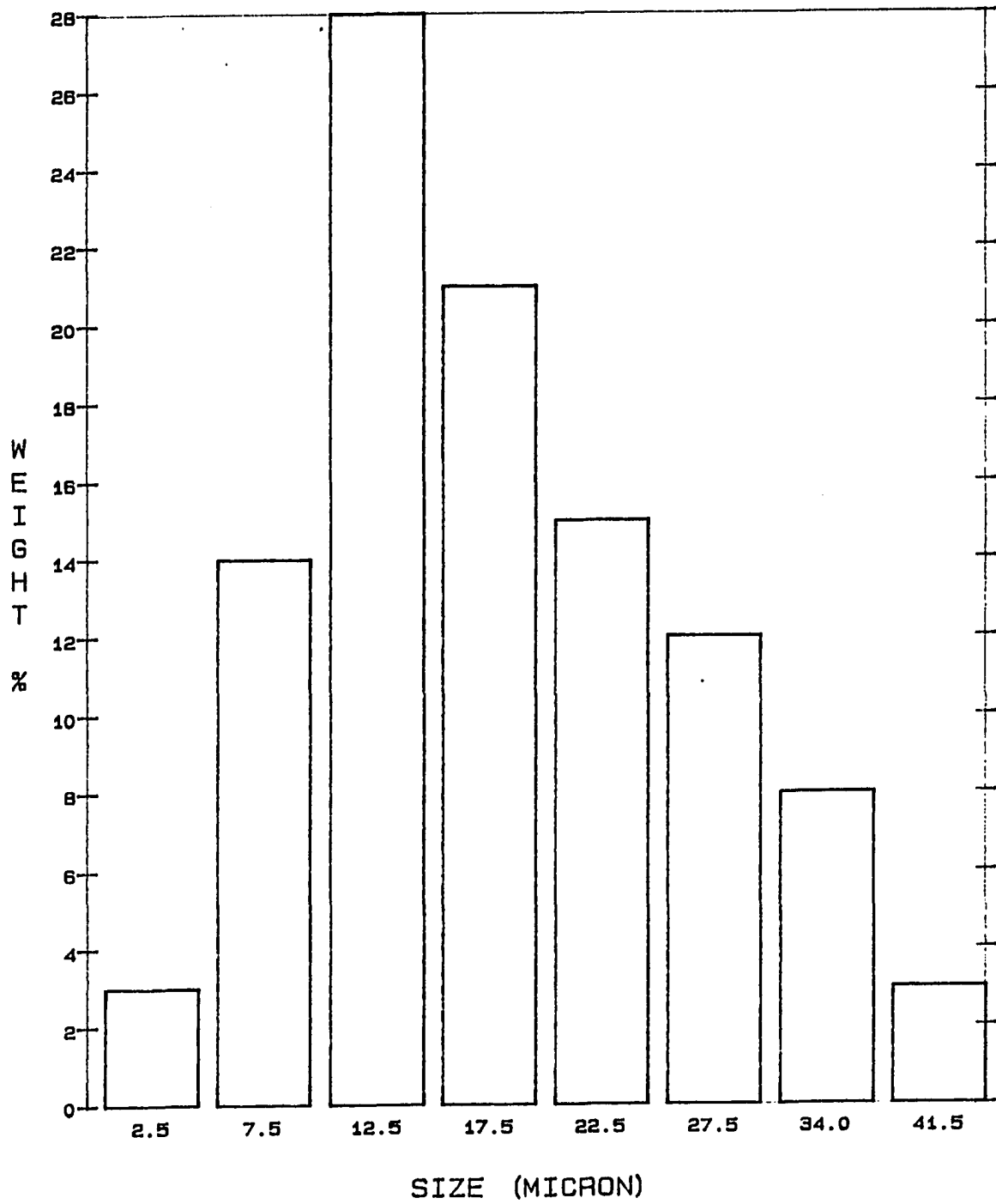


Figure 4.24: Size distribution of spherical batch aluminum particles

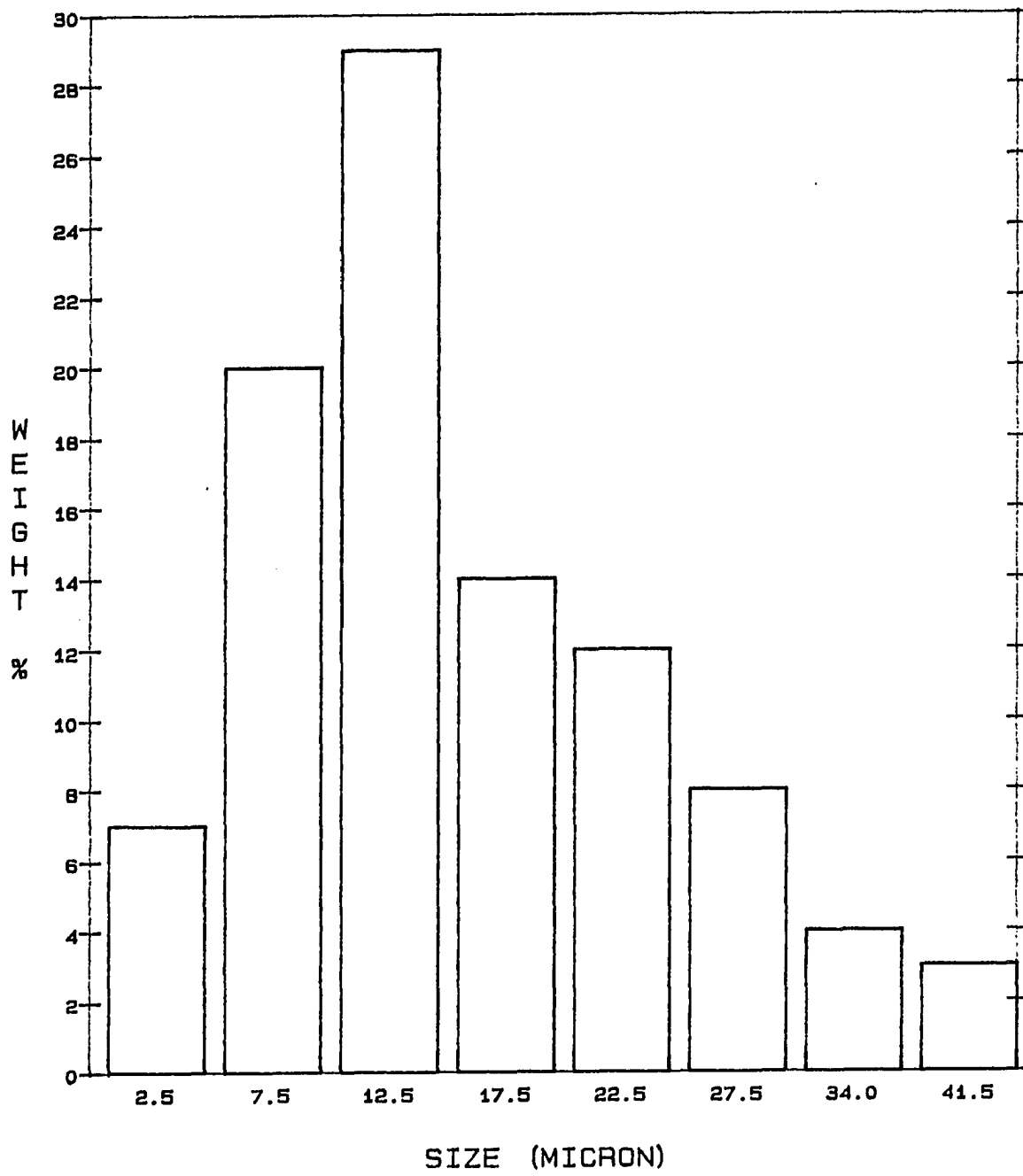


Figure 4.25: Size distribution of irregular batch aluminum particles

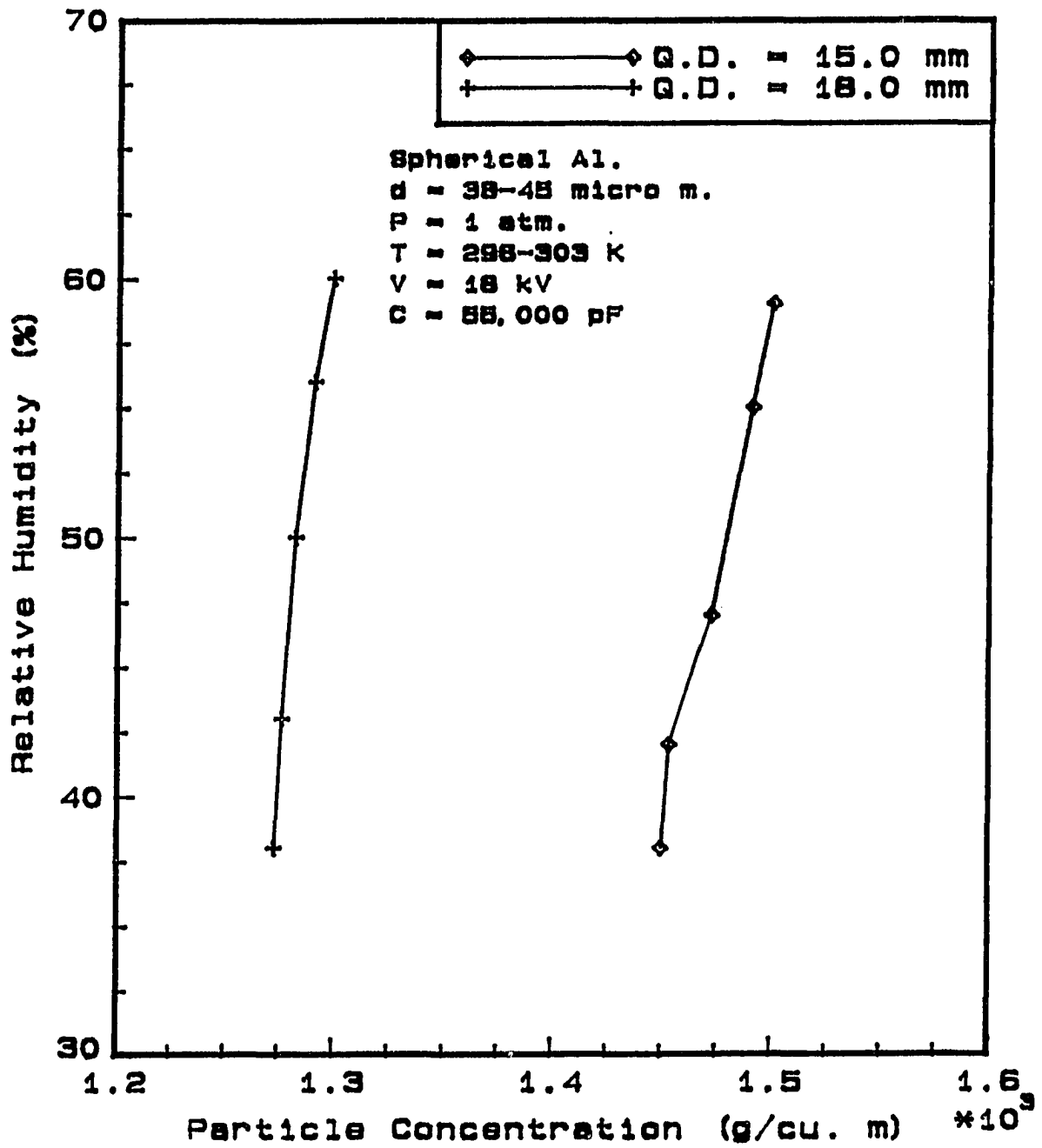


Figure 4.26: Effect of relative humidity on quenching distance of $41.5 \mu\text{m}$ spherical aluminum particles

differences were quite small enough to neglect the effect of an ignition energy. One explanation for the small differences is that stratification of the particle is occurring at the reduced external voltage.

4.4 Burning Velocity of Aluminum-air Flame

Cassel [1964] measured the burning velocities of aluminum particles for particles less than $10 \mu m$ in diameter using a Bunsen burner stabilized flames 1.4 cm and 1.9 cm diameter. He reported values of 50 cm/sec and 40 cm/sec for a 1.4 cm diameter and a 1.9 cm diameter respectively. Nagy and Lenoir [1970] reported a burning velocity of 7 cm/sec for the particle concentration of $500 g/m^3$ in a Hartmann tube.

Ballal [1983a] measured the burning velocities of $11 \mu m$ and $38 \mu m$ mean diameter aluminum particles using his zero-gravity combustion chamber. He measured the burning velocities in the concentration range from $100 g/m^3$ to stoichiometric concentration of $306.5 g/m^3$. His values are close to Cassel's values. At the stoichiometric concentration using $11 \mu m$ mean diameter particle, Ballal reported the value of 42 cm/sec.

The burning velocity of spherical aluminum of size ranges from 12.5 to $41.5 \mu m$ are tested. A high speed photographic method was used to measure the flame front position with time. A video camera as well as high speed camera was used to measure the burning velocity. The difficulties encountered with the video camera due to the slow recording speed (30 frames/sec) were overcome by carefully observing the 16 mm film taken using a high speed camera at the speed of 400 frames/sec which could precisely distinguish the starting point of the flame and the position of the flame front.

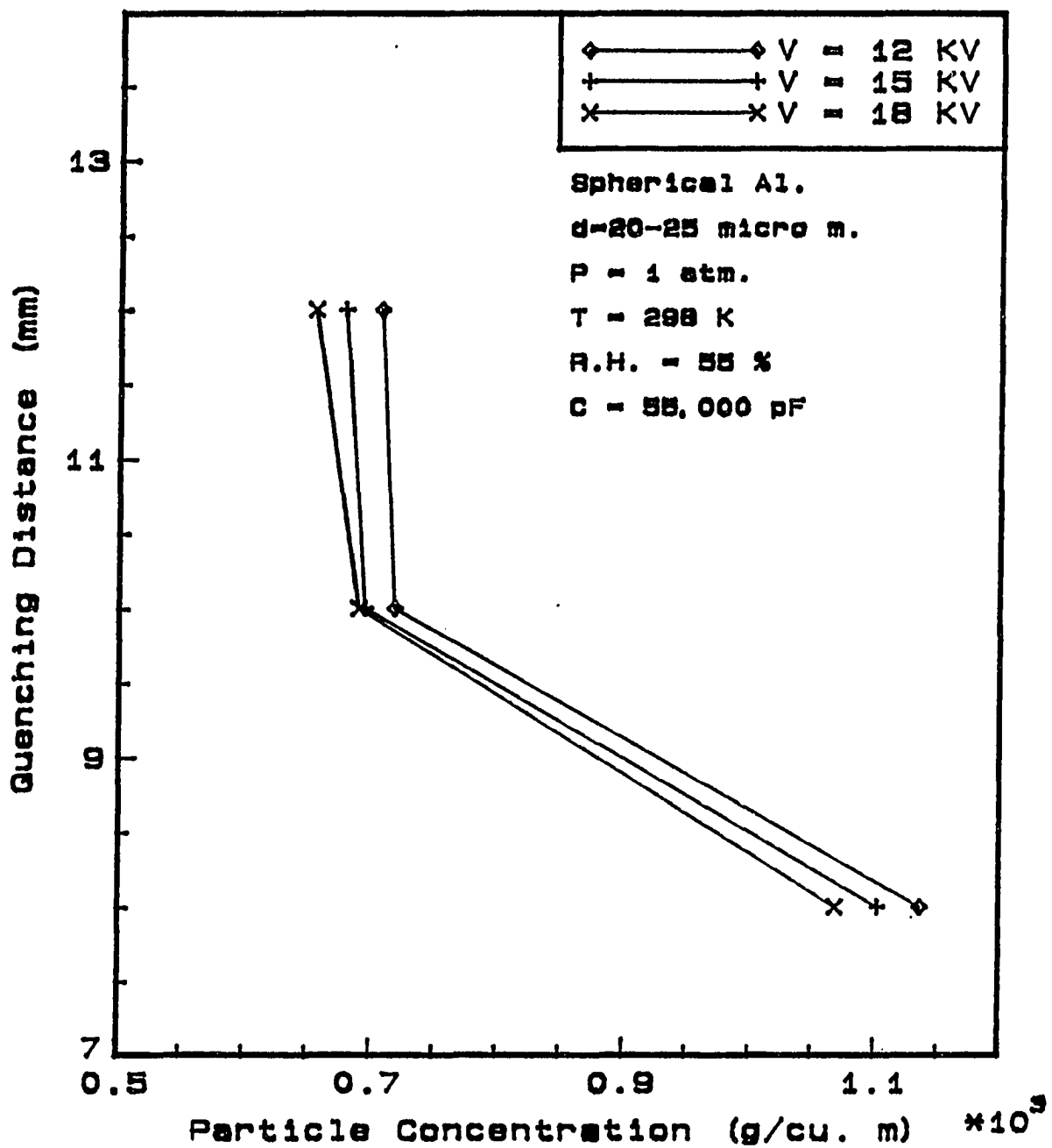


Figure 4.27: Effect of ignition energy on quenching distance of $22.5 \mu\text{m}$ spherical aluminum particles

A video camera has the advantage of being an economical and convenient method, but has the disadvantage of being too slow to analyze the flame front exactly. Thus, for video camera, each data point was averaged after at least 3 times of repetition. The error was within $\pm 20\%$.

4.4.1 Flame propagation behavior

The flame propagation characteristic of three different sizes of aluminum powder were determined. Figure 4.28 shows the photographs of flame propagation of $27.5\ \mu\text{m}$ aluminum powder at a particle concentration of $810.0\ \text{g}/\text{m}^3$. The photographs are taken by the high speed camera. Successive frames in Figure 4.28 are shown at about every $8/100$ second. The pictures clearly show the movement of flame front of an aluminum-air flame.

The movement of the flame front for each of the three aluminum samples were observed by recording and the distance of travel of the flame front from the center of the electrode with time. It is shown in Figure 4.29. The flame moves almost linearly with time. The flame velocities for each of three samples were determined by dividing the flame front travelling distance by the corresponding time. They are shown in Figure 4.30. The burning velocity is seen to increase linearly to a steady-state value. The steady burning velocity for $17.5\ \mu\text{m}$ aluminum particles at $783.2\ \text{g}/\text{cm}^3$ concentration is $39.0\ \text{cm}/\text{sec}$. This value is very close to the value of Ballal [1983a], $42\ \text{cm}/\text{sec}$. The steady burning velocity for $34.0\ \mu\text{m}$ particles at $626.8\ \text{g}/\text{cm}^3$ is $28.0\ \text{cm}/\text{sec}$ and the burning velocity for $27.5\ \mu\text{m}$ particles at $810.0\ \text{g}/\text{cm}^3$ is $38.0\ \text{cm}/\text{sec}$ which is very close to that of the $17.5\ \mu\text{m}$ particles. A sudden rise in the flame

velocity for the initial few milliseconds is thought to be due to the effect of ignition energy.

4.4.2 Effect of particle concentration

The burning velocity for each size of aluminum particles was measured for various particle concentrations starting with the lean flammability limit into the rich concentrations. Figures 4.31, 4.32, 4.33 show the effect of particle concentration on burning velocity for three spherical aluminum particles, 12.5, 17.5, and 22.5 μm respectively.

For 12.5 μm particles, the maximum burning velocity is 44.0 cm/sec which occurs at 420.0 g/cm^3 . Maximum burning velocities of 36.5 cm/sec and 33.5 cm/sec are obtained at 570 and 760 g/cm^3 for 17.5 and 22.5 μm particles respectively.

Generally, the burning velocity is seen to increase rapidly until it reaches a maximum value then decreases slowly as the particle concentration increases.

4.4.3 Effect of particle size

Figure 4.34 shows the effect of particle size. The maximum burning velocity increases as the particle size decreases. The particle concentration at the maximum burning velocity increases with an increase in the particle size.

The effect of particle size is sensitive to particle size at the lean particle concentration ranges, and becomes less sensitive for the rich concentration ranges. Also, the burning velocity is observed to increase with a decrease in particle diameter in the lean concentration ranges but decreases with a decreases in particle diameter at rich

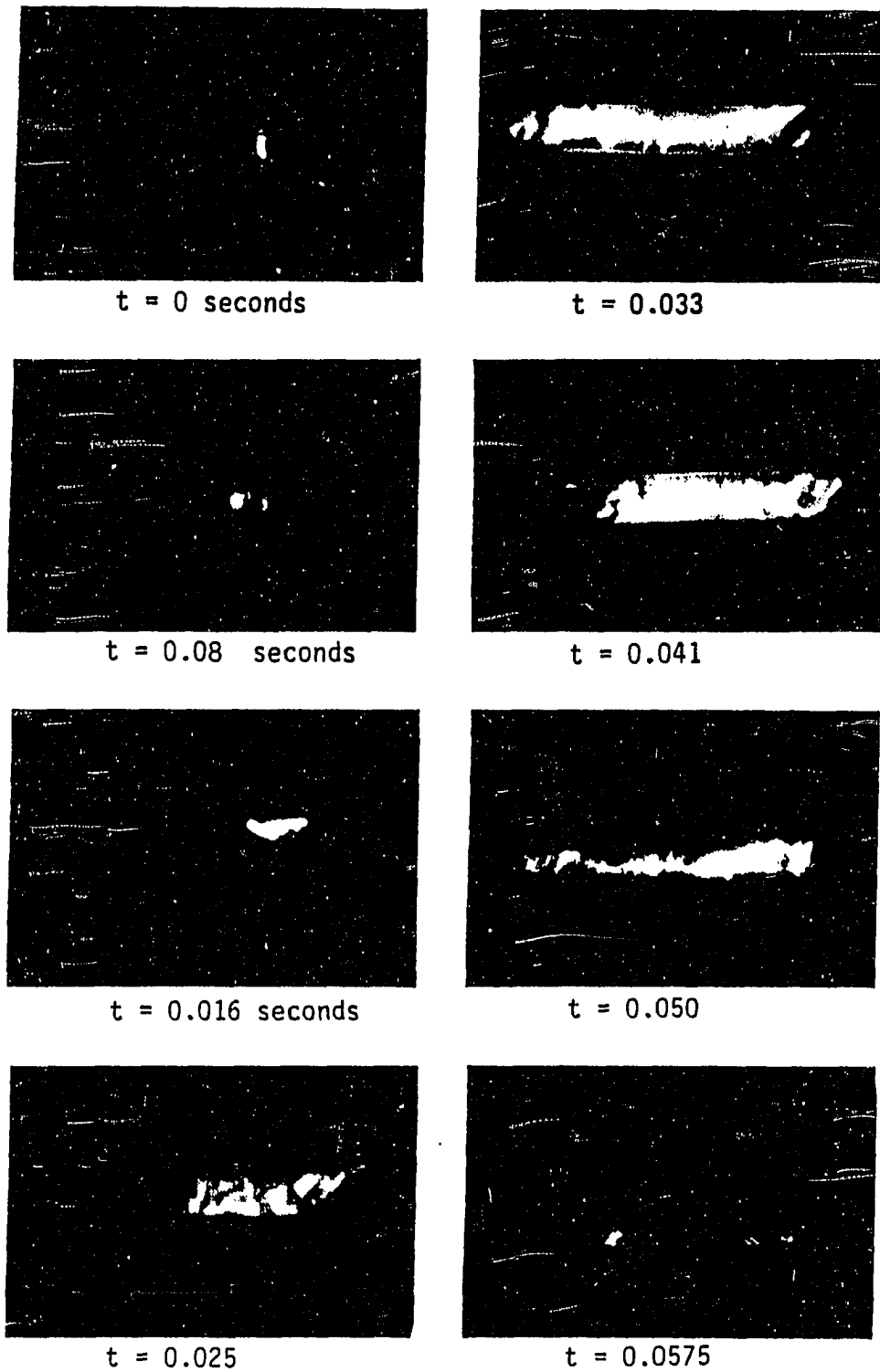


Figure 4.28: Photographs of flame propagation of 27.5 μm spherical aluminum powder

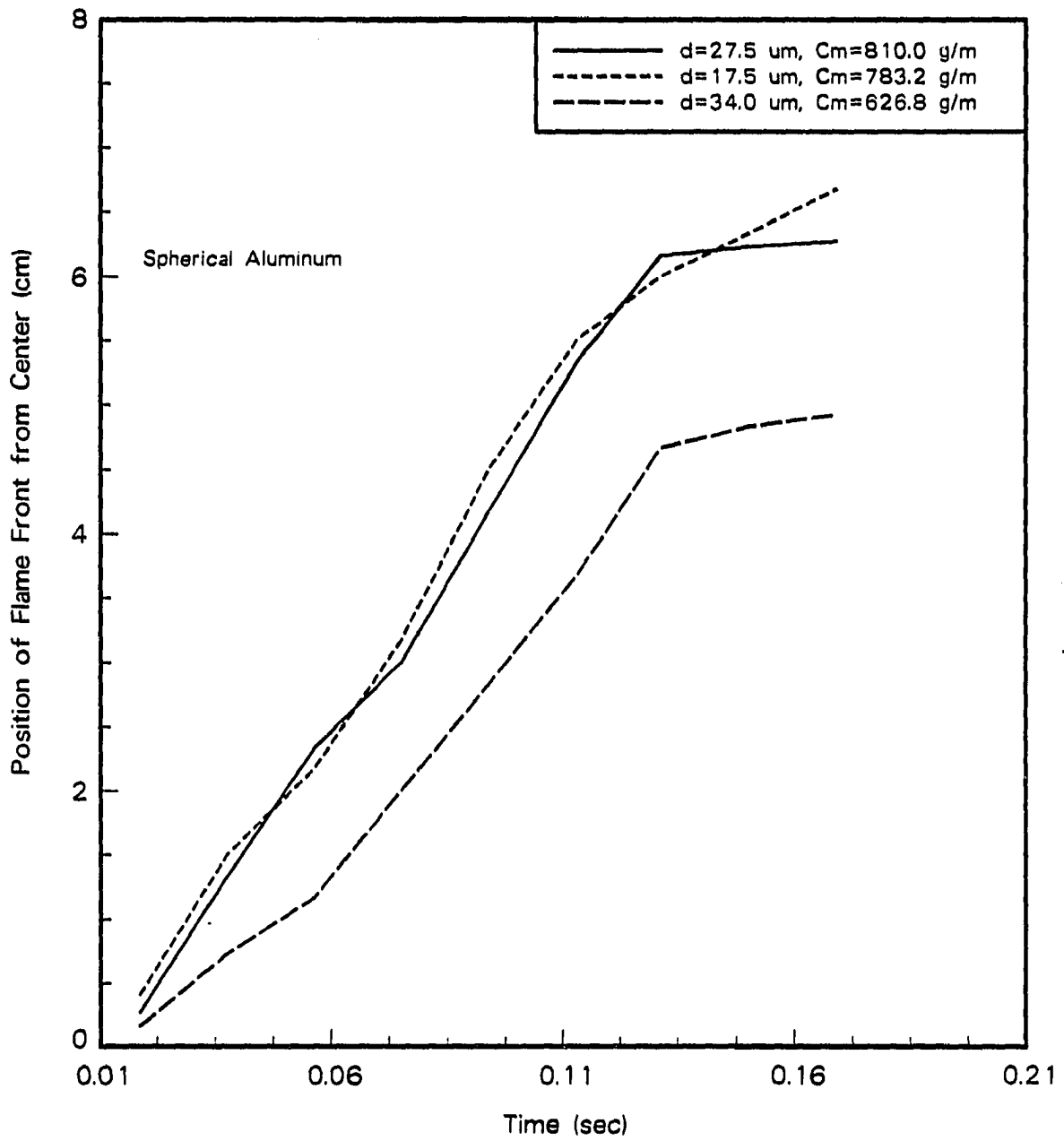


Figure 4.29: Distance of flame front with time

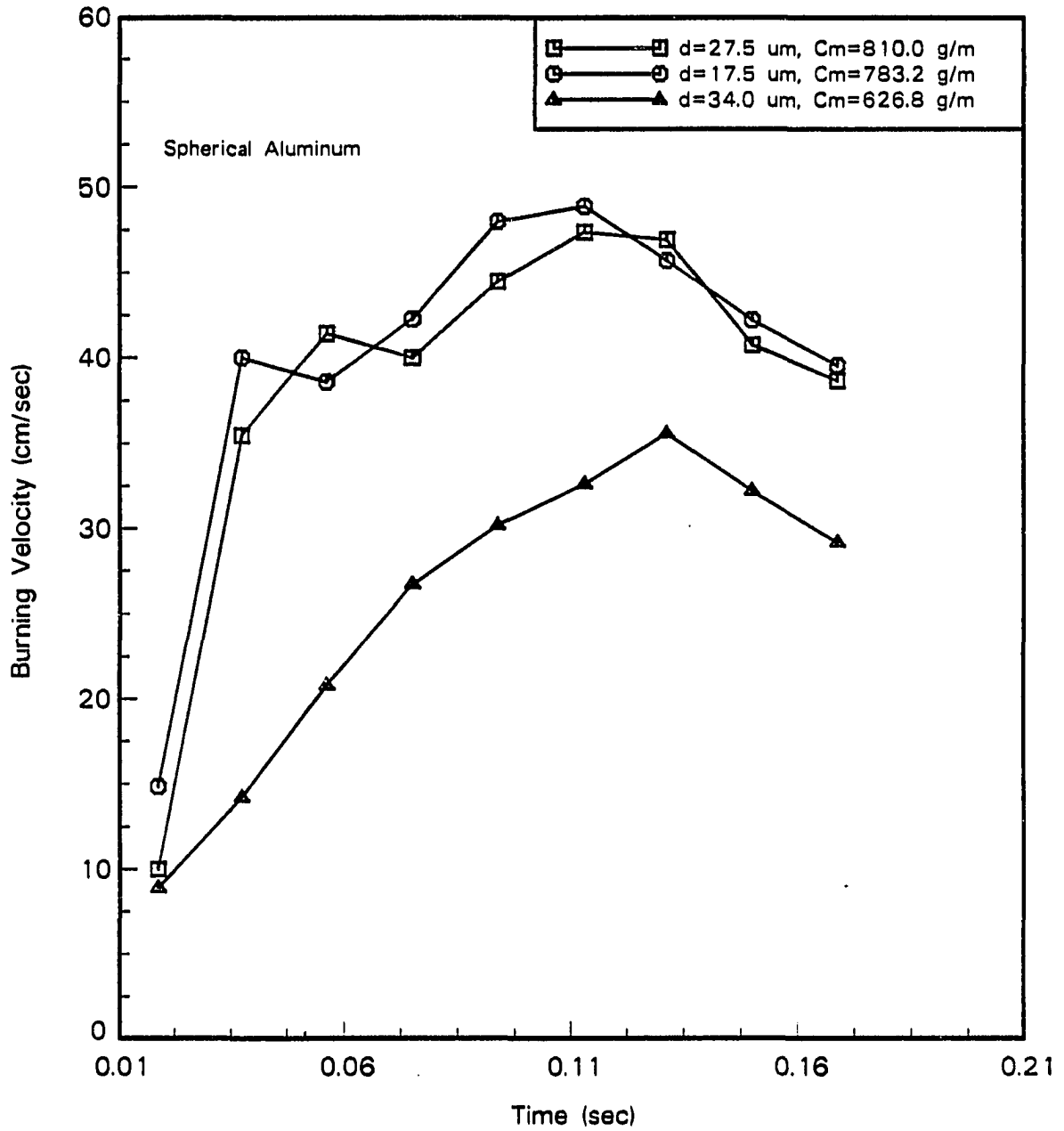


Figure 4.30: Burning velocity vs. time of three aluminum powders

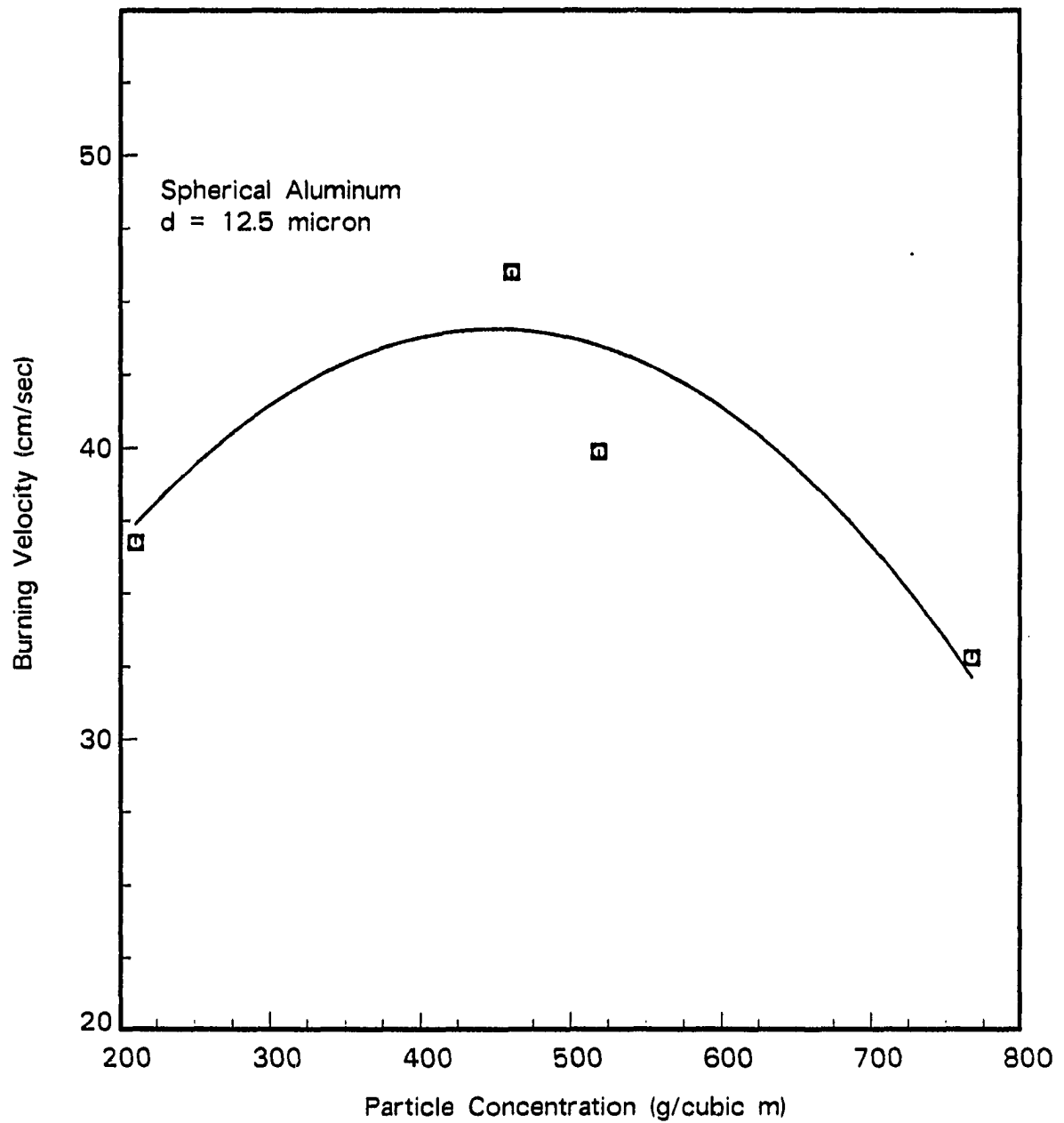


Figure 4.31: Burning velocity vs. particle concentration of 12.5 μm aluminum particle

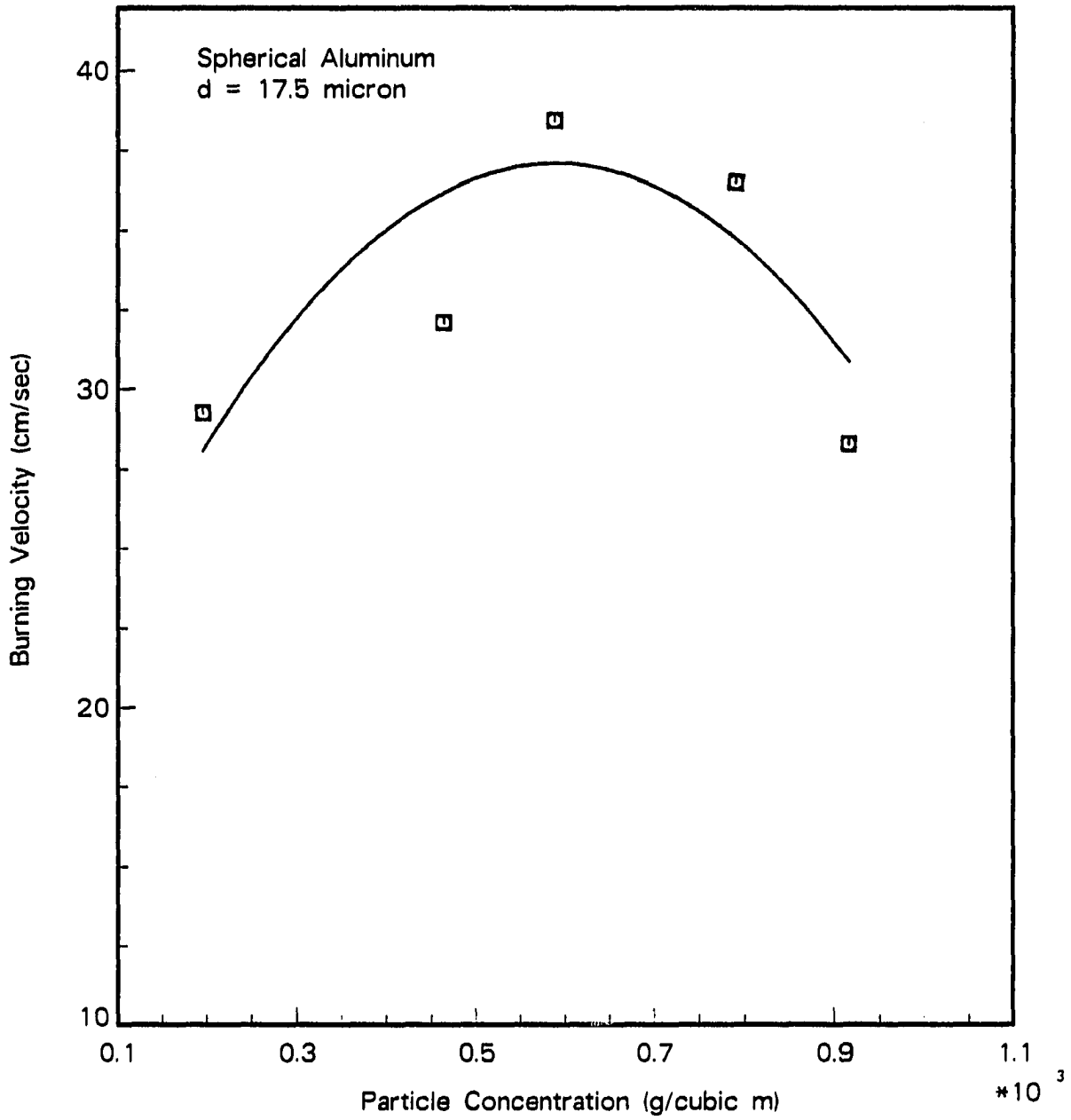


Figure 4.32: Burning velocity vs. particle concentration of 17.5 μm aluminum particle

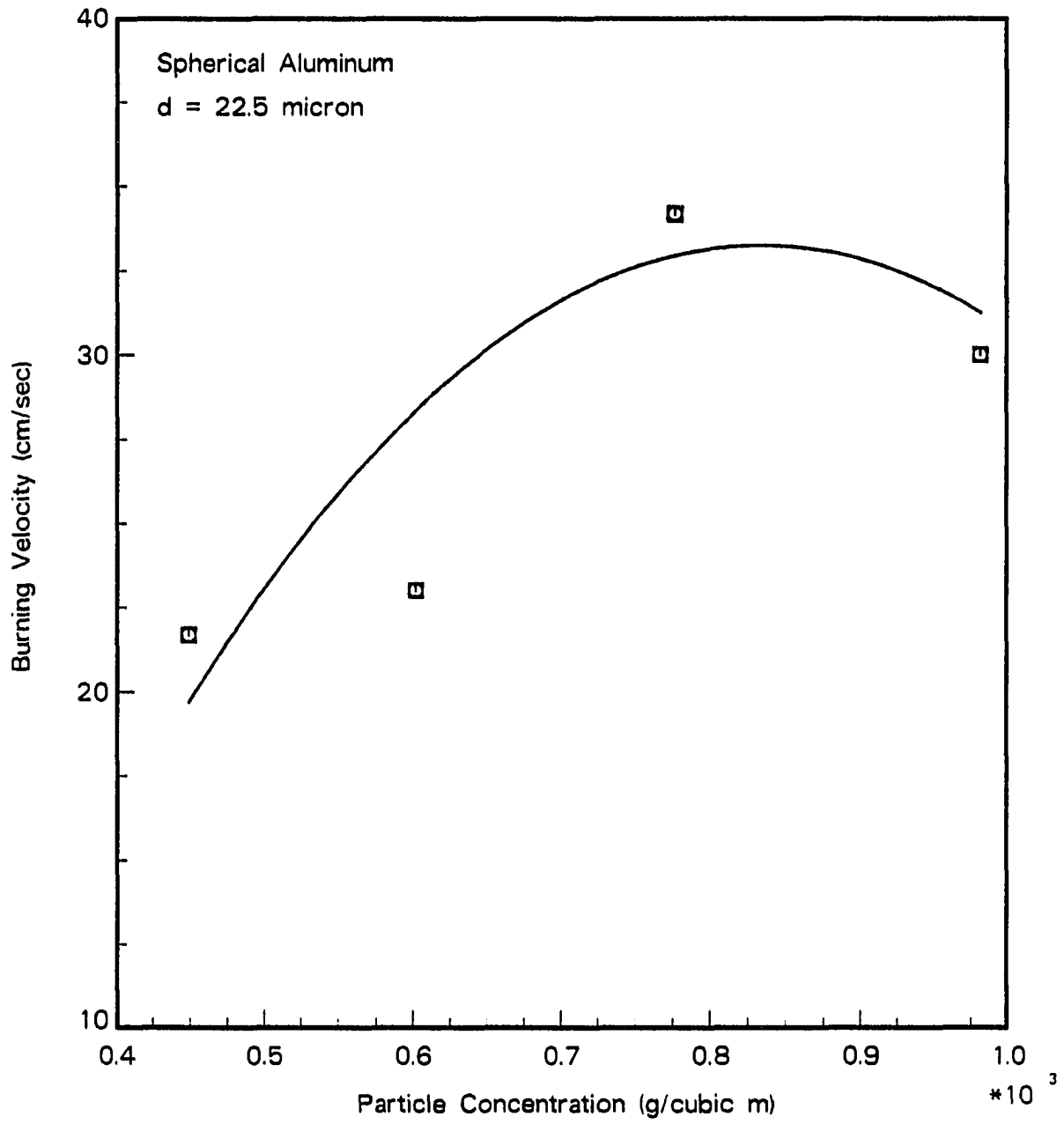


Figure 4.33: Burning velocity vs. particle concentration of 22.5 μm aluminum particle

concentration ranges, above 700.0 g/m^3 in this case.

4.5 Conclusion

An electrostatic particulate suspension system with an adjustable needle electrode spark ignition system has been developed for this study. The quenching distance of methane-air flame was measured and compared with previous researcher's data to justify the experimental technique and apparatus used in this study. The result shows that quenching distance and flammability limits measured in this study are in agreement with the results found by other researcher.

The quenching distances of aluminum powder were found to be greatly influenced by particle concentration, size, shape, and size distribution. Generally, the quenching distance was observed to increase with a increase of particle size. The quenching distance decreases until it reaches a minimum then increases as the particle concentration increases. Irregular aluminum has a smaller quenching distance than that of spherical aluminum of the same mean diameter below particle diameter of $25 \mu\text{m}$, but the reverse is true for particles above $25 \mu\text{m}$. Batch aluminum powders were found to have a higher quenching distance than mono-sized aluminum powder of same mean diameter.

The burning velocity of spherical aluminum powder was determined using a photographic method with the effect of particle size and concentration being studied. The burning velocity increases as the particle size increases and increases until it reaches a maximum then decreases as the particle concentration increases.

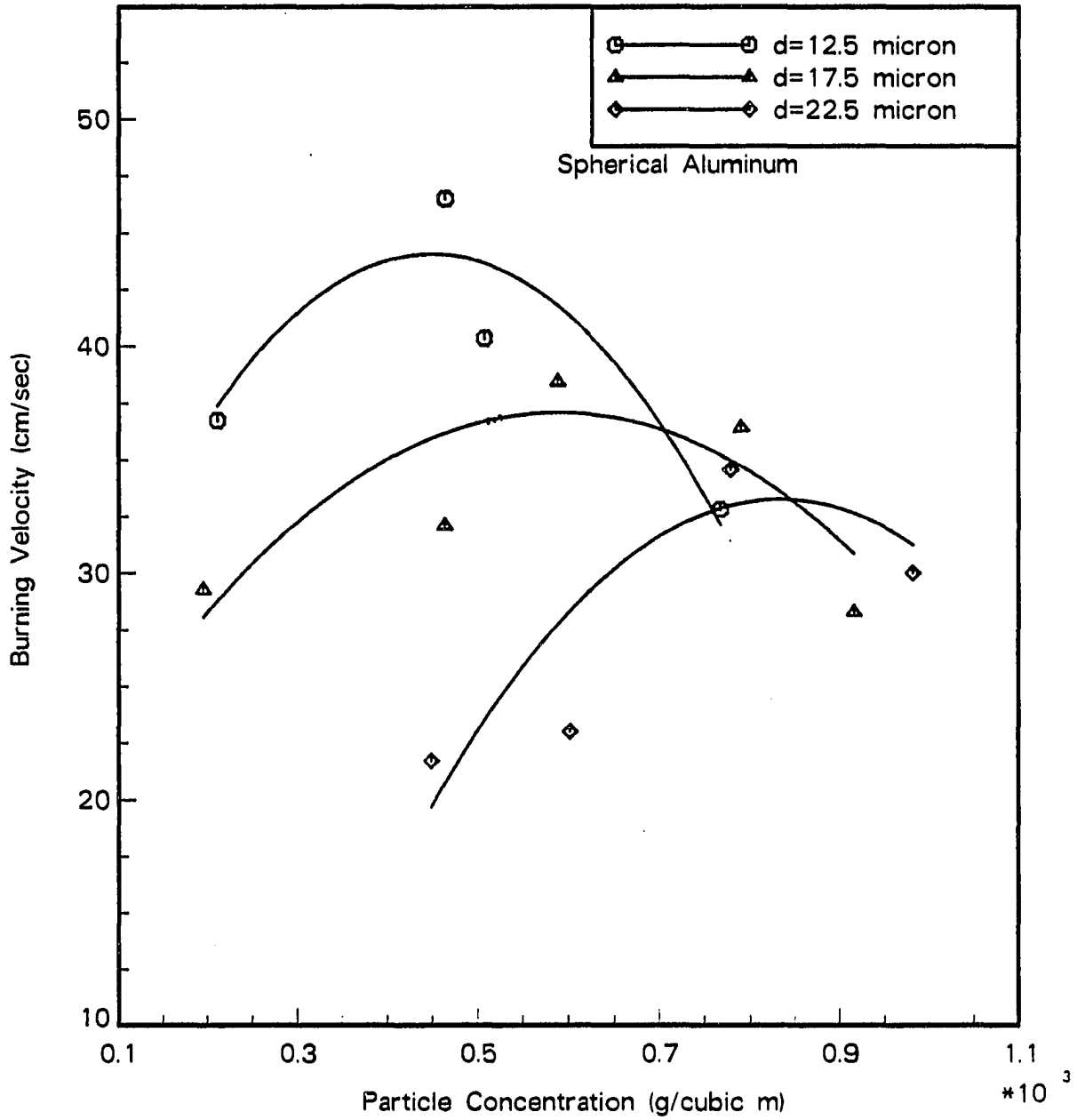


Figure 4.34: Burning velocity vs. particle concentration of three particle sizes

5 FLAME PROPAGATION AND QUENCHING OF COAL PARTICLES

5.1 Experimental Technique and Procedure

An electric suspension of coal powder was generated with the aids of vibration and air flow into the test section. A light absorption method was used for the measurement of the particle concentration.

The experimental procedure used for the quenching tests on coal flames is as follows:

1. Set the electrode gap distance large enough distance for flame ignition and propagation, around 30.0 mm.
2. Adjust the needle electrode penetrating distance so that the needle doesn't affect the particle motion but be able to initiate a spark when the uniform suspension of coal particulate clouds are accomplished.
3. Put the coal powder inside the glass container.
4. Set the frequency of the function generator at a very low frequency with an amplitude of few millimeters, around 100 Hz, to vibrate the test section so that the coal powder can be distributed all around the lower electrode.

5. Turn on the He-Ne laser and align the particle suspension monitoring system so that the laser beam passes through the center of the test section such that the intensity of the beam without the particle, I_0 , is as large as possible.
6. Turn on the air flow so that only a small amount of coal particles escape through the openings at the bottom of the glass cylinder.
7. Set the frequency of the function generator around 750 Hz, for the best suspension of coal particles and a low amplitude such that particles are not suspended.
8. Apply the electric field.
9. Increase the amplitude of the function generator until a uniform suspension is formed and a large amount of coal powders is observed to be in suspension.
10. Record the intensity of the laser beam with the laser power meter and oscilloscope.
11. Increase the electric field until spark breakdown occurs and test for propagation of a flame visually.
12. Repeat the above procedure for the whole range of particle concentrations until the lower and/or upper flammability limits are obtained.
13. Decrease the electrode gap distance and repeat the above procedure.
14. When no flame propagation is observed over the whole range of particle concentrations at some fixed electrode gap distance, stop the experiment. That

electrode gap distance is the minimum quenching distance for the type and size of coal particle.

The experimental procedure for the measurement of burning velocity of coal is same except the electrode gap distance is maintained at a large enough distance so that the effect of quenching can be neglected. That is, in this research, only the adiabatic burning velocity is measured. Thus, burning velocity is measured at a varying particle concentrations and a fixed electrode gap distance, starting from the lean flammability limit obtained from the quenching data.

5.2 Quenching of Coal-air Flame

To date, relatively little data are known for coal powder in regards to its quenching distance. Pioneering work on the behavior of coal dust-air mixtures has been carried out at the Pittsburgh Mining and Safety Research Center. Litchfield [1981] reported a quenching distance of about 1 cm for the coal dust tested. Powell [1962] reported that a coal dust-air flame could not propagate through tubes less than 14 cm in diameter. Recently, Jarosinski et al. [1986] gave the minimum quenching distance of 25.0 mm for less than 5 μm using Devco no. 26 bituminous coal (32.1 % V.M.).

In the present study, five different type of coal with a different volatile contents was sieved in 3 - 4 size ranges, from 9.1 to 36.6 μm , and tested.

5.2.1 Effect of particle concentration

As with flammable gases, combustible dusts when mixed with air exhibit upper and lower explosion limits. These limits are well defined for gases where combustion

reaction involves homogeneous mixtures of molecular-size particles. For dusts, the upper flammability limit is difficult to determine since uniform particle concentrations are virtually impossible to achieve. The lean flammability limit is the smallest suspension density of particles that is capable of igniting and propagating a flame, and is somewhat dependent on the particle size. At dust concentrations below this limit, the particles are separated by relatively large distances, the heat liberated by the oxidation of single particle is not sufficient to ignite adjacent particles. Above the upper flammability limit, which may be of the order 5 to 10 times the stoichiometric particle concentration, the particles are so densely packed that ready access of oxygen necessary for combustion is prevented, and flame propagation is inhibited. The quenching distance measured for coal was found to be much higher than that of aluminum. Generally, quenching distance of coal decreases until it reaches a minimum and then increase as the particle concentration increases.

5.2.1.1 Lower Kittaining coal Lower Kittaining coal of 3 different size ranges are tested. This coal has the lowest volatile content (16.9 %) among the five type of coals tested in this research.

For 16.7 μm particles, the minimum quenching distance measured was 15.50 mm at a particle concentration of 274.0 g/m^3 , which is 1.3 times higher than the stoichiometric concentration (210.0 g/m^3). The lean flammability limit was 180.0 g/m^3 as shown in Figure 5.1. The minimum quenching distance is determined to be the average value between highest separation distance that quenches the flame and the lowest separation distance that propagates a flame.

Figure 5.2 shows the results for 25.5 μm coal powder. The minimum quenching

distance is 19.50 mm at a particle concentration of 402.0 g/m^3 . The lean flammability limit is 230.0 g/m^3 .

The minimum quenching distance for $36.6 \mu\text{m}$ particle is 25.50 mm at a particle concentration of 484.0 g/m^3 . The lean flammability limit is 290.0 g/m^3 . Their values are shown in Figure 5.3. Larger size coal particles were tested, but it was impossible to ignite them.

5.2.1.2 Illinois no. 6 coal Illinois no. 6 bituminous coal with a 27.9 % volatile content was tested for three particle size ranges. For $16.7 \mu\text{m}$ in diameter particle, the minimum quenching distance is 13.50 mm at a particle concentration of 320.0 g/m^3 which is 1.5 times higher than the stoichiometric concentration as shown in Figure 5.4. The lean flammability limit is 170.0 g/m^3 .

Figure 5.5 shows the result for $25.5 \mu\text{m}$ particles. The minimum quenching distance is 16.5 mm at a particle concentration of 398.0 g/m^3 . The lean flammability limit is 220.0 g/m^3 .

Figure 5.6 shows the results for $36.6 \mu\text{m}$ particles. The minimum quenching distance is 22.5 mm at a concentration of 438.0 g/m^3 . The lean flammability limit is 290.0 g/m^3 .

5.2.1.3 Penn. Seam coal A third type of coal tested was a Penn. Seam coal having a 34.4 % volatile content. This type of coal was sieved in four size ranges and tested. For the $9.1 \mu\text{m}$ particle size, the minimum quenching distance is 9.5 mm at a particle concentration of 290.0 g/m^3 which is 1.4 times higher than the stoichiometric concentration. The lean flammability limit is 140.0 g/m^3 . These are

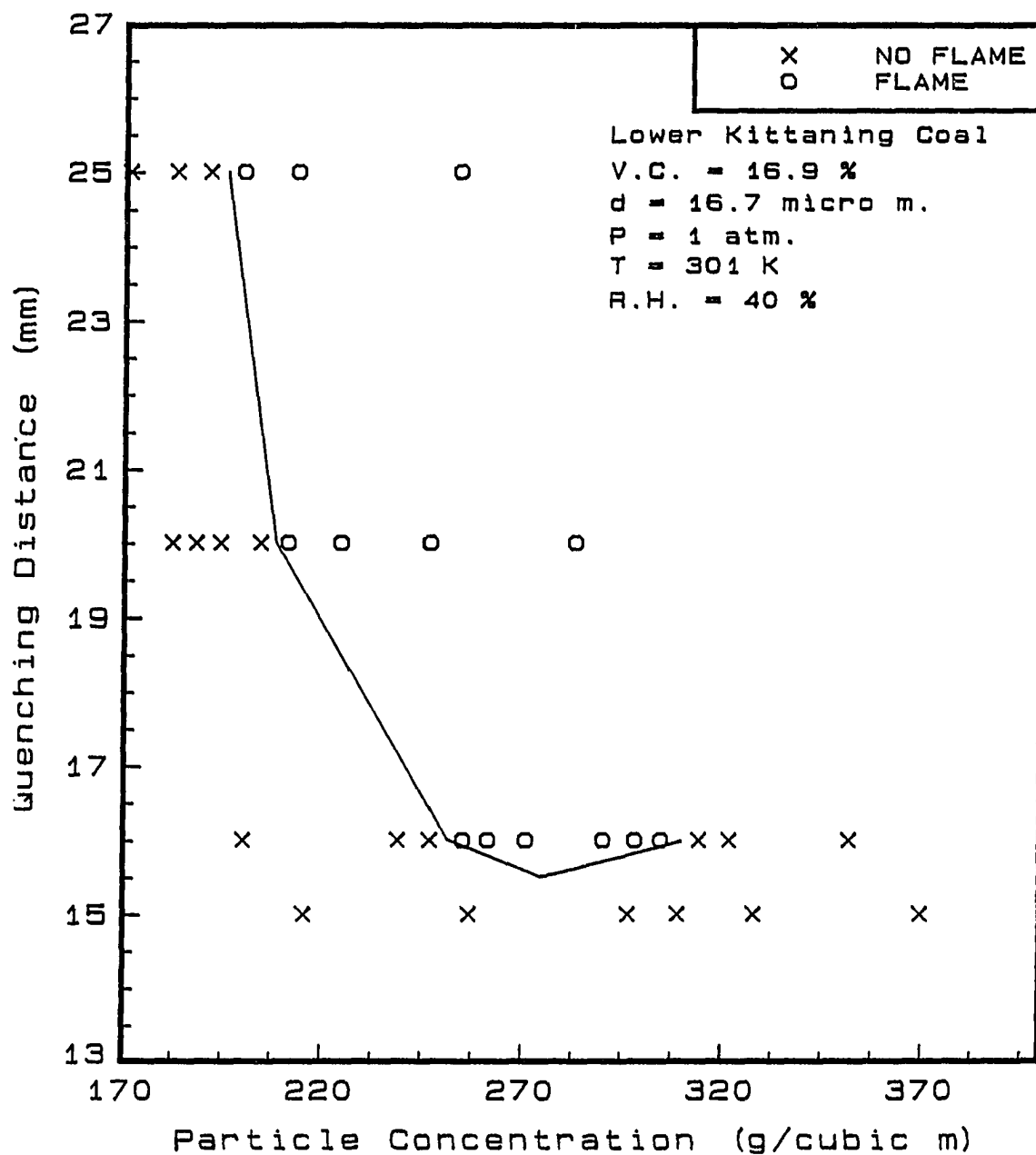


Figure 5.1: Quenching distance vs. particle concentration of 16.7 μm Lower Kittanning coal

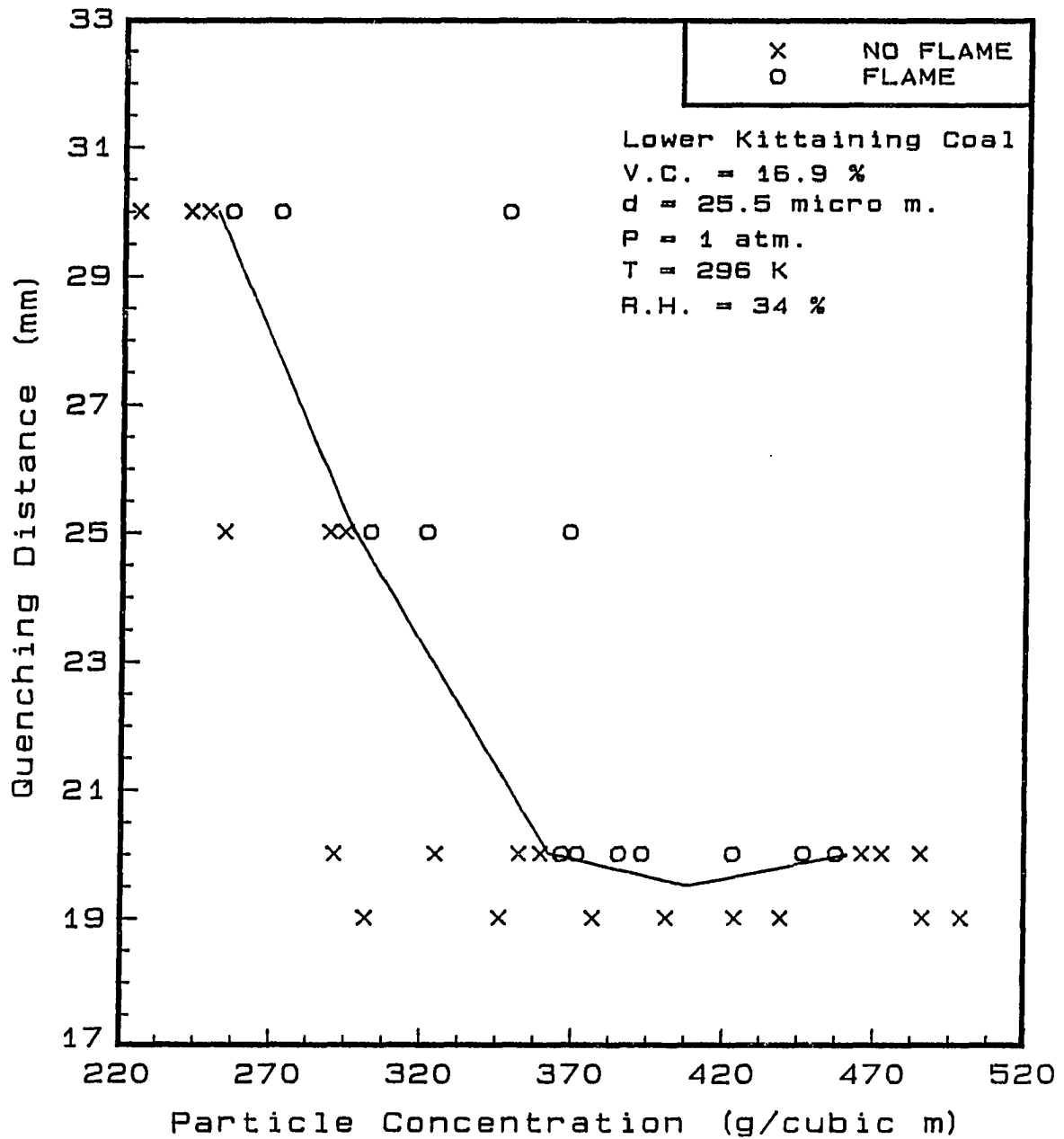


Figure 5.2: Quenching distance vs. particle concentration of 25.5 μm Lower Kittaining coal

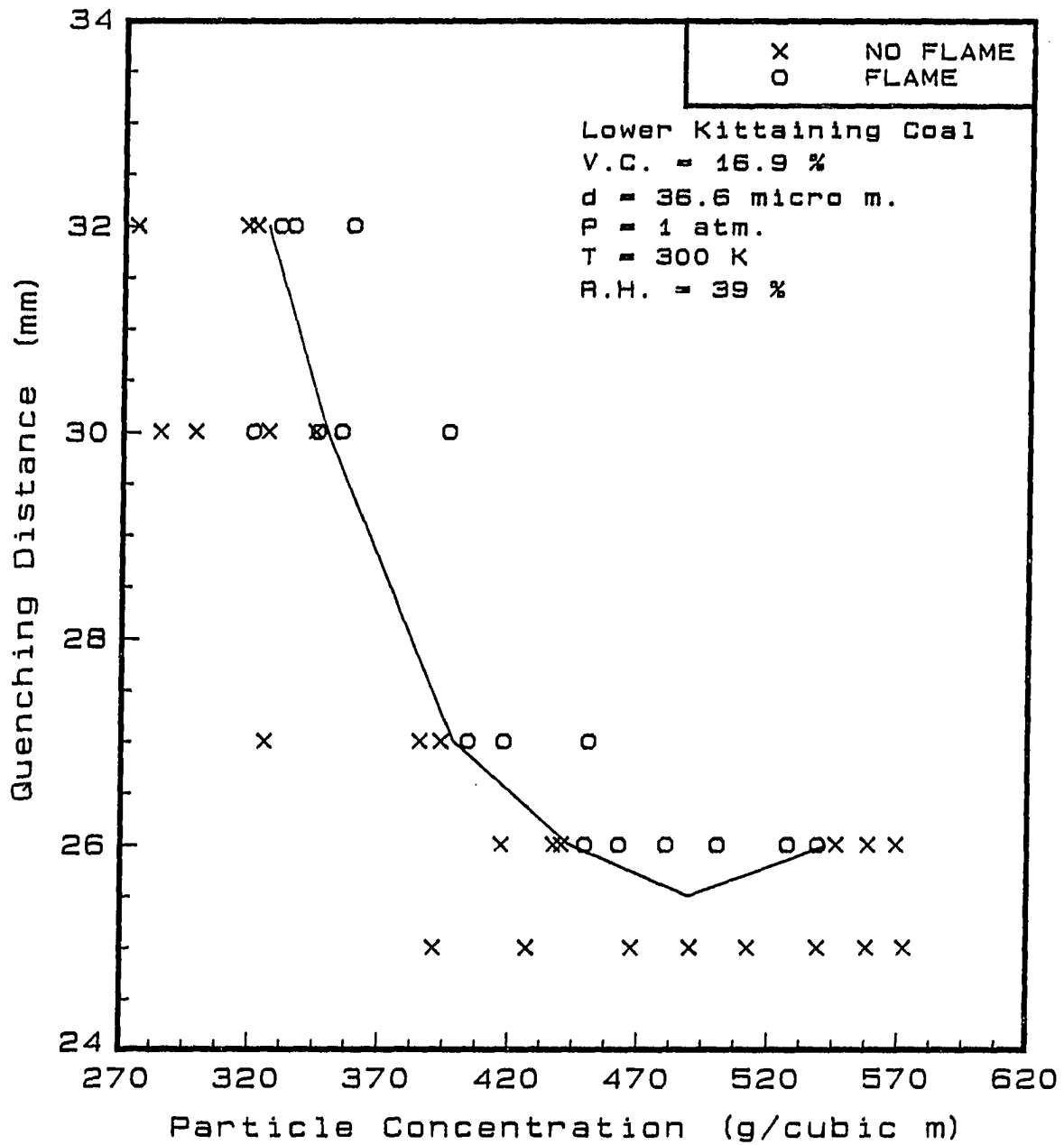


Figure 5.3: Quenching distance vs. particle concentration of 36.6 μm Lower Kittaining coal

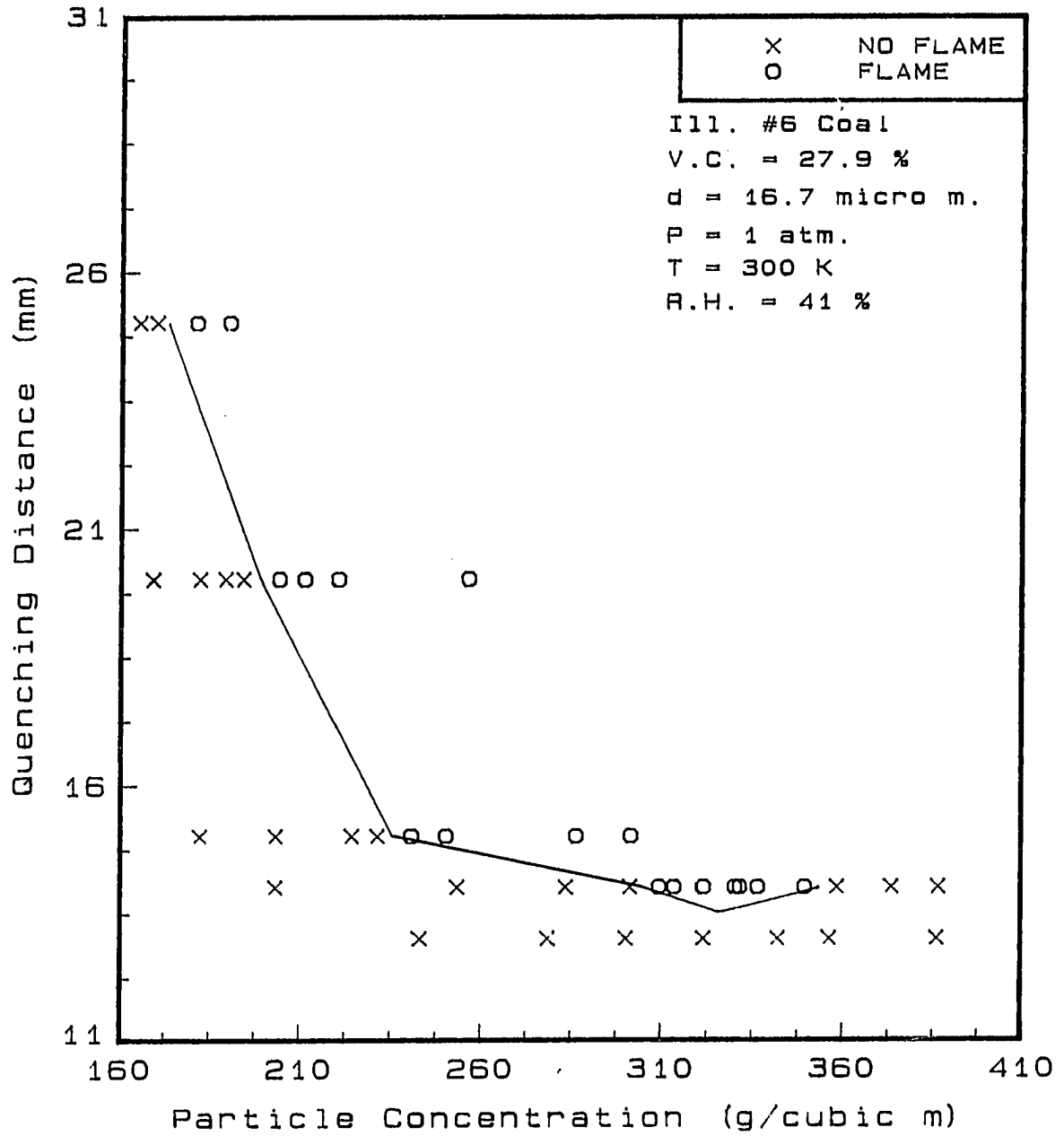


Figure 5.4: Quenching distance vs. particle concentration of $16.7 \mu\text{m}$ Illinois # 6 coal

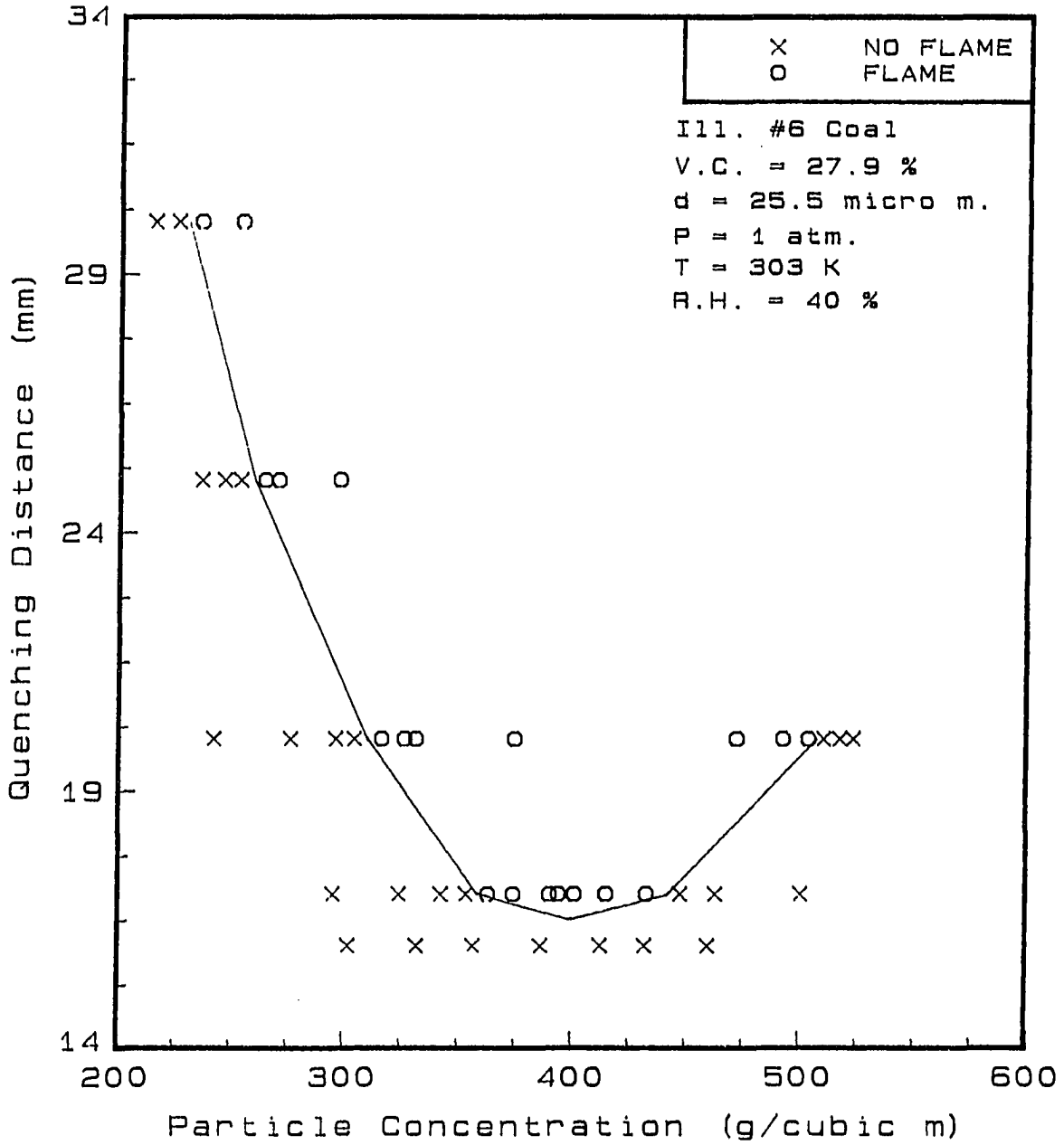


Figure 5.5: Quenching distance vs. particle concentration of 25.5 μm Illinois # 6 coal

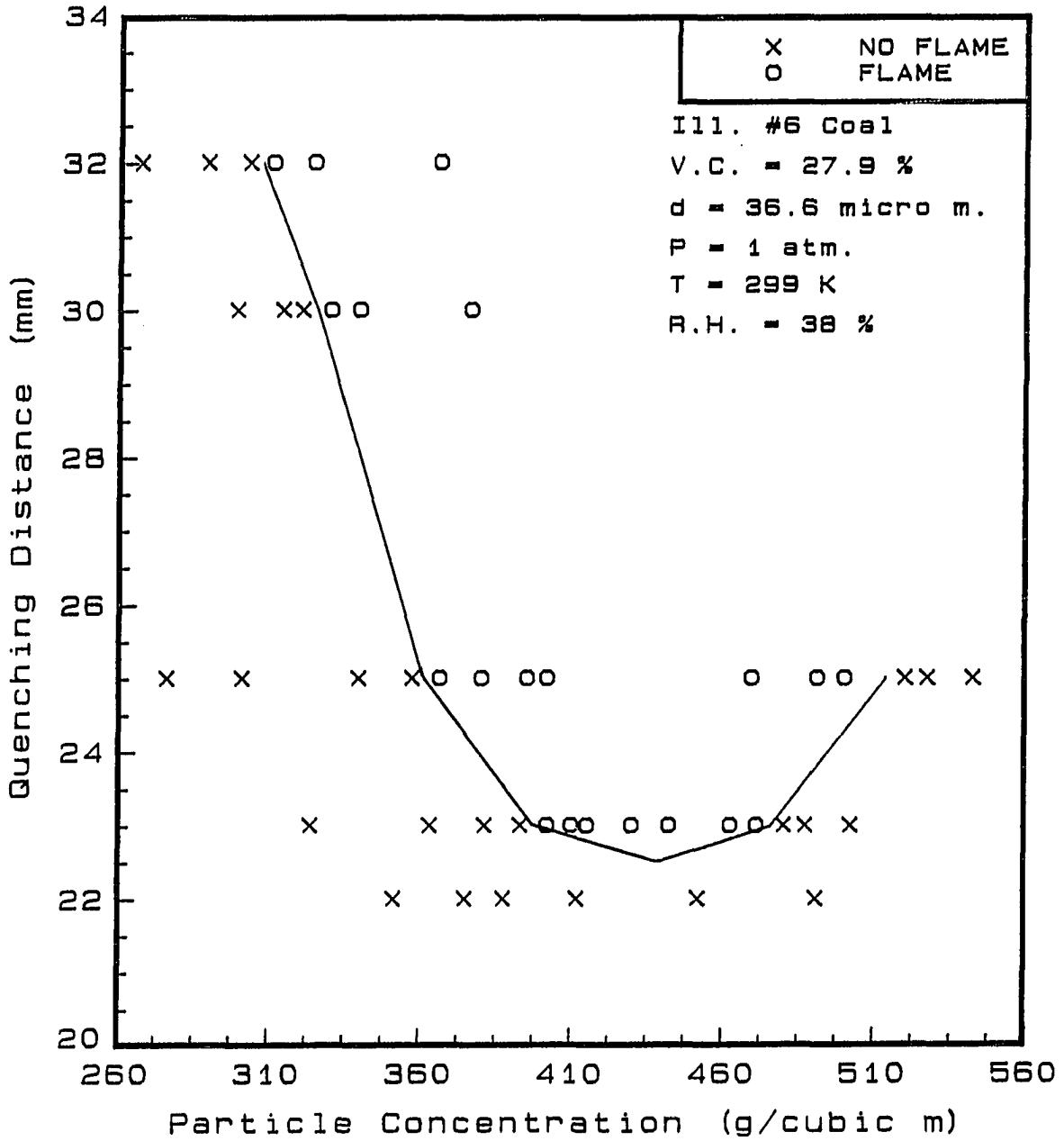


Figure 5.6: Quenching distance vs. particle concentration of 36.6 μm Illinois # 6 coal

shown in Figure 5.7.

Figure 5.8 shows the result for 16.7 μm particles. The minimum quenching distance is 12.0 mm at a concentration of 312.0 g/m^3 . The lean flammability limit is 165.0 g/m^3 .

Figure 5.9 shows, for 25.5 μm particles, that the minimum quenching distance is 14.5 mm at a particle concentration of 365.0 g/m^3 . The lean flammability limit is 205.0 g/m^3 . Figure 5.10 shows, for 36.6 μm particle size, the minimum quenching distance is 18.5 mm at a particle concentration of 430.0 g/m^3 . The lean flammability limit is 270.0 g/m^3 . In the case of Penn. Seam coal, the lean flammability is more obvious than for any other types of coal dust tested. That is, the slope increases rapidly as the particle concentration decreases. As mentioned earlier, Jarosinski et al. [1986] reported a minimum quenching distance of 25.0 mm for a 32.1 % volatile content bituminous coal of less than 5 μm in diameter which has a very similar volatile content as the Penn. Seam coal (34.4 %) tested here. In the case of Penn. Seam coal for a 9.1 μm particle size, the minimum quenching distance is 9.5 mm which is 1/2.6 smaller than his value. The discrepancy is probably due to the difference in the definition of quenching distance, which, in his definition, is the quenching distance is the maximum spacing between the walls for which heat outflow to the walls is able to quench the fully developed freely propagating flames.

5.2.1.4 Avaville no. 11 coal A high-volatile bituminous Adaville no. 11 coal was sieved in three size ranges and tested for quenching. The volatile content of this coal is 41.8 %.

Figure 5.11 shows the effect of particle concentrations on the quenching distance

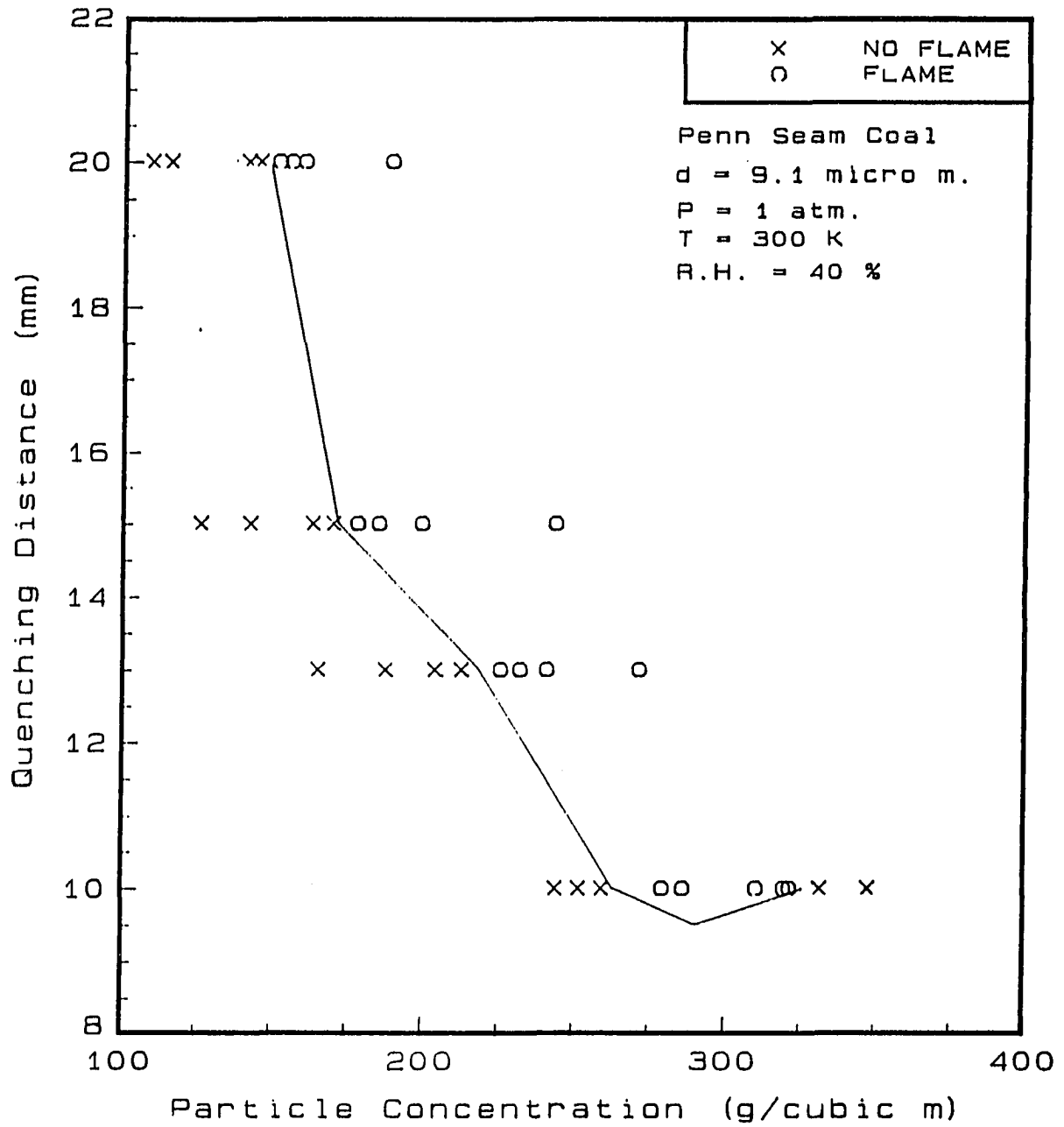


Figure 5.7: Quenching distance vs. particle concentration of $9.1 \mu\text{m}$ Penn. Seam coal

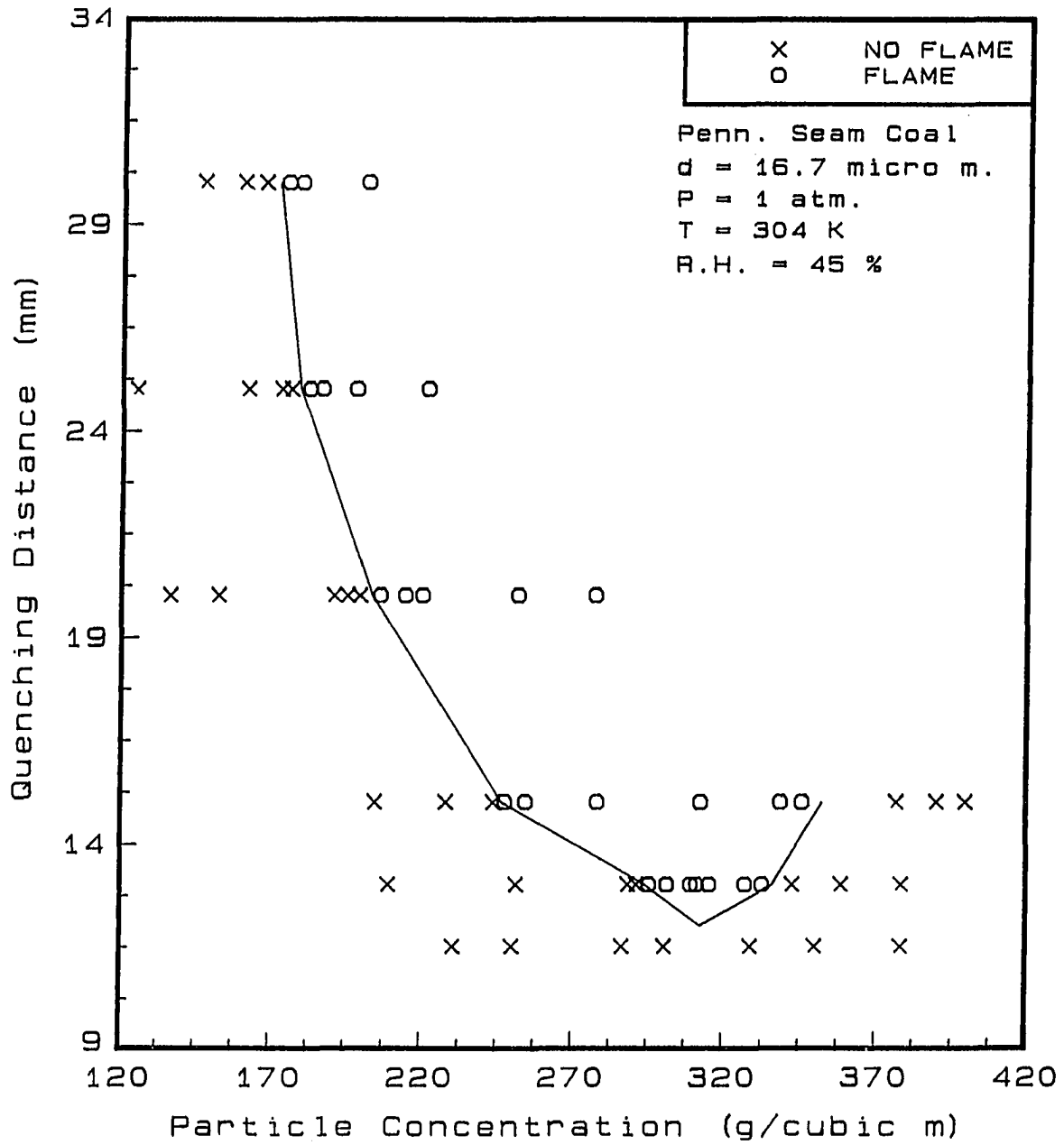


Figure 5.8: Quenching distance vs. particle concentration of $16.7 \mu\text{m}$ Penn. Seam coal

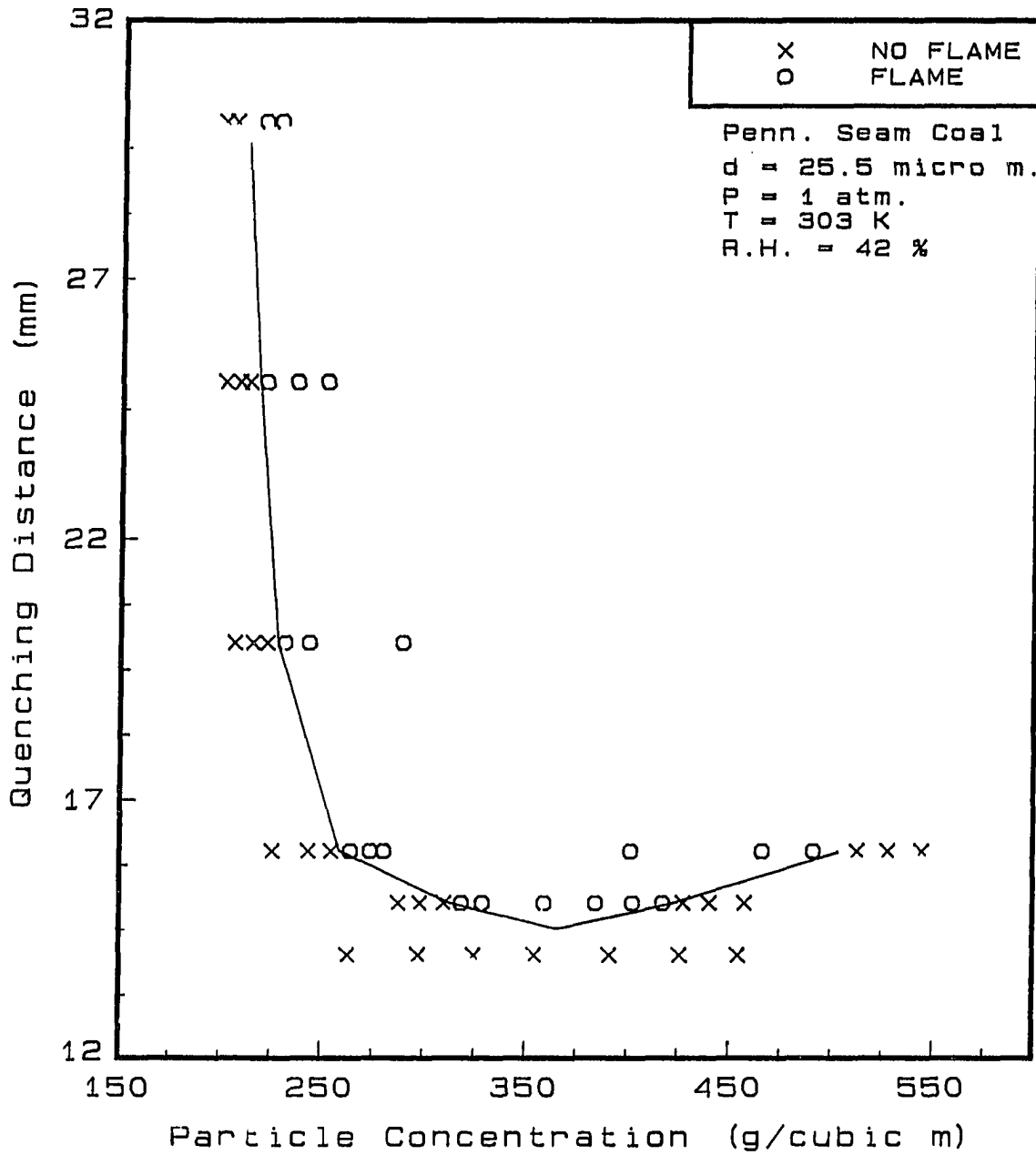


Figure 5.9: Quenching distance vs. particle concentration of 25.5 μm Penn. Seam coal

of 16.7 μm coal powder. The minimum quenching distance is 10.5 mm at 300 g/m^3 particle concentration which is 1.4 times higher than stoichiometric concentration. The lean flammability limit is difficult to determine, but it is estimated to be around 150.0 g/m^3 . Also, this particle has a relatively well defined rich flammability limit, around 370.0 g/m^3 .

Figure 5.12 shows the effect of particle concentrations on the quenching distance for 25.5 μm coal powder. The minimum quenching distance is 13.5 mm at a particle concentration of around 360.0 g/m^3 . In these cases, the point is determined as the center of the two limits. The lean flammability limit is well defined as 190.0 g/m^3 .

Figure 5.13 shows the effect of particle concentrations on the quenching distance for 36.6 μm in diameter coal particles. The minimum quenching distance is 18.5 mm at the particle concentration of 426.0 g/m^3 . The lean flammability limit is about 260.0 g/m^3 which is 2.0 times higher than stoichiometric concentration. The lean limit is difficult to be determined.

5.2.1.5 Hanna no. 80 coal Hanna no. 80 coal has the highest volatile content (44.4 %) among the coals tested in this research. This coal was sieved into three size ranges and tested for quenching.

Figure 5.14 shows the results for 16.7 μm coal. The minimum quenching distance is 8.5 mm at a particle concentration of 293.0 g/m^3 which is 1.4 times higher than stoichiometric concentration. The lean flammability is 130.0 g/m^3 . This minimum quenching distance is the lowest one among all types and sizes of coals tested.

For 25.5 μm in diameter particles, the minimum quenching distance is 10.5 mm at a particle concentration of 301.0 g/m^3 as shown in Figure 5.15. The lean flammability

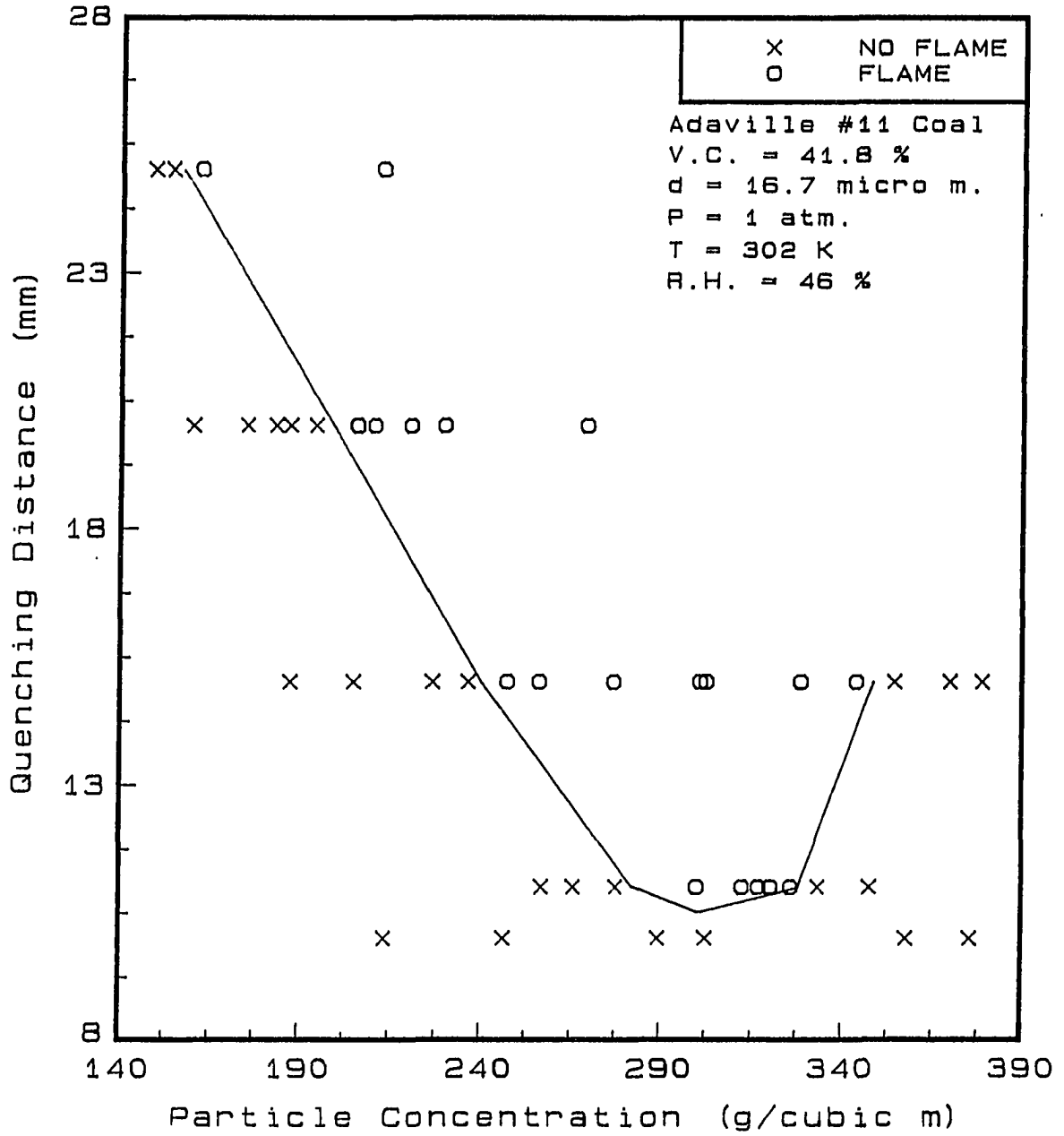


Figure 5.11: Quenching distance vs. particle concentration of 16.7 μm Adaville no. 11 coal

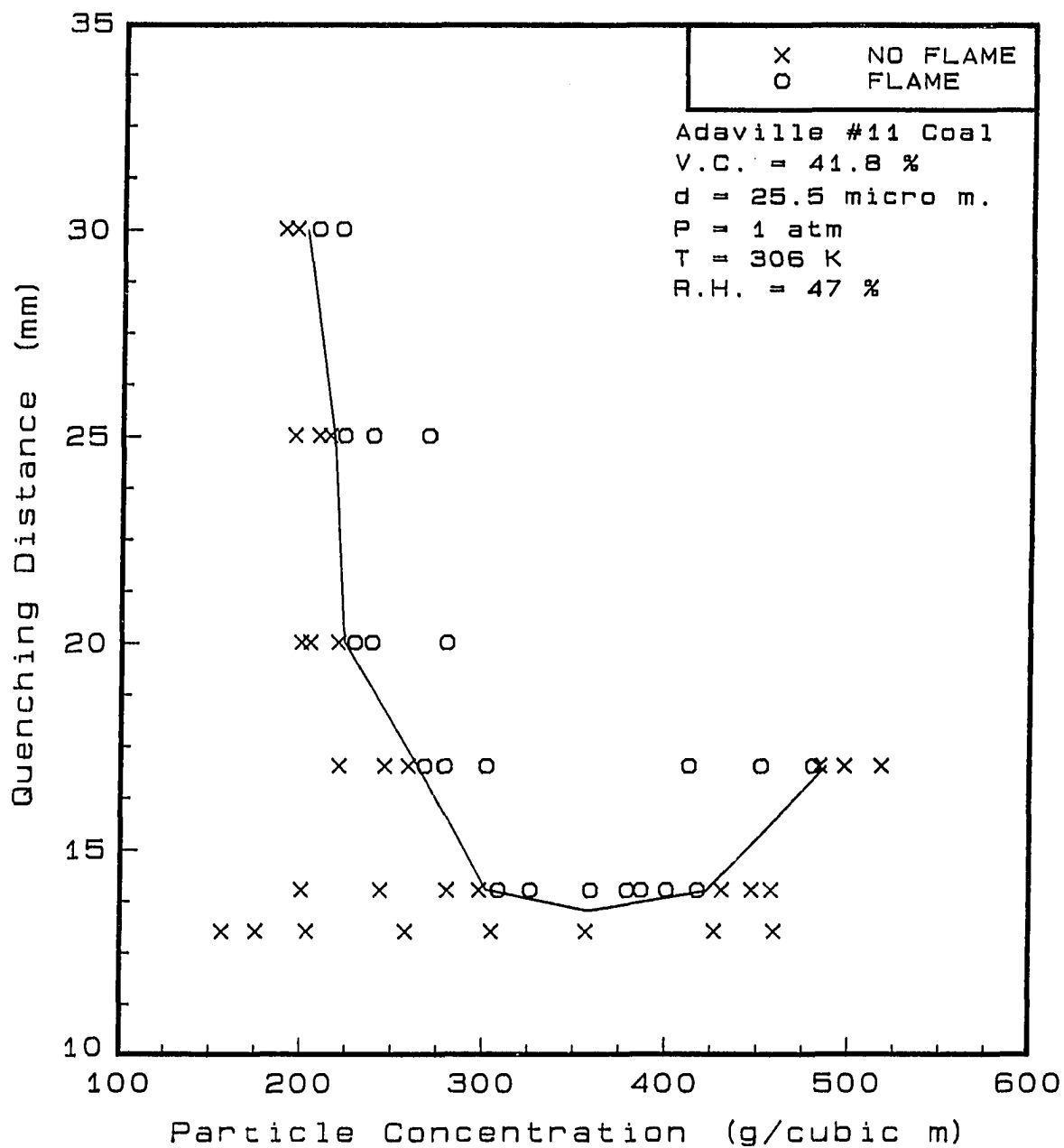


Figure 5.12: Quenching distance vs. particle concentration of 25.5 μm Adaville no. 11 coal

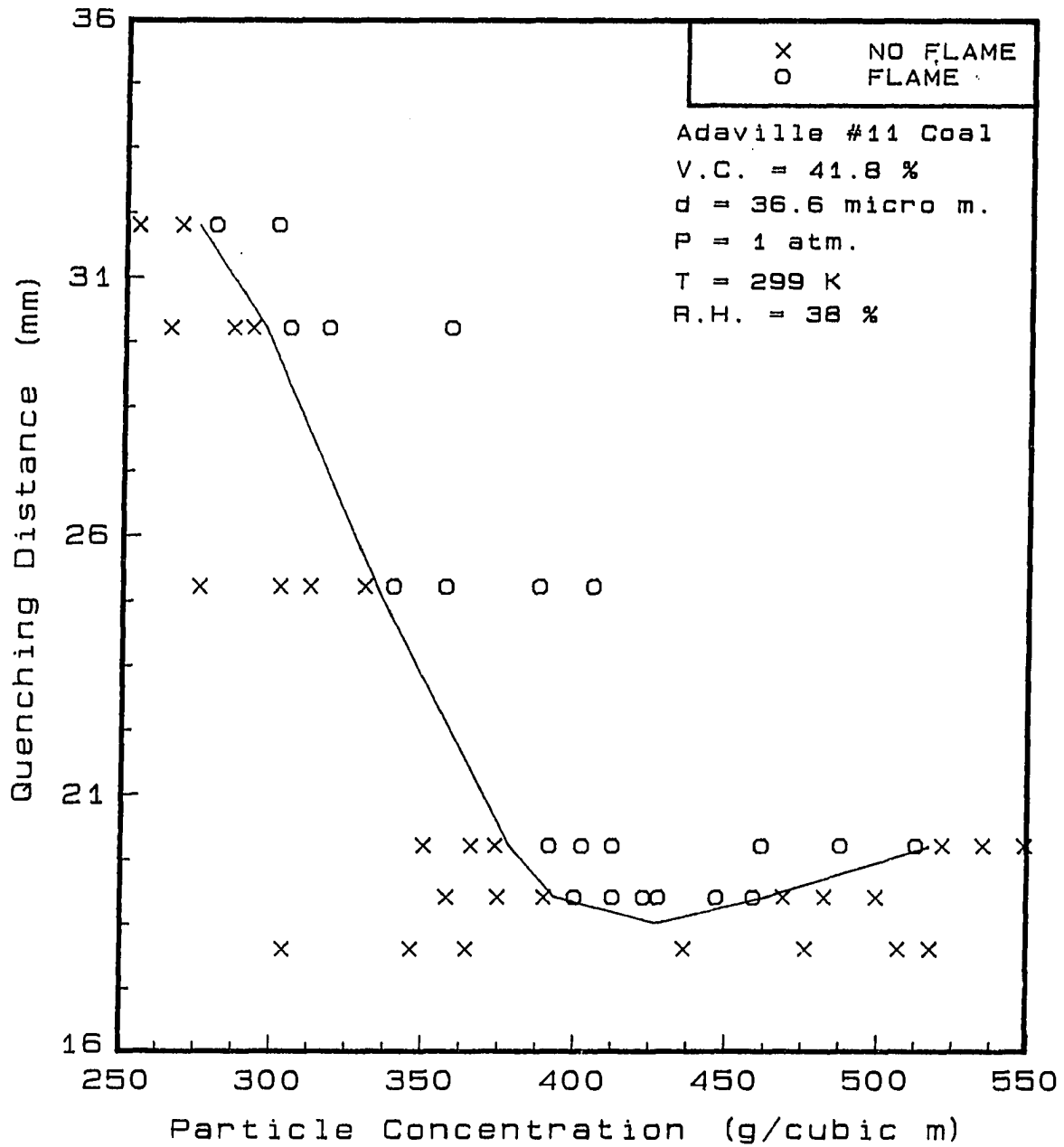


Figure 5.13: Quenching distance vs. particle concentration of 36.6 μm Adaville no. 11 coal

limit is 160.0 g/m^3 . The slope of right-hand side of this curve does not become steeper as the particle concentration increases. That means either the rich flammability limit does not exist or too high to be determined. It is shown in Figure 5.15.

Figure 5.16 shows the result for $36.6 \mu\text{m}$ coal. The minimum quenching distance is 14.5 mm at the particle concentration of 365.0 g/m^3 . The lean flammability limit is 220.0 g/m^3 .

5.2.2 Effect of particle size

The combustion processes occurring during a dust explosion involves chemical reaction at the solid-oxygen interface. Consequently the surface area available for oxidation and heat transfer has a significant effect on the initiation and progress of a dust explosion. As the particle size increases, the specific surface area decreases. Thus smaller particles are easier to ignite, and have a lower quenching distance and wider flammability limits.

The effect of particle size on quenching distance for each type of coal powder is shown in Figures 5.17 - 5.21. For all type of particles, the quenching distance and lean flammability limit increases as the particle size increases. Also, the particle concentration at the minimum quenching distance increases as the particle size increases. For Penn. Seam coal and Adaville no. 11 coal, the quenching distance of the smaller particle size is larger than the quenching distance of the bigger particle size at some higher concentrations. Nagy and Verakis [1983] reported that the ignition temperature increases as the particle size increases for the bituminous coal dust, and as particle diameter becomes smaller a limiting ignition temperature is approached.

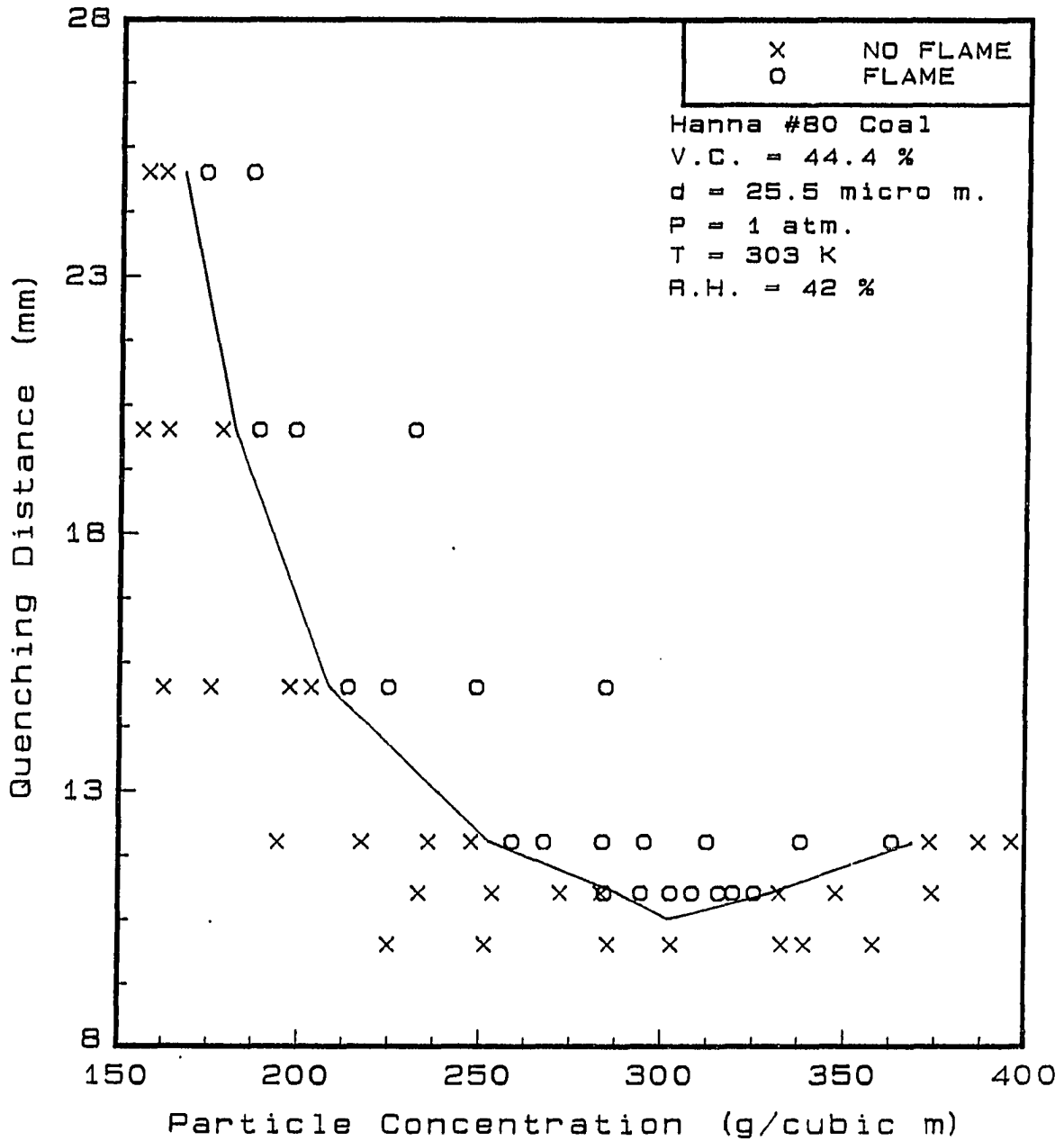


Figure 5.15: Quenching distance vs. particle concentration of 25.5 μm Hanna # 80 coal

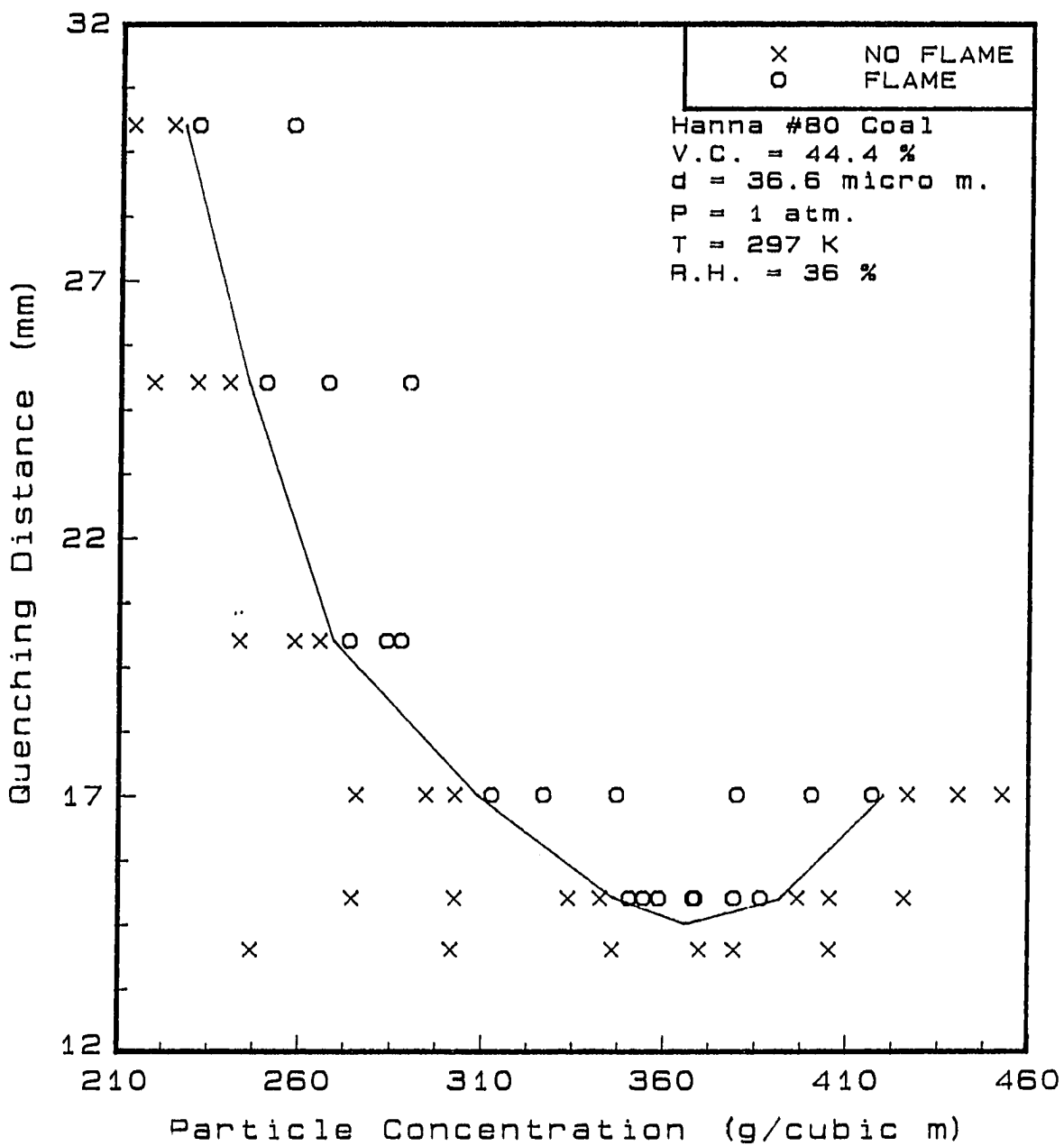


Figure 5.16: Quenching distance vs. particle concentration of $36.6 \mu\text{m}$ Hanna # 80 coal

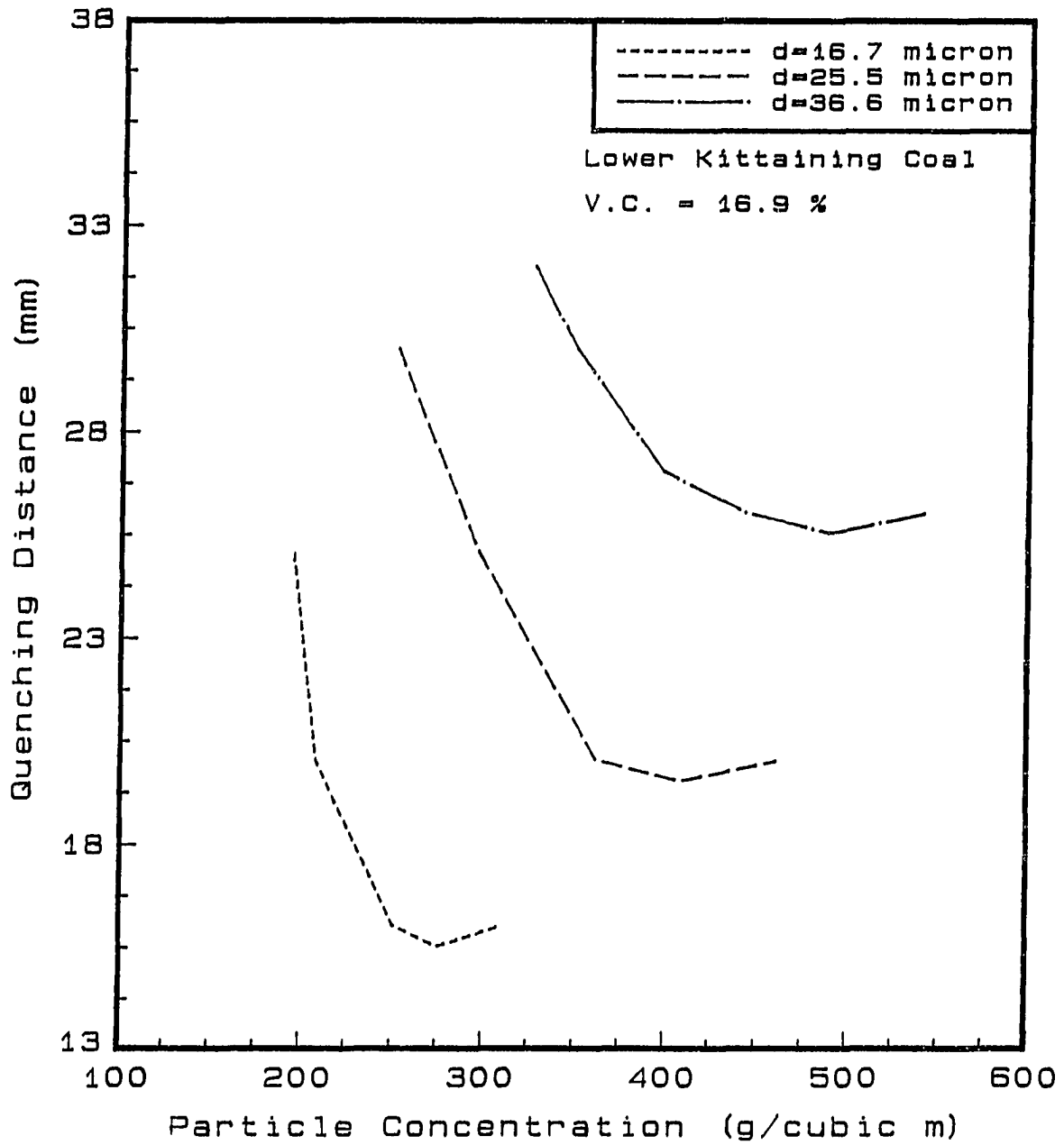


Figure 5.17: Quenching distance vs. particle concentration of Lower Kittaining coal of each particle sizes

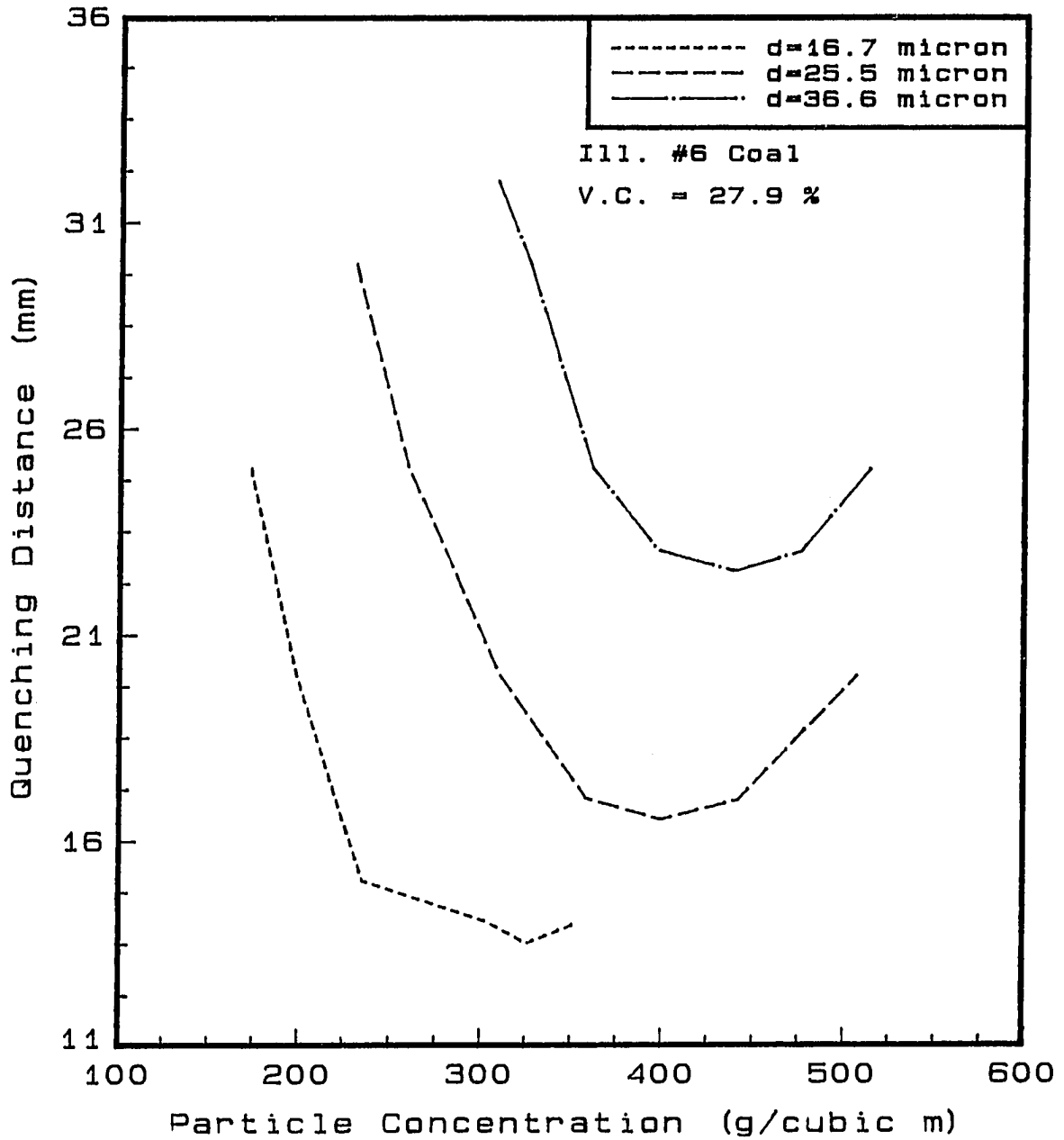


Figure 5.18: Quenching distance vs. particle concentration of Illinois # 6 coal of each particle sizes

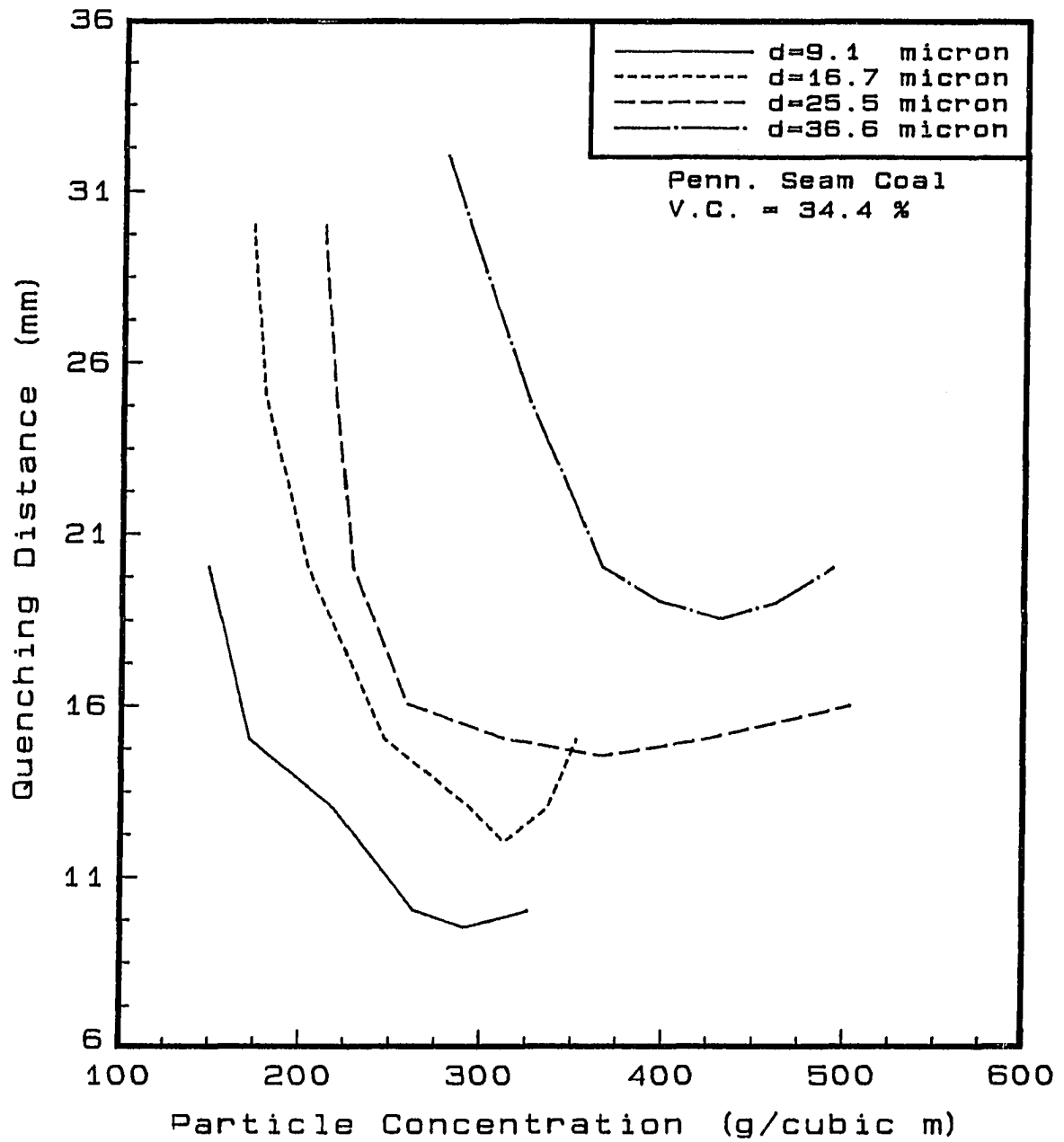


Figure 5.19: Quenching distance vs. particle concentration of Penn. Seam coal of each particle sizes

Also, they reported that a coal particles greater than $100 \mu m$ could not be ignited by electric sparks. However, they showed that as the particle size decreases, the minimum ignition energy decreases. That means the quenching distance decreases as the particle diameter decreases. Figure 5.22 shows such a trend. As the particle size increases, the slope becomes steeper. As mentioned earlier, the quenching distance for the biggest size particles is greater than 32.0 mm, proving that the slope of quenching distance vs. particle diameter curve becomes steeper as particle size increases.

5.2.3 Effect of volatile content

Nagy and Verakis [1983] reported that the ignition energy by a spark decreases and approaches a limiting value as the volatile content of the coal increases.

Field [1982] mentioned that for pure chemical compounds, or natural products, combustion generally result in the formation of carbon dioxide and moisture, with atmospheric nitrogen. Dust explosion pressures in this case result from the expansion of the gases due to the heat of combustion. The heat of combustion influences the rate of combustion but no simple relationship exists between them and it is possible that the activation energy for the intermediates in the combustion process has a more significant effect. He also mentions that the explosion hazard tends to increase with an increase in the volatile content.

Figure 5.23, 5.24, and 5.25 show the effect of volatile contents on the quenching distance of the same particle size at various particle concentrations. Figure 5.23 shows that the minimum quenching distance decreases as the volatile content of the coal

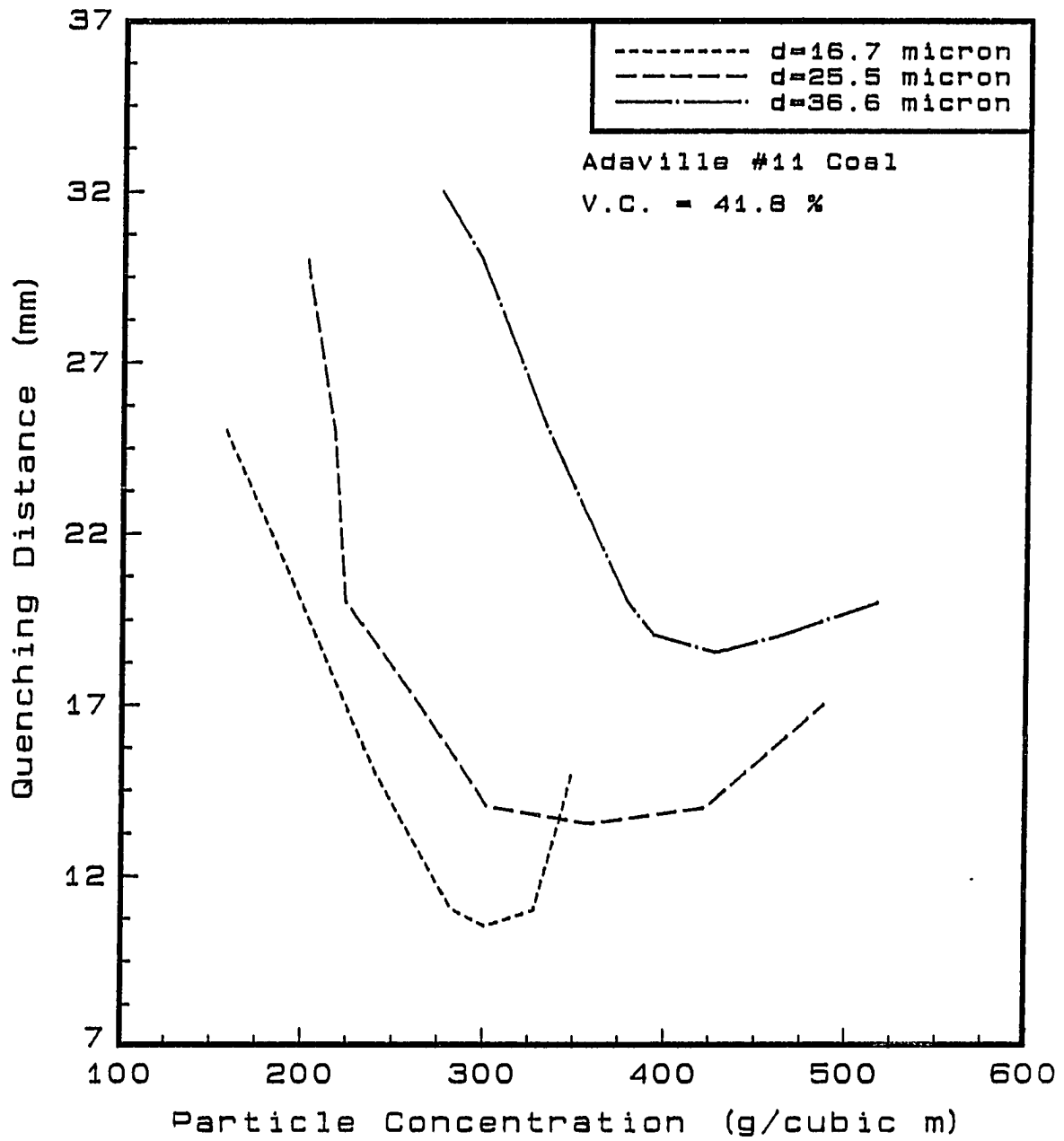


Figure 5.20: Quenching distance vs. particle concentration of Adaville # 11 coal for various particle sizes

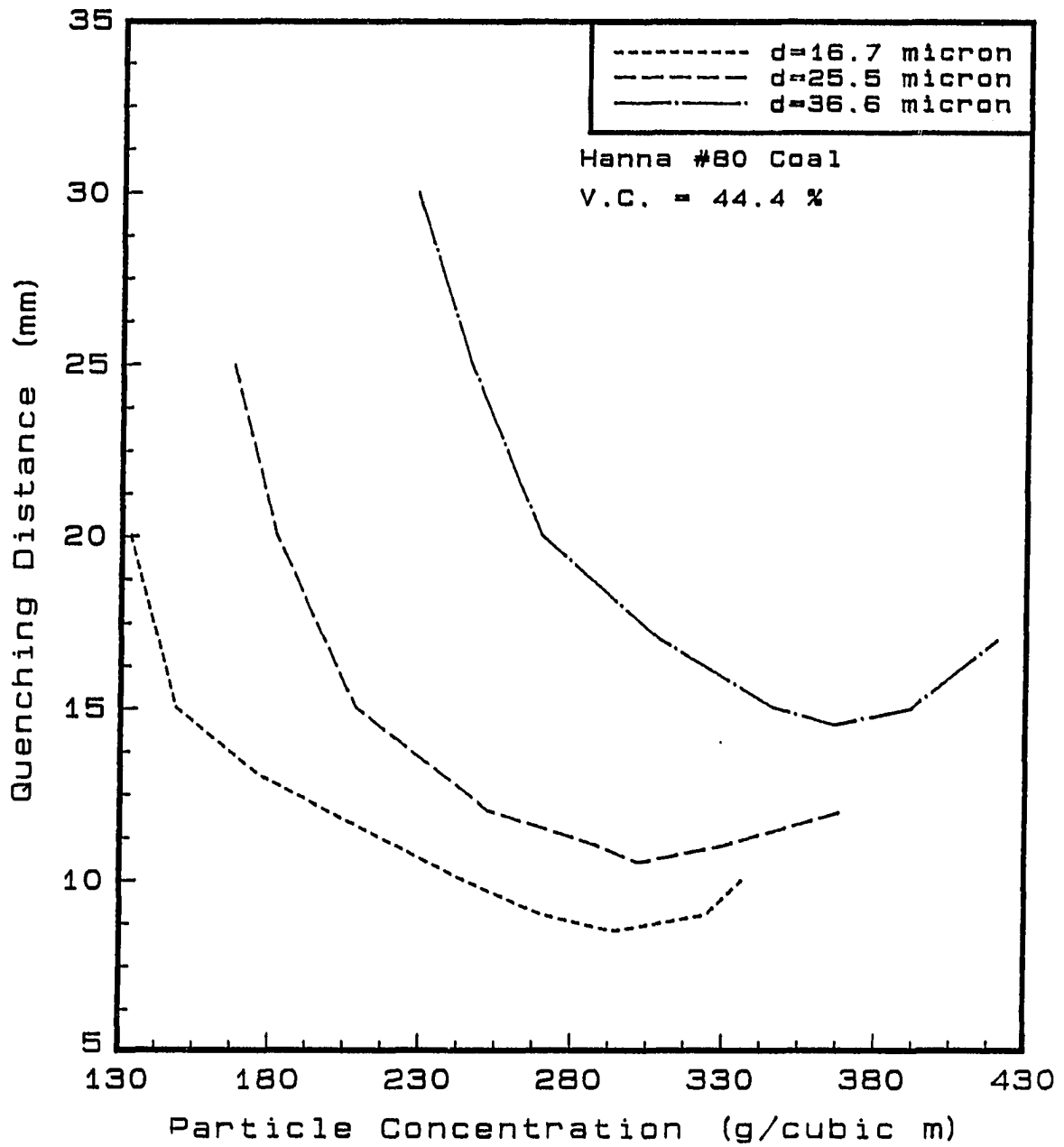


Figure 5.21: Quenching distance vs. particle concentration of Hanna # 80 coal of each particle sizes

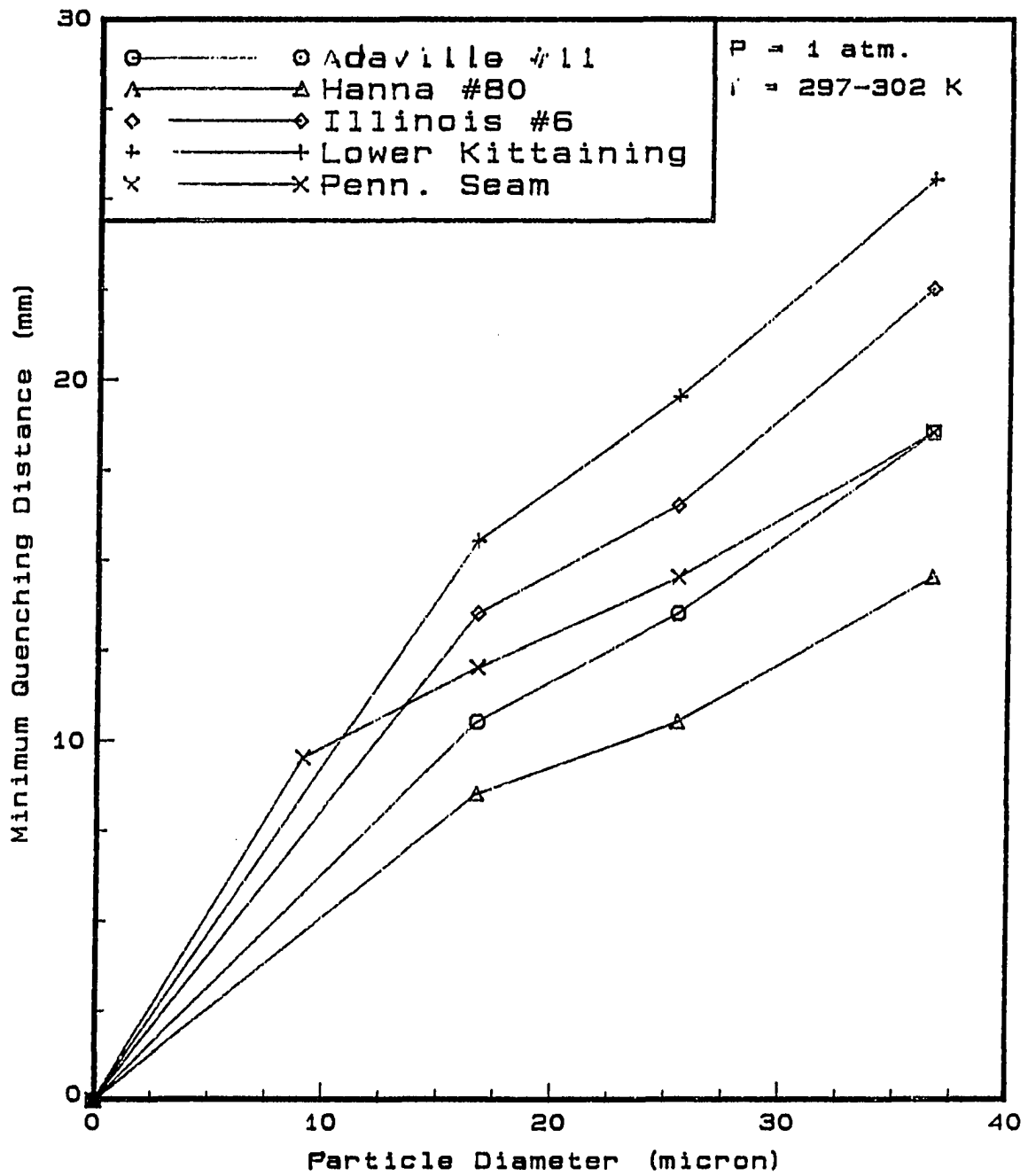


Figure 5.22: Minimum quenching distance vs. particle diameter for each type of coal

increases. But the difference in the quenching distance for 3 types of coals, 27.9 %, 34.4 %, and 41.8 % volatile content coals, below the particle concentration of about 250.0 g/m^3 are very small. Also, the flammability limits generally increase with decreasing volatile content.

Figure 5.24 shows the results for $25.5 \mu\text{m}$ coal particles. The minimum quenching distance increases with a decreasing volatile content. The difference in the quenching distance between 34.4 % and 41.8 % volatile content coal below the particle concentration of 280.0 g/m^3 are very small.

The similarity between these two types of coals, Penn. Seam coal and Adaville no. 11 coal, is due to the fact that the volatile content on a wet basis is similar even though on a dry basis there is about 7.4 % difference. The volatile contents of these two coals on a wet basis is; Penn. Seam coal (33.7 %); Adaville no. 11 coal (33.9 %).

Figure 5.25 shows the results for particles of $36.6 \mu\text{m}$ in diameter. As in previous graphs, the difference in quenching distance between the Penn. Seam coal and Adaville no. 11 coal is very slim. For this particle size, the minimum quenching distance between these two types of coals is same. The effect of volatile content on the minimum quenching distance is more clearly shown in Figure 5.26. The minimum quenching distance decreases slowly up to 41.8 % and then decreases rapidly. But the difference in minimum quenching distance among different sizes of coal particles becomes smaller as the volatile content increases. That means the effect of volatile content is reduced as the particle size becomes larger. It is generally believed that a significant amount of volatiles remains in the char downstream of flame front as the particle size increases.

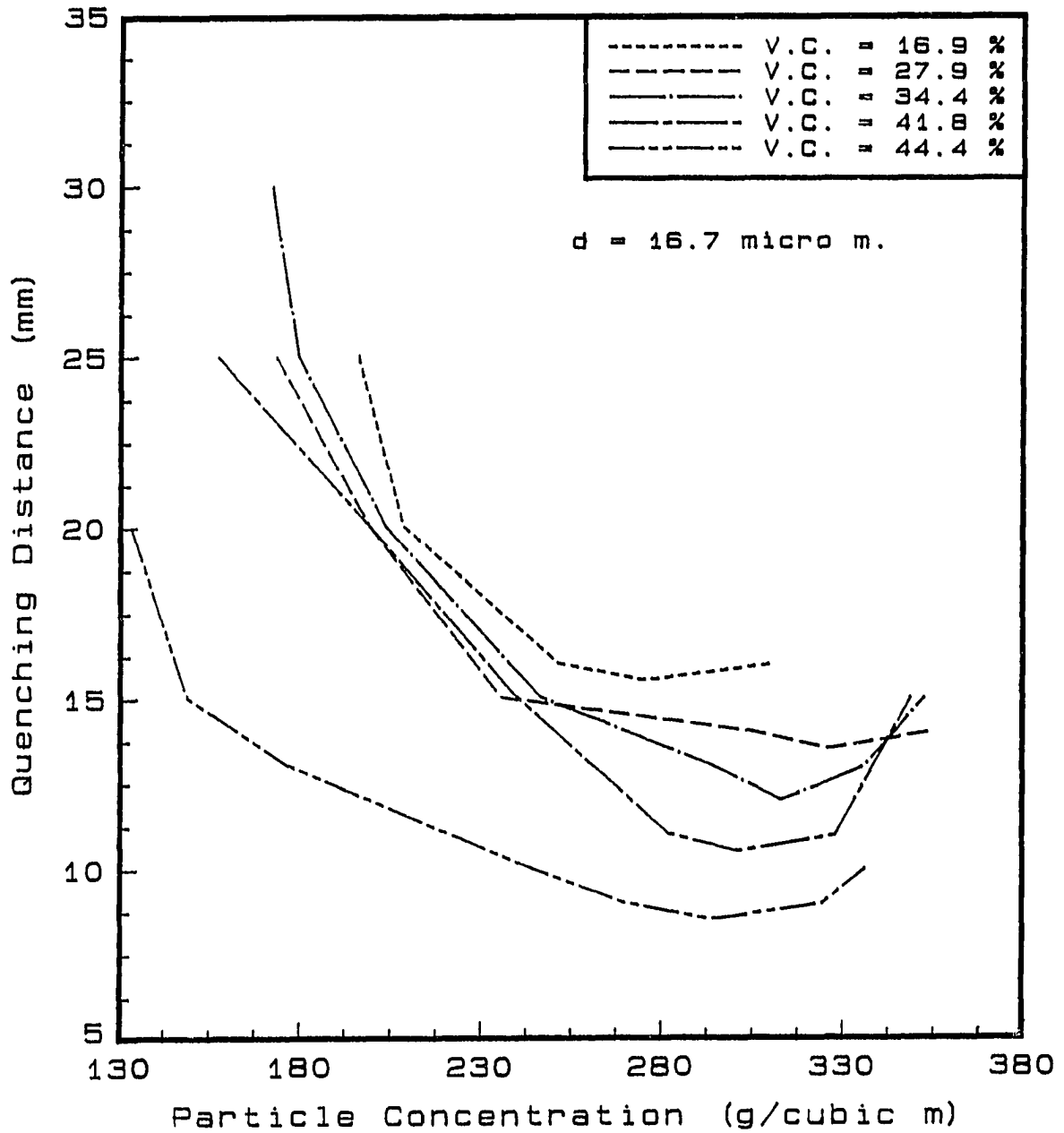


Figure 5.23: Quenching distance vs. particle concentration of $16.7 \mu\text{m}$ coal for different volatile content

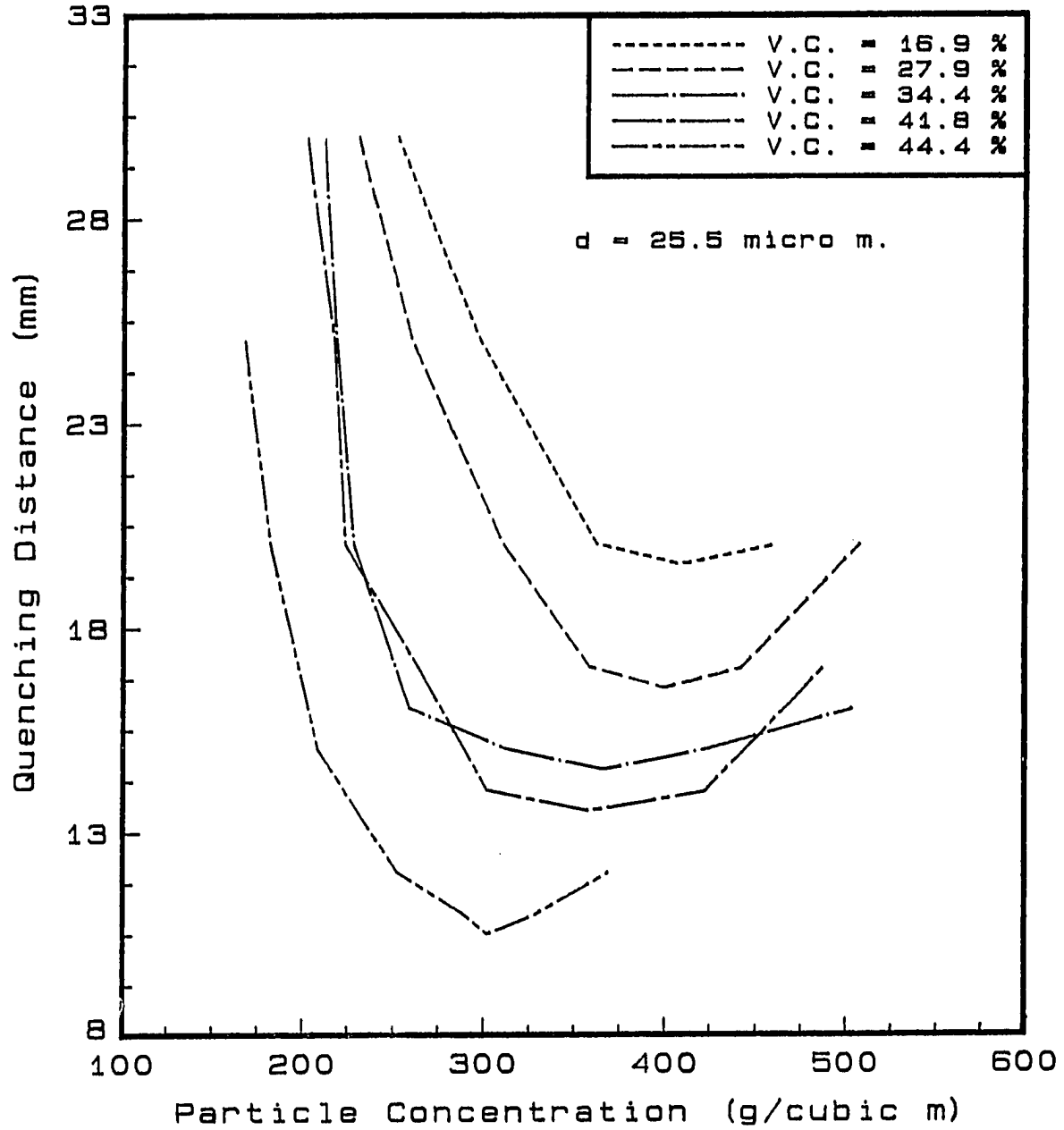


Figure 5.24: Quenching distance vs. particle concentration of $25.5 \mu\text{m}$ coal for different volatile content

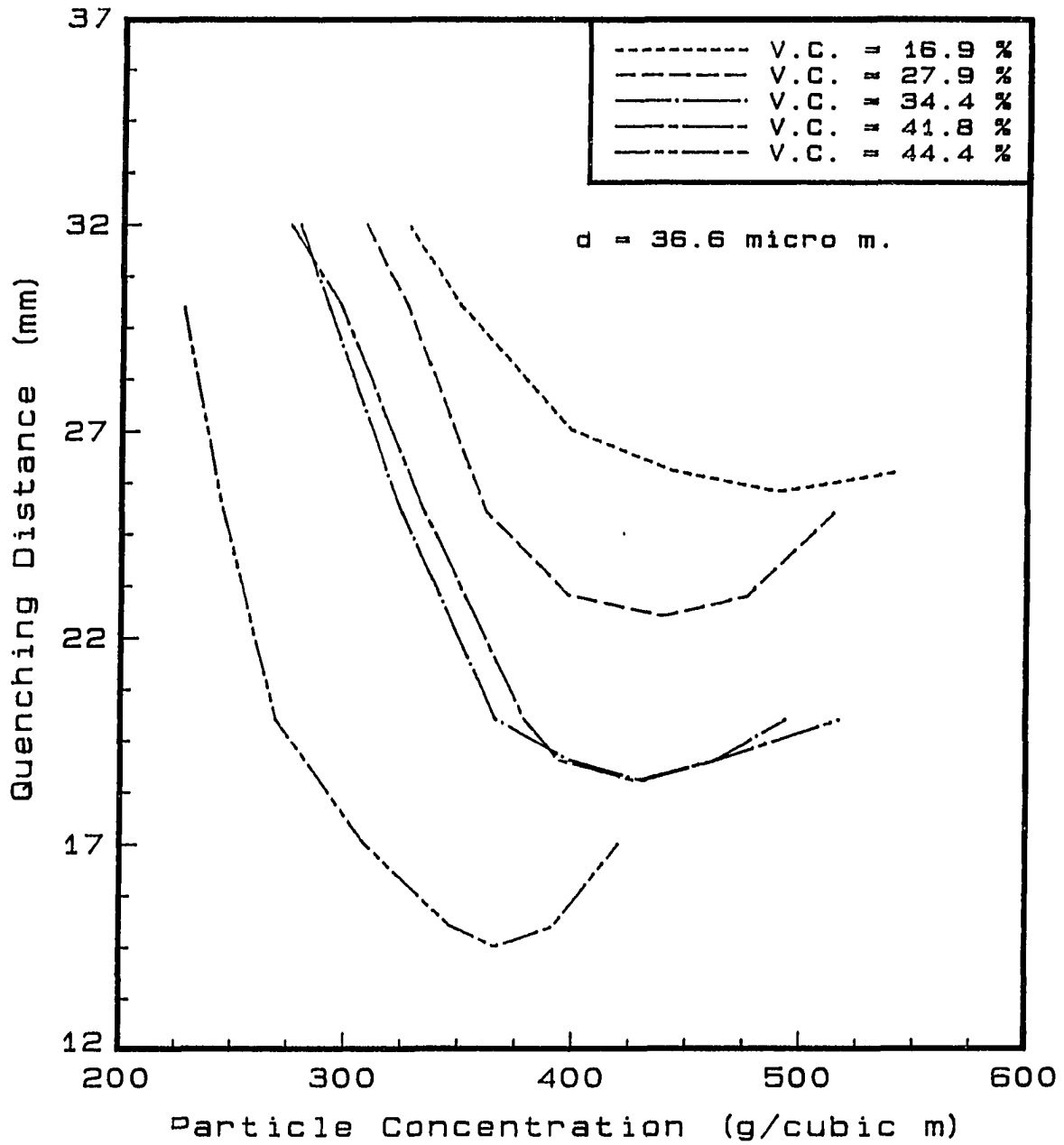


Figure 5.25: Quenching distance vs. particle concentration of $36.6 \mu\text{m}$ coal of for different volatile content

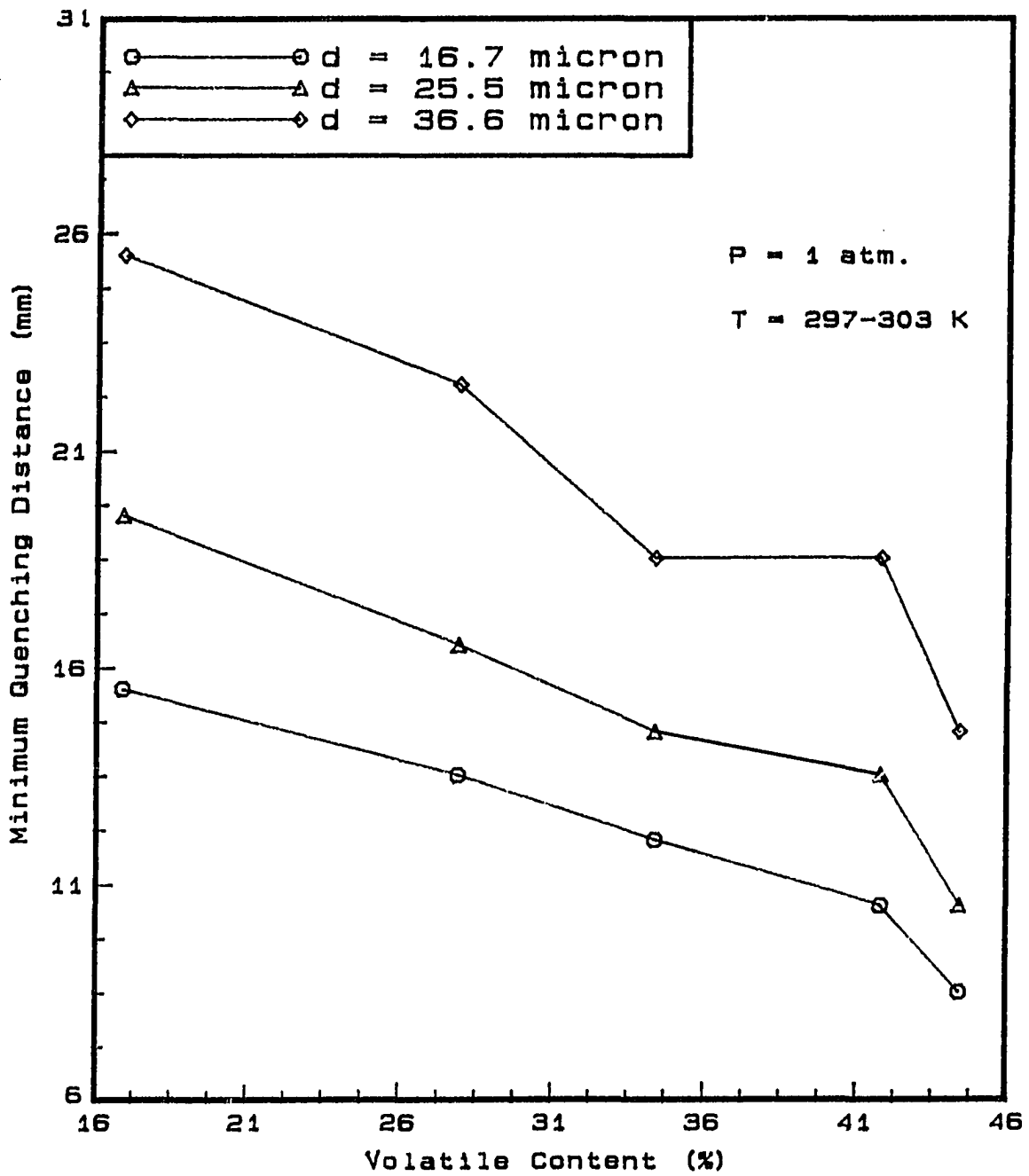


Figure 5.26: Minimum quenching distance vs. volatile content of each sizes of coal

5.3 Burning Velocity of Coal-air Flames

As mentioned in the Literature Review part of this dissertation, the burning velocity of coal given by previous researchers varies from 3 cm/sec to 130 cm/sec. A variety of test conditions and setups makes it difficult to generalize results but generally it appears that

1. The burning velocity increases as the particle size decreases.
2. The burning velocity increases as the coal particle concentration increases until the system becomes quite fuel rich and decreases thereafter.
3. The maximum burning velocity varies greatly.
4. The burning velocity increases as the volatile content of the coal increases.

5.4 Observation of Flame Propagation of Coal

A flame propagation behavior of Adaville no. 11 coal was investigated using a high speed photographic method. Figure 5.27 shows the position of the flame front with time as it burns rapidly outward in the test section. The figure shows that the flame moves nearly linearly with time. Figure 5.28 shows the burning velocity behavior with time. The burning velocity increases with time till it reaches a maximum value, then decrease slowly to the steady state value. The initial sudden increase of burning velocity is due the effect of ignition energy.

A video camera was also used to measure the burning velocities of Penn. Seam coal at various particle concentrations, as shown in Figures 5.29 and 5.30. The maximum velocities for the 16.7 μm and 25.5 μm Penn. Seam coal are 11.5 cm/sec

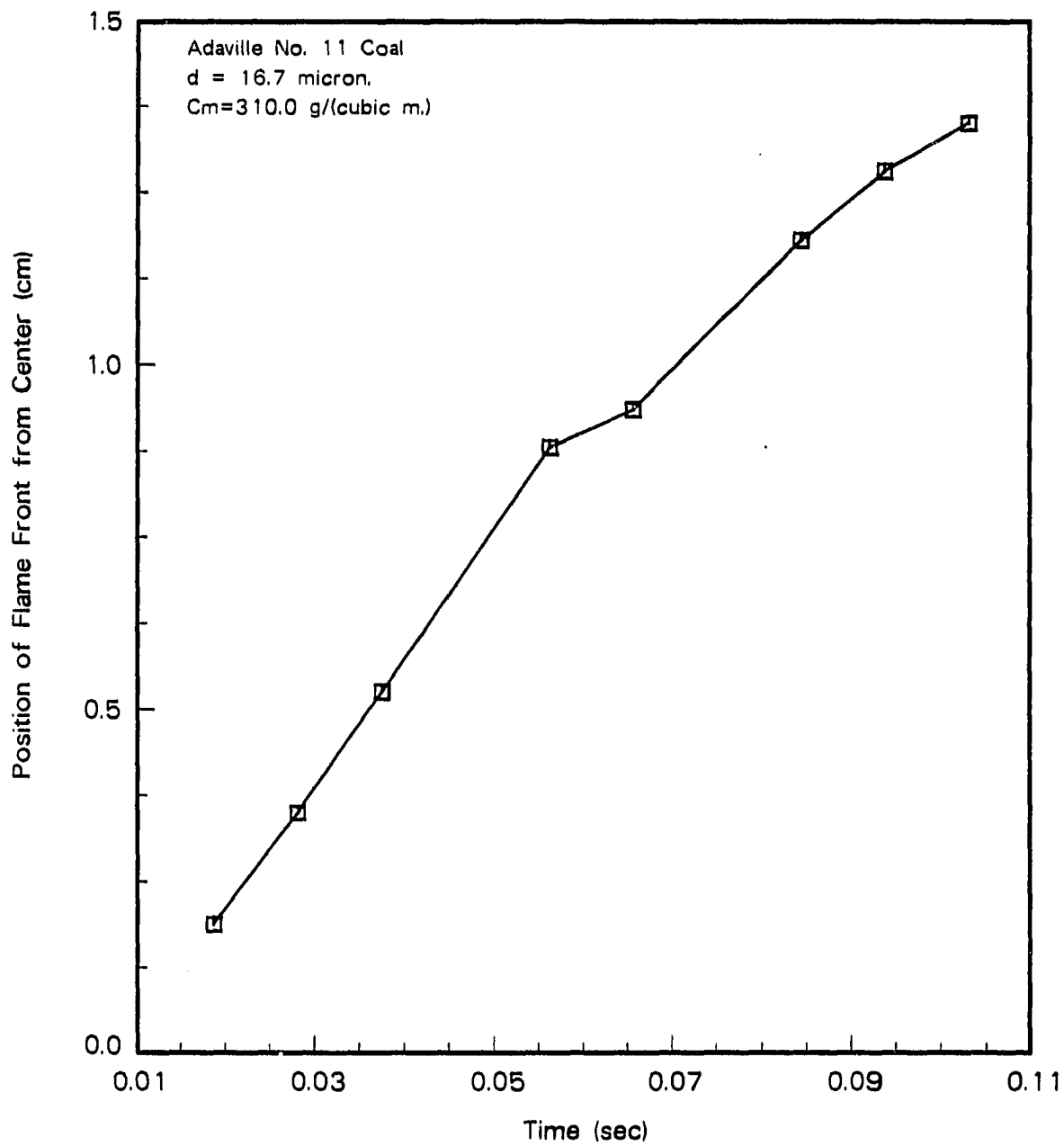


Figure 5.27: Position of flame front with time of Adaville no. 11 coal

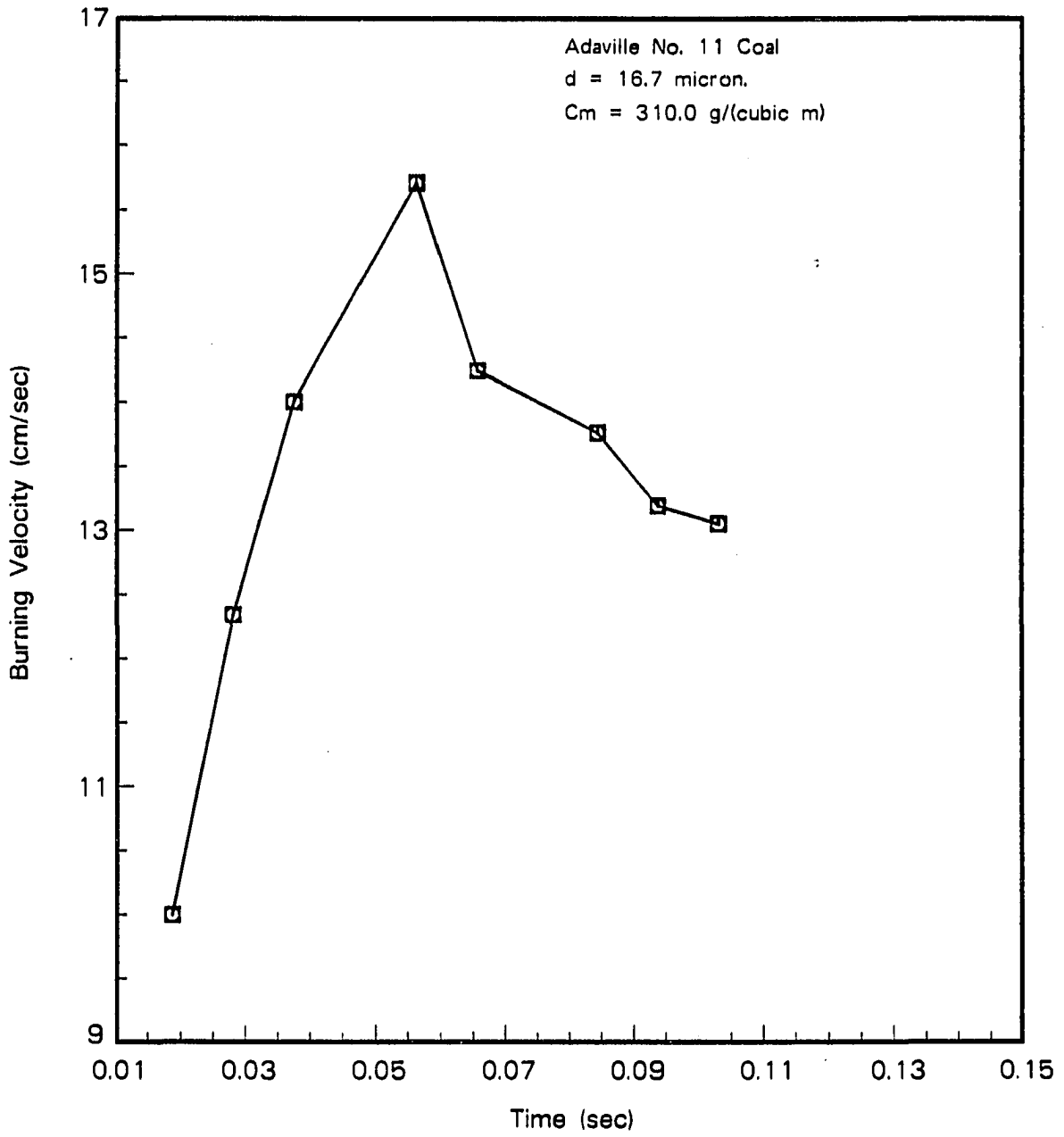


Figure 5.28: Burning velocity vs. time of Adaville no. 11 coal

and 10.6 cm/sec, respectively. The burning velocity of coal increases rapidly until it reaches a maximum then decreases slowly as the particle concentration increases. The maximum burning velocity increases as the particle size decreases.

5.5 Conclusion

A vibration exciter and air flow control to the upper electrode was used in conjunction with an electrostatic particulate suspension to achieve a uniform suspension of coal powder. Quenching distance and burning velocity of five different types of different sizes of coal powder were measured. The quenching distance of coal was observed to be influenced by particle size, concentration, and volatile content.

The quenching distance was found to increase with an increase of particle size and with a decrease in the volatile content. The volatile content does not affect the quenching distance as much as the particle size, especially in the high volatile content range. Finally, quenching distance of the coal is seen to decrease until it reaches a minimum and then increases as the particle concentration increases.

The burning velocity of Adaville no. 11 coal was measured with a high speed camera. The effect of particle concentration on quenching distance of Penn. Seam coal was investigated using two different sizes of coal powder. It is found that the burning velocity increases rapidly until it reaches a maximum and then decreases slowly as the particle concentration increases. In addition, the maximum burning velocity of this coal is on the order of 10.0 cm/sec, and it decreases as the particle size increases.

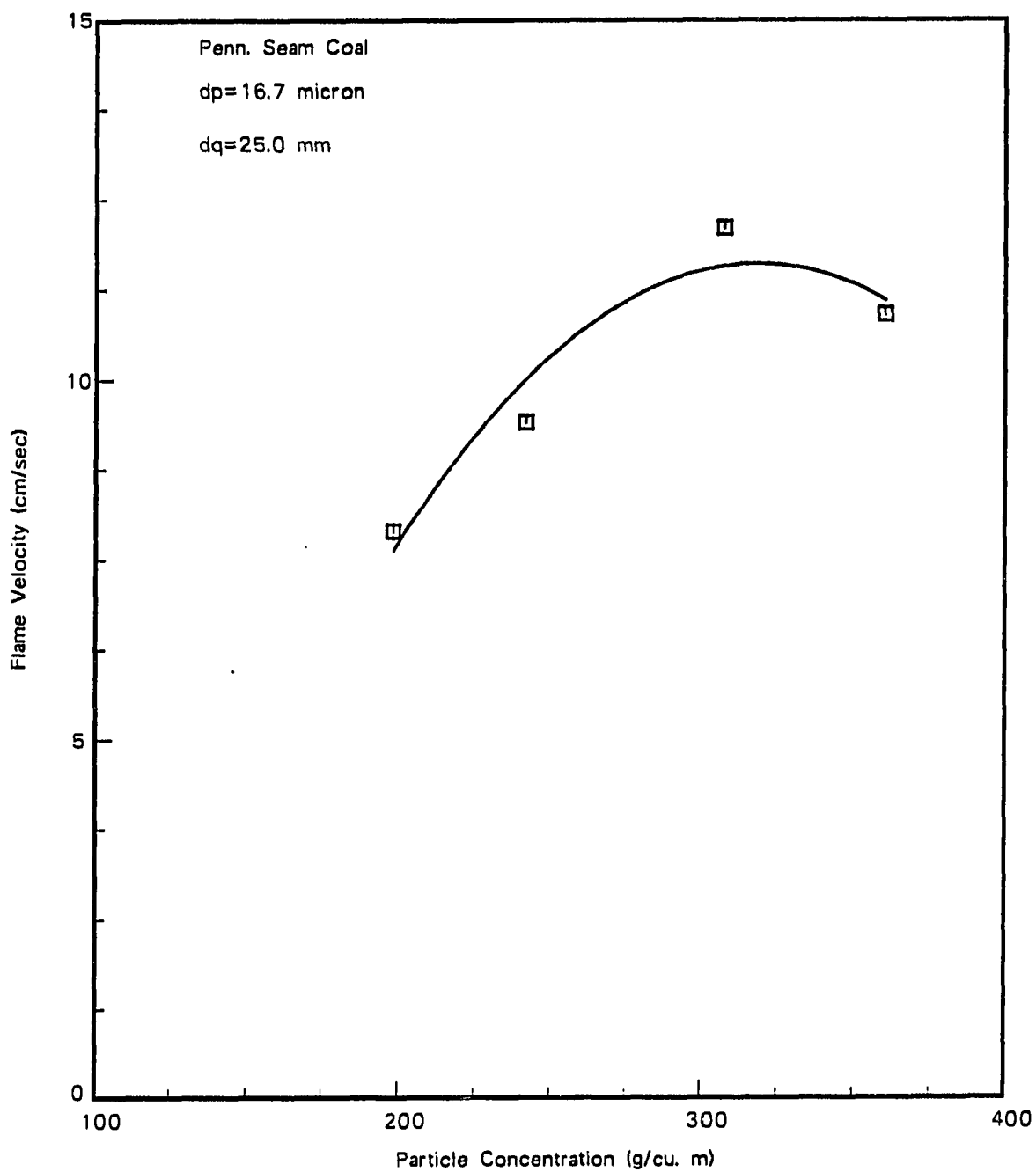


Figure 5.29: Burning velocity vs. particle concentration of $16.7 \mu\text{m}$ Penn. Seam coal

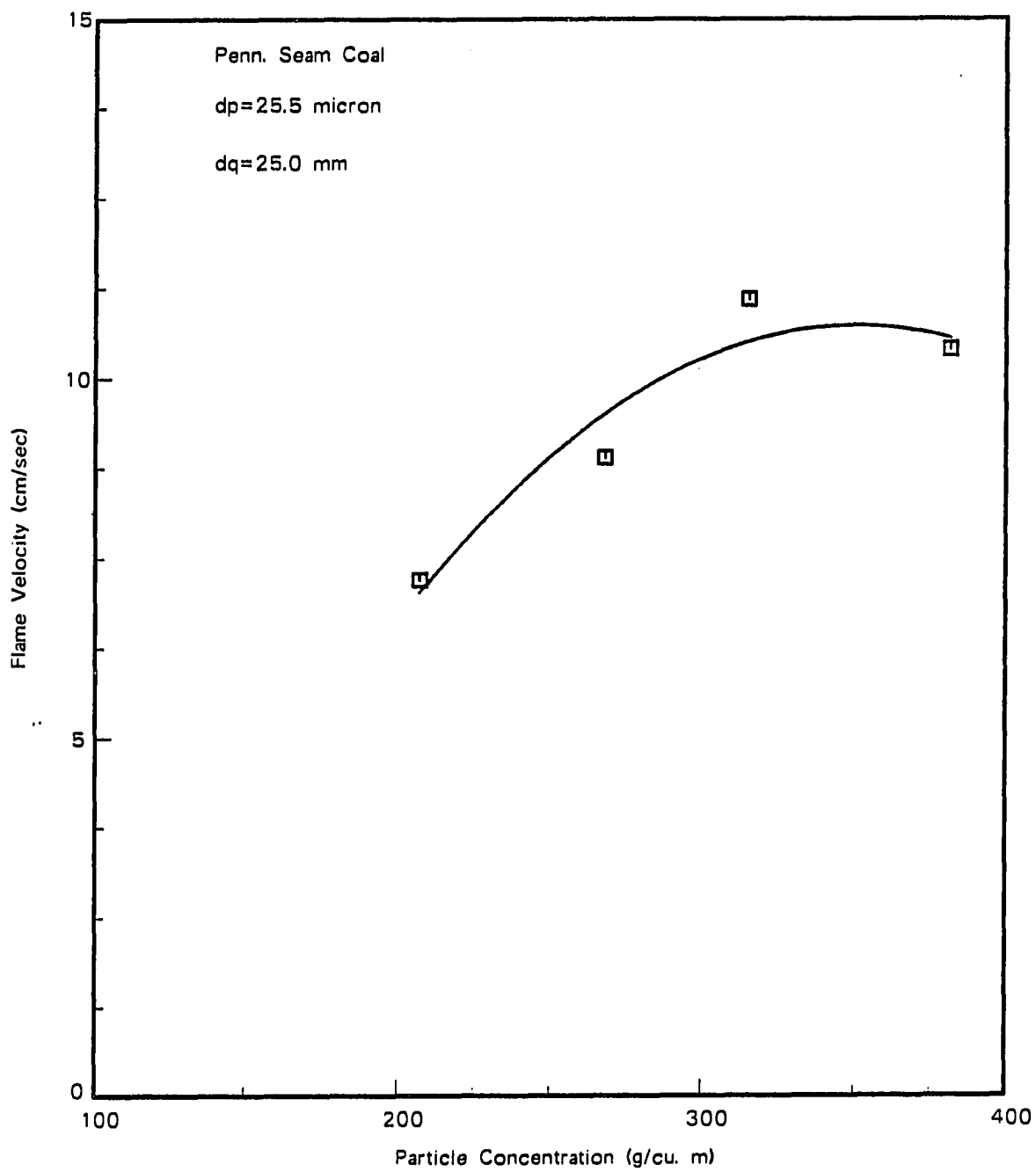


Figure 5.30: Burning velocity vs. particle concentration of $25.5 \mu m$ Penn. Seam coal

6 CORRELATIONS OF QUENCHING DISTANCE

Correlation of the experimental data is important in a sense that necessary and important experimental quantities can be found from a correlation equation without referring to graphs or tables. Also, correlation equations clearly show the effect of each independent variables on the dependent variable.

A multiple regression method was used to correlate the quenching distance to the independent variables; particle concentration, particle diameter, volatile content. A summary of regression theories is well documented in Kennedy and Neville [1976].

For this multiple regression analysis, RS/1 a statistical package has been used. A least square multiple regression of polynomial fit facility called FITGLM in RS/1 is used.

6.1 Quenching Distance Correlation of Aluminum Powder

In the case of aluminum, experimental data for quenching distance, d_q , were collected for two independent variables, particle concentration C_m and particle diameter d_p . Even though the effect of relative humidity and external voltage were investigated, these two independent variables are not considered in the correlation, because they are found not to be significant enough to affect the quenching distance.

The equation is in functional form,

$$d_q = f(C_m, d_p) \quad (6.1)$$

The variables are non-dimensionalized by dividing each variables by dimensional constants. The quenching distance d_q is non-dimensionalized by dividing by $d_{q,min}$, which is the minimum quenching distance of all the aluminum powders tested, where $d_{q,min}$ equals to 3.50 mm. The particle concentration C_m is non-dimensionalized by dividing by the stoichiometric concentration of aluminum $C_{m,stoi}$, which has a value of 302.0 g/m^3 . The particle diameter d_p is non-dimensionalized by dividing by the minimum particle diameter of aluminum powders tested in this research, $d_{p,min}$, which is equal to 12.5 μm . Thus, the non-dimensionalized form of the variables are;

$$\bar{d}_q = \frac{d_q}{d_{q,min}} \quad (6.2)$$

$$\bar{C}_m = \frac{C_m}{C_{m,stoi}} \quad (6.3)$$

$$\bar{d}_p = \frac{d_p}{d_{p,min}} \quad (6.4)$$

A quadratic form of multiple least square regression is used, which takes the following form.

$$y = c_1 + a_1x_1 + a_2x_2 + a_3x_1^2 + a_4x_1x_2 + a_5x_2^2 \quad (6.5)$$

where, y is the dependent variable, x_1 and x_2 are independent variables, and c_1, a_1, \dots, a_5 are constants. The data that is used for this correlation is listed in Tables 14.4 - 14.18. The regression analysis is performed in RS/1 and the coefficients, standard error, significance level, mean square values are listed in Table 6.1.

Table 6.1: Regression coefficients and analysis of variance of spherical aluminum

Parameter	Coef.	Standard Error	Sig. level
CONSTANT	-0.5138	0.5757	0.3727
X1: Dp	4.1348	0.4682	0.0001
X2: Cm	-1.1498	0.0998	0.7056
X1**2	-0.0377	0.0998	0.7056
X1*X2	-0.6044	0.0369	0.0001
X2**2	0.2848	0.0161	0.0001

The final result is as follows.

$$\bar{d}_q = -0.514 + 4.135\bar{d}_p - 1.150\bar{C}_m - 0.038\bar{d}_p^2 - 0.604\bar{d}_p\bar{C}_m + 0.285\bar{C}_m^2 \quad (6.6)$$

The plot of observed and predicted values in quenching distance versus particle concentration curves of each particle size is shown in Figure 6.1. The predicted values of all particle sizes except for 22.5 μm matches very well. The predicted values match very well at the lean particle concentrations, but they deviate as they reaches to the rich particle concentrations. The reason for this discrepancy is because, in case of 22.5 μm particles, the particle concentration goes to richer concentrations than any other particle sizes.

The residuals are plotted along with the predicted values to observe more closely how well this correlation equation estimates the experimental data. They are shown in Figure 6.2. All the residuals are within $\pm 5\%$ of observed values above the non-dimensionalized quenching distance of 6.0. Overall, the residuals are within $\pm 7\%$ of observed values.

6.2 Quenching Distance Correlation of Coal Powders

For coal, three independent variables were correlated; particle concentration, particle diameter, and volatile content. In functional form, the correlation equation takes the following form.

$$d_q = f(C_m, d_p, \phi) \quad (6.7)$$

The variables are non-dimensionalized at the same manner as the case of aluminum correlation. The quenching distance d_q is non-dimensionalized by dividing

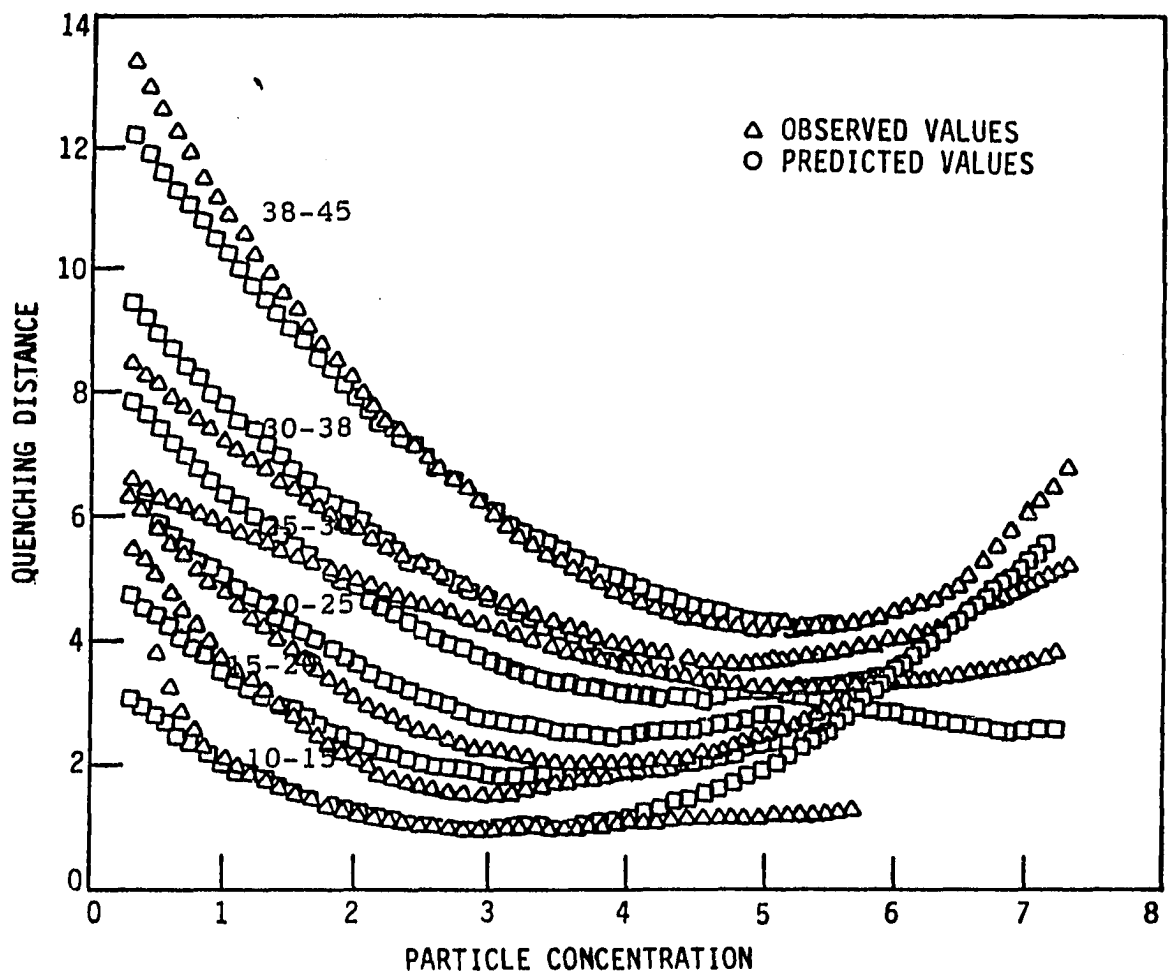


Figure 6.1: Predicted vs. observed data of regression of aluminum powders

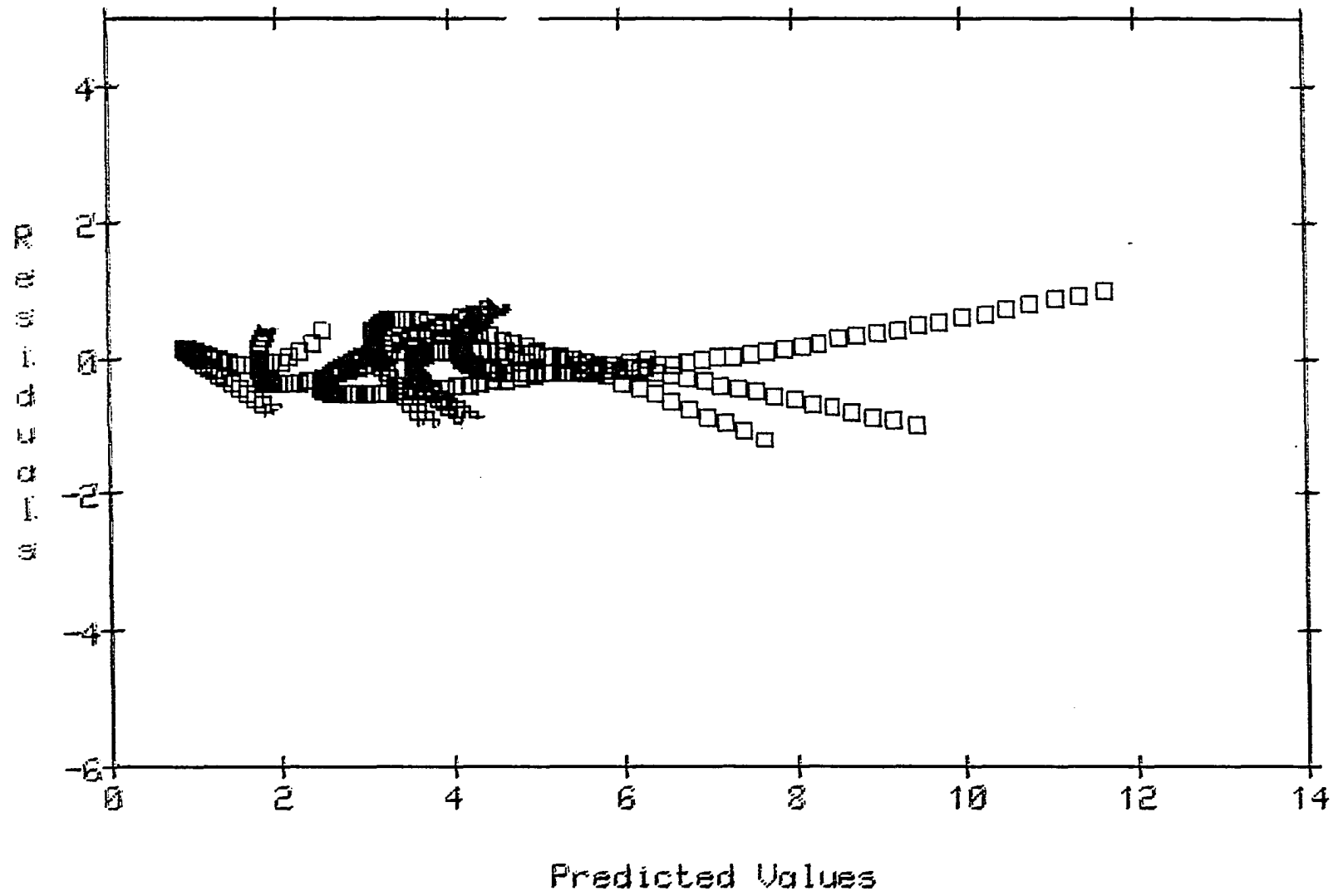


Figure 6.2: Residual vs. predicted values of regression of aluminum powders

by the minimum quenching distance of all the coal powders tested, $d_{q,min}$, which is 8.50 mm. The particle concentration C_m is non-dimensionalized by dividing by the stoichiometric particle concentration of coal $C_{m,stoi}$ which equals to 210.0 g/m^3 . The particle diameter d_p is non-dimensionalized by dividing by the minimum particle diameter of coal tested in this research $d_{p,min}$ which equals to 9.1 mm. The volatile content ϕ is already dimensionless so does not need to be non-dimensionalized. So, the non-dimensionalized form of the variables are

$$\bar{d}_q = \frac{d_q}{d_{q,min}} \quad (6.8)$$

$$\bar{C}_m = \frac{C_m}{C_{m,stoi}} \quad (6.9)$$

$$\bar{d}_p = \frac{d_p}{d_{p,min}} \quad (6.10)$$

$$\bar{\phi} = \phi \quad (6.11)$$

A quadratic form of least square multiple regression is used for this correlation of coal data. A quadratic form takes the following form.

$$y = c_1 + a_1x_1 + a_2x_2 + a_3x_3 + a_4x_1^2 + a_5x_1x_2 + a_6x_1x_3 + a_7x_2^2 + a_8x_2x_3 + a_9x_3^2 \quad (6.12)$$

where, y is the dependent variable, x_1 , x_2 and x_3 are independent variables, and c_1 , a_1, \dots, a_9 are constants. the experimental data that are used for this correlation is listed in Tables 14.28 - 14.58. The regression analysis is performed in RS/1 and the coefficients, standard error, significance level, mean square values are listed in Table 6.2.

Table 6.2: Regression coefficients and analysis of variance of spherical aluminum

Parameter	Coef.	Standard Error	Sig. level
CONSTANT	4.3636	0.5375	0.0001
X1: Dp	-6.0069	0.4673	0.0001
X2: Cm	1.8880	0.1949	0.0001
X3: psi	0.0176	0.0194	0.3658
X1**2	2.0189	0.1485	0.0001
X2*X2	-0.9547	0.1006	0.0001
X1*X3	0.0386	0.0073	0.0001
X2**2	0.1753	0.0302	0.0001
X2*X3	-0.207	0.0032	0.0001
X3**2	-0.0010	0.0003	0.0002

The final result is as follows.

$$\begin{aligned} \bar{d}_q = & 4.364 + 1.888\bar{d}_p - 6.007\bar{C}_m + 0.018\phi + 2.019\bar{C}_m^2 \\ & - 0.955\bar{d}_p\bar{C}_m + 0.039\bar{C}_m\bar{\phi} + 0.175\bar{d}_p^2 - 0.021\bar{d}_p\bar{\phi} - 0.001\bar{\phi}^2 \end{aligned} \quad (6.13)$$

The plot of observed and predicted values in quenching distance versus particle concentration curves for each particle size and volatile content is shown in Figure 6.3. The predicted values match very well at all particle concentration ranges.

The residuals are plotted with the predicted values to observe more closely how well this correlation equation estimates the experimental data. They are shown in Figure 6.4. All the residuals are within $\pm 5\%$ of observed values.

6.3 Conclusion

The correlation equations are obtained for the experimental data of aluminum and coal powder. The predicted values match well with the experimental data, specifically the errors are within $\pm 7\%$ and $\pm 5\%$ for aluminum and coal powders, respectively.

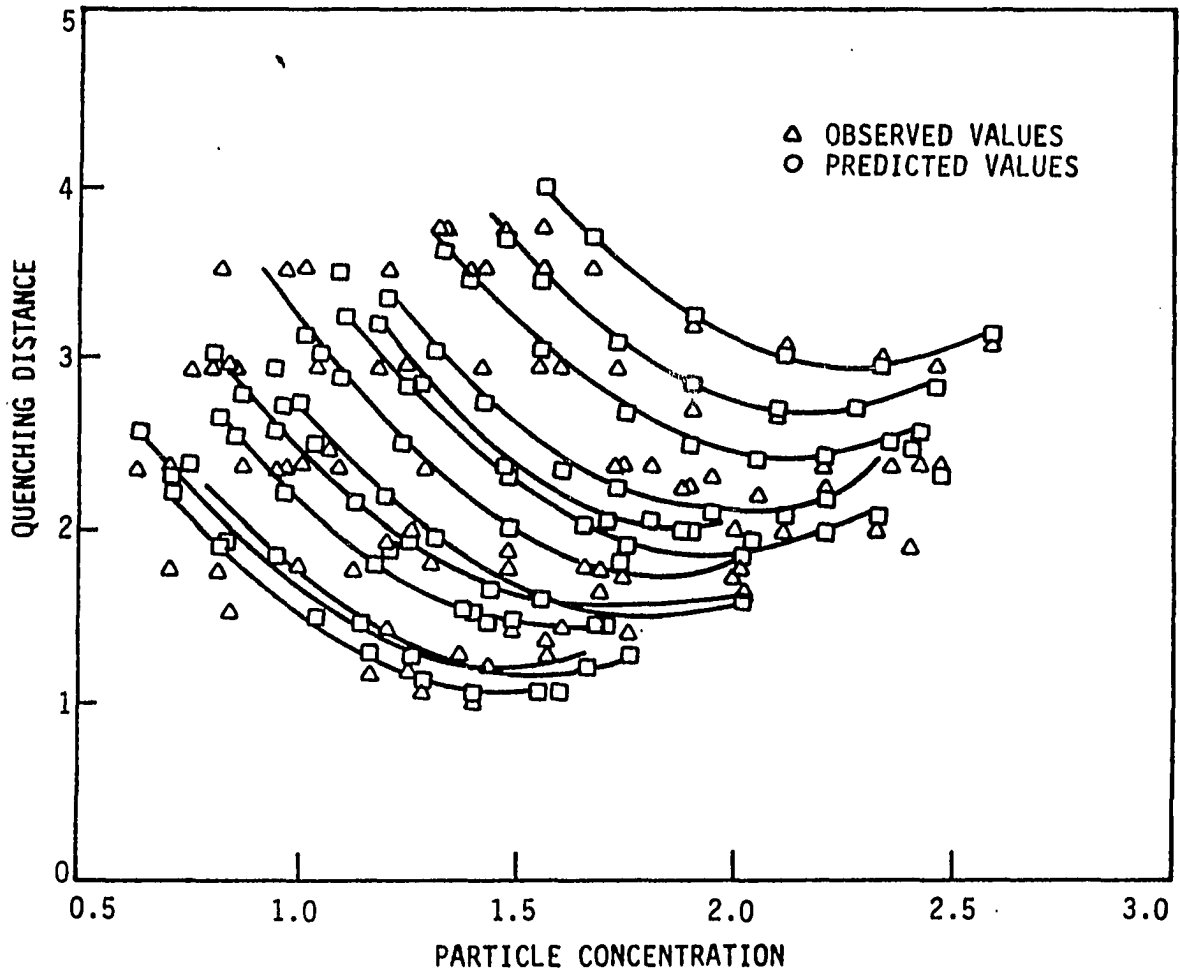


Figure 6.3: Predicted vs. observed data of regression of coal powders

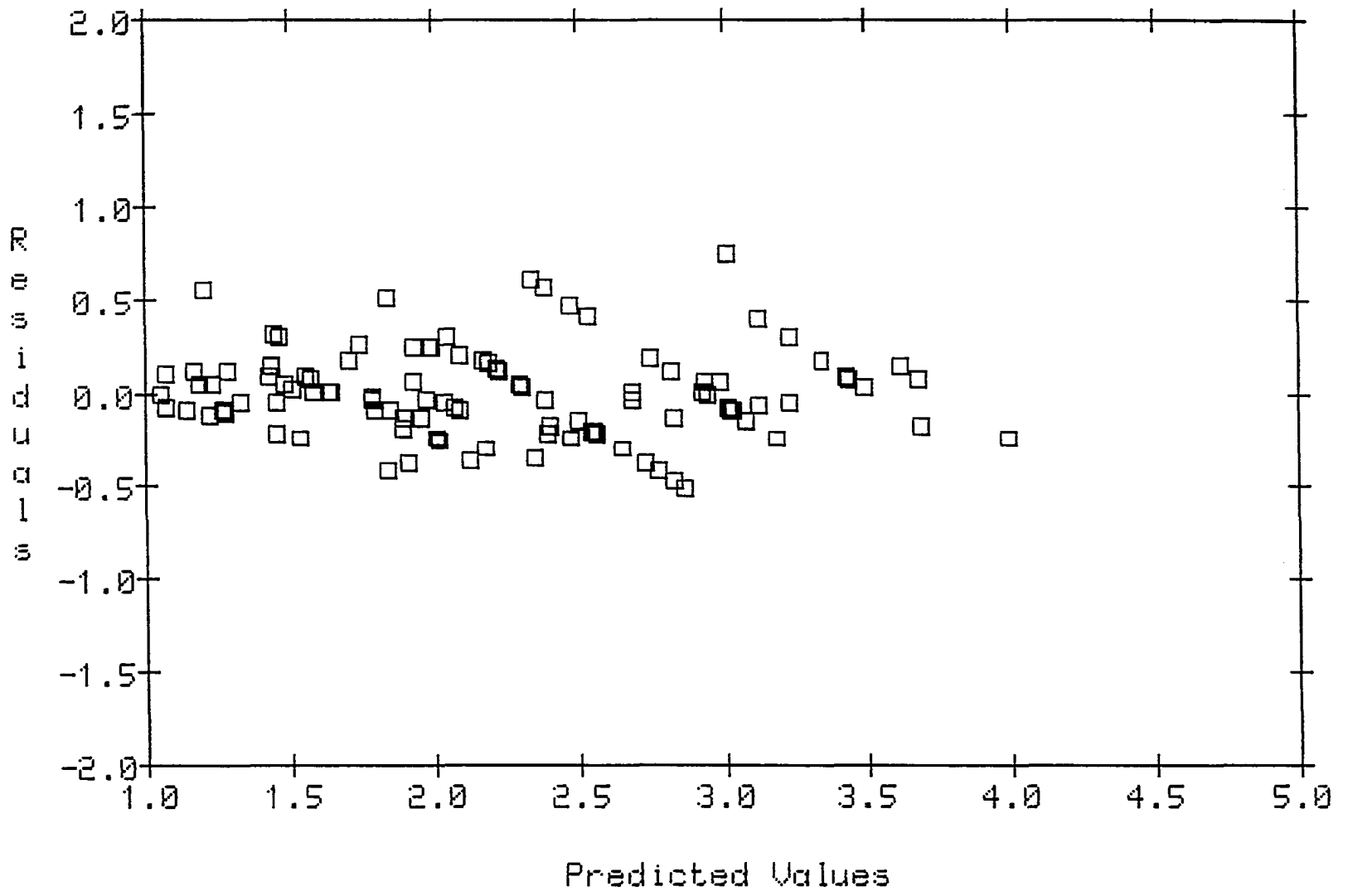


Figure 6.4: Residual vs. predicted values of regression of coal powders

7 COMPUTER SIMULATION OF ALUMINUM COMBUSTION

7.1 Formulation

The mathematical model developed here simulates the flame propagation of an aluminum-air flame. The propagation of aluminum flame is idealized as one-dimensional in a cylindrical test section with a spark ignition at the center.

A dust explosion is a multiphase reactive flow, and a key question is how to describe the physical and chemical processes occurring in the multiphase mixture. Wallis [1969] treated the multiphase mixture as a locally homogeneous fluid. The local values of the continuum field variables; temperature, velocity, concentration, density are defined by taking the average over each phase within the neighborhood of a point (Slattery [1981]). A local volume averaging technique is used in this analysis.

Kuo [1983] described the detailed mathematical formulation of locally homogeneous flow models. Ramos [1983a, b] developed a model incorporating transport models for gaseous combustion and Aggarwal and Sirignano [1985] developed a model for droplet combustion. One advantage of this method is that chemical kinetics directly appear in model considerations to replace the empirically determined burning velocity. Figure 7.1 shows the schematics of a dust explosion in a cylindrical test section.

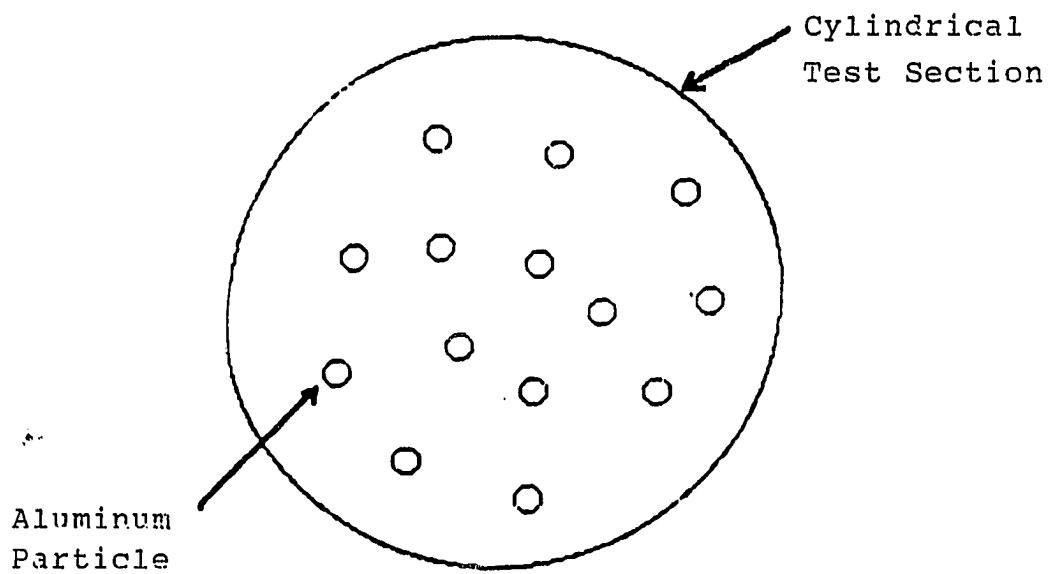


Figure 7.1: Schematics of a dust explosion in a cylindrical test section

7.2 Governing Equations

The local volume average of any field variable ψ is defined as

$$\psi_m = \frac{1}{V} \int_V \psi dV \quad (7.1)$$

The above equation states that the mixture of ψ , ψ_m , is the average of ψ at each point within the averaging volume V .

Most dust explosions are turbulent rather than laminar flows. Therefore, a suitable time-averaging technique must be employed in the analysis as well. A density-weighted time averaging technique is used. The density-weighted average of any field variable ψ is defined as

$$\bar{\psi} = \bar{\rho}\psi / \bar{\rho} \quad (7.2)$$

where the overbar denotes the conventional time average for an unsteady flow;

$$\bar{\psi} = \frac{1}{\Delta t} \int_t^{t+\Delta t} \psi d\tau \quad (7.3)$$

It has been implicitly assumed that the local volume averages and density-weighted averages are commutative.

The major assumptions invoked in this analysis are as follows.

1. One-dimensional, unsteady radial flow with cylindrical symmetry.
2. Body forces and viscous dissipation is neglected.
3. Uniform pressure distribution throughout the test section, so that momentum equation can be safely neglected.
4. Gas mixture obeys the ideal gas law.

5. Gas-particle mixture is optically thick.

6. Temperature lag and velocity drag between the particle and the gas are neglected.

The energy equation includes turbulent diffusion, thermal radiation, and an heat generation due to chemical reaction.

The conservation equations of mass, species continuity, and energy equation are given below:

Mixture continuity:

$$\frac{\partial \rho_m}{\partial t} + \frac{1}{r} \frac{\partial}{\partial r} (\rho_m v r) = 0 \quad (7.4)$$

Mixture thermal energy:

$$\rho_m C_{p,m} \left(\frac{\partial T}{\partial t} + v \frac{\partial T}{\partial r} \right) = \frac{\partial P}{\partial t} + \sum_{i=1}^N H_i^0 r_i''' + \frac{1}{r} \frac{\partial}{\partial r} [(k_m + k_t + k_r) r \frac{\partial T}{\partial r}] \quad (7.5)$$

Mixture species continuity:

$$\rho_m \left(\frac{\partial Y_i}{\partial t} + v \frac{\partial Y_i}{\partial r} \right) = \frac{1}{r} \frac{\partial}{\partial r} [(D_m + D_t) \rho_m r \frac{\partial Y_i}{\partial r}] + r_i''' \quad (7.6)$$

Mass fraction:

$$Y_N = 1 - \sum_{i=1}^{N-1} Y_i \quad (7.7)$$

Equation of state:

$$PW = \rho_g R_g T, (W = [\sum_{i=1}^N (Y_i / W_i)]^{-1}) \quad (7.8)$$

Mixture momentum:

$$P = P(t) \quad (7.9)$$

where, v is a radial velocity of the mixture, D_m and D_t are mixture and turbulent mass diffusivities, respectively, k_m , k_t , and k_r are thermal, turbulent, and radiative thermal conductivities respectively, H_i^0 is a enthalpy of formation of specie i , and r_i''' is volumetric heat source term due to homogeneous and heterogeneous chemical reactions.

7.3 Formulation of Reaction Mechanism

To date, there is no experimental study on reaction mechanism. Law [1973] proposed a model for vapor-phase combustion of metal particles. Recently, Ogle [1986] postulated a reaction mechanism of aluminum combustion consisting of four gas phase reactions and one heterogeneous reaction at the aluminum surface which is a rate determining step, and one heterogeneous reaction at the surface of aluminum oxide. His model is based on Markstein's [1966] model for a burning aluminum droplet. In his model for droplet combustion, the fuel is oxidized through a number of homogeneous and heterogeneous reactions. The schematic of a burning aluminum droplet is shown in Figure 7.2. The metal droplet is surrounded by a region of homogeneous reactions and this is surrounded by a cloud of metal oxide droplets created by a heterogeneous reaction. In this computer simulation of aluminum combustion, Ogle's model is adopted.

The sequence of steps are as follows.



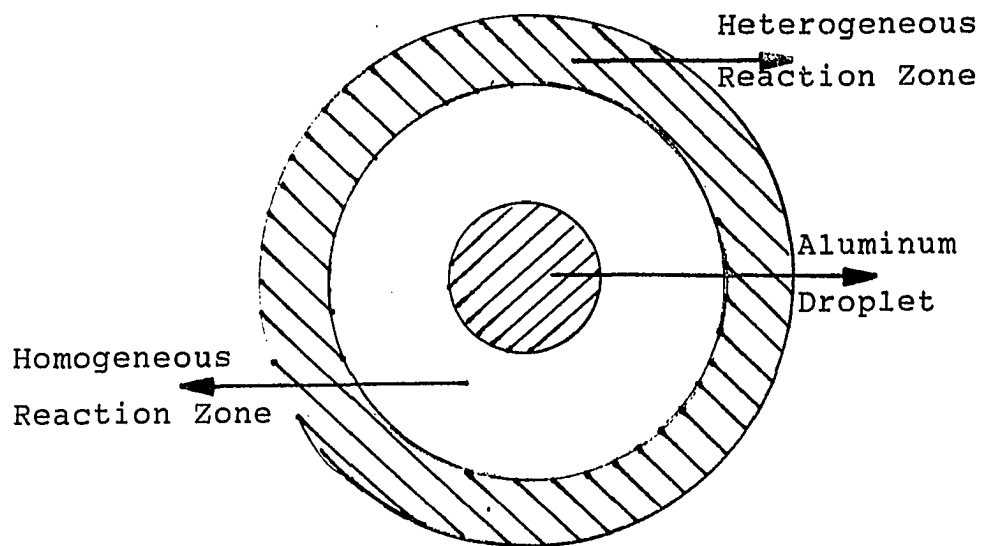


Figure 7.2: Schematics of a burning aluminum droplet (Markstein [1966])



The rate of heterogeneous reaction is transformed into a quasi-homogeneous reaction rate.

$$r_{Al}''' = \alpha S_v r_{Al}'' \quad (7.16)$$

where, R_{Al}'' is the reaction rate in moles of aluminum per unit surface area of particles per time, S_v is the surface to volume fraction of aluminum particle. The reaction rate in mass unit is as follows.

$$r_{Al}''' = -\alpha S_v k \rho_m^{3/2} Y_{Al} Y_{O_2}^{1/2} \quad (7.17)$$

And, the rate coefficient k is written in Arrhenius form;

$$k = A \exp(-E/R_g T) \quad (7.18)$$

Thus, the reaction rate takes the following form.

$$r_{Al}''' = \alpha S_v A \rho_m^{3/2} Y_{Al} Y_{O_2}^{1/2} \exp(-E/R_g T) \quad (7.19)$$

Ogle [1986] found the pre-exponential factor A and activation energy E by trial and error by fitting his experimental data on pressure rise into his mathematical model.

No data are yet available for an overall rate equation for aluminum combustion. Using the conservation of total mass,

$$\sum_{i=1}^N r_i''' = 0 \quad (7.20)$$

the rate of reaction of other species can be related to the rate of reaction of aluminum.

$$\overset{///}{r}_{O_2} = s \overset{///}{r}_{Al} \quad (7.21)$$

$$\overset{///}{r}_{N_2} = 0 \quad (7.22)$$

$$\overset{///}{r}_{Al_2O_3} = \overset{///}{r}_{Al} - \overset{///}{r}_{O_2} = -(s + 1) \overset{///}{r}_{Al} \quad (7.23)$$

where, s is a mass of oxidizer required to react with a unit mass of fuel.

7.4 Transformations

Ramos [1983a, b] used two transformations to solve model of flame propagation of gaseous fuels. Those two transformation will be used in the present model.

First, the adiabatic transformation is used to remove the rate of pressure change term in energy equation. The adiabatic transformation is defined as,

$$\phi = TP^{\frac{1-\gamma_m}{\gamma_m}} \quad (7.24)$$

where, γ_m is a heat capacity ratio of the mixture.

Second, the Lagrangian transformation is used to remove the convective terms in the governing equations, and this transformation satisfies the continuity equation automatically. The transformation is defined as follows in cylindrical coordinates.

$$\rho_m r = M \frac{\partial \psi}{\partial r} \quad (7.25)$$

$$\rho_m v r = -M \frac{\partial \psi}{\partial t} \quad (7.26)$$

and M is defined as,

$$M = \int_0^R \rho_m r dr = \frac{\rho_m R^2}{2} \quad (7.27)$$

7.5 Transport Properties

The relations to describe the radiative and turbulent heat fluxes, mass fluxes, chemical reaction rate, heat capacity, thermal conductivity, and viscosity of the gas and mixture are to be used to solve the governing equations.

Many researchers proposed that thermal radiation plays an important role in dust flame propagation. Diffusion approximation of radiative heat flux is used assuming optically thick flame. In the limit of the diffusion approximation, the radiative heat flux is obtained as follows.

$$q_r = -k_r \frac{\partial T}{\partial r} \quad (7.28)$$

where,

$$k_r = \frac{16}{3} \frac{\sigma}{a} T^3 \quad (7.29)$$

where, K_r is a radiative conductivity and dependent on particle size and concentration.

Turbulence is important transport process in a dust explosion, but there are very little data available. Abdel-Gayed et al. [1978] developed an eddy diffusivity correlation for turbulent combustion of gaseous fuels. This correlation will be used in this study, and the eddy diffusivity takes the following form.

$$\frac{\epsilon}{\nu} = 11 Re_t^{0.56} \quad (7.30)$$

where, ϵ is an eddy diffusivity, ν is a kinematic viscosity, and Re_t is a turbulent Reynolds number.

The transport properties of the mixture of pure substances are well described by Bird et al. [1960]. The heat capacity of the gas are found from polynomial correlation

of the form,

$$C_{pg,i} = \sum Z_n/T^n, T < 1200 K \quad (7.31)$$

$$C_{pg,i} = \sum Z_m/T^m, T > 1200 K \quad (7.32)$$

The viscosity of the each component of gas are calculated using the equation of the form,

$$\mu_{gi} = 1.34 \times 10^{-8} (W_i T)^{1/2} / \sigma^2 \Omega_\mu \quad (7.33)$$

The viscosity of the gas mixture is calculated using the Wilke approximation,

$$\mu_g = \sigma_i [X_i \mu_{gi} / \sigma_k X_k \phi_{ik}] \quad (7.34)$$

Thermal conductivity of each gas species are calculated from,

$$k_{gi} = (5/4) [C_{pgi} + R/2W_i] \mu_{gi} \quad (7.35)$$

and the thermal conductivity of the gas mixture is calculated using the Wilke approximation.

$$k_g = \sigma_i [X_i k_{gi} / \sigma_k X_k \phi_{ik}] \quad (7.36)$$

The above transport equations are used to solve the governing equations. The values of the various parameters are listed in Table 7.1.

7.6 Transformation of Energy Equation

An energy and species continuity equations have a similar form. So the derivation of one equation will be satisfactory.

Table 7.1: Numerical values of the parameters

Parameter	Value	Unit
W	28.9	kg/kmol
Q	3.73E6	J/kg
E	100.0	kJ/kmol
R	14.7	cm
C_{p1}	987.0	J/kgK
C_{p4}	1012.0	J/kgK
ρ_1	2700.0	kg/ m^3
ρ_4	3970.0	kg/ m^3

7.6.1 Adiabatic transformation

The adiabatic transformation is defined as,

$$\phi = TP^{\frac{1-\gamma m}{\gamma m}} \quad (7.37)$$

Define the exponent of the transformation as,

$$\Gamma = \frac{\gamma m - 1}{\gamma m} \quad (7.38)$$

The time-derivative of temperature is transformed;

$$\frac{\partial T}{\partial t} = \frac{\partial}{\partial t}(\phi P^\Gamma) = P^\Gamma \frac{\partial \phi}{\partial t} + \phi \Gamma P^{\Gamma-1} \frac{\partial P}{\partial t} \quad (7.39)$$

The spatial-derivative of temperature is transformed;

$$\frac{\partial T}{\partial r} = \frac{\partial}{\partial r}(\phi P^\Gamma) = P^\Gamma \frac{\partial \phi}{\partial r} \quad (7.40)$$

And the second-order derivative term is,

$$\frac{1}{r} \frac{\partial}{\partial r} \left(r \frac{\partial T}{\partial r} \right) = \frac{1}{r} \frac{\partial}{\partial r} \left(r P^\Gamma \frac{\partial \phi}{\partial r} \right) = P^\Gamma \frac{1}{r} \frac{\partial}{\partial r} \left(r \frac{\partial \phi}{\partial r} \right) \quad (7.41)$$

Substituting the above equations, the energy equation is transformed into the following form.

$$\frac{\partial \phi}{\partial t} + v \frac{\partial \phi}{\partial r} = \frac{S_r}{P^\Gamma \rho_m C_{p,m}} + \frac{1}{\rho_m C_{p,m}} \frac{1}{r} \frac{\partial}{\partial r} \left[(k_m + k_t + k_r) r \frac{\partial \phi}{\partial r} \right] \quad (7.42)$$

7.6.2 Lagrangian transformation

As mentioned in previous section, the transformation is defined as follows in cylindrical coordinates.

$$\rho_m r = M \frac{\partial \psi}{\partial r} \quad (7.43)$$

$$\rho_m v r = -M \frac{\partial \psi}{\partial t} \quad (7.44)$$

and M is defined as,

$$M = \int_0^R \rho_m r dr = \frac{\rho_m R^2}{2} \quad (7.45)$$

This transformation satisfies the continuity equation automatically, and transform the independent variables from Eulerian coordinate (r,t) to Lagrangian coordinate (ψ,t) .

The time-derivative term is transformed to,

$$\frac{\partial}{\partial t} = \frac{\partial}{\partial t} - (\rho_m v r) \frac{1}{M} \frac{\partial}{\partial \psi} \quad (7.46)$$

The spatial-derivative is transformed to,

$$\frac{\partial}{\partial r} = (\rho_m r) \frac{1}{M} \frac{\partial}{\partial \psi} \quad (7.47)$$

Using the above equations, the energy equation is transformed to the following form.

$$\frac{\partial \phi}{\partial t} = \frac{1}{M^2} \frac{\partial}{\partial \psi} \left[\frac{k_m}{C_{p,m}} k^* \rho_m r^2 \frac{\partial \phi}{\partial \psi} \right] + \frac{S_r}{\rho_m C_{p,m} P \Gamma} \quad (7.48)$$

where,

$$k^* = 1 + \frac{k_t}{k_m} + \frac{k_r}{k_m} \quad (7.49)$$

Also, the species continuity equation is transformed into the following form.

$$\frac{\partial Y_i}{\partial t} = \frac{1}{M^2} \frac{\partial}{\partial \psi} \left[D_m D^* \rho_m r^2 \frac{\partial Y_i}{\partial \psi} \right] + \frac{r_i'''}{\rho_m} \quad (7.50)$$

where,

$$D^* = 1 + \frac{D_t}{D_m} \quad (7.51)$$

In the above transformed energy equation, S_r represent the enthalpy source term due to chemical reaction.

7.7 Formulation of Parameters

Each of the independent variables are evaluated in terms of the transformation parameters, ψ and ϕ .

7.7.1 Temperature

Temperature T is,

$$T = \phi P^\Gamma \quad (7.52)$$

7.7.2 Density

Densities of the gas and mixture, ρ_g and ρ_m are, respectively,

$$\rho_g = P^{1/\gamma m} \frac{W}{R_g \phi} \quad (7.53)$$

$$\rho_m = \frac{\rho_g}{Y_g} \quad (7.54)$$

7.7.3 Radial coordinate

Radial coordinate r is,

$$\rho_m r dr = M d\psi \quad (7.55)$$

Integrate the above equation and substitute the above relationship,

$$r = \left[\frac{2M R_g}{W P^{1/\gamma m}} \int_0^\psi Y_g \phi d\psi \right]^{1/2} \quad (7.56)$$

7.7.4 Mixture velocity

From the mixture continuity equation,

$$\frac{\partial \rho_m}{\partial t} = -\frac{1}{r} \frac{\partial}{\partial r} (\rho_m v r) \quad (7.57)$$

Integrate the above equation using the equation,

$$\rho_m r dr = M d\psi \quad (7.58)$$

to get a relationship for the mixture velocity v ,

$$v = \frac{M}{r} \int_0^\psi \frac{\partial}{\partial t} \left(\frac{1}{\rho_m} \right) d\psi \quad (7.59)$$

7.7.5 Pressure

Using the ideal gas law and definition of adiabatic transformation,

$$P^{1/\gamma_m} = \rho_g R_g \phi / W \quad (7.60)$$

Integrate the above equation over the entire volume of the test section, and noting that ρ_g and ϕ are function of position and P is function of time.

$$2\pi h \int_0^R P^{1/\gamma_m} r dr = 2\pi h \frac{R_g}{W} \int_0^R \rho_g \phi r dr \quad (7.61)$$

Evaluate the above integral using the definition of the Lagrangian transformation.

Then,

$$P = \left[\frac{2M(R_g/W)}{R^2} \int_0^1 Y_g \phi d\psi \right]^{\gamma_m} \quad (7.62)$$

7.7.6 Total mass

Total mass of the mixture can be calculated using the above relationships starting from,

$$\rho_m r dr = M d\psi \quad (7.63)$$

$$M = \frac{P^{1/\gamma_m} W R^2}{2R_g} \left[\int_0^1 Y_g \phi d\psi \right]^{-1} \quad (7.64)$$

7.8 Burning Velocity

First, the mixture continuity equation is,

$$\frac{\partial \rho_m}{\partial t} + \frac{1}{r} \frac{\partial}{\partial r} (\rho_m v r) = 0 \quad (7.65)$$

At steady state, the time-derivative term goes to zero. Thus,

$$(\rho_m v r)_{unburned} = (\rho_m v r)_{burned} \quad (7.66)$$

From the species continuity equation,

$$\rho_m \left(\frac{\partial Y_i}{\partial t} + v \frac{\partial Y_i}{\partial r} \right) = \frac{1}{r} \frac{\partial}{\partial r} [(D_m + D_t) \rho_m r \frac{\partial Y_i}{\partial r}] + r_i''' \quad (7.67)$$

And, the Lagrangian transformation,

$$\frac{\partial}{\partial t} = \frac{\partial}{\partial t} - (\rho_m v r) \frac{1}{M} \frac{\partial}{\partial \psi} \quad (7.68)$$

The time-derivative term and the diffusion term disappear at the steady state.

Thus,

$$\frac{(\rho_m v r)_u}{M} (Y_{ib} - Y_{iu}) = \int_{\psi_u}^{\psi_b} \frac{r_i'''}{\rho_m} d\psi \quad (7.69)$$

where, the subscripts u and b represent the unburned and burned state, respectively.

Finally, the burning velocity S_u is,

$$S_u = \frac{M \int_{\psi_u}^{\psi_b} \frac{r_i'''}{\rho_m} d\psi}{(\rho_m r)_u (Y_{ib} - Y_{iu})} \quad (7.70)$$

7.9 Boundary and Initial Conditions

Boundary conditions are set by assuming that the cylinder wall is adiabatic and impermeable, also the heat and mass flux are zero at the center. Therefore, at $r = 0$

and R

$$\frac{\partial Y_i}{\partial r} = 0 \quad (7.71)$$

And,

$$\frac{\partial T}{\partial r} = 0 \quad (7.72)$$

The initial condition for temperature is based on the release of 10 joules into a volume of 1/10 of the total volume. This corresponds to the activation of the spark ignition. The temperature inside the central ignition zone is set at the temperature higher than the boiling temperature of the aluminum. The mass fraction initial condition is set such that a stoichiometric mixture are ignited initially at the central ignition zone, and also it is assumed that half of aluminum particle and oxygen reacts at the central ignition zone. And the pressure is set at the atmospheric pressure initially.

7.10 Finite Difference Method

Ramos [1983b] used nine different finite difference methods including explicit, implicit, Crank-Nicolson method, and method of lines to solve problem of a flame propagation of gaseous fuels. He reported that the explicit method is the most efficient method and the error is within 2 %. Thus, an explicit method is used in this simulation. A forward differencing is used for the time-derivatives and central differencing is used for spatial derivatives.

The governing system of equations can be represented in the following form.

$$\frac{\partial A}{\partial t} = B \frac{\partial}{\partial \psi} [Cr^2 \frac{\partial A}{\partial \psi}] + S \quad (7.73)$$

The staggered grid method is used along with central differencing method for spatial derivatives.

$$\frac{A^{n+1} - A^n}{\Delta t} = \frac{B}{\Delta \psi^2} [C_{i+1/2} r_{i+1/2}^2 (A_{i+1} - A_i) - C_{i-1/2} r_{i-1/2}^2 (A_i - A_{i-1})] \quad (7.74)$$

where,

$$r_{i+1/2} = \frac{r_i + r_{i+1}}{2} \quad (7.75)$$

$$r_{i-1/2} = \frac{r_i + r_{i-1}}{2} \quad (7.76)$$

$$C_{i+1/2} = \frac{C_i + C_{i+1}}{2}$$

$$C_{i-1/2} = \frac{C_i + C_{i-1}}{2}$$

7.11 Trapezoidal Method

A trapezoidal method is used to integrate the equations. When the distance x is divided into k sub-divisions from $x = a$ to $x = b$ with a width of h for each subdivision, the integration of function $f(x)$ is represented as follows.

$$\int_{x=a}^{x=b} f(x) dx = \frac{h}{2} [f(a) + 2 \left(\sum_{j=1}^{k-1} f(a + jh) \right) + f(b)] \quad (7.77)$$

7.12 Results and Discussions

The numerical productions are made for $12.5 \mu\text{m}$ aluminum powder at the concentration of 302.0 g/m^3 which is a stoichiometric concentration. The predicted burning velocity value was 22.8 cm/sec comparing to the experimental value of 41.0 cm/sec . The predicted burning velocity is lower than the experimental value. Figure

7.3 shows the temperature profile. The temperature at the center is 3630.0 K and decreases slowly to 2500 K at 5.3 cm from the center then decreases sharply to room temperature. Since the temperature profile is not experimentally determined, it was impossible to compare with the experimental data. Figure 7.4 shows the profile of mass fraction of aluminum, oxygen, and aluminum oxide. As expected the amount reactants decreases and the amount product increases as time progresses. Figure 7.5 shows the pressure history with time. Initially, the pressure increases sharply to 3.1 atm at 1 msec then increases slowly to 5 atm at 20 msec. About 3 minutes of CPU time is taken to reach the steady-state which is $t = 30$ msec. Burning velocities at 214.2 and 459.0 g/m^3 are predicted numerically to see the effect of particle concentration. The burning velocity of 19.23 cm/sec and 23.05 cm/sec are obtained at the concentrations of 214.2 and 459.0 g/m^3 , respectively. They are plotted at Figure 7.6 and compared with experimental value. The predicted values are about 20.0 cm/sec below the experimental values, but the trends are same. The discrepancies are mainly due to the homogeneous model of governing equations. A heterogeneous model that solves the balance equations for each of the gas and particle phase in the system should be adopted for better estimation of combustion characteristics.

The predicted burning velocity values are used to predicted the quenching distance of aluminum-air flame using Ballal's model of quenching. The equation take the following form.

$$d_q = (8\alpha)^{1/2} \left[\left(\frac{C_3^3 \rho_f D_{32}^2}{8C_1 f^2 (k/C_p) \phi \ln(1+B)} + \frac{12.5\alpha}{S_u^2} \right)^{-1} - \frac{9qC_1^2 \epsilon \sigma T_p^4}{C_p \rho_f C_3^3 f D_{32} \Delta T_{st}} \right]^{-1/2} \quad (7.78)$$

The derivation of the Ballal's model is given in Appendix 2. The predicted quench-

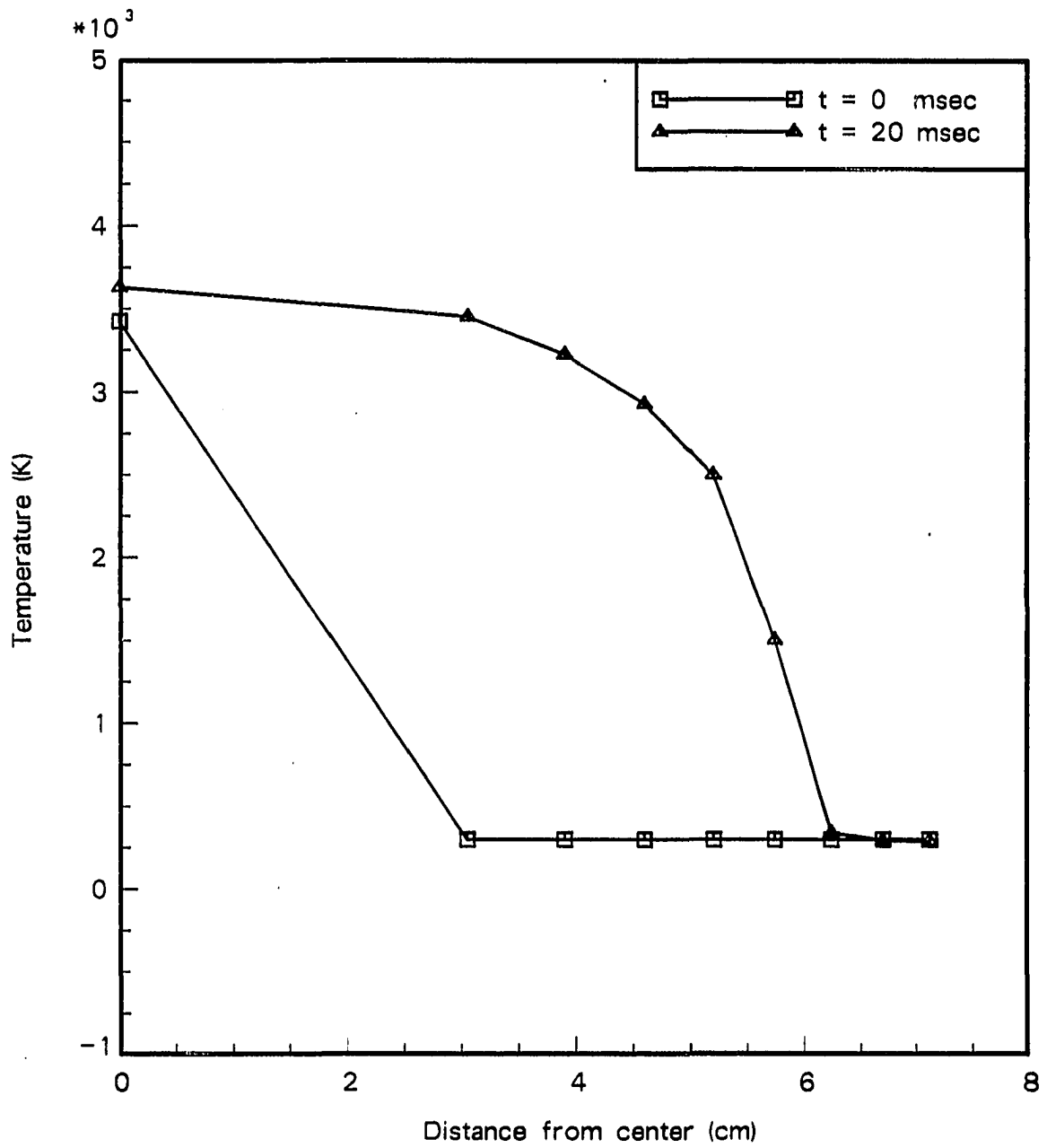


Figure 7.3: Predicted temperature profile

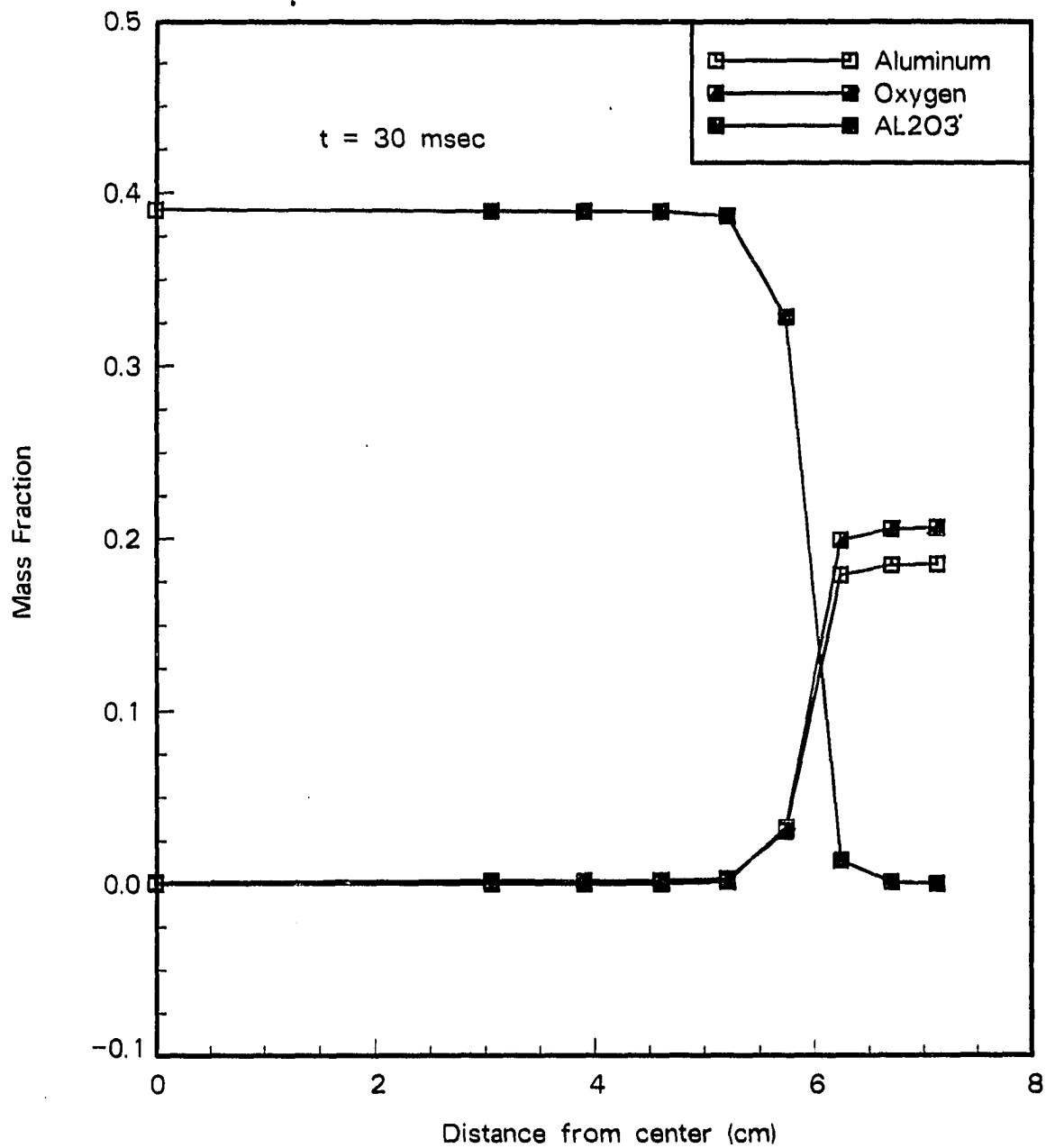


Figure 7.4: Predicted profile of mass fractions of reactants and product

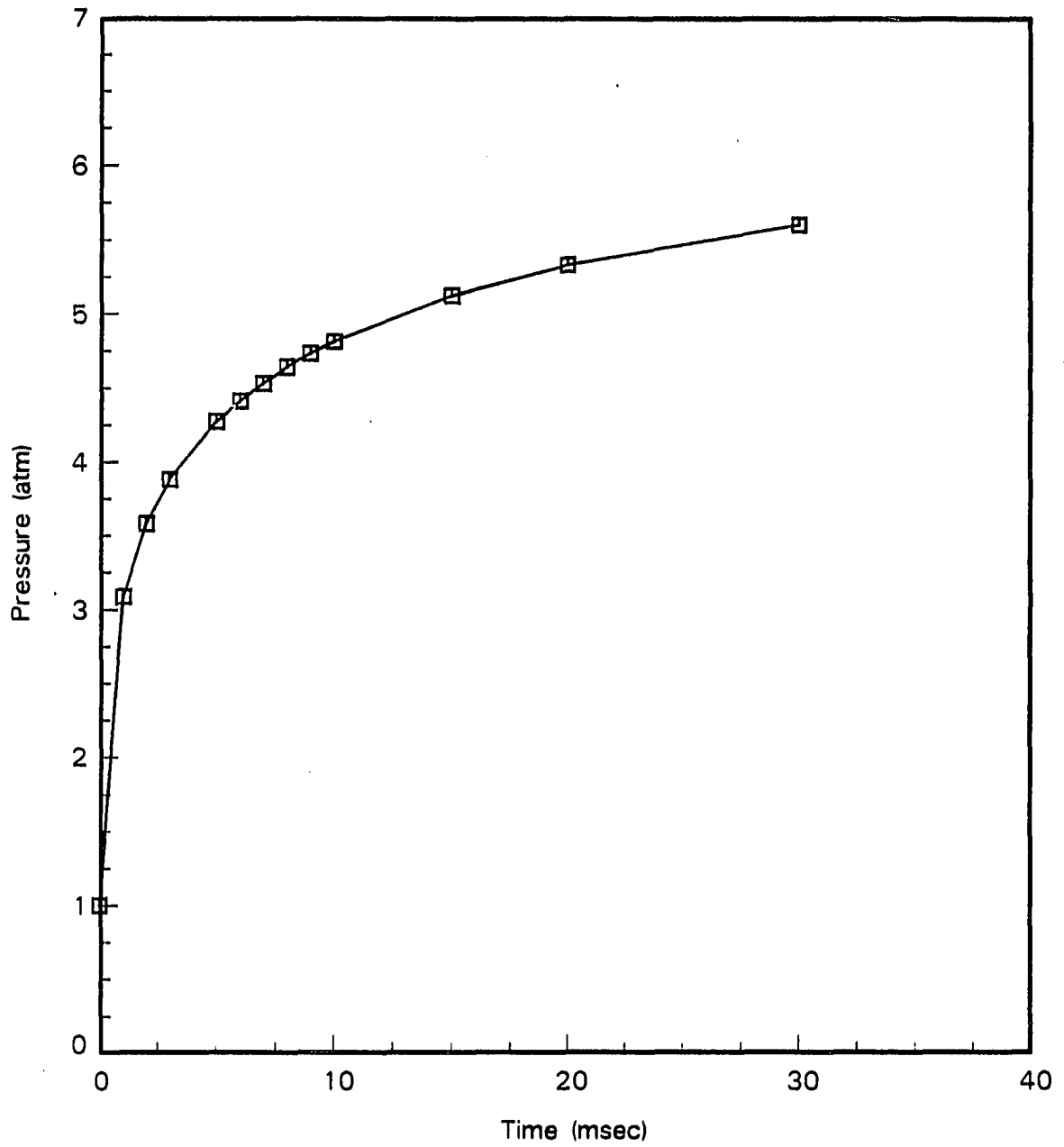


Figure 7.5: Predicted pressure history

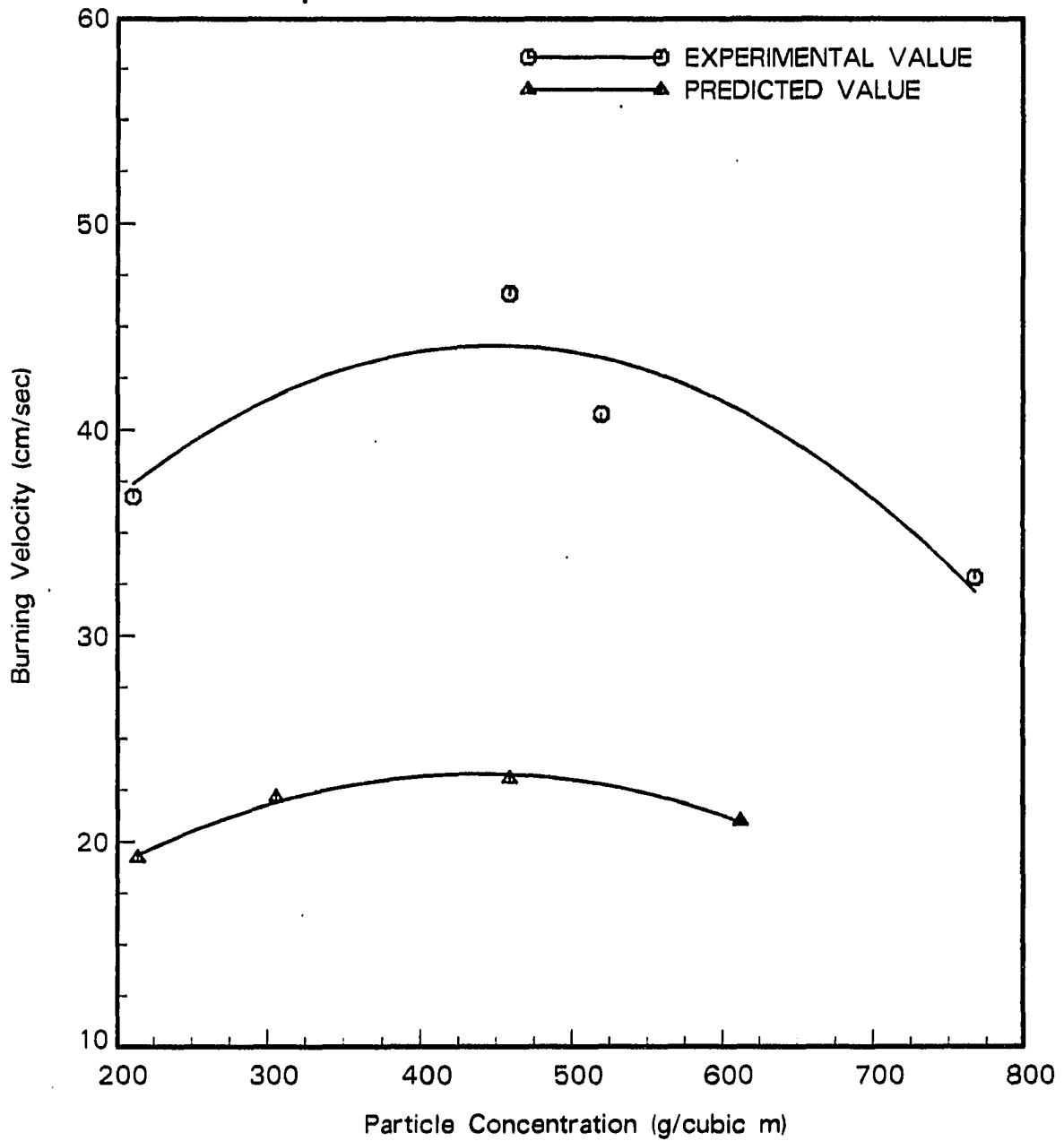


Figure 7.6: Predicted burning velocities

ing distance are compared with the experimental data and it is shown in Figure 7.7. The predicted quenching distance matches very well with the experimental quenching distance at the particle concentration range of 250.0 to 410.0 g/m^3 . As the particle concentration increases, the predicted values over-predict the experimental data. This deviation is mainly due to the uncertain reaction mechanism and homogeneous formulation of this mathematical model.

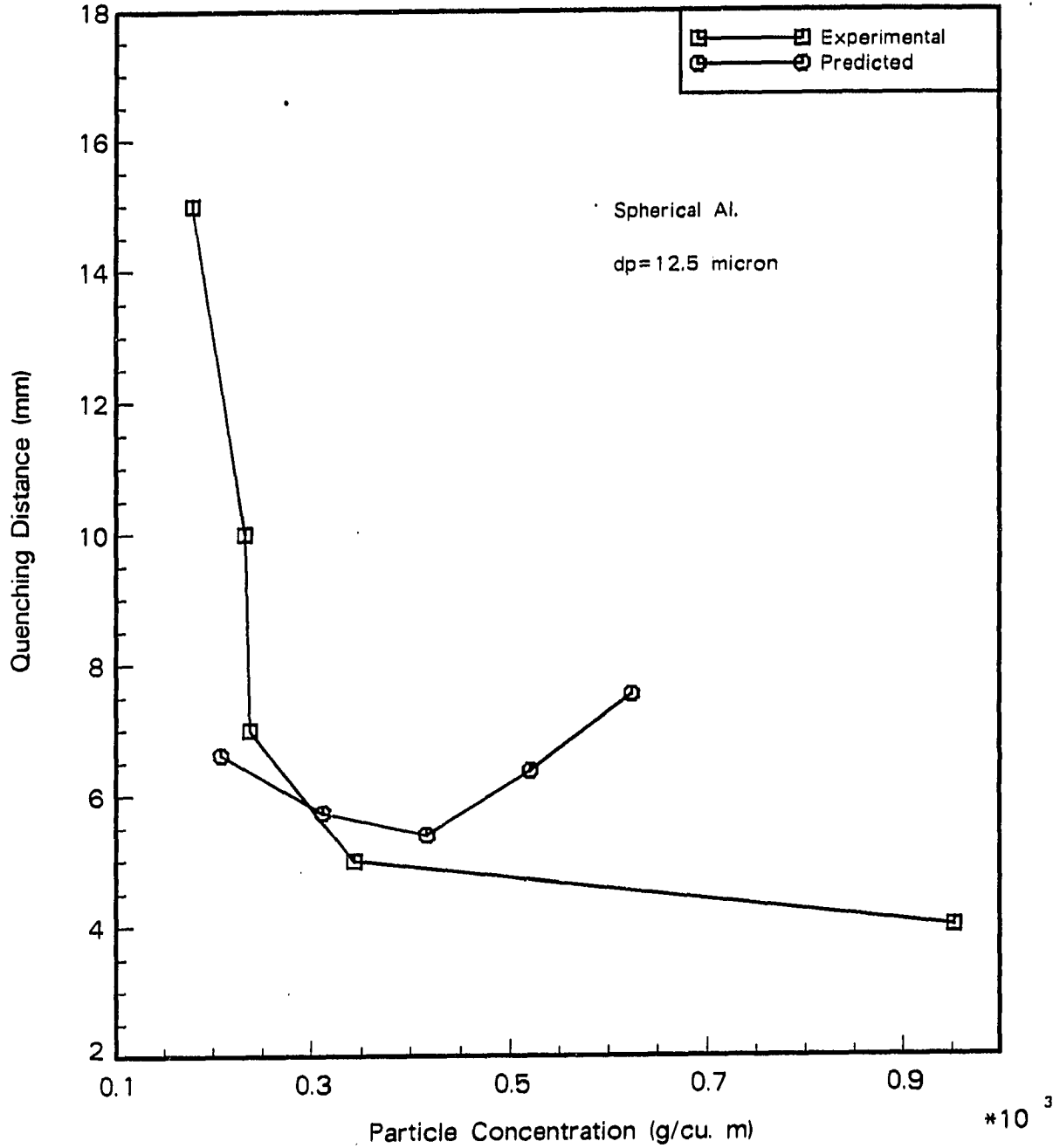


Figure 7.7: Predicted quenching distance vs. particle concentration of $12.5 \mu m$ spherical aluminum

7.13 List of Computer Program

```

C *****
C *
C * TMOAC
C * SE-WON KIM
C * DEPARTMENT OF MECHANICAL ENGINEERING
C * IOWA STATE UNIVERSITY
C *
C * TMOAC (Time-dependent Model of Aluminum Combustion)
C * is a one-dimensional time-dependent computer program
C * for aluminum particle/air flame propagation in a
C * cylindrical chamber. The mass fraction of aluminum,
C * oxygen, product, burning velocity, temperature, and
C * reaction rates are obtained as a function of time
C * and radial distance. Also, the steady-state burning
C * velocities are obtained as a function of aluminum
C * concentration.
C *
C * The differential equations are solved by using
C * forward differencing for the time differential terms,
C * and central differencing for the spatial differential
C * terms by the staggered grid method. The integral
C * equations are solved by using trapezoidal method.
C *
C *****
C
C -----
C |
C | Nomenclature
C |
C | (All the units are in SI units.)
C | A : Arrhenius Pre-exponent Factor (M**3/Kg.sec)
C | ALCON : Aluminum Concentration (g/m**3)
C | AMASS : Molecular Weight of Air
C | ALPHA : Constant in the Species Continuity Equation.
C | (RHO*RMU/RMASS**2)
C | BETA : (1.0 - GAMMA)/GAMMA
C | BURNV : Burning Velocity

```

C	CALSTO	: Stoichiometric Aluminum Concentration	
C		(0.3602 Kg/m**3)	
C	CM1	: Total Mass of Fuel in the Chamber (Kg)	
C	CM2	: Total Mass of Oxidizer in the Chamber (Kg)	
C	CM3	: Total Mass of Inert in the Chamber (Kg)	
C	CM4	: Total Mass of Product in the Chamber (Kg)	
C	CMTOT	: Total Mass of the Mixture in the Chamber (Kg)	
C	CP	: Constant Pressure Specific Heat (J/Kg.mole)	
C	CV	: Constant Volume Specific Heat (J/Kg.mole)	
C	CMASS	: Total Mass in the Chamber for each Time-step	
C	DIFM	: Mass Diffusivity of the Gas Species	
C	DIFMIX	: Mixture Mass Diffusivity	
C	DTAU	: Time-step (Sec.)	
C	DTDZ	: Gradient of Temperature-Distance Curve (K/m)	
C	E	: Activation Energy (J/Kg.mole)	
C	ER	: Equivalence Ratio	
C	EQUI	: Equivalence Ratio, (Y1/Y2)actual/(Y1/Y2)stoi	
C	GAMMA	: Cp/Cv	
C	H	: Spatial-step (m)	
C	ICOUNT	: Time-step Counter	
C	IFREQ	: Counter for Number of Time-steps	
C	NG	: Total Number of Spatial Grids	
C	NG1	: NG - 1	
C	OLDRHO	: Mixture Density at the Previous Time Step	
C	OLDT	: Temperature at the Previous Time Step	
C	P	: Pressure (N)	
C	PINIT	: Initial Pressure (N)	
C	PR	: Prantle Number of the Mixture	
C	Q	: Heat of Combustion (J/Kg)	
C	R	: Radial Coordinate (m)	
C	RADIUS	: Radius of the Cylindrical Chamber (m)	
C	RADN	: Radiation Coefficient	
C	RGAS	: Universal Gas Constant (J/Kg.mole.K)	
C	RHEIG	: Height of the Cylindrical Chamber (m)	
C	RHO1	: Density of Fuel (Kg/m**3)	
C	RHO4	: Density of Product (Kg/m**3)	
C	RHOMU	: Constant (Density*Viscosity)	
C	RMASS	: Total Mass/(2.0*PI*RHEIG)	
C	RMU	: Viscosity (Kg/m.sec)	

C	ROSS	: Absorption Coefficient	
C	RXN	: Reaction Rate (Kg/sec.m**3)	
C	S	: Stoichiometric Coefficient	
C	SC	: Schmit Number of the Mixture	
C	SOURCE	: Source term in the Energy Equation	
C	T	: Absolute Temperature (K)	
C	TAU	: Time (sec)	
C	TATM	: Atmospheric Temperature	
C	TURB	: Turbulence Coefficient	
C	VOL	: Volume of the Cylindrical Chamber (m**3)	
C	W	: Average Molecular Weight of Air (Kg/mole)	
C	WLE	: Lewis Number of the Mixture	
C	XG	: Mole Fraction of the Gas Species	
C	Y1	: Mass Fraction of Fuel	
C	Y2	: Mass Fraction of Oxidizer	
C	Y3	: Mass Fraction of Inert	
C	Y4	: Mass Fraction of Product	
C	YG	: Mass Fraction of the Gas Species	
C	Y1S	: Stoichiometric Mass Fraction of Fuel	
C	Y2S	: Stoichiometric Mass Fraction of Oxidizer	
C	Y3S	: Stoichiometric Mass Fraction of Inert	
C	Y4S	: Stoichiometric Mass Fraction of Product	
C	YACT	: Actual Actual Mass Fraction Ratio of Fuel	
C		and Oxidizer, Y1/Y2	
C	YSTO	: Y1S/Y2S	
C	Y1NEW	: New Mass Fraction of Fuel after New Time-step	
C	Z	: Spatial Coordinate	
C			

C
C
C
C

```

IMPLICIT DOUBLE PRECISION (A-H,O-Z)
COMMON/VAR1/RHOG,CPG,TEMP,CPI(20),XG(20),WI(20),
& SD(20),VMUG,DS,ISPECIE,RGAS,CVG,CVI(20)
COMMON/VAR2/P,V,AREA,DIFMW,EK(20),RHO(5),
& DELTA(20),DIFM(20),CK(20),VMU(20),CKG,EL(5,5),
& PHIJWK(5,9),IEUCKEN,Z(10,10),G(5,8),B(5)
COMMON/VAR3/Y1(201),Y2(201),Y1NEW(201),Y2NEW(201),T(201),
&PHI(201),PHINEW(201),R(201),RHOGAS(201),Y4(201),CPMIX(201),

```

```
&RXN(201),SOURCE(201),Y3(201),OLDRHO(201),VEL(201),CVMIX(201),
&RHOMIX(201),TURB(201),RADN(201),TURBF(201),TURBB(201),
&YG(201),DTDZ(201),OLDT(201),BURNV3(201),DV(201)
COMMON/VAR4/YGAS(20),DIFMIX(201),PR(201),WLE(201),SC(201),
&    BFR(201),BBK(201),PGN(201),PG(201),PB(201),GAMMA(201),
&    BETA(201),CKMIX(201),VMUMIX(201)

C
C   SET THE OUTPUT FILENAMES
C
OPEN(12,FILE='TMOAC1S.OUT',STATUS='NEW')
OPEN(13,FILE='TMOAC2S.OUT',STATUS='NEW')

C
C   READ THE INPUT DATA
C
READ(11,*) DTAU,TAUMAX,IFREQ,NG

C
C   -----
C   INPUT PARAMETERS
C   -----
C
C   CPGAS   = 1.0131E03
C   CP1     = 9.87E02
C   CP4     = 1.012E03
C   CVGAS   = 7.236E02
C   RH01    = 2.7E03
C   RH04    = 3.97E03
C   E       = 2.4*4.184E07
C   A       = 3.0E05
C   Q       = 3.106E07
C   PI      = 3.1415927
C   RGAS    = 8.3143E03
C   RADIUS  = 7.125E-02
C   RHEIG   = 5.0E-2
C   RHOMU   = 2.1718E-05
C   S       = 8.889E-01
C   W       = 2.896E01
C   WI(1)   = 32.0
C   WI(2)   = 28.0
C   P       = 1.0133E05
```

ROSS = 1.38E01
 TATM = 2.98E01
 DPDT1 = 0.0E00
 CALSTO = 3.062E-01

C

NG1 = NG-1
 HNG = NG1
 H = 1.0/HNG

C

C

C

C

C

 STOICHIOMETRIC MASS FRACTION

 Y1S = 2.0776E-01
 Y2S = 1.8647E-01
 Y3S = 6.0757E-01
 Y4S = 0.000E00
 YSTO= Y1S/Y2S

C

C

C

C

C

C

C

C

C

 INITIAL CONDITION OF MASS FRACTION IN THE CHAMBER.
 EQUIVALENCE RATIO = 0.25 - 2.5

ER = 1.0

DO 120 I = 2,NG
 T(I) = 2.98E02
 Y2(I) = 1.0/(4.29 + YSTO*ER)
 Y1(I) = Y2(I)*YSTO*ER
 Y3(I) = 1.0 - Y2(I) - Y1(I)
 Y4(I) = 0.0

120

CONTINUE

C

C

C

C

C

 INITIAL CONDITIONS OF MASS FRACTION AT THE CENTER OF
 THE CHAMBER, SPARK IGNITION ZONE.
 ASSUME 1/100 OF TOTAL VOLUME IS THE IGNITION ZONE.

```

C   ASSUME 1/2 OF FUEL AND OXIDANT REACT IN THIS ZONE.
C   -----
C
      T(1) = 3.424E03
      Y1(1) = 0.5*Y1(5)
      Y2(1) = 0.5*Y2(5)
      Y3(1) = Y3(5)
      Y4(1) = 1.0-Y1(1)-Y2(1)-Y3(1)
C
C   CHECK THE EQUIVALENCE RATIO
C
      YACT = Y1(5)/Y2(5)
      EQUI = YACT/YSTO
C
C   -----
C   INITIAL TOTAL MASS, VOLUME OF CHAMBER, AND INITIAL
C   MASS OF EACH REACTANTS AND PRODUCT
C   -----
C
      VOL = PI*RADIUS**2.0*RHEIG
      CM1 = VOL*CALSTO*EQUI
      CM2 = (CM1/Y1(5))*Y2(5)
      CM3 = (CM1/Y1(5))*Y3(5)
      CM4 = 0.0E00
      CMTOT = CM1+CM2+CM3+CM4
C
C   CALCULATE RMASS AND ALPHA
C
125  RMASS = CMTOT/(2.0E00*PI*RHEIG)
      ALPHA = RHOMU/(RMASS**2.0)
C
C   CALCULATE THE ALUMINUM CONCENTRATION (g/m**3)
C
      ALCON = (CM1*1.0E03)/VOL
C
C   WRITE THE EQUIVALENCE RATIO AND ALUMINUM CONCENTRATION
C
      WRITE(12,800)

```

```

WRITE(12,810) ER,EQUI,ALCON
WRITE(12,800)

```

```

C
C
C
C
C
C
C

```

```

-----
CALCULATE THE TRANSPORT PROPERTIES OF THE MIXTURE,
SPECIFIC HEATS, DENSITY, THERMAL CONDUCTIVITY, VISCOSITY,
AND MASS DIFFUSIVITY OF THE GAS SOLID MIXTURE
-----

```

```

DO 130 I=1,NG
  Y1NEW(I) = 0.0E00
  Y2NEW(I) = 0.0E00
  PHINNEW(I) = 0.0E00

```

```

C
C
C
C
C

```

```

-----
MASS FRACTION AND MOLE FRACTIONS OF THE GAS SPECIES
-----

```

```

YGAS(1) = Y2(I)/(Y2(I)+Y3(I))
YGAS(2) = 1-YGAS(1)

```

```

C

```

```

X1 = YGAS(1)/WI(1)
X2 = YGAS(2)/WI(2)
XG(1) = X1/(X1+X2)
XG(2) = X2/(X1+X2)

```

```

C

```

```

-----
CALL TPGAS
CALL TPSOLID

```

```

C

```

```

YG(I) = Y2(I) + Y3(I)
CPMIX(I) = Y1(I)*CP1 + Y4(I)*CP4 + YG(I)*CPG
CVMIX(I) = Y1(I)*CP1 + Y4(I)*CP4 + YG(I)*CVG
RHOGAS(I) = P*W/(RGAS*T(I))
RHOMIX(I) = 1.0/(Y1(I)/RHO1 + Y4(I)/RHO4 + YG(I)/RHOGAS(I))
CKMIX(I) = 1.0/(Y1(I)/CK1+Y4(I)/CK4+YG(I)/CKG)
VMUMIX(I) = 1.0/(Y1(I)/VMU1+Y4(I)/VMU2+YG(I)/VMUG)
DIFMIX(I) = VMUMIX(I)/RHOMIX(I)

```

```

C
C

```

```

C      DIMENSIONLESS PARAMETERS
C      Pr, Le, Sc
C      -----
C
C      PR(I) = CPMIX(I)*VMUMIX(I)/CKMIX(I)
C      WLE(I) = CKMIX(I)/(RHOMIX(I)*CPMIX(I)*DIFMIX(I))
C      SC(I) = VMUMIX(I)/(RHOMIX(I)*DIFMIX(I))
C
C      CALCULATE THE REACTION RATES
C
C      RXN(I) = A*EXP(-1.0*E/(RGAS*T(I)))*(RHOMIX(I)**1.5)*
&          Y1(I)*(Y2(I)**0.5)
130    CONTINUE
C
C      CALCULATE AVERAGE SPECIFIC HEATS
C
C      CCP1 = 0.0E00
C      CCV1 = 0.0E00
C      DO 140 I=2,NG1
C          CCP1 = CCP1 + CPMIX(I)
C          CCV1 = CCV1 + CVMIX(I)
C      140    CONTINUE
C      CPAVG = H*(((CPMIX(1)+CPMIX(NG))/2.0) + CCP1)
C      CVAVG = H*(((CVMIX(1)+CVMIX(NG))/2.0) + CCV1)
C
C
C      -----
C      CALCULATE THE ADIABATIC VARIABLE, PHI
C      -----
C
C      GAMMA = CPAVG/CVAVG
C      BETA = (1.0-GAMMA)/GAMMA
C      PG = P**(BETA)
C      DO 150 I=1,NG
C          PHI(I) = T(I)*PG
C      150    CONTINUE
C
C      DO 142 I=1,NG
C          GAMMA(I) = CPMIX(I)/CVMIX(I)

```

```

      BETA(I) = (1.0-GAMMA(I))/GAMMA(I)
      PG(I) = P**(BETA(I))
      PHI(I) = T(I)*PG(I)
142  CONTINUE
C
C -----
C  CALCULATE THE RADIAL COORDINATES
C -----
C
      ZETA = H
      RSUM = 0.0E00
      R(1) = 0.0E00
      COEF = 2.0*RMASS*RGAS/W
      DO 166 I=2,NG
        JJ = I-1
        FJ = JJ
C      R(I) = ((2.0*RMASS*RGAS/(W*(P**(1.0/GAMMA)))))*((ZETA/FJ)*
C &      (0.5*(YG(1)*PHI(1)+YG(I)*PHI(I))+RSUM))**(1.0/2.0)
      R(I)=(COEF*(ZETA/FJ)*(0.5*(YG(1)*PHI(1)*(P**(-1.0/GAMMA(1)))+
&      YG(I)*PHI(I)*(P**(-1.0/GAMMA(I))))+RSUM))**(1.0/2.0)
      RSUM = RSUM + YG(I)*PHI(I)*(P**(-1.0/GAMMA(I)))
      ZETA = ZETA + H
166  CONTINUE

C
C -----
C  CALCULATE THE INITIAL PRESSURE
C -----
C
      PSUM = 0.0E00
      DO 170 I=2,NG1
        PSUM = PSUM + YG(I)*PHI(I)
170  CONTINUE
C
      GSUM = 0.0
      DO 173 I=1,NG
        GSUM = GSUM + GAMMA(I)
173  CONTINUE
      GAMAVG = GSUM/NG
      PINIT = ((2.0*RMASS*RGAS/(W*(RADIUS**2.0)))*H*(0.5*(YG(1)*

```

```

&          PHI(1)+YG(NG)*PHI(NG))+PSUM)**(GAMAVG)

C
C  -----
C  SET THE INITIAL GAS VELOCITIES TO ZERO
C  -----
C
DO 180 I=1,NG
    VEL(I) = 0.0E00
180 CONTINUE
C
C  -----
C  CALCULATE THE TOTAL MASS
C  -----
C
    CSUM = 0.0
    REPT = 0.0
DO 447 I = 2,NG1
    CSUM = CSUM + YG(I)*PHI(I)*P**(-1.0/GAMMA(I))
447 CONTINUE
    REPT = H*(0.5*(YG(1)*PHI(1)*P**(-1.0/GAMMA(1))+
&          YG(NG)*PHI(NG)*P**(-1.0/GAMMA(NG)))+CSUM)
    CMASS = PI*W*RHEIG*(RADIUS**2.0)/(RGAS*REPT)
C
C  -----
C  WRITE THE OUTPUT VALUES
C  -----
C
WRITE(12,851)
WRITE(12,820) CMTOT,CMASS
WRITE(12,851)
IF((CMASS-CMTOT).LT.1.0E-5) GO TO 195
IF((CMASS-CMTOT).GE.1.0E-5) CMTOT = CMASS
GO TO 125

C
C  CALCULATE THE TURBULENT FLOW AND RADIATIVE TRANSFER PARAMETERS
C
195 DO 200 I=1,NG
    TURB(I) = 3.41E02*RHOMIX(I)**1.12

```

```

      RADN(I) = (3.024E-07/ROSS)/(RHOMIX(I)*CPMIX(I))*T(I)**3.0
200  CONTINUE
C
C  -----
C  PRINT OUT THE INITIAL PROPERTIES
C  -----
C
      WRITE(12,840) DTAU,TAUMAX,H,IFREQ,NG
        WRITE(12,851)
        WRITE(12,898)
        WRITE(12,851)
        WRITE(12,852) TAU
        WRITE(12,851)
        WRITE(12,854)
        WRITE(12,851)
        WRITE(12,858)
        WRITE(12,851)
      DO 215 I = 1,NG,10
        WRITE(12,850) Y1(I),Y2(I),Y3(I),Y4(I),PHI(I)
215  CONTINUE
        WRITE(12,851)
        WRITE(12,853)
        WRITE(12,851)
      DO 225 I=1,NG,10
        WRITE(12,859) T(I),R(I),RHOMIX(I),VEL(I),RXN(I)
225  CONTINUE
        WRITE(12,851)
        WRITE(12,855)
        WRITE(12,851)
      DO 235 I=1,NG,10
        WRITE(12,856) TURB(I),RADN(I),CPMIX(I),CVMIX(I)

235  CONTINUE
      WRITE(12,851)
      WRITE(12,857)
      WRITE(12,851)
      DO 236 I=1,NG,10
        WRITE(12,869) PR(I),SC(I),WLE(I),GAMMA(I)
236  CONTINUE
      WRITE(12,851)

```

```

WRITE(12,868) GAMMA,CM1,CMASS,P
WRITE(12,851)
WRITE(12,898)

C
C WRITE FOR THE ANOTHER OUTPUT FILE
C

WRITE(13,863) DTAU,TAUMAX,H,IFREQ,NG
WRITE(13,861)
WRITE(13,865) TAU
WRITE(13,861)

C
C *****
C *
C * ITERATE OVER SUCCESSIVE TIME STEP, DTAU *
C *
C *****

TAU = 0.0E00
ICOUNT = 0
JCOUNT = 0
990 TAU = TAU + DTAU
ICOUNT = ICOUNT + 1
JCOUNT = JCOUNT + 1

C
C -----
C CALCULATE THE NEW MASS FRACTION OF FUEL, AND NEW REACTION RATES
C FOR A SUCCESSIVE TIME STEP
C -----
C

RXN(1) = A*EXP(-1.0*E/(RGAS*T(1)))*(RHOMIX(1)**1.5)*
& Y1(1)*(Y2(1)**0.5)
Y1NEW(1) = Y1(1)-(DTAU*RXN(1)/RHOMIX(1))
RXN(NG) = A*EXP(-1.0*E/(RGAS*T(NG)))*(RHOMIX(NG)**1.5)*
& Y1(NG)*(Y2(NG)**0.5)
Y1NEW(NG) = Y1(NG)-(DTAU*RXN(NG)/RHOMIX(NG))
DO 300 I = 2,NG1
RXN(I) = A*EXP(-1.0*E/(RGAS*T(I)))*(RHOMIX(I)**1.5)*
& Y1(I)*(Y2(I)**0.5)
C TURBF(I) = 2.0 + TURB(I+1) + TURB(I)

```

```

C      TURBB(I) = 2.0 + TURB(I) - TURB(I-1)
      BFR(I)=(1.0+TURB(I+1))*SC(I+1)*RHOMIX(I+1)*VMUMIX(I+1)+
&      (1.0+TURB(I))*SC(I)*RHOMIX(I)*VMUMIX(I)
      BBK(I)=(1.0+TURB(I-1))*SC(I-1)*RHOMIX(I-1)*VMUMIX(I-1)+
&      (1.0+TURB(I))*SC(I)*RHOMIX(I)*VMUMIX(I)
C      Y1NEW(I) = Y1(I)+(DTAU*ALPHA/(8.0*(H**2.0)))*(((
C      R(I)+R(I+1))
C      &      **2.0)*(Y1(I+1)-Y1(I))*TURBF(I))-(TURBB(I)*((R(I)
C      &      +R(I-1))*2.0)*(Y1(I)-Y1(I-1))))-(DTAU*RXN(I)/
C      &      RHOMIX(I))
      Y1NEW(I) = Y1(I)+(DTAU/(8.0*(RMASS**2.0)*(H**2.0)))*
&      (((R(I)+R(I+1))*2.0)*(Y1(I+1)-Y1(I))*BFR(I))-
&      (BBK(I)*((R(I)+R(I-1))*2.0)*(Y1(I)-Y1(I-1))))-
&      (DTAU*RXN(I)/RHOMIX(I))
      IF(Y1NEW(I).LE.0.0) Y1NEW(I)=0.0
300  CONTINUE

C
C  -----
C  CALCULATE THE NEW MASS FRACTION OF OXIDIZER
C  FOR A SUCCESSIVE TIME STEP
C  -----
C
      Y2NEW(1) = Y2(1)-(DTAU*S*RXN(1)/RHOMIX(1))
      Y2NEW(NG) = Y2(NG)-(DTAU*S*RXN(NG)/RHOMIX(NG))
      DO 310 I = 2,NG1
C      Y2NEW(I) = Y2(I)+(DTAU*ALPHA/(8.0*(H**2.0)))*(((R(I)+
C      &      R(I+1))*2.0)*(Y2(I+1)-Y2(I))*TURBF(I))-
C      &      (TURBB(I)*((R(I)+R(I-1))*2.0)*(Y2(I)-Y2(I-1))))-
C      &      (DTAU*S*RXN(I)/RHOMIX(I))
      Y2NEW(I) = Y2(I)+(DTAU/(8.0*(H**2.0)))*(((R(I)+
&      R(I+1))*2.0)*(Y2(I+1)-Y2(I))*BFR(I))-
&      (BBK(I)*((R(I)+R(I-1))*2.0)*(Y2(I)-Y2(I-1))))-
&      (DTAU*S*RXN(I)/RHOMIX(I))
      IF(Y2NEW(I).LE.0.0) Y2NEW(I)=0.0
310  CONTINUE

C
C  -----
C  CALCULATE THE NEW ADIABATIC VARIABLE FOR A SUCCESSIVE TIME
C  STEP

```

```

C -----
C
PHINEW(1)=PHI(1)-DTAU*Q*A*Y1(1)*(Y2(1)*RHOMIX(1))**(0.5)*
& EXP(-1.0*E/(RGAS*T(1)))/(CPMIX(1)*(P**(-1.0*BETA(1))))
PHINEW(NG)=PHI(NG)-DTAU*Q*A*Y1(NG)*(Y2(NG)*RHOMIX(NG))**
& (0.5)*EXP(-1.0*E/(RGAS*T(NG)))/(CPMIX(NG)*
& (P**(-1.0*BETA(NG))))
DO 320 I=2,NG1
SOURCE(I)=Q*RXN(I)/(RHOMIX(I)*CPMIX(I)*(P**(-1.0*BETA(I))))
BFR(I) = (1.0+TURB(I+1)+RADN(I+1))*PR(I+1)*RHOMIX(I+1)*
& VMUMIX(I+1)+(1.0+TURB(I)+RADN(I))*PR(I)*RHOMIX(I)*
& VMUMIX(I)
BBK(I) = (1.0+TURB(I-1)+RADN(I-1))*PR(I-1)*RHOMIX(I-1)*
& VMUMIX(I-1)+(1.0+TURB(I)+RADN(I))*PR(I)*RHOMIX(I)*
& VMUMIX(I)
PHINEW(I)=PHI(I)+(DTAU/(8.0*(RMASS**2.0)*(H**2.0)))*
& (((R(I)+R(I+1))**2.0)*
& (PHI(I+1)-PHI(I))*BFR(I))-
& (BBK(I)*((R(I)+R(I-1))**2.0)*(PHI(I)-PHI(I-1))))-
& DTAU*SOURCE(I)
320 CONTINUE

C -----
C
C SUBSTITUTE NEW MASS FRACTION OF REACTANTS AND PRODUCT
C TEMPERATURE MIXTURE DENSITY, AND ADIABATIC VARIABLE
C FOR A SUCCESSIVE TIME STEP
C -----
C
DO 330 I=1,NG
Y1(I) = Y1NEW(I)
Y2(I) = Y2NEW(I)
Y4(I) = 1.0-Y1(I)-Y2(I)-Y3(I)
PHI(I) = PHINEW(I)
OLDT(I) = T(I)
OLDRHO(I) = RHOMIX(I)
YG(I) = Y2(I)+Y3(I)
330 CONTINUE

C -----
C

```

```

C      CALCULATE A NEW PRESSURE FOR A SUCCESSIVE TIME STEP
C      -----
C
      PSUM = 0.0
      DO 340 I=2,NG1
        PSUM = PSUM + YG(I)*PHI(I)
340    CONTINUE
      P = ((2.0*RMASS*RGAS/(W*(RADIUS**2.0)))*H*(0.5*(YG(1)*
&        PHI(1)+YG(NG)*PHI(NG))+PSUM)**(GAMAVG)

C
C
C      CALCULATE A NEW TEMPERATURE FOR A SUCCESSIVE TIME STEP
C
      DO 350 I=1,NG
        PB(I) = P**(-1.0*BETA(I))
        T(I) = PB(I)*PHI(I)
350    CONTINUE
C
C      EVALUATE THE TRANSPORT PROPERTIES AT EVERY 10TH
C      TIME STEP
C
      ITP = 10
      IF(JCOUNT.NE.ITP) GO TO 358
      DO 355 I=1,NG

C
C      -----
C      MASS FRACTION AND MOLE FRACTIONS OF THE GAS SPECIES
C      -----
C
      YGAS(1) = Y2(I)/(Y2(I)+Y3(I))
      YGAS(2) = 1-YGAS(1)

C
      X1 = YGAS(1)/WI(1)
      X2 = YGAS(2)/WI(2)
      XG(1) = X1/(X1+X2)
      XG(2) = X2/(X1+X2)

C      -----
      CALL TPGAS

```

```

      CALL TPSOLID
C -----
355 CONTINUE
      JCOUNT = 0

C -----
C CALCULATE A NEW GAS DENSITY FOR A SUCCESSIVE TIME STEP
C -----
C
358 DO 360 I=1,NG
      PGN(I) = (P**(1.0/GAMMA(I)))*W/RGAS
      RHOGAS(I) = PGN(I)/PHI(I)
360 CONTINUE

C -----
C CALCULATE A NEW RADIAL COORDINATES FOR A SUCCESSIVE TIME STEP
C -----
C
      ZETA = H
      RSUM = 0.0E00
      R(1) = 0.0E00
      COEF = 2.0*RMASS*RGAS/W
      DO 160 I=2,NG
        JJ = I-1
        FJ = JJ
        R(I)=(COEF*(ZETA/FJ)*(0.5*(YG(1)*PHI(1)*(P**(-1.0/GAMMA(1))))+
&      YG(I)*PHI(I)*(P**(-1.0/GAMMA(I))))+RSUM)**(1.0/2.0)
        RSUM = RSUM + YG(I)*PHI(I)*(P**(-1.0/GAMMA(I)))
        ZETA = ZETA + H
160 CONTINUE

C -----
C CALCULATE A NEW SPECIFIC HEATS AND A MIXTURE DENSITIES
C FOR A SUCCESSIVE TIME STEP
C -----
C
      DO 380 I = 1,NG
        CPMIX(I) = Y1(I)*CP1 +Y4(I)*CP4 + YG(I)*CPG
        CVMIX(I) = Y1(I)*CP1 +Y4(I)*CP4 + YG(I)*CVG

```

```

      RHOMIX(I)=1.0/(Y1(I)/RHO1 + Y4(I)/RHO4 + YG(I)/RHOGAS(I))
380  CONTINUE

C
C  -----
C  CALCULATE AN AVERAGE SPECIFIC HEATS FOR A SUCCESSIVE TIME STEP
C  -----
C
C      CP2 = 0.0E00
C      CV2 = 0.0E00
C      DO 390 I=2,NG1
C          CP2 = CP2 + CPMIX(I)
C          CV2 = CV2 + CVMIX(I)
C      390  CONTINUE
C          CPAVG = H*((CPMIX(1)+CPMIX(NG))/2.0) + CP2)
C          CVAVG = H*((CVMIX(1)+CVMIX(NG))/2.0) + CV2)
C      DO 390 I=2,NG1
C          GAMMA(I) = CPMIX(I)/CVMIX(I)
C          BETA(I) = (1.0-GAMMA(I))/GAMMA(I)
390  CONTINUE

C
C  -----
C  CALCULATE A NEW TURBULENT FLOW AND RADIATIVE TRANSFER
C  PARAMETERS FOR A SUCCESSIVE TIME STEP
C  -----
C
C      DO 400 I=1,NG
C          TURB(I) = 3.41E02*RHOMIX(I)**(1.12)
C          RADN(I)=(3.024E-07/ROSS)/(RHOMIX(I)*CPMIX(I))*T(I)**3.0
C      400  CONTINUE

C
C  -----
C  CALCULATE A NEW GAS VELOCITIES FOR A SUCCESSIVE TIME STEP
C  -----
C
C      ZETA = H
C      VSUM = 0.0
C      DO 410 I =2,NG1
C          JM = I-1

```

```

      VJ = JM
      VEL(I) = (RMASS/(DTAU*R(I)))*(ZETA/VJ)*
&             (0.5*((1.0/RHOMIX(1))-(1.0/OLDRHO(1)))+
&             ((1.0/RHOMIX(I))-(1.0/OLDRHO(I))))+VSUM)
      VSUM = VSUM+((1.0/RHOMIX(I))-(1.0/OLDRHO(I)))
      ZETA = ZETA + H
410  CONTINUE
      C
      C -----
      C  METHOD 1:
      C  CALCULATE THE BURNING VELOCITY USING THE ZELDOVICH
      C  THERMAL THEORY
      C -----
      C
      DTDZ(1) = ABS((T(2)-T(1))/H)
      DTDZ(NG) = ABS((T(NG)-T(NG1))/H)
      DO 420 I=2,NG1
      DTDZ(I) = ABS((T(I+1)-2.0*T(I)+T(I-1)))/(2.0*H))
420  CONTINUE
      SUM = 0.0
      DO 430 I=2,NG1
      SUM = SUM + RXN(I)*DTDZ(I)
430  CONTINUE
      BURN1 = SUM + (RXN(1)*DTDZ(1)+RXN(NG)*DTDZ(NG))/2.0
      RXNAVG = BURN1*H/(T(1)-T(NG))
      BURNV1=(2.0*Q*CKMIX(NG))**(0.5)/(RHOMIX(NG)*CPMIX(NG))*
&          *(RXNAVG/(T(1)-T(NG)))*(0.5)

      C
      C -----
      C  SET THE CONVERGENCE LIMIT
      C  CHECK THE TEMPERATURE VARIATION WITH DISTANCE
      C -----
      C
      DO 450 I=3,NG
      C      IF(DTDZ(I).LE.10.0) GO TO 455
      TLIM = ABS(T(I)-OLDT(I))
      IF(TLIM.LE.1.0) GO TO 455
450  CONTINUE
455  ISTOP = I

```

```

C
C   FIND THE MAXIMUM SLOPE POINT
C
      DTMAX=MAX(DTDZ(2),DTDZ(1))
      DO 412 I=3,NG1
          DTM=MAX(DTMAX,DTDZ(I))
          DTMAX=DTM
412  CONTINUE
C
C   -----
C   METHOD 2:
C   CALCULATE THE BURNING VELOCITY
C   BURNV2 = (DISTANCE/TIME FOR REACTION)
C   -----
C
      BURNV2 = R(ISTOP)/TAU
C
C   -----
C   METHOD 3:
C   CALCULATE THE STEADY STATE BURNING VELOCITY
C   DERIVED FROM THE STEADY-STATE CONTINUITY AND
C   SPECIES CONTINUITY EQUATIONS
C   -----
C
      IC = ICOUNT
      BSUM = 0.0
      DO 470 I=2,NG1
          BSUM = BSUM + RXN(I)/RHOMIX(I)
470  CONTINUE
      BURN3 = H*(0.5*(RXN(1)/RHOMIX(1)+RXN(NG)/RHOMIX(NG))+BSUM)
      BURNV3(IC) = RMASS*BURN3/((Y1(NG)-Y1(1))*RHOMIX(NG)*R(NG))
C
C   -----
C   METHOD 4:
C   BURNING VELOCITY = VELOCITY DIFFERENCE ACROSS THE FLAME
C                       = MAXIMUM VELOCITY DIFFERENCE
C   -----
C
      DO 471 I=1,NG1

```

```

      DV(I) = ABS(VEL(I+1)-VEL(I))
471  CONTINUE
      DVMAX=MAX(DV(2),DV(1))
      DO 472 I=3,NG1
          DVM=MAX(DVMAX,DV(I))
          DVMAX=DVM
472  CONTINUE
      BURNV4 = DVMAX

C
C  -----
C  PRINT OUT THE RESULTS FOR EVERY IFREQ TIME STEP
C  -----
C
      IF(ICOUNT.NE.IFREQ) GO TO 600
      ICOUNT=0

C
C
      WRITE(13,899)
      WRITE(13,861)
      WRITE(13,864) TAU,ALCON,R(ISTOP),BURNV1,BURNV2,BURNV3(IC),
&                BURNV4
      WRITE(13,861)
      WRITE(13,899)

C
C  -----
C  CALCULATE THE TOTAL MASS FOR A SUCCESSIVE TIME STEP
C  -----
C
      CSUM = 0.0
      REPT = 0.0
      DO 440 I = 2,NG1
          CSUM = CSUM + YG(I)*PHI(I)*P**(-1.0/GAMMA(I))
440  CONTINUE
          REPT = H*(0.5*(YG(1)*PHI(1)*P**(-1.0/GAMMA(1))+
&                YG(NG)*PHI(NG)*P**(-1.0/GAMMA(NG)))+CSUM)
          CMASS = PI*W*RHEIG*(RADIUS**2.0)/(RGAS*REPT)

C
C  PRINT OUT THE OUTPUT
C

```

```

        WRITE(12,851)
        WRITE(12,871) TAU
        WRITE(12,851)
        WRITE(12,898)
        WRITE(12,851)
        WRITE(12,872)
        WRITE(12,851)
    DO 315 I=1,NG,3
        WRITE(12,873) Y1(I),Y2(I),Y3(I),Y4(I)
315    CONTINUE
        WRITE(12,851)
        WRITE(12,874)
        WRITE(12,851)
    DO 325 I=1,NG,3
        WRITE(12,875) T(I),R(I),VEL(I),RXN(I)

325    CONTINUE
        WRITE(12,851)
        WRITE(12,826)
        WRITE(12,851)
    DO 329 I=1,NG,3
        WRITE(12,827) DTDZ(I),DTMAX
329    CONTINUE
        WRITE(12,851)
        WRITE(12,876) RXNAVG,CMASS,P
        WRITE(12,851)
        WRITE(12,898)
        WRITE(12,851)
        WRITE(12,877) ALCON,ISTOP,R(ISTOP),BURNV1,BURNV2,BURNV3(IC),
&          BURNV4
        WRITE(12,851)

C
C    SET THE MAXIMUM ITERATION LIMIT
C
600    IF((TAU-TAUMAX).LT.0.0) GO TO 990
C
C    FORMAT THE OUTPUT
C
437    FORMAT(5X,3(E12.5,4X))
438    FORMAT(10X,'TAU',13X,'TURB(I)',14X,'RADN(I)')
```

```

800  FORMAT(//,5X,70('*'),//)
810  FORMAT(/,5X,'EQUIVALENCE RATIO = ',E12.5/,5X,
&      'EQUIVALENCE RATIO = ',E12.5/,5X,'ALUMINUM ',
&      'CONCENTRATION = ',E12.5,//)
820  FORMAT(/,5X,'TOTAL MASS OF ALUMINUM = ',2(E12.5,3X))
826  FORMAT(8X,'DTDZ(I)',13X,'DTMAX')
827  FORMAT(5X,2(E12.5,2X))

840  FORMAT(//,5X,'DT = ',E10.5/,5X,'TMAX = ',E10.5/,5X,
&      'H = ',E10.5/,5X,'IFREQ = ',I5/,5X,'TOTAL GRIDS = ',
&      I5,//)
851  FORMAT(5X,70('-'))
852  FORMAT(5X,'TIME-STEP(SEC) = ',E10.5)
854  FORMAT(5X,'INITIAL CONDITIONS AT EACH 10TH GRID POINTS')
858  FORMAT(10X,'Y1',12X,'Y2',12X,'Y3',12X,'Y4',11X,'PHI')
850  FORMAT(5X,5(E12.5,2X))
853  FORMAT(10X,' T ',13X,' R ',8X,'RHOMIX',11X,'VEL',11X,'RXN')
859  FORMAT(5X,5(E12.5,2X))
855  FORMAT(8X,'TURB',10X,'RADN',9X,'CPMIX',9X,'CVMIX')
856  FORMAT(5X,4(E12.5,2X))
857  FORMAT(10X,'Pr',12X,'Sc',12X,'Le',12X,'GAMMA')
868  FORMAT(5X,'CM1 = ',E12.5/,5X,
&      'CMASS = ',E12.5/,5X,'P = ',E12.5)
869  FORMAT(5X,4(E12.5,2X))
863  FORMAT(//,5X,'DT = ',E10.5/,5X,'TMAX = ',E10.5/,5X,
&      'H = ',E10.5/,5X,'IFREQ = ',I5/,5X,'TOTAL GRIDS = ',
&      I5,//)
861  FORMAT(5X,70('-'))
865  FORMAT(5X,'TIME-STEP(SEC) = ',E10.5)
864  FORMAT(5X,'TAU = ',E12.5/,5X,'AL. CONC. = ',E12.5/,5X,
&      'R(ISTOP) = ',E12.5/,5X,'BURNV1 = ',E12.5/,5X,
&      'BURNV2 = ',E12.5/,5X,'BURNV3 = ',E12.5/,5X,
&      'BURNV4 = ',E12.5)
871  FORMAT(5X,'TIME-STEP(SEC) = ',E10.5)
872  FORMAT(10X,'Y1',14X,'Y2',14X,'Y3',14X,'Y4')
873  FORMAT(5X,4(E12.5,4X))
874  FORMAT(11X,' T ',15X,' R ',13X,'VEL',13X,'RXN')
875  FORMAT(5X,4(E12.5,4X))
876  FORMAT(5X,'RXNAVG = ',E12.5/,5X,'CMASS = ',E12.5/,5X,
&      'P = ',E12.5)

```

```

877  FORMAT(5X,'AL. CONC. = ',E12.5,/,5X,'ISTOP = ',I5,/,5X,
&      'R(ISTOP) = ',E12.5,/,5X,'BURNV1 = ',E12.5,/,5X,
&      'BURNV2 = ',E12.5,/,5X,'BURNV3 = ',E12.5,/,5X,
&      'BURNV4 = ',E12.5)

```

C

C PRINT THE COMPLETED MESSAGE

C

```

WRITE(12,898)
WRITE(12,891)
WRITE(12,892)
WRITE(12,891)
WRITE(13,899)
WRITE(13,893)
WRITE(12,894)
WRITE(12,893)
891  FORMAT(5X,70('-'))
893  FORMAT(5X,70('-'))
881  FORMAT(5X,'ALUMINUM CONCENTRATION = ',E12.5,/,5X,
&      'BURNV4 = ',E12.5)
882  FORMAT(5X,'ALUMINUM CONCENTRATION = ',E12.5,/,5X,
&      'BURNV4 = ',E12.5)
898  FORMAT(///)
899  FORMAT(///)
892  FORMAT(5X,'1 EQUIVALENCE RATIO COMPLETED')
894  FORMAT(5X,'1 EQUIVALENCE RATIO COMPLETED')

```

C

C CLOSE THE OPEN STATEMENT

C

```

CLOSE(12)
CLOSE(13)
STOP
END

```

\clearpage

C

C

```

*****
SUBROUTINE TPGAS

```

C

Evaluate the transport properties of the gas mixture

C

```

*****

```

```

C
C
C |-----|
C | Nomenclature :
C |   D1      : Diameter of the particle (m)
C |   DELTA   : Stockmayer polar parameter
C |   DS      : Diameter of the reaction Chamber
C |   EK      : Stockmayer parameter
C |   GMW     : Molecular weight of input gas
C |   RHOG    : Initial gas density
C |   SD      : Stockmayer collision Diameter
C |   Z       : Coefficient of the heat capacity equation
C |   VMU     : Viscosity of the gas element
C |   VMUG    : Viscosity of the Mixture gas
C |   CK      : Thermal Conductivity of the Gas Element
C |   CKG     : Thermal Conductivity of the Mixture Gas
C |   PHIJK   : Parameter of the Mixture Viscosity and
C |             Thermal Conductivity Equations
C |   CP1     : Heat Capacity below 1200 K
C |   CP2     : Heat Capacity above 1200 K
C |   CPG     : Mixture Heat Capacity
C |   DIF     : Mass Diffusivity of the Gas Element
C |   DIFMW   : Mass Diffusivity of the Mixture Gas
C |   WI      : Molecular Weight of the Elements
C |-----|

```

```

C
C CALCULATE THE TRANSPORT DATA. THESE DATA DO NOT CHANGE
C SIGNIFICANTLY FROM ONE POINT TO THE NEXT THROUGH THE
C CHAMBER. SO, EVALUATE THESE DATA ONLY WHEN THEIR IS A
C SIGNIFICANT CHANGE, NOT EVERY TIME STEP.
C

```

```

IMPLICIT DOUBLE PRECISION (A-H,O-Z)
COMMON/VAR1/RHOG,CPG,TEMP,CPI(20),XG(20),WI(20),
& SD(20),VMUG,DS,ISPECIE,RGAS,CVG,CVI(20)
COMMON/VAR2/P,V,AREA,DIFMW,EK(20),RHO(5),
& DELTA(20),DIFM(20),CK(20),VMU(20),CKG,EL(5,5),
& PHIJK(5,9),IEUCKEN,Z(10,10),G(5,8),B(5)
COMMON/VAR3/Y1(201),Y2(201),Y1NEW(201),Y2NEW(201),T(201),
& PHI(201),PHINEW(201),R(201),RHOGAS(201),Y4(201),CPMIX(201),
& RXN(201),SOURCE(201),Y3(201),OLDRHO(201),VEL(201),CVMIX(201),

```

```
&RHOMIX(201),TURB(201),RADN(201),TURBF(201),TURBB(201),  
&YG(201),DTDZ(201),OLDT(201),BURNV3(201),DV(201)  
COMMON/VAR4/YGAS(20),DIFMIX(201),PR(201),WLE(201),SC(201),  
&      BFR(201),BBK(201),PGN(201),PG(201),PB(201),GAMMA(201),  
&      BETA(201),CKMIX(201),VMUMIX(201)
```

C

IEUCKEN = 1

C

READ THE PARAMETER VALUES

C

C

C

C

O2 HEAT CAPACITY PARAMETERS

C

C

```
Z(1,1) = 10.994  
Z(1,2) = -1.03  
Z(1,3) = -16.889  
Z(1,4) = 32.394  
Z(1,5) = -17.5193  
Z(1,6) = 7.1663  
Z(1,7) = -3.3897  
Z(1,8) = 12.9769  
Z(1,9) = -12.1542  
Z(1,10) = 3.736
```

C

C

C

C

C

```
-----  
N2 HEAT CAPACITY PARAMETERS  
-----  
Z(2,1) = 9.7325  
Z(2,2) = -4.9604  
Z(2,3) = 11.2348  
Z(2,4) = -15.2917  
Z(2,5) = 7.2885  
Z(2,6) = 7.5309  
Z(2,7) = -4.0828  
Z(2,8) = 8.9494  
Z(2,9) = -5.9095  
Z(2,10) = 1.3277
```

C
C
C
C
C

02 of Cv eq.

G(1,1) = -1.294427E06
G(1,2) = 5.982317E04
G(1,3) = -8.978508E02
G(1,4) = 6.552362E02
G(1,5) = -1.131313E-02
G(1,6) = 3.498107E-06
G(1,7) = 4.21065E-09
G(1,8) = 2.67997E02
B(1) = 2239.81

C
C
C
C
C

N2 OF Cv EQ.

G(2,1) = -2.182035E05
G(2,2) = 1.015736E04
G(2,3) = -1.655047E02
G(2,4) = 7.43176E02
G(2,5) = -5.14606E-03
G(2,6) = 5.18347E-06
G(2,7) = -1.05922E-09
G(2,8) = 2.98389E02
B(2) = 3353.4061

C

EK(1) = 113.0
EK(2) = 91.5
DELTA(1) = 0.0
DELTA(2) = 0.0
SD(1) = 3.433
SD(2) = 3.681

C
C
C
C

COLLISION INTEGRAL FOR VISCOSITY

```

C
    ISPECIE = 2
    DO 10 I1=1,ISPECIE
        TEK=T(I)/EK(I1)
        COLMU=SIGMAM(TEK,DELTA(I1))
C
C -----
C SPECIE VISCOSITY AND THERMAL CONDUCTIVITY
C -----
C
    VMU(I1)=2.67E-05*SQRT(WI(I1)*T(I))/(SD(I1)**2*COLMU)
    CK(I1)=1.25*(CPI(I1)+RGAS/(2.0*WI(I1)))*VMU(I1)
    IF (EUCKEN.EQ.1) CK(I1)=(CPI(I1)+1.25*RGAS/WI(I1))*VMU(I1)
10 CONTINUE
C
C -----
C MIXTURE VISCOSITY AND THERMAL CONDUCTIVITY
C -----
C
    SUMXMU=0.0
    SUMXK=0.0
    DO 20 I2=1,ISPECIE
        SUMXFI=0.0
        DO 30 K1=1,ISPECIE
            PHIIK=.3535534*SQRT(1.0/(1.0+WI(I2)/WI(K1)))*
1 (1.0+SQRT(VMU(I2)/
2 VMU(K1)))*(WI(K1)/WI(I2)**(0.25))**2
C
C***  DEBUG
C
30 SUMXFI=SUMXFI+XG(K1)*PHIIK
    IF(XG(I2).LT.1.0E-30)GO TO 20
    SUMXK=SUMXK+XG(I2)*CK(I2)/SUMXFI
    SUMXMU=SUMXMU+XG(I2)*VMU(I2)/SUMXFI
20 CONTINUE
    CKG=SUMXK*418.4
    VMUG=SUMXMU*0.1
C
C SPECIES HEAT CAPACITY AT CONSTANT PRESSURE

```

C

```

DO 11 I1=1,ISPECIE
IF(T(I).GT.1200.0) GO TO 14
  SUMCP1=0.0
  DO 78 I3=1,5
    SUMCP1=SUMCP1+Z(I1,I3+5)*(T(I)/1000.0)**(I3-1)
78  CONTINUE
    CPI(I1)=SUMCP1
14  SUMCP2=0.0
    DO 12 I3=1,5
      SUMCP2=SUMCP2+Z(I1,I3)*(1000.0/T(I))**(I3-1.0)
12  CONTINUE
      CPI(I1)=SUMCP2
11  CONTINUE

```

C

C

MIXTURE HEAT CAPACITY AT CONSTANT PRESSURE

C

```

SCPG = 0.0
DO 27 I1=1,ISPECIE
SCPG = SCPG + YGAS(I1)*CPI(I1)
27  CONTINUE
CPG = SCPG*4184.0

```

27

C

C

SPECIES HEAT CAPACITY AT THE CONSTANT VOLUME

C

```

DO 31 I1=1,ISPECIE
  SUMCV1=0.0
  DO 36 I3=1,7
    SUMCV1=SUMCV1+G(I1,I3)**(I3-4)
36  CONTINUE
    CVI(I1)=SUMCV1+G(I1,8)*EXP(B(I1)/T(I))*((B1/T(I))/
&    (EXP(B1/T(I))-1.0))**2.0
31  CONTINUE

```

31

C

C

C

```

-----
MIXTURE HEAT CAPACITY AT CONSTANT VOLUME
-----

```

C

C

SCVG = 0.0

```

DO 37 I1=1, ISPECIE
SCVG = SCVG + YGAS(I1)*CVI(I1)
37 CONTINUE
CVG = SCVG*4184.0

C
C -----
C DIFFUSIVITIES
C -----
C

DIFMW=0.0
DO 50 I1=1, ISPECIE
SUMXD=0.0
DO 40 KI=1, ISPECIE
IF (I1.EQ.KI) GO TO 40
TEK=T(I)/SQRT(EK(I1)*EK(KI))
COLDIF=SIGMAD(TEK)
DIF=0.00186*T(I)**(1.5)*SQRT(1.0/WI(I1)+1.0/WI(KI))/
1 (P*((SD(I1)+SD(KI))/2.0)**2*COLDIF)
SUMXD=SUMXD+XG(KI)/DIF
40 CONTINUE
DIFM(I1)=(1.0-XG(I1))/SUMXD
DIFMW=DIFM(I1)*1.0E-04
50 CONTINUE
RETURN
END

```

\clearpage

```

C
C *****
C SUBROUTINE TPSOLID
C *****
C -----
C TRANSPORT PROPERTIES OF SOLID PARTICLES
C TRANSPORT PROPERTIES CHANGES SIGNIFICANTLY ABOVE THE
C MELTING TEMPERATURE OF THE SOLID.
C -----
C
C
C IMPLICIT DOUBLE PRECISION (A-H,O-Z)
COMMON/VAR1/RHOG,CPG,TEMP,CPI(20),XG(20),WI(20),
& SD(20),VMUG,DS,ISPECIE,RGAS,CVG,CVI(20)

```

```

COMMON/VAR2/P,V,AREA,DIFMW,EK(20),RHO(5),
&    DELTA(20),DIFM(20),CK(20),VMU(20),CKG,EL(5,5),
&    PHIJWK(5,9),IEUCKEN,Z(10,10),G(5,8),B(5)
COMMON/VAR3/Y1(201),Y2(201),Y1NEW(201),Y2NEW(201),T(201),
&PHI(201),PHINEW(201),R(201),RHOGAS(201),Y4(201),CPMIX(201),
&RXN(201),SOURCE(201),Y3(201),OLDRHO(201),VEL(201),CVMIX(201),
&RHOMIX(201),TURB(201),RADN(201),TURBF(201),TURBB(201),
&YG(201),DTDZ(201),OLDT(201),BURNV3(201),DV(201)
COMMON/VAR4/YGAS(20),DIFMIX(201),PR(201),WLE(201),SC(201),
&    BFR(201),BBK(201),PGN(201),PG(201),PB(201),GAMMA(201),
&    BETA(201),CKMIX(201),VMUMIX(201)

```

C
C
C

HEAT CAPACITY

```

CP1=1.4222E-06*T(I)**3-2.30647E-03*T(I)**2+1.64437*T+580.05
CP4 = 1012.0

```

C
C
C

THERMAL CONDUCTIVITY

```

CK1=1.6595E-07*T(I)**3-3.8165E-04*T(I)**2+0.2174*T(I)+202.70
IF(T(I).GE.933.0) CK1 = 105.0
CK4 = 105.0

```

C
C
C

DENSITY

```

RHO1 = 2700.0
IF(T(I).GE.933.0) RHO1 = 2330.0
RHO4 = 3970.0

```

C
C
C

VISCOSITY

```

VMU1 = 0.1*EXP((720.0/T(I))-2.68)
IF(T(I).GE.933.0) VMU1 = 1.492E-04*EXP(1984.5/T(I))
VMU4 = 1.492E-04*EXP(1984.5/T(I))

```

C
C
C
C

NUMBER OF SPATIAL-STEPS

DISTANCE BETWEEN EACH SPATIAL GRIDS

RETURN

END
 \clearpage

```

C
C *****
  FUNCTION SIGMAD(TEK)
C *****
C
  DIMENSION ABC(3,3)
  DATA (ABC(I,1),I=1,3)/0.36934,-0.48595,0.02574/
  DATA (ABC(I,2),I=1,3)/0.343,-0.44203,0.07548/
  DATA (ABC(I,3),I=1,3)/0.09454,-0.17612,0.00272/
  IF (TEK.LT.0.3) TEK=0.3
  IF (TEK.GT.100.0) TEK=100.0
  M = 1
  IF (1.55.LE.TEK.AND.TEK.LT.7.0) M=2
  IF (TEK.GT.7.0) M=3
  ALOGT = ALOG(TEK)
  SIGMAD=EXP(ABC(1,M)+ALOGT*(ABC(2,M)+ALOGT*ABC(3,M)))
  RETURN
  END

```

\clearpage

```

C
C *****
  FUNCTION SIGMAM(TEK,DEL)
C *****
C
  DIMENSION DELTA(8),AM(8,3),BM(8,3),CM(8,3)
  DATA(DELTA(I),I=1,8)/0.0,0.25,0.5,0.75,1.0,1.5,2.0,2.5/
  DATA(AM(I,1),I=1,8)/0.47395,0.47808,0.50119,0.54868,0.60910,
1 0.45351,0.89016,1.01037/
  DATA(AM(I,2),I=1,8)/0.43969,0.44882,0.48192,0.53732,0.60815,
1 0.76710,0.91660,1.04383/
  DATA(AM(I,3),I=1,8)/0.16152,0.16285,0.17807,0.20258,0.23287,
1 0.31112,0.41063,0.52600/
  DATA(BM(I,1),I=1,8)/-0.53203,-0.51551,-0.49752,-0.49670,
1 -0.51945,-0.57471,-0.60747,-0.62594/
  DATA(BM(I,2),I=1,8)/-0.44832,-0.45212,-0.47283,-0.50951,
1 -0.55388,-0.64309,-0.70603,-0.73772/

```

```

DATA(BM(I,3),I=1,8)/-0.15835,-0.15840,-0.16626,-0.17878,
1 -0.16314,-0.23119,-0.27807,-0.33159/
DATA(CM(I,1),I=1,8)/-0.05410,-0.04057,-0.01404,0.01,0.01832,
1 0.01467,0.00901,0.00461/
DATA(CM(I,2),I=1,8)/0.07758,0.07756,0.08067,0.08685,0.09367,
1 0.10489,0.10718,0.10078/
DATA(CM(I,3),I=1,8)/0.00186,0.00178,0.00281,0.00442,0.00627,
1 0.01075,0.01625,0.02242/
DATA IDEL/1/
IF (DEL.GT.2.5) DEL=2.5
IF (TEK.LT.0.1) TEK=0.1
IF (TEK.GT.100.0) TEK=100.0
M=1
IF(TEK.LT.9.0.AND.1.4.LE.TEK) M=2
IF(TEK.GE.9.0) M=3
ALOGT=ALOG(TEK)
CALL FIND (DEL,A,DELTA,AM(1,M),8,IDEL)
CALL FIND (DEL,B,DELTA,BM(1,M),8,IDEL)
CALL FIND (DEL,C,DELTA,CM(1,M),8,IDEL)
SIGMAM=EXP(A+ALOGT*(B+C*ALOGT))
RETURN
END

```

C

\clearpage

C

C

```

*****
SUBROUTINE FIND(ARG,ANS,X,Y,NPTS,I)

```

C

```

*****

```

C

C

```

EXTRAPOLATES FOR THE VALUES OUT OF TABLE RANGE
CALLING SEQUENCE IS ....

```

C

C

```

CALL FIND(ARG,ANS,X,Y,NPTS,MEM)

```

C

C

```

ARG IS THE ARGUMENT

```

C

```

ANS CONTAINS RESULTS ON EXIT

```

C

```

DIMENSION X(50), Y(50)

```

1

```

IF(X(I)-ARG) 4,2,2

```

```
2      I=I-1
      IF (I-1) 3,3,1
3      I=1
      GO TO 3
4      IF(X(I+1)-ARG) 5,7,7
5      I=I+1
      IF (I-NPTS) 4,6,6
6      I=NPTS-1
      GO TO 9
7      ANS=Y(I)+(Y(I+1)-Y(I))*(ARG-X(I))/(X(I+1)-X(I))
      RETURN
8      ANS = Y(1)
      RETURN
9      ANS = Y(NPTS)
      RETURN
      END
```

8 MODEL OF FLAME PROPAGATION AND QUENCHING OF COAL-AIR FLAME

A mathematical model of coal dust-air flame propagation is developed and numerical prediction of the detailed laminar flame structure, temperature distribution, and flame velocity and comparison with the experimental data are performed wherever possible.

8.1 Introduction

A system of time-dependent, non-linear partial differential equations governing the flame propagation phenomena are solved numerically. Researchers started these studies to find a way to describe the processes involved in the flame propagation hoping to either prevent the coal mine explosions or to find a way to control them. Analytical models, some complex and some very simple, have been used to predict the experimental data. However, the equations describing the flame fronts during coal combustion are very complex and have made the analytical treatments almost impossible. Recent advances of fast digital computers enabled the numerical analysis of these models.

An approach to the numerical solution of the equations of the coal combustion is discussed in the following sections. This model is used to investigate the flame

velocity and the species profiles of coal-air flames. This study is based on the model developed by Smoot and Horton [1977].

8.2 Model Assumptions and Advantages

The governing general equations are reduced to the time-dependent one-dimensional equations using the following set of assumptions.

1. One-dimensional laminar flow.
2. Negligible gravity effects, viscous dissipation, thermal diffusion.
3. Coal particles are spherical in shape.
4. Dynamic equilibrium of the particle-gas mixture.
5. Pressure is uniform throughout the test section.

Despite the above simplifications, the following significant complexities are included in this model.

1. Variable gas density, and transport properties.
2. Gas phase non-equilibrium throughout the flame front.
3. Multi-components in the gas phase.
4. An arbitrary number of particle sizes.

8.3 Governing Equations

The schematics of this model is shown in Figure 8.1. On one side of the coal-air flame, a mixture of unburned particle-gas exists, and the combustion products of this mixture exist on the other side of the flame front. Gases continually enter the unburned edge of the flame and exit from the burned edge. This might be visualized either as a moving wall of unburned fuel mixture entering a stationary flame, or as a moving flame propagating into a region of unburned fuel mixture. The governing equations for each phase are described as follows.

Gas phase:

Total continuity;

$$\frac{\partial \rho_g}{\partial t} + \frac{\partial \rho_g v_g}{\partial y} = \sum_j r_{pj} \quad (8.1)$$

Species Continuity;

$$\begin{aligned} \rho_g \frac{\partial \omega_{ig}}{\partial t} + \rho_g v_g \frac{\partial \omega_{ig}}{\partial y} &= \frac{\partial}{\partial y} \left(\rho_g D_{ig} \frac{\partial \omega_{ig}}{\partial y} \right) \\ &+ r_{ig} + \sum_j (r_{pi})_j - \sum_j r_{pj} \omega_{ig} \end{aligned} \quad (8.2)$$

Energy;

$$\begin{aligned} \rho_g \frac{\partial h_g}{\partial t} + \rho_g v_g \frac{\partial h_g}{\partial y} &= \frac{\partial}{\partial y} \left(\frac{k_g}{C_{pg}} \frac{\partial h_g}{\partial y} \right) + \sum_j Q_{pj} + \sum_j r_{pj} (h_{pj} - h_g) \\ &= -Q_{gs} \frac{\partial}{\partial y} \sum_i \left[D_{ig} \rho_g - \frac{k_g}{C_{pg}} \right] h_{ig} \frac{\partial \omega_{ig}}{\partial y} \end{aligned} \quad (8.3)$$

Particle phase:

Total continuity;

$$\frac{\partial \rho_{pj}}{\partial t} + \frac{\partial \rho_{pj} v_{pj}}{\partial y} = - \sum_j r_{pj} \quad (8.4)$$

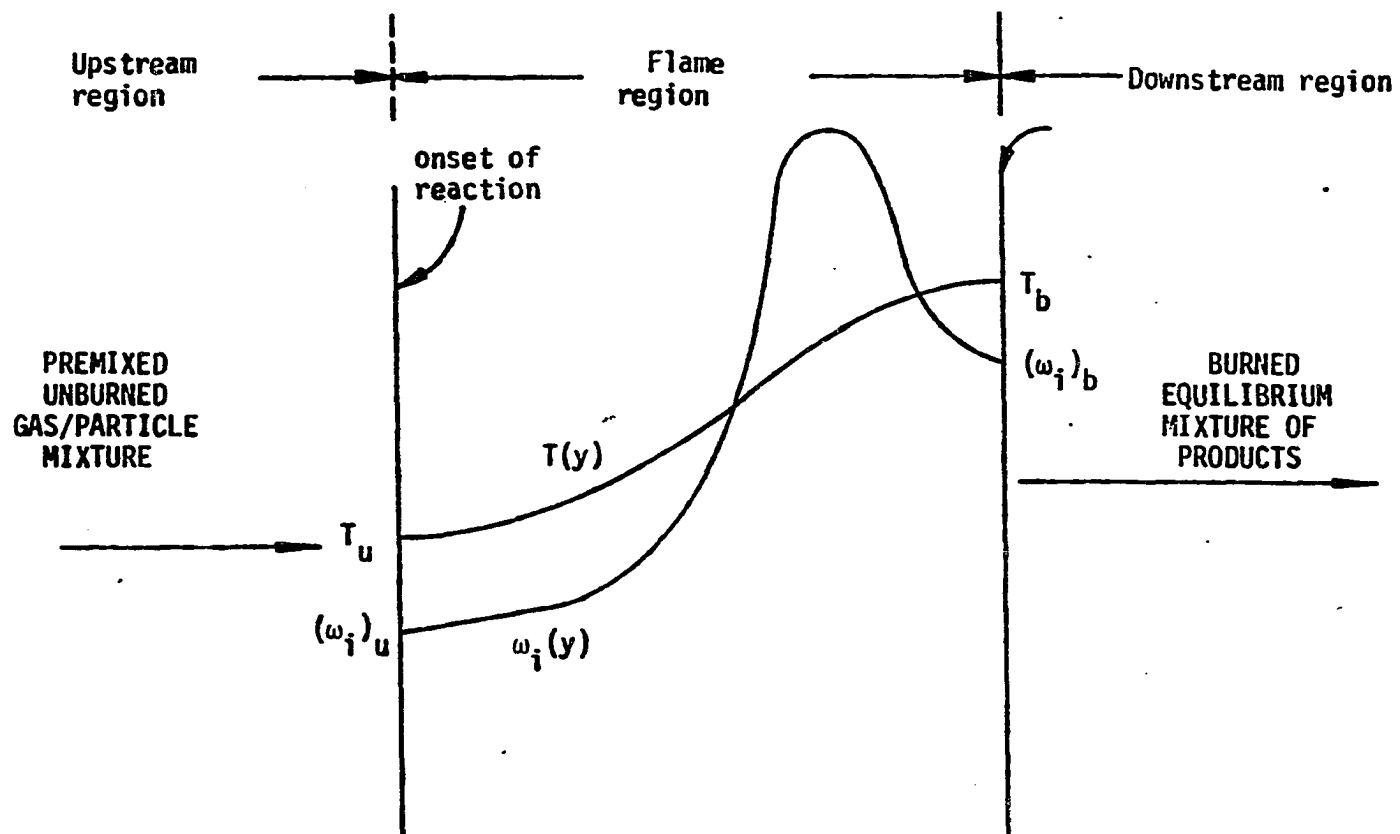


Figure 8.1: Schematics of flame region

Species Continuity;

$$\rho_p \frac{\partial \omega_{pj}}{\partial t} = \omega_{pj} \sum_j (r_{pj}) - r_{pj} \quad (8.5)$$

Energy;

$$\begin{aligned} \rho_{pj} \frac{\partial h_g}{\partial t} + \rho_{pj} v_{pj} \frac{\partial h_{pj}}{\partial y} = & -Q_{pj} - Q_{ps} - Q_{pf} \\ & -r_{pj} [(h_{pjg} - h_{pj}) - p/\rho_{pgj}] \end{aligned} \quad (8.6)$$

Total density; adding the gas phase and particle continuity equations the total continuity is obtained.

$$\frac{\partial \rho_t}{\partial t} + \frac{\partial \rho_t v}{\partial y} = 0 \quad (8.7)$$

where,

$$\rho_t = \rho_g + \sigma_j \rho_{pj} \quad (8.8)$$

Particle number balance;

$$\frac{\partial n_{pj}}{\partial t} = -\frac{\partial n_{pj} v}{\partial y} \quad (8.9)$$

Combine the above equation with the total continuity equation to give;

$$\frac{1}{\rho_t} \frac{\partial \rho_t}{\partial t} = \frac{1}{n_{pj}} \frac{\partial n_{pj}}{\partial t} \quad (8.10)$$

Finally, combine this equation with the equation of the total density with $\rho_{pj} = \omega_{pj} \rho_p$,

$$\frac{\rho_t}{n_{pj}} \frac{\partial n_{pj}}{\partial t} \sum_k [m_{pk} \frac{\partial n_{pk}}{\partial t} n_{pk} \frac{\partial n_{pk}}{\partial t}] = \frac{\partial \rho_g}{\partial t} \quad (8.11)$$

Particle mass balance:

$$\frac{\partial m_{pj}}{\partial t} = -\frac{r_{pj}}{n_{pj}} \quad (8.12)$$

8.4 Flame Velocity

From the total continuity equation, the steady state flame velocity can be defined as,

$$S_u = -S_b = -\rho_t v \quad (8.13)$$

Generally, the steady state flame velocity is calculated from the species continuity equations. Assuming steady state and noting that the diffusion term is negligible when it is integrated over the entire flame region, the following equation can be obtained.

$$[(\rho g \omega_{ig} + \sum \rho_{pj})v]_u - [(\rho g \omega_{ig} + \sum \rho_{pj})v]_b = \int_b^u (r_{ig} + \sum_j [(\omega_{ig} - 1)r_{pj}]) dy \quad (8.14)$$

Where the subscripts u and b represent the unburned and burned states, respectively. Thus, the flame velocity is calculated by simultaneously solving the above equation and the mass balance equation:

$$[(\rho g + \sum \rho_{pj})v]_u = [(\rho g + \sum \rho_{pj})v]_b \quad (8.15)$$

8.5 Transformation

The Lagrangian transformation is used to transform the differential equations from (y,t) coordinate to (ψ ,t) coordinate.

$$\frac{\partial \psi}{\partial t} = -\rho_t v \quad (8.16)$$

$$\frac{\partial \psi}{\partial y} = \rho_t \quad (8.17)$$

The Lagrangian transformation satisfies the total continuity equations automatically, and this transformation makes the convective terms containing the velocity disappear. Thus, it is unnecessary to know the flame velocity v to integrate the model equations.

The above Lagrangian transformation can be used to proceed the numerical solution without further transformation. But the flame region, $\psi_b - \psi_u$, changes with time, making it difficult to initially predict the flame width. To avoid the problem of iterating the flame width as the solution marches with time, Spalding et al. [1971] suggested a further transformation by non-dimensionalizing the ψ coordinate as follows.

$$s(\psi, t) = \frac{\psi - \psi_u}{\psi_b - \psi_u} \quad (8.18)$$

This transformation further transforms the (ψ, t) coordinates into (s, t) coordinates. The transformed equations, using the fact that $\rho_t v = S_b$, take the following general form.

$$\frac{\partial \phi}{\partial t} + \left(\frac{sm_b + (1-s)m_u}{\psi_b - \psi_u} \right) \frac{\partial \phi}{\partial s} = A \frac{\partial}{\partial s} \left[B \frac{\partial \phi}{\partial s} + C \right] \quad (8.19)$$

It can be seen from the above equation that the s transformation re-introduces the convective term, even though it normalizes the grid spacing.

8.6 Auxiliary Equations

The auxiliary equations are required to complete the mathematical model. These auxiliary equations are divided into six groups.

1. Thermal equations of temperature, enthalpy, heat capacity, equation of state.

2. Transport properties equations of viscosity, conductivity, density, and diffusivity.
3. Radiative heat transfer equations.
4. Coal reactions equations.
5. Particle-gas interaction equations of convective heat transfer and chemical reaction.
6. Gas phase kinetic equations.

The enthalpy of gas and particle are calculated from the differential equations. Thus, the thermal equations of heat capacity of gas species and mixture, enthalpies of each species and mixture and equation of state are required to solve the governing equations.

The radiation is assumed to occur only among particles. The flame region is divided into three radiation regions, preheat region, flame region, and post-burn region.

The following assumptions are made for the calculation of the coal reaction equations.

1. A particle is composed of raw coal, char, moisture, and ash.
2. Moisture losses during coal combustion are controlled by heat transfer and water vapor diffusion from the coal to the gas.
3. Ash is inert and remains in the solid phase during reaction.

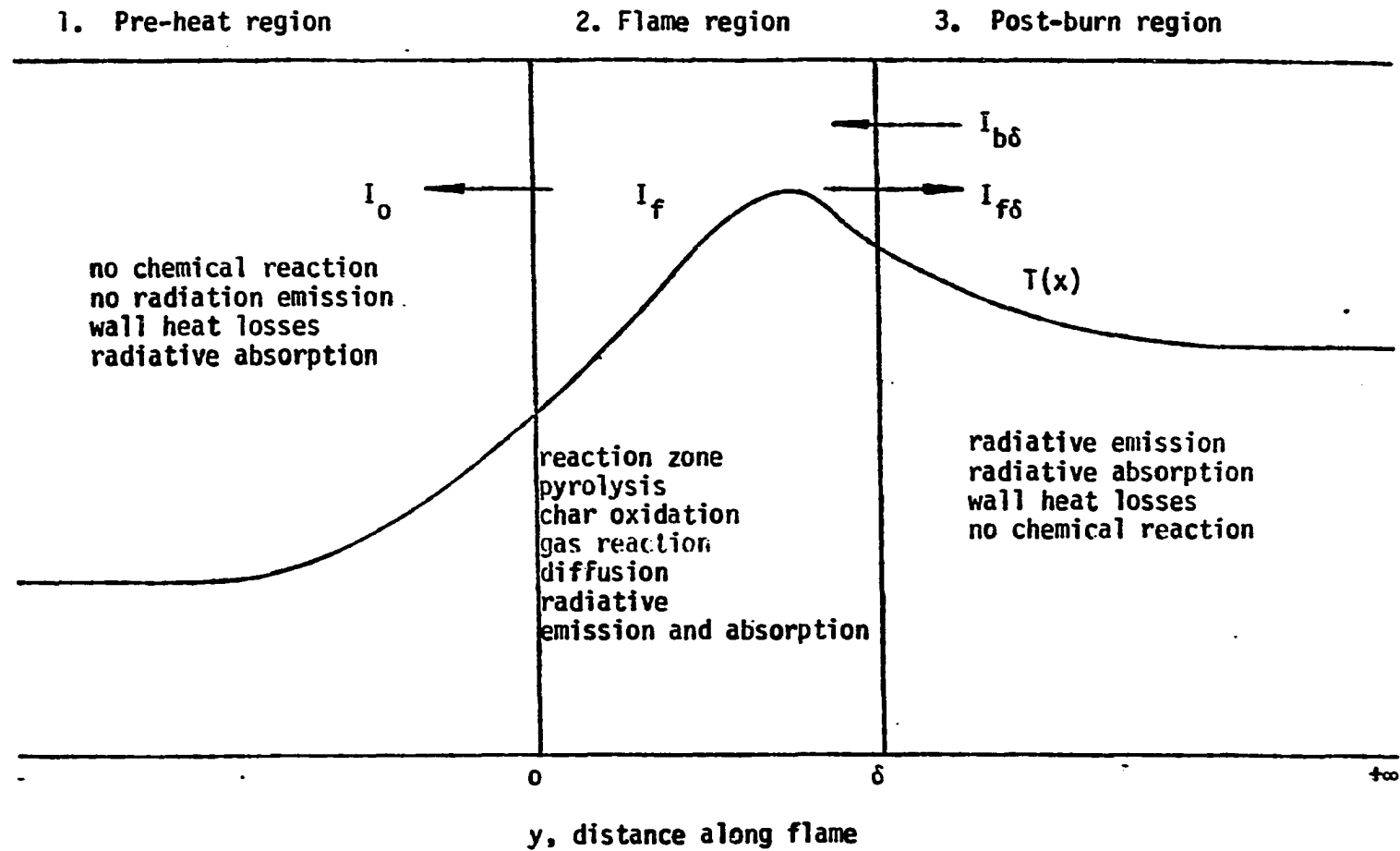


Figure 8.2: Schematics of coal flame model.

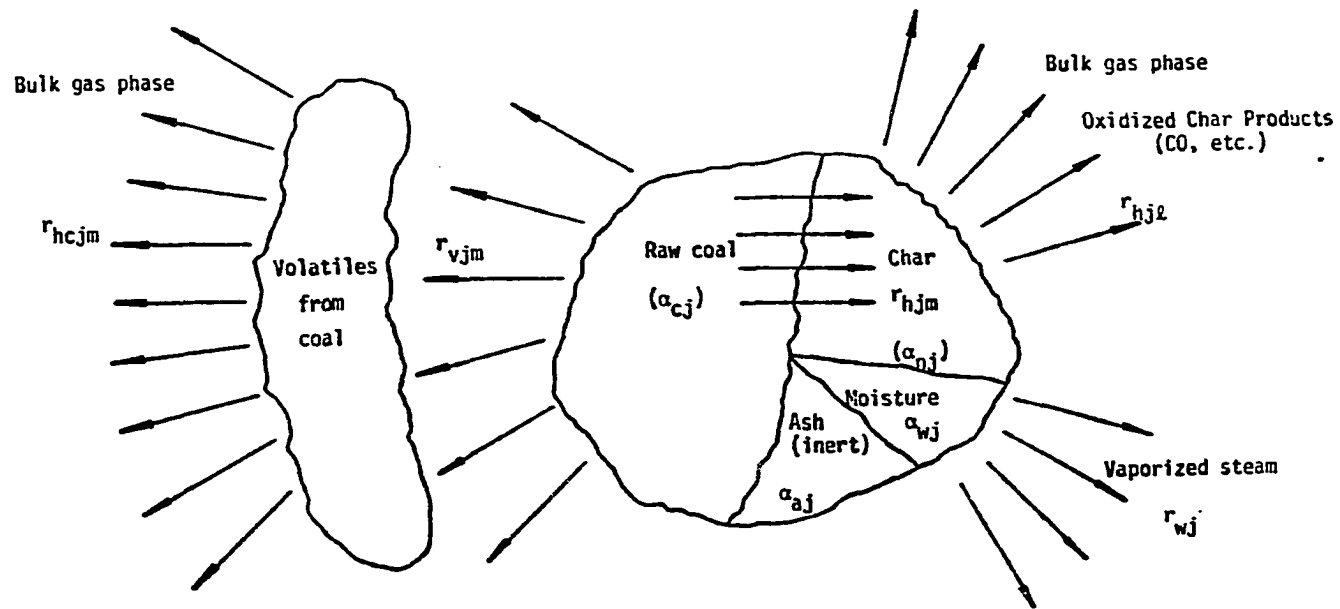


Figure 8.3: Coal particle constituents and reaction rates (Smoot and Horton [1977])

Figure 8.3. shows this model of coal particle reaction scheme.

The general sequence of chemical reactions is; a). devolatilization reactions, b). char oxidation, c). and gaseous volatiles oxidation.

For devolatilization, the formulation by Anthony et al. [1974] is used. The kinetic rates of volatile production are,

$$r_{vjm} = Y_{jm} k_{jm} \rho_{cj} \quad (8.20)$$

where,

$$k_{jm} = A_{jm} \exp(-E_{jm}/RT) \quad (8.21)$$

Char is assumed to oxidize heterogeneously by a gaseous oxidizer that diffuses to the particle, absorbs, reacts with the carbon and desorbs as carbon monoxide. The reaction equation is,

$$r_{hjk} = \phi_l k_{cj} k_{jl} \zeta A_j C_{0j}^{n_j} \quad (8.22)$$

where

$$k_{jl} = A_{jl} \exp(-E_{jl}/RT_j) \quad (8.23)$$

Some coals contain high percentages of moisture. The vaporization of from the coal particle is described by,

$$r_{wj} = M_w Nu_{im} C_g D_{wm} A_j A (X_{wj} - X_{wg}) / dg (1 - X_w r_j / r_{wj}) \quad (8.24)$$

Density, diameter, heat capacity, and enthalpy of each of the coal particle and components, reaction rate of particle devolatilization, heterogeneous char reaction rate, and total particle reaction rate equations are necessary for the solution

8.7 Solution Technique

The numerical method used to reach the solution of this problem is accomplished by treating the gas and particle equations separately. The fundamental reason for this separation is the differences between the two equation sets. The second-order diffusion term in the gas equations and the presence of the gas kinetics terms introduce difficulties.

8.7.1 Initial and boundary conditions

The initial distribution of chemical species and enthalpy is not essential for the solution of this problem. Spalding et al. [1971] proposed the initial profile of the form.

When $t=0$,

$$\frac{\phi - \phi_u}{\phi_b - \phi_u} = 10s^3 - 15s^4 + 6s^5 \quad (8.25)$$

where, ϕ is a variable.

Radical concentrations are assumed initially to be zero. The equilibrium composition and temperature of the final flame are evaluated to provide the initial burned gas values. As the computation proceeds, these burned gas values are allowed to float with the boundary conditions so that the slope of the species composition, temperature, etc., are zero at the burned edge of the flame. Unburned values of these parameters remain fixed. Thus, the boundary conditions take the following form.

At the unburned edge ($s=0$),

$$\omega_{ig} = \omega_{ig,u} \quad (8.26)$$

$$\omega_{jp} = \omega_{jp,u}$$

$$h_g = h_{g,u}$$

$$h_{jp} = h_{jp,u}$$

At the burned edge ($s=1$),

$$\begin{aligned} \frac{\partial \omega_{ig}}{\partial s} &= 0 \\ \frac{\partial \omega_{jp}}{\partial s} &= 0 \\ \frac{\partial h_g}{\partial s} &= 0 \\ \frac{\partial h_{jp}}{\partial s} &= 0 \end{aligned} \quad (8.27)$$

8.7.2 Finite difference formulation

The gas species equations contain reversible non-linear kinetic reaction terms. Equations involving this type of reaction terms are referred to as “stiff” equations, and standard method of solving partial differential equations numerically tend to fail to solve this stiffness problem.

The gas reaction term in the gas species equation, r_{ig} at the new time step is evaluated from the linear terms of a Taylor series which is expanded at the previous time step. The following expression is obtained.

$$r_{ig}^{n+1} = r_{ig}^n + \sum \frac{\partial r_{ig}^n}{\partial \omega_k} (\omega_k^{n+1} - \omega_k^n) \quad (8.28)$$

Explicit method is used for all spatial derivatives. After insertion of the linearized kinetics terms, the finite difference equation for species continuity appears as follows.

$$B\omega^{n+1} = B\omega^n + L^n + P^n + R^n \quad (8.29)$$

A matrix system results which must be solved at each grid position, yielding the gas composition at the new time step, but only for that grid position.

Because spatial derivatives are handled explicitly, the stability of the program is a strong function of the grid size, the time step used, and also of the mass flow rates. In most cases, the instabilities are observed to dampen out, regardless of the previous magnitude.

The above-described "explicit-implicit" method has been used only for gas species equations. The equation describing gas enthalpy variation was treated using an implicit Crank-Nicolson algorithm. This process yields a simple tri-diagonal matrix for each equation.

Implicit numerical techniques were also tried for the particle equations; however, the implicit methods used for these differential equations was not stable. Analyses of this second order diffusion term are first order hyperbolic, while the gas-phase equations are parabolic. An implicit finite difference method is used for first order hyperbolic equations.

In summary, the various techniques used for each of the govern equations are as follows. A mixed implicit-explicit method is used for the gas species equation, an implicit method is used for gas energy equation, and an implicit method is used for all of the particle equations.

8.8 Results and Discussions

Numerical predictions are performed for coal-air flame for various particle sizes, concentrations, and volatile contents, and they are compared with the experimental

data. About 100 minutes of CPU time is taken for the solution to reach the steady state.

The results are plotted in Figures 8.4 to 8.8. Figure 8.4 shows a predicted flame velocities of 16.7 μm Penn. Seam coal at various particle concentrations. The predicted flame velocities are higher than experimental values. Figures 8.5 and 8.6 shows species mass fraction and temperature profiles of coal-air flame. In this model, the gaseous volatile is assumed to be composed of $C_5H_{7.25}$. It shows that gas temperature is little higher than particle temperature. Figures 8.7 and 8.8 shows the effect of particle diameter and volatile content on the flame velocity of coal-air flame. They shows that flame velocities increase with a decrease in particle diameter and with a increase in volatile content.

The predicted burning velocity data are used to predicted the quenching distance of coal-air flame using Ballal's model. His equation takes the following form.

$$d_q = (8\alpha)^{1/2} \left[\left(\frac{C_3^3 \rho_f D_{32}^2}{8C_1 f^2 (k/C_p) \phi \ln(1+B)} + \frac{12.5\alpha}{S_u^2} \right)^{-1} - \frac{9qC_1^2 \epsilon \sigma T_p^4}{C_p \rho_f C_3^3 f D_{32} \Delta T_{st}} \right]^{-1/2} \quad (8.30)$$

The predicted quenching distances are compared with experimental data and it is plotted in Figure 8.9. The predicted quenching distances are little lower than experimental data. But the effect of particle concentration on quenching distance are well predicted by this model.

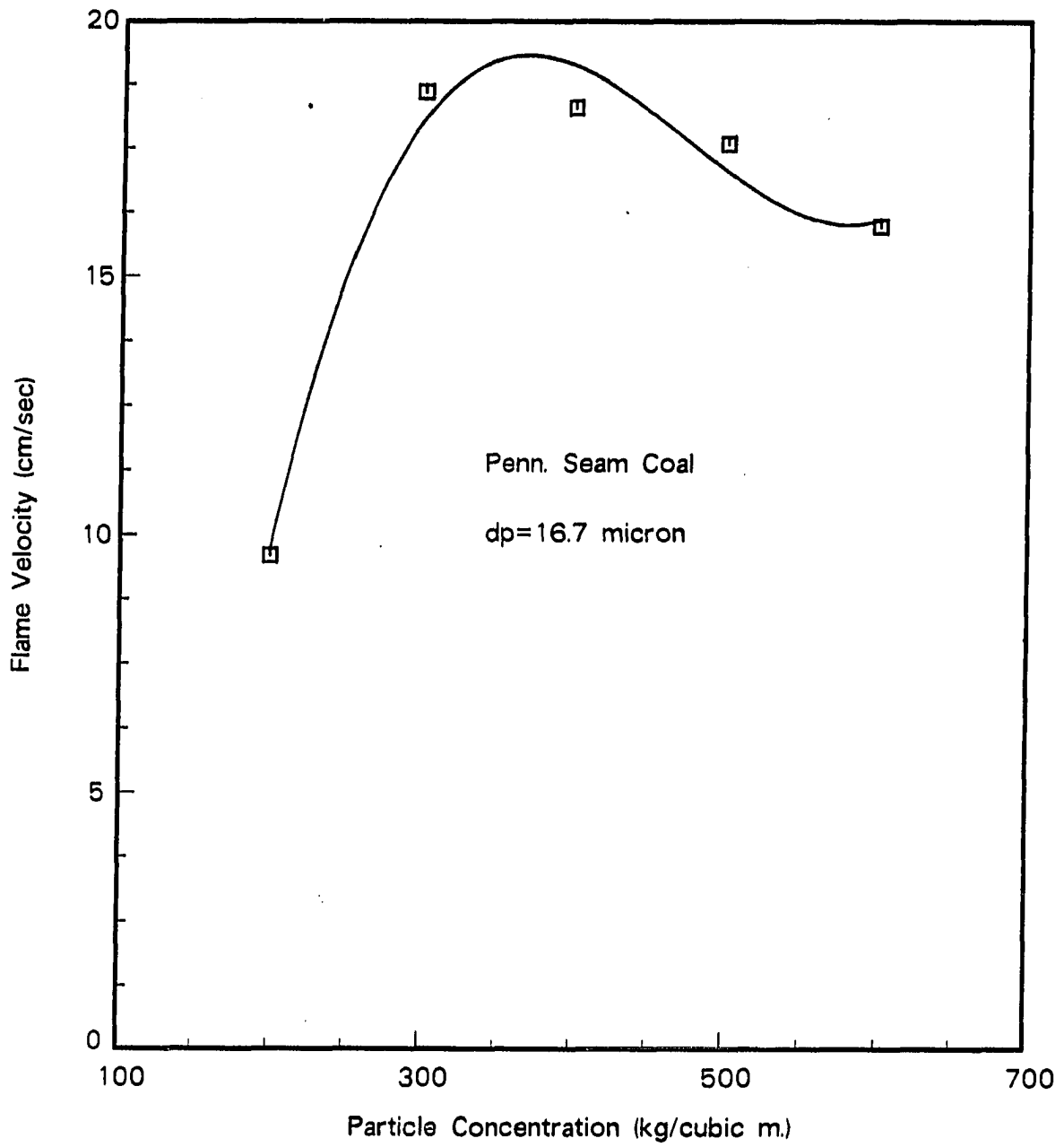


Figure 8.4: Predicted flame velocity vs. particle concentration

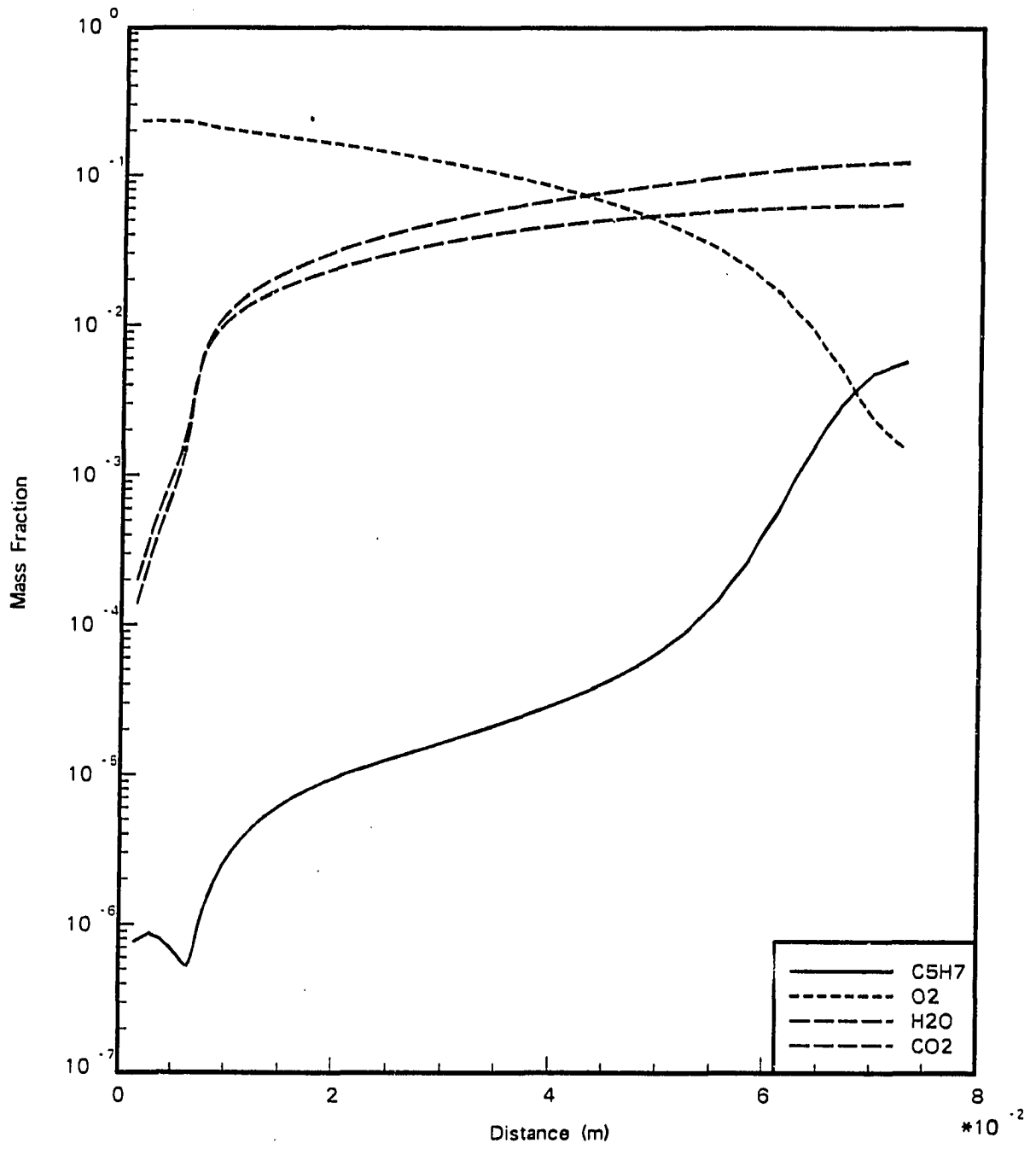


Figure 8.5: Predicted species profile variation with distance

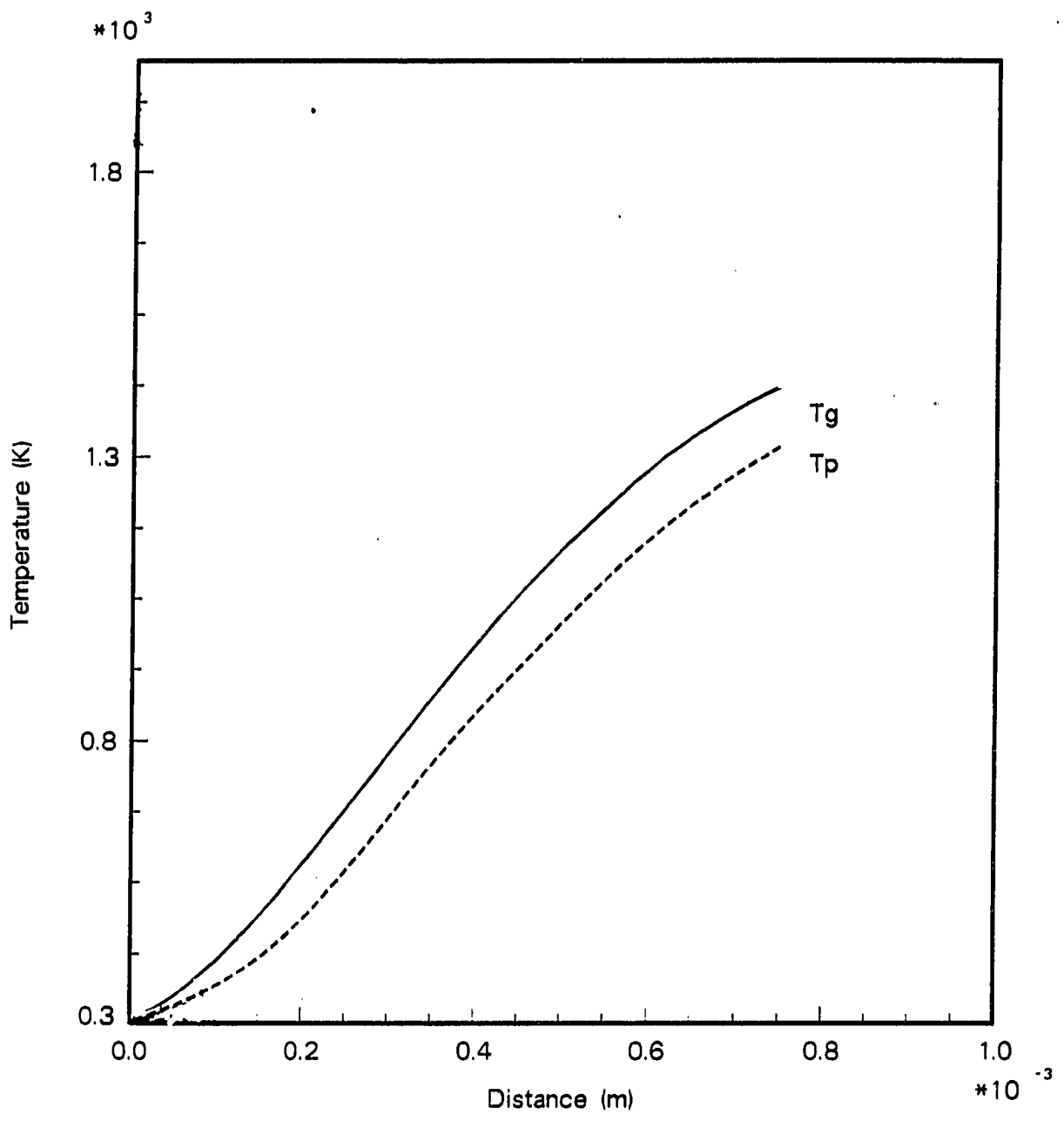


Figure 8.6: Predicted particle and gas temperature variation with distance

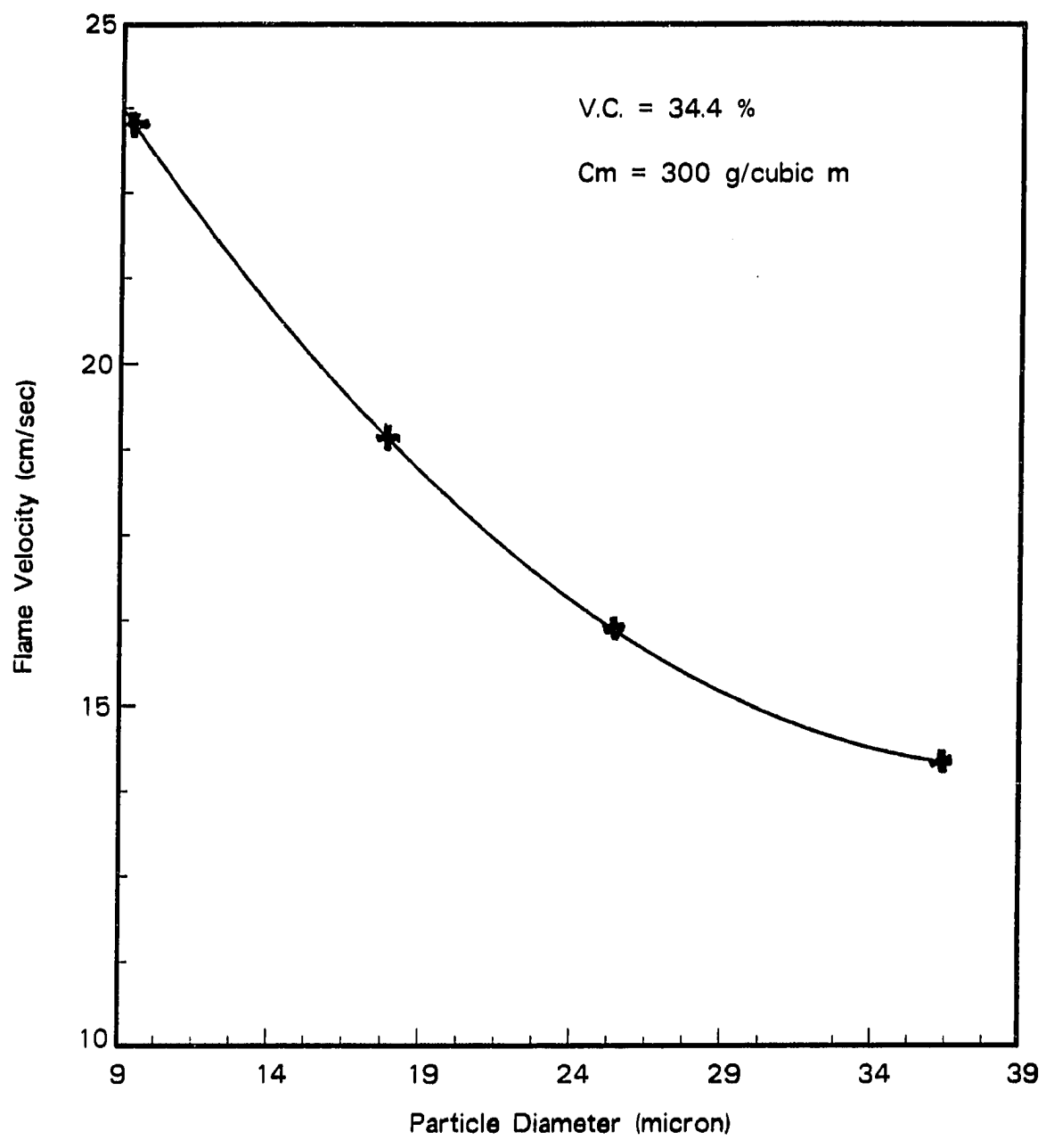


Figure 8.7: Predicted flame velocity vs. particle diameter

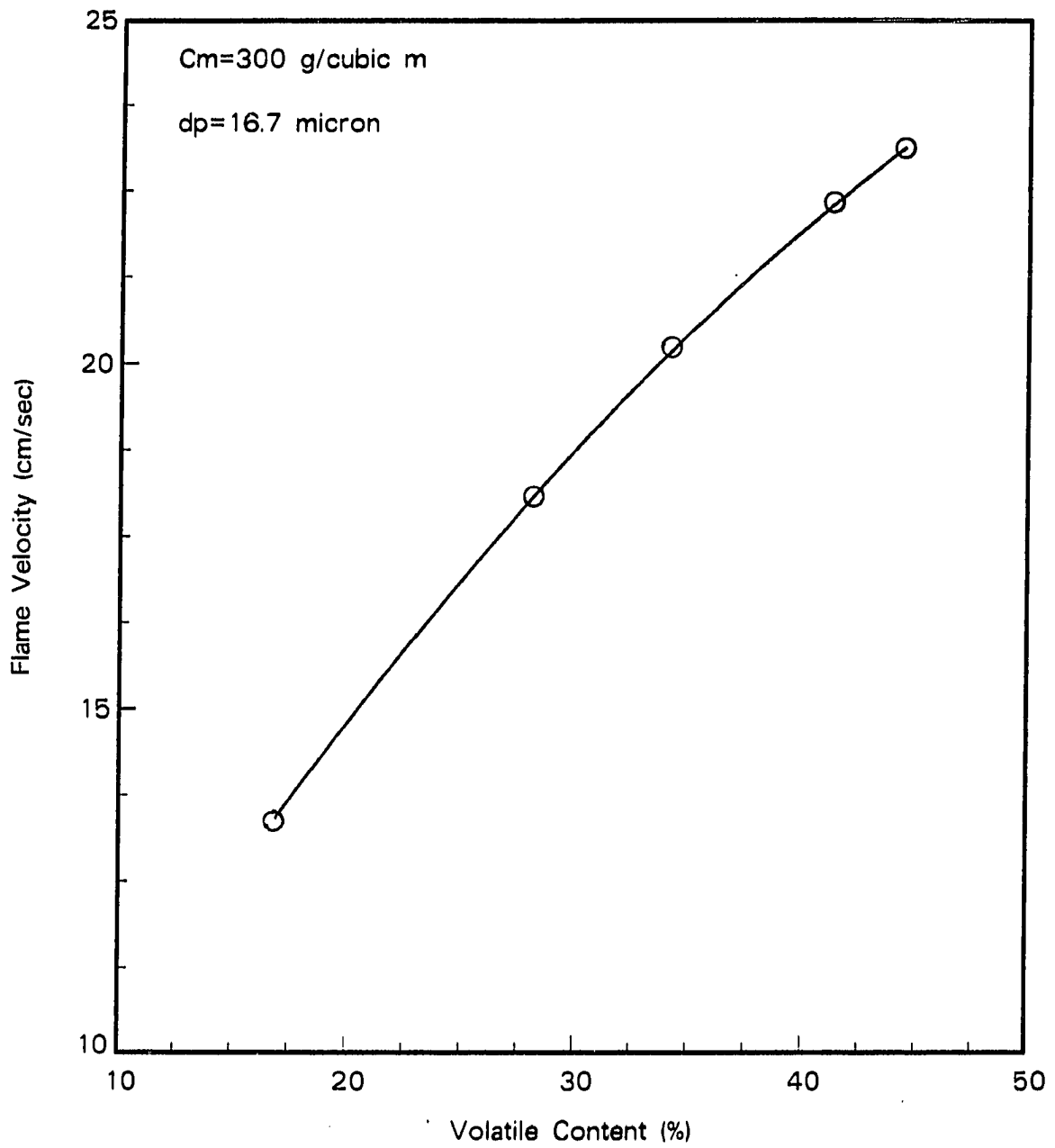


Figure 8.8: Predicted flame velocity vs. volatile content

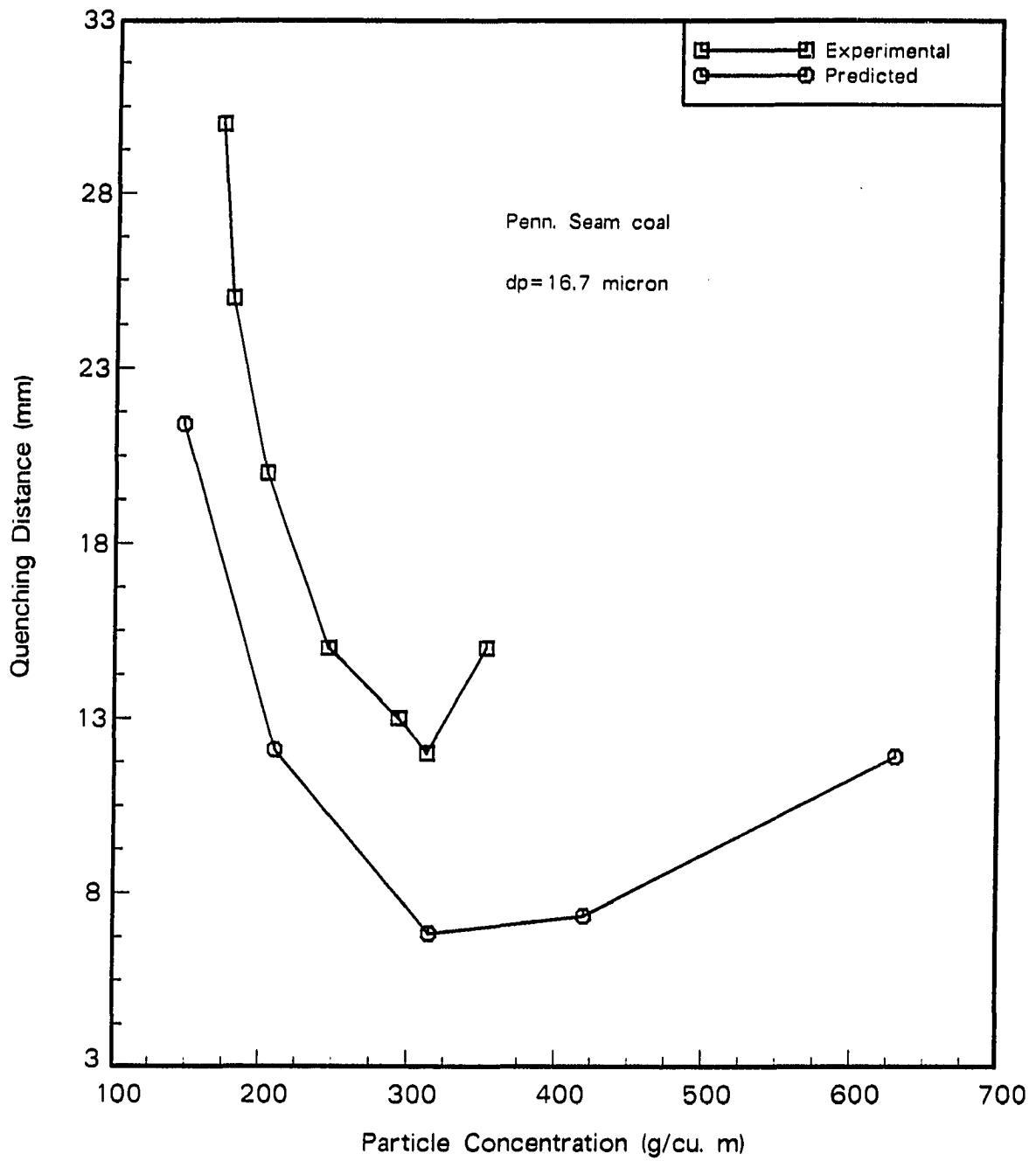


Figure 8.9: Predicted quenching distance vs. particle concentration of Penn. Seam coal

9 CONCLUSIONS AND RECOMMENDATIONS

A comprehensive theoretical and experimental study has been carried out at atmospheric pressure on the flame propagation and quenching of spherical and irregular aluminum powder of various particle sizes, and for five different types of coal powders of various particle sizes. Much of the data are presented here for the first time, and therefore only limited comparisons can be made with the literature. Theoretical and numerical studies were performed to predict the burning velocity and quenching distance of the aluminum and coal powders, and compared with the experimental data. The study includes the effects of particle diameter, particle concentration, volatile content on burning velocity and quenching distance of powdered fuels. A multiple regression is performed and a correlation equation of quenching distance as a function of particle diameter, particle concentration, and volatile content (coal only) was obtained for both aluminum and coal powder.

The experimental apparatus utilized a new concept in ignition of powders using a needle electrode mounted at the upper plate in an electric particulate suspension of powder. A vibration exiter and air flow were used along with an electrostatic particulate suspension to augment the suspension of coal powder. The advantages of this technique are that a highly uniform particulate cloud is generated and that testing is steady state. In contrast, a Hartmann type test tubes relies on a transient

testing method utilizing aerodynamics to create the suspension.

Disadvantages to the present testing method are that the test section volume is physically limited and that excess energy may be required to trigger a spark. However, this distance limitation was used to advantage in the quenching studies where small separation distance are needed. A helium neon laser with a photo-sensor was used to measure the particle concentration. High speed pictures taken at 400 frames/sec were used to observe the flame propagation behavior of dust clouds, the ignition delay time and the burning velocity. The following observations summarize important characteristics and behavior of powdered flames tested in the course of this research:

- For burner experiment, a cone-shaped flame could be obtained above the upper electrode for all sizes of spherical aluminum powder.
- A flat flame with aluminum powder could be stabilized after a long time while a flat flame with a medium volatile bituminous coal (Penn. Seam) was obtained but did not stabilize itself.
- The application of an electric field lifted the flame a few millimeters above the upper screen; for a higher electric field, the flame is blown off.
- For a flat flame burner utilizing powdered fuel, the pneumatic transport of particles is of primary importance, and with the electric field augmenting the transport.
- The minimum quenching distance of both aluminum and coal increases as the particle size increases and generally, the lean flammability limit appears to increase as the particle size increases.

- In general, the quenching distance of both aluminum and coal decreases as the particle concentration increases until it reaches the minimum quenching distance, then increases as the particle concentration increases.
- A rich flammability limit does not exist or impossible to find.
- Batch aluminum powder was found to be more difficult to ignite than mono-sized aluminum of the same mean diameter.
- For irregular shaped aluminum, the minimum quenching distance increases monotonically as the particle size increase up to $27 \mu m$, then it increases rapidly with the particle diameter. However, for spherical aluminum, the minimum quenching distance was seen to increase monotonically with an increase of the particle size.
- The quenching distance of irregular aluminum is lower than for spherical aluminum of the same mean diameter for particles below $25 \mu m$ in diameter, but for particles above $25 \mu m$ in diameter, irregular aluminum has a higher quenching than spherical aluminum.
- The quenching distance increases as the moisture content of air increases, but the differences are small enough to be negligible.
- The quenching distance decreases as the external electric field strength increases but the differences are small enough to be negligible.
- The burning velocity of both aluminum and coal decreases as the particle size increases.

- The shape of the burning velocity vs. particle concentration curve is concave downward, which is the reverse of the quenching distance vs. particle concentration curve.
- The minimum quenching distance of coal is much higher than that of aluminum powder for the same particle size.
- It was impossible to ignite coal larger than 40 μm diameter in this apparatus.
- The minimum quenching distance increases as the volatile content of the coal decreases for the same particle size; however, the quenching distance does not always increase as the volatile content of the coal decreases (for the same particle size).
- However, the burning velocity of coal is much slower than that of aluminum powder of the same diameter.
- The correlation equations for both aluminum and coal predict the experimental quenching distance quite well.
- The mathematical model of aluminum combustion predicts burning velocity values lower than the experimental ones, but the trends are same.
- The aluminum combustion model is a very efficient but nontrivial model, and it proved useful as a rough estimate for predicting the effect of various parameters on the combustion.
- The predicted quenching distance of an aluminum-air flame matches the experimental data quite well considering the simplified characteristics of the aluminum

combustion model.

- Mathematical model for coal combustion predicts burning velocity values close to the experimental values. Also the coal combustion model is useful for a detailed parametric study of various combustion characteristics.
- The predicted quenching distance of coal-air flame is little lower than the experimental quenching distance, but the effect of particle concentration is well predicted by this model.

Overall the present study shows that quenching distance and burning velocity of aluminum and coal powders are influenced by particle size, concentration, volatile content, moisture content, external voltage, particle size distribution, particle shape.

To further clarify the phenomena and to extend the investigation, the following recommendations are suggested:

- A refinement of the particle transport system on the particle burner is needed, so that a comparison of burning velocities measured with this method and the burner method can be made.
- A bigger test section, if possible, is more suitable for the burning velocity measurement of a dust flame.
- A new two or three dimensional model of flame quenching needs to be developed for a better prediction of the quenching distance and flame propagation behavior of particulate fuels.

- Other ignition method than spark ignition are needed to investigate the effect of spark ignition on the quenching and flame propagation behavior of powdered fuels.
- A test needs to be conducted at various pressures and at different oxygen-inert gas ratios to investigate the effects of pressure and oxygen contents on quenching distance.
- A coal-air mixture with a small percentage of methane needs to be tested for the investigation the effect of presence of a flammable gas from the practical point of view.

10 ACKNOWLEDGEMENT

The author first wishes to thank Professor Gerald M. Colver, his thesis advisor, for his considerate advice and guidance in the course of this study. Five years of graduate work with him was both challenging and very rewarding.

The author also wishes to thank each member of the author's committee. Professor George H. Junkhan contributed significantly to the author's understanding of heat transfer theory which is invaluable in this research and gave the author an opportunity to work on his heat exchanger project. Professor Thomas D. Weelock provided a large amount of Illinois No. 6 coal for this research and also permitted the author to use his laboratory for pulverizing and sieving the coals. Professor Thomas R. Rogge introduced a new numerical method to the author and gave a continuous encouragement to the author. Professor R. C. Brown taught the author a combustion theory and generously lent a YAG laser for this study.

The author wishes to thank Professor L. D. Smoot in Brigham Young University for providing the computer program for coal combustion modeling. Thanks are extended to Mr. Gaylord Scandrett for his continuous technical assistance and friendship. The author also thanks to Dr. Chetan Desai for his constant companionship in the course of the graduate program.

The author is thankful to the Power Affiliates group for their financial support

of this research.

The author want to give special thanks to his wife, Jae-Hee Kim, for her encouragement and friendship. She also typed a great deal of this dissertation.

11 BIBLIOGRAPHY

Abdel-Gayed, R. G., Bradley, D., and McMahon, M. "Turbulent Flame Propagation in Premixed Gases: Theory and Experiment." *Seventeenth Symposium (International) on Combustion* 17 (1978):245-254.

Adamczyk, A. A., and Lavoie, G. A. "Laminar Head-On Flame Quenching: A Theoretical Study." SAE paper 730969, *SAE Transactions* 87 (1978):1-48.

Adams, G. K., and Cook, G. B. "The Effect of Pressure on the Mechanism and Speed of the Hydrazine Decomposition Flame." *Combustion and Flame* 4 (1960):9-18.

Aggarwal, S. K., and Sirignano, W. A. "Numerical Modeling of One-Dimensional Enclosed Homogeneous and Heterogeneous Deflagrations." *Computers and Fluids* 12 (1984):145-158.

Aggarwal, S. K., and Sirignano, W. A. "Unsteady Spray Flame Propagation in a Closed Volume." *Combustion and Flame* 62 (1985):69-84.

Aly, S. L., and Hermance, C. E. "A Two-Dimensional Theory of Laminar Flame Quenching." *Combustion and Flame* 40 (1981):173-185.

Aly, S. L., Simpson, R. B., and Hermance, C. E. "Numerical Solution of the Two-Dimensional Premixed Laminar Flame Equations." *AIAA Journal* 17 (1979):56-63.

Andrews, G. E., and Bradley, D. "The Burning Velocity of Methane-Air Mixtures." *Combustion and Flame* 19 (1972):275-288.

Anthony, D. B., Howard, J. B., Hottel, H. C., and Messner, H. P. "Rapid Devolatilization of Pulverized Coal." *Fifteenth Symposium (International) on Combustion* 15 (1974):1303-1317.

Arpaci, V. S., and Tabaczynski, R. J. "Radiation-Affected Laminar Flame Propagation." *Combustion and Flame* 46 (1982):315-322.

- Arpaci, V. S., and Tabaczynski, R. J. "Radiation-Affected Laminar Flame Quenching." *Combustion and Flame* 57 (1984):169-178.
- Ballal, D. R. "Ignition and Flame Quenching of Quiescent Dust Clouds of Solid Fuels." *Proceedings of Royal Society of London A* 369 (1980):479-500.
- Ballal, D. R. "Further Studies on the Ignition and Flame Quenching of Quiescent Dust Clouds." *Proceedings of Royal Society of London A* 385 (1983a):1-19.
- Ballal, D. R. "Flame Propagation through Dust Clouds of Carbon, Coal, Aluminum and Magnesium in an Environment of Zero Gravity." *Proceedings of Royal Society of London A* 385 (1983b):21-51.
- Ballal, D. R., and Lefebvre, H. "Flame Quenching in Turbulent Flowing Gaseous Mixtures." *Sixteenth Symposium (International) on Combustion* 16 (1976):1689-1698.
- Ballal, D. R., and Lefebvre, A. H. "Ignition and Flame Quenching in Flowing Gaseous Mixtures." *Proceedings of Royal Society of London A* 357 (1977):163-181.
- Ballal, D. R., and Lefebvre, A. H. "Ignition of Liquid Fuel Spray at Subatmospheric Pressures." *Combustion and Flame* 31 (1978a):115-126.
- Ballal, D. R., and Lefebvre, A. H. "Ignition and Flame Quenching of Quiescent Fuel Mists." *Proceedings of Royal Society of London A* 364 (1978b):277-294.
- Ballal, D. R., and Lefebvre, A. H. "Ignition and Flame Quenching of Flowing Heterogeneous Fuel-Air Mixtures." *Combustion and Flame* 35 (1979):155-168.
- Ballal, D. R., and Lefebvre, A. H. "A General Model of Spark Ignition for Gaseous and Liquid Fuel-Air Mixtures." *Eighteenth Symposium (International) on Combustion* 18 (1980a):1737-1746.
- Ballal, D. R., and Lefebvre, A. H. "Flame Propagation in Heterogeneous Mixtures of Fuel Droplets, Fuel Vapor and Air." *Eighteenth Symposium (International) on Combustion* 18 (1980b):321-328.
- Bartknecht, W. *Explosions*. Berlin, West Germany: Springer-Verlag, 1981.
- Berlad, A. L., and Potter, A. E., Jr. "Prediction of the Quenching Effect of Various Surface Geometries." *Sixth Symposium (International) on Combustion* 6 (1956):728-735.
- Berlad, A. L., and Yang, C. H. "A Theory of Flame Extinction Limits." *Combustion*

and Flame 4 (1960):325-333.

Bhaduri, D., and Bandyopadhyay, S. "Combustion in Coal Dust Flames." *Combustion and Flame* 17 (1971):15-27.

Bird, R. B., Stewart, W. E., and Lightfoot, E. N. *Transport Phenomena*. New York: Wiley, 1960.

Blanc, M. V., Guest, P. G., von Elbe, G., and Lewis, B. "Ignition of Explosive Gas Mixtures by Electric Sparks I. Minimum Ignition Energies and Quenching Distances of Mixtures of Methane, Oxygen and Inert Gases." *J. of Chem. Phys.* 15 (1947):11-26.

Bledjian, L. "Computations of Time-Dependent Laminar Flame Structure." *Combustion and Flame* 20 (1973):5-17.

Bradley, D., and Mitcheson, A. "Mathematical Solutions for Explosions in Spherical Vessels." *Combustion and Flame* 26 (1976):201-217.

Bregeon, B., Gordon, A. S., and Williams, F. H. "Near-Limit Downward Propagation of Hydrogen and Methane Flames in Oxygen-Nitrogen Mixtures." *Combustion and Flame* 33 (1978a):33-42.

Bregeon, B., Gordon, A. S., and Williams, F. H. "Raman Scattering Measurements of Nitric Oxide in Ammonia/Oxygen Flames." *Combustion and Flame* 33 (1978b):23-32.

Brewer, L., and Searcy, A. W. "The Gaseous Species of the $Al - Al_2O_3$ System." *J. Am. Chem. Soc.* 73 (1951):5308-5314.

Brown, W. G., Porter, R. P., Verlin, J. D., and Clark, A. H. "A Study of Acetylene-Oxygen Flames." *Twelfth Symposium (International) on Combustion* 12 (1968):1035-1047.

Buckmaster, J. "The Quenching of Deflagration Waves." *Combustion and Flame* 26 (1976):151-162.

Buckmaster, J. "The Quenching of Two-Dimensional Premixed Flames." University of Wisconsin - Madison, Mathematics Research Center, *Technical Summary Report* No. 1814, 1977.

Burgoyne, J. H., and Long, V. D. "Some Measurements of the Burning Velocity of Coal-in-Air Suspensions." *Conference on Science in the Use of Coal* Paper No. 28,

Institute of Fuel, London, (1958):D16-D20.

Carrier, G. F., Fendell, F. E., Bush, W. B., and Feldman, P. S. "Nonisenthalpic Interaction of a Planar Premixed Laminar Flame with a Parallel End Wall." SAE Paper 790245, *SAE Transactions* 89 (1979):135-151.

Carrier, G. F., Fendell, F. E., and Feldman, P. S. "Laminar Flame Propagation/Quench for a Parallel-Wall Duct." *Twentieth Symposium (International) on Combustion* 20 (1984):67-74.

Cassel, H. M. "Some Fundamental Aspects of Dust Flames." Report of Investigations No. 6551, USDI-Bureau of Mines, 1964.

Cassel, H. M., das Gupta, A. K., and Guruswamy, S. "Factors Affecting Flame Propagation Through Dust Clouds." *Third Symposium on Combustion, Flames, and Explosions* 3 (1949):185-190.

Cassel, H. M., Liebman, I. "The Cooperative Mechanism in the Ignition of Dust Dispersions." *Combustion and Flame* 3 (1959):467-475.

Coffee, T. P., and Heimerl, J. M. "Transport Algorithms for Premixed, Laminar Steady-State Flames." *Combustion and Flame* 43 (1981):273-289.

Colver, G. M. "Dynamics and Stationary Charging of Heavy Metallic and Dielectric Particles against a Conducting Wall in the Presence of a DC Applied Electric Field." *Journal of Applied Physics* 47 (1976):4839-4849.

Colver, G. M., and Howell, D. L. "Particle Diffusion in an Electric Suspension." *IEEE Conference Record - IAS Annual Meeting*, New York, 1980.

Cotroneo, J. A., and Colver, G. M. "Electrically Augmented Pneumatic Transport of Copper Spheres at Low Particle and Duct Reynolds Numbers." *J. of Electrostatics* 5 (1978):205-223.

Daniel, W. A. "Flame Quenching at the Walls of an Internal Combustion Engine." *Sixth Symposium (International) on Combustion* 6 (1956):275-293.

Dixon-Lewis, G. "Flame Structure and Flame Reaction Kinetics: I. Solution of Conservation Equations and Applications to Rich Hydrogen-Oxygen Flames." *Proc. Royal Society of London* A298 (1967):495-513.

Dixon-Lewis, G. "Flame Structure and Flame Reaction Kinetics: II. Transport Phe-

nomena in Multicomponent Systems." *Proc. Royal Society of London A*307 (1968):111-135.

Dixon-Lewis, G. "Flame Structure and Flame Reaction Kinetics: V. Investigation of Reaction Mechanism in a Rich Hydrogen-Nitrogen-Oxygen Flame by a Solution of Conservation Equations." *Proc. Royal Society of London A*317 (1970):235-247.

Dixon-Lewis, G. "Kinetic Mechanism, Structure and Properties of Premixed Flames in Hydrogen-Oxygen-Nitrogen Mixtures." *Phil. Trans. Royal Society of London A*292 (1979):45-99.

Dixon-Lewis, G. "Computer Modeling of Combustion Reactions in Flowing Systems with Transport." Pp. 21-125 in W. C. Gardiner, ed. *Combustion Chemistry* New York: Springer-Verlag, 1984.

Dixon-Lewis, G., and Shepherd, I. G. "Some Aspects of Ignition by Localized Sources, and of Cylindrical and Spherical Flames." *Fifteenth Symposium (International) on Combustion* 15 (1974):1483-1491.

Drowart, J., Demaria, G., Burns, R. P., and Ingham, M. G. "Thermodynamic Study of Al_2O_3 Using a Mass Spectrometer." *J. of Chem. Phys.* 32 (1960):1366-1372.

Eraslan, A. N., and Brown, R. C. "Chemiiionization and Ion-Molecule Reactions in Fuel-Rich Acetylene Flames." *Combustion and Flame* 74 (1988):19-37.

Essenhigh, R. H. "Combustion and Flame Propagation in Coal Systems: A Review." *Sixteenth Symposium (International) on Combustion* 16 (1976):127-153.

Essenhigh, R. H., and Csaba, J. "The Thermal Radiation Theory for Plane Flame Propagation in Coal Dust Clouds." *Ninth Symposium (International) on Combustion* 9 (1962):11-125.

Essenhigh, R. H., and Csaba, J. "The Thermal Radiation Theory for Plane Flame Propagation in Coal Dust Clouds." *Eleventh Symposium (International) on Combustion* 11 (1966):111-125.

Fendell, F. E. "Wall Quench and Flammability Limit Effects on Exhaust Hydrocarbon Emissions." *Final Report*, Phase 2, ERDA Contract E(04-3)-1261, 1977.

Ferguson, C. R., and Keck, J. C. "On Laminar Flame Quenching and its Application to Spark Ignition Engines." *Combustion and Flame* 28 (1977):197-211.

- Field, M. A. "Measurements of the Effects of Rank on Combustion Rates of Pulverized Coal." *Combustion and Flame* 14 (1970):237-248.
- Field, P. *Dust Explosions. Handbook of Powder Technology*. Vol. 4. Amsterdam, Netherlands: Elsevier, 1982.
- Friedman, R. "The Quenching of Laminar Oxyhydrogen Flames by Solid Surfaces." *Third Symposium (International) on Combustion* 3 (1949):110-120.
- Friedman, R., and Johnston, W. C. "The Wall-Quenching of Laminar Propane Flames as a Function of Pressure, Temperature, and Air-Fuel Ratio." *Journal of Applied Physics* 21 (1950):791-795.
- Gerstein, M., and Stine, W. "Analytical Criteria for Flammability Limits." *Fourteenth Symposium (International) on Combustion* 14 (1973):1109-1118.
- Ghosh, B., Basu, D., and Roy, N. K. "Studies of Pulverized Coal Flames." *Sixth Symposium (International) on Combustion* 6 (1956):595-602.
- Gray, D., Cogoli, J. C., and Essenhigh, R.H. "Problems in Pulverized Coal and Char Combustion." *Advances in Chemistry Series of American Chemical Society Coal Gasification* 131 (1974):72-91.
- Grosse, A V., and Conway, J. B. "Combustion of Metals in Oxygen." *Industry and Engineering Chemistry* 50 (1958):663-672.
- Grumer, J. "Recent Research Concerning Extinguishment of Coal Dust Explosions." *Fifteenth Symposium (International) on Combustion* 15 (1974):103-114.
- Harris, M. E., Grumer, J., von Elbe, G., and Lewis, B. "Combustion and Flame and Explosion Phenomena." *Third Symposium (International) on Combustion* 3 (1949):80-89.
- Hartman, I., Jacobson, M., and Williams, R. P. "Laboratory Explosibility Study of American Coals." Report of Investigations No. 5052. USDI-Bureau of Mines, 1954.
- Hattori, H. "Flame Propagation in Pulverized Coal-Air Mixtures." *Sixth Symposium (International) on Combustion* 6 (1956):590-595.
- Hertzberg, M. "The Theory of Flammability Limits Natural Convection." Report of Investigations No. 8127, USDI-Bureau of Mines, 1980a.
- Hertzberg, M. "The Theory of Flammability Limits Conductive and Convective Wall

Losses and Thermal Quenching." Report of Investigations No. 8469. USDI-Bureau of Mines, 1980b.

Hirschfelder, J. O., Curtiss, C. F., and Campbell, D. E. "The Theory of Flames and Detonations." *Fourth Symposium (International) on Combustion* 4 (1952):190-210.

Hirschfelder, J. O., Curtiss, C. F., Henkel, M. J., Spaulding, W. P., and Hummel, H. "Theory of Propagation of Flames." *Third Symposium (International) on Combustion and Flame and Explosion Phenomena* 3 (1949):121-139.

Holm, J. M. "On the Initiation of Gaseous Explosions by Small Flames." *Phil. Mag.* 14 (1932):18-56.

Horton, M. D., Goodson, F. P., and Smoot, L. D. "Characteristics of Flat, Laminar Coal-Dust Flames." *Combustion and Flame* 23 (1977):175-183.

Howard, J. B., and Essenhigh, R. H. "Mechanism of Solid Particle Combustion with Simultaneous Gas Phase Volatiles Combustion." *Eleventh Symposium (International) on Combustion* 11 (1966):399-408.

Ishikawa, N. "Studies of Wall Flame Quenching and Hydrocarbon Emissions in a Model Spark Ignition Engine." University of California - Lawrence Berkeley Laboratory Report No. LBL-8819, 1978.

Ishikawa, N., Branch, M. C., "A Simple Model of Transient Thermal Flame Quenching." *SAE Transactions* 8 Paper No. 770648, 1978.

Jacobson, M., Cooper, A. R., and Nagy, J. "Explosibility of Metal Powders." Report of Investigations No. 6516. USDI- Bureau of Mines, 1964.

Jarosinski, J. "Flame Quenching by a Cold Wall." *Combustion and Flame* 50 (1983):167-175.

Jarosinski, J. "The Thickness of Laminar Flames." *Combustion and Flame* 56 (1984):337-342.

Jarosinski, J. "A survey of Recent Studies on Flame Extinction." *Progress in Energy and Combustion Science* 12 (1986):81-116.

Jarosinski, J., Lee, J. H., Knystautas, R., and Crowley, J. D. "Quenching of Dust-Air Flames." *Twenty-first Symposium (International) on Combustion* 21 (1986):1917-1924.

- Kanury, A. M. *Introduction to Combustion Phenomena*. New York: Gordon and Breach, 1975.
- Kennedy, J. B., and Neville, A. M. *Basic Statistical Methods for Engineers and Scientists*. New York: Harper and Row Publishers, 1976.
- Kim, S. "Spark Ignition of Aluminum Powder." *Master of Science Thesis*. Iowa State University, Ames, Iowa, 1986.
- King, M. K. "Modeling of Single Particle Aluminum Combustion in $CO_2 - N_2$ Atmospheres." *Seventeenth Symposium (International) on Combustion* 17 (1978):1317-1328.
- Klein, G. "A Contribution to Flame Theory." *Phil. Trans. Royal Society of London* A249 (1957):389-415.
- Kobayashi, H., Howard, J. B., and Sarofim, A. F. "Coal Devolatilization at High Temperatures." *Sixteenth Symposium (International) on Combustion* 16 (1976):411-425.
- Kooker, D. E. "Numerical Study of a Confined Premixed Laminar Flame: Oscillatory Propagation and Wall Quenching." *Combustion and Flame* 49 (1983):141-149.
- Krazinski, J. L., Buckius, R. O., and Krier, H. "Coal Dust Flames: A Review and Development of a Model for Flame Propagation." *Progress on Energy Combustion and Science* 5 (1979):31-71.
- Krier, H., and Krazinski, J. L. "Theory of Coal Dust-Air Flame Propagation." *AIAA/SAE Tenth Propulsion Conference* 10 (1974):74-92.
- Kuo, K. K. *Principles of Combustion*. New York: John Wiley & Sons, 1983.
- Kurkov, A P., and Mirsky, W. "An Analysis of the Mechanism of Flame Extinction by a Cold Wall." *Twelfth Symposium (International) on Combustion* 12 (1968):615-624.
- Kydd, P. h., and Foss, W. I. "A Comparison of the Influence of Heat Losses and Three-dimensional Effects on Flammability Limits." *Combustion and Flame* 8 (1964):267-273.
- Lavoie, G A. "Correlations of Combustion Data for S. I. Engine Calculations: Laminar Flame Speed, Quench Distance and Global Reaction Rates." *SAE Transactions* 87 paper 780229, 1978.

Law, C. K. "A Simplified Theoretical Model for the Vapor-Phase Combustion of Metal Particles." *Combustion Science and Technology* 7 (1973):197-212.

Lewis, B., and von Elbe, G. *Combustion, Flames and Explosions of Gases*. Second Edition, New York: Academic Press, 1961.

Litchfield, E. L. Private Communication, In Green, F. T., and J. E. O'Donnell. "The Quenching Behavior of Coal Dust-Air Mixtures." *Final Technical Report* 9. U. S. Bureau of Mines Contract No. J0166076. Kansas City, Mo.: Midwest Research Institute, 1981.

Lund, C. M. "A General Computer Program for Calculating Time-Dependent Phenomena Involving One-Dimensional Hydrodynamics, Transport and Detailed Chemical Kinetics." *University of California Lawrence Livermore Laboratory Report UCRL-52504*, 1978.

Macek, A. "Fundamentals of Combustion of Single Aluminum and Beryllium Particles." *Eleventh Symposium (International) on Combustion* 11 (1966):203-214.

Markstein, G. H. "Heterogeneous Reaction Processes in Metal Combustion." *Eleventh Symposium (International) on Combustion* 11 (1966):219-234.

Marshall, W. F., Palmer, H. B., and Seery, D. H. "Particle Size Effects and Flame Propagation Rate Control in Laminar Dust Flames." *J. Inst. Fuel* 37 (1964):342-349.

Massey, B. S., and Lindley, B. C. "Flame Quenching." *J. of the Royal Aeronautical Society* 62 (1958):32-42.

Mayer, E. "A Theory of Flame Propagation Limits Due to Heat Loss." *Combustion and Flame* 1 (1957):438-452.

Mitani, T. "A Flame Inhibition Theory by Inert Dust and Spray." *Combustion and Flame* 43 (1981):243-253.

Nagy, A. R., and Lenoir, J. M. "Absorption and Scattering of Thermal Radiation by a Cloud of Small Particles." *AIChE J.* 16 (1970):286-292.

Nagy, J., and Verakis, H. C. *Development and Control of Dust Explosions*. New York: Marcel Dekker Inc., 1983.

Ogle, R. A. "A New Strategy for Dust Explosion Research: A Synthesis of Combustion Theory, Experimental Design and Particle Characterization." *Ph.D. Dissertation*.

University of Iowa, Iowa City, Iowa, 1986.

Palmer, K. N. *Dust Explosions and Fires*. London, England: Chapman and Hall, 1973.

Patankar, S. V., and Spalding, D. B. *Heat and Mass Transfer in Boundary Layers*. Second Edition. London, U. K.:Intertext Books, 1970.

Payman, W., and Wheeler, R. V. "The Combustion of Complex Gaseous Mixtures. Part II. Mixtures of Carbon Monoxide and Hydrogen with Air." *J. of Chem. Society of London* 123 (1923):1251-1259.

Porter, R. F., Schissel, P., and Inghram, M. G. "A Mass Spectrometric Study of Gaseous Species in the Al- Al_2O_3 System." *J. of Chem. Phys.* 23 (1955):339-342.

Potter, A. E., and Berlad, A. L. "The Effect of Fuel Type and Pressure on Flame Quenching." *Sixth Symposium (International) on Combustion* 6 (1951):27-34.

Potter, A. E., and Berlad, A. L. "A Thermal Equation for Flame Quenching." NACA TN 3398, 1955.

Potter, A. E., and Berlad, A. L. "The Effect of Fuel Type and Pressure on Flame Quenching." *Sixth Symposium (International) on Combustion* 6 (1956):27-36.

Powell, F. "The Effect of Inert Dust on the Combustion Limits of Lycopodium Stones Dispersed in Air." *Combustion and Flame* 6 (1962):75-87.

Price, E. W. "Combustion of Metalized Propellants." Pp. 479-513 in K. K. Kuo, and M. Summerfeld, eds. *Fundamentals of Solid-Propellant Combustion* New York: Academic Press, 1983.

Ramos, J. I. "Numerical Studies of Laminar Flame Propagation in Spherical Bombs." *AIAA J.* 21 (1983a):415-422.

Ramos, J. I. "A Numerical Study of One-Dimensional Enclosed Flames." Pp. 529-546 in *Numerical Properties and Methodologies in Heat Transfer*. Washington, D.C.: Hemisphere, 1983b.

Rosner, D. E. "Convective Diffusion Limitations on the Rates of Chemical Reactions at Solid Surfaces-Kinetic Implications." *Eleventh Symposium (International) on Combustion* 11 (1966):181-196.

Rosner, D. E. "High-Temperature Gas-Solid Reactions." *Annual Review of Materials*

Science 12 (1972):573-606.

Simon, D. M., Belles, F. E., and Spakowski, A. E. "Investigation and Interpretation of the Flammability Region for Some Lean Hydrocarbon-Air Mixtures." *Fifth Symposium (International) on Combustion* 5 (1954):927-938.

Singer, J. M., Bruszak, A. E., and Grumer, J. "Equivalence of Coal Dust and Methane at Lower Quenching Limits of Flames of Their Mixtures." Report of Investigation No. 6761. USDI-Bureau of Mines, 1966.

Slattery, J. C. *Momentum, Energy and Mass Transfer in Continua*. 2nd. Ed. Huntington, New York: Rober E. Krieger Publ. Co., 1981.

Slezak, S. E., Buckius, R. O., and Krier, H. "A Model of Flame Propagation in Rich Mixtures of Coal Dust in Air." *Combustion and Flame* 59 (1985):251-265.

Sloan, D. G., Smith, P. J., and Smoot, L. D. "Modeling of Swirl in Turbulent Flow Systems." *Progress on Energy Combustion and Science* 10 (1984):359-441.

Smith, P. J., Smoot, L. D., and Brewster, B. S. "Revised User's Manual Pulverized Coal Gasification or Combustion." *Final Report Vol. 2*. Brigham Young University, Provo, Utah, 1987.

Smooke, M. D. , "Solution of Burner-Stabilized Pre-mixed Laminar Flames by Boundary Value Methods." Sandia National Laboratories, Livermore, SAND 81-8040, 1982.

Smoot, L. D., Hecker, W. C., and Williams, G. A. "Prediction of Propagating Methane-Air Flames." *Combustion and Flame* 26 (1976):323-342.

Smoot, L. D., and Horton, M. D. "Propagation of Laminar Pulverized Coal-Air Flames." *Progress on Energy Combustion and Science* 3 (1977):235-258.

Smoot, L. D., and Smith, P. J. *Coal Combustion and Gasification*. New York, New York: Plenum Press, 1985.

Spalding, D. B. "The Theory of Flame Phenomena with a Chain Reaction." *Phil. Trans. Roy. Soc. Lond.* A249 (1956):1-25.

Spalding, D. B. "A Theory of Inflammability Limits and Flame-Quenching." *Proceedings of Royal Society of London* A240 (1957):83-100.

Spalding, D. B., Stephenson, P. L., and Taylor, R. G. "A Calculation Procedure for the Prediction of Laminar Flame Speeds." *Combustion and Flame* 17 (1971):55-64.

- Takeno, T., and Iijima, T. "Theoretical Study of Nonsteady Flame Propagation in Closed Vessels." *Progress Astro. Aero.* Vol. 76. New York, New York: Academic Press, 1981:578-595.
- Tsatsaronis, G. "Prediction of Propagating Laminar Flames in Methane, Oxygen, Nitrogen Mixtures." *Combustion and Flame* 33 (1978):217-239.
- Ubhayakar, S. K., Stickler, D. B., von Rosenberg, C. W., Jr., and Gannom, R. E. "Rapid Devolatilization of Pulverized Coal in Hot Combustion Gases." *Sixteenth Symposium (International) on Combustion* 16 (1976):427-436.
- von Karman, T., and Millan, G. "Thermal Theory of a Laminar Flame Front near a Cold Wall." *Fourth Symposium (International) on Combustion* 4 (1952):173-177.
- Wallis, G. B. *One-Dimensional Two-Phase Flow* New York: McGraw-Hill, 1969.
- Warnatz, J. "Concentration-, Pressure-, and Temperature-Dependence of the Flame Velocity in Hydrogen-Oxygen-Nitrogen Mixtures." *Combustion Science and Technology* 26 (1981):203-213.
- Westbrook, C. K., and Dryer, F. L. "A Comprehensive Mechanism for Methanol Oxidation." *Combustion Science and Technology* 20 (1979):125-140.
- Westbrook, C. K., and Dryer, F. L. "Chemical Kinetics and Modeling of Combustion Processes." *Eighteenth Symposium (International) on Combustion* 18 (1980):749-761.
- Westbrook, C. K., Adamczyk, A. A., and Lavoie, G. A. "A Numerical Study of Laminar Flame Wall Quenching." *Combustion and Flame* 40 (1981):81-99.
- Wilde, K. A. "Boundary-Value Solutions of the One-Dimensional Laminar Flame Propagation Equations." *Combustion and Flame* 18 (1972):43-52.
- Williams, F. A. *Combustion Theory*. London, U. K.: Addison-Wesley Publishing Company, 1964.
- Williams, F. A. *Combustion Theory*. Second Edition. Menlo Park, CA: Benjamin Cummings, 1985.
- Zeldovich, Y. B. *The Theory of Combustion and Detonation*. USSR: Publication of Academy of Sciences, 1944. (Russian).
- Zeldovich, Y. B., and Barenblatt, G. I. "Theory of Flame Propagation." *Combustion and Flame* 3 (1959):61-73.

12 APPENDIX A: ERROR ANALYSIS

Whenever measurements are made, uncertainties in the raw data occur usually because of three types of errors, illegitimate, systematic, and random errors. Illegitimate errors are caused by mistakes in reading instruments and performing calculations or variations in experimental conditions. Such errors can be reduced by using care and repetition of the experiments and calculations. Systematic errors are of a consistent form and result from inaccurate calibration of the instruments, improper condition or incorrect procedures. These errors can be reduced through calibration. However, the third type of error, random error, deals with irregularity and originate from a variety of causes such as fluctuating experimental conditions or disturbances. Random error cannot usually be avoided since these errors are inherently present in any measuring system. However, the random uncertainties can be minimized through experimental design. Hence, to estimate the accuracy of the experimental data, it is necessary to determine the total uncertainty through the use of statistics in a propagation of error analysis. The uncertainty of a calculated quantity depends on the uncertainty of the measured quantities required for the calculation. If the measured quantities are determined independently, and if their distribution about a measure of central tendency is approximately symmetrical, the following expression can be used to calculate the uncertainty, U , in any calculated quantity, Z (Kennedy and Neville

[1976]).

$$U_z^2 = \frac{\partial Z}{\partial Y_1}^2 U_{Y_1}^2 + \frac{\partial Z}{\partial Y_2}^2 U_{Y_2}^2 + \dots + \frac{\partial Z}{\partial Y_n}^2 U_{Y_n}^2 \quad (12.1)$$

In this equation, Y_1, Y_2, \dots, Y_n represent a measured independent variables so that mathematically we have the following relation;

$$Z = f(Y_1, Y_2, \dots, Y_n) \quad (12.2)$$

When the uncertainty of a measured quantity, U_{Y_i} , is chosen to be the absolute value of the maximum expected deviation from a measured result Y_i , the uncertainty of calculated quantity U_z indicates the maximum expected deviation from the reported experimental results. A simplified form of the above propagation of error equation results if the function Z is of the form,

$$Z = Y_1^a Y_2^b \dots Y_n^m \quad (12.3)$$

where, the exponents a, b, \dots, m may be positive or negative, integer or real. The simplified result is

$$\left(\frac{U_z}{Z}\right)^2 = a^2 \left(\frac{\partial Y_1}{Y_1}\right)^2 + b^2 \left(\frac{\partial Y_2}{Y_2}\right)^2 + \dots + m^2 \left(\frac{\partial Y_n}{Y_n}\right)^2 \quad (12.4)$$

The uncertainties of the each variables will be evaluated and finally the total uncertainty of this experiment will be calculated.

12.1 Particle Diameter

12.1.1 Particle diameter of aluminum particle

In estimating the uncertainty of the particle diameter U_d , difficulties arise to find the representative particle diameter of sieved particles, since they are not of the same

size and shape. By assuming spherical particles, an arithmetic average of the particle diameter is,

$$d_p = \sum d_{pi}/n \quad (12.5)$$

In case of aluminum particles, the average sieve size was used as the particle diameter. For example, for the particles sieved between 20 - 25 μm range, 22.5 μm is used as the particle diameter. Since an actual distribution has somewhat wider range than the sieved range, the uncertainty in particle diameter $U_{d,a}$ is chosen to be $\pm 2 \mu m$. Thus,

$$\frac{U_{d,a}}{d_p} = 0.089 \quad (12.6)$$

12.1.2 Particle diameter of coal particle

In case of coal particles, the particle size distribution and average particle diameter is measured by using the scanning electron microscope and the uncertainty in the particle diameter is smaller than that of the aluminum particle. Thus, it can be reasonably assumed that the uncertainty of particle diameter of coal particles, $U_{d,c}$ is $\pm 1 \mu m$.

$$\frac{U_{d,c}}{d_p} = 0.044 \quad (12.7)$$

In average, the uncertainty in particle diameter is,

$$\frac{U_d}{d_p} = 0.067 \quad (12.8)$$

12.2 Breakdown Voltage

The breakdown voltage is a strong function of environmental pressure. It was observed during the course of experiments that pressure, P, is 760 ± 40 mm Hg.

There is at present no clear way to estimate how much the pressure change affects the breakdown voltage of the needle-to-plane particulate cloud system as used in this study. So, it is assumed that a ± 40 mm Hg pressure deviation causes $\pm 5\%$ difference in the breakdown voltage of a uniform field system.

$$\frac{U_{v1}}{V_1} = 0.050 \quad (12.9)$$

12.3 Capacitance

The uncertainty in the capacitance of this experimental system U_c is caused by the uncertainty in the capacitance of the external capacitor. The uncertainty of the capacitance is assumed to be 500 pF. The total capacitance is $0.055 \mu F$. Thus the uncertainty in the capacitance is,

$$\frac{U_c}{C} = 0.009 \quad (12.10)$$

12.4 External Voltage

The uncertainty of the external voltage U_{v2} is the average of the uncertainty of the electrostatic voltmeter reading and the uncertainty of the calibration. The uncertainty of the voltmeter reading is the resolution of the reading, which is 0.1 kV. The uncertainty of the calibration is assumed to be 0.5 % of the reading. Thus, when the external voltage of 20 kV is chosen, the uncertainty of the voltage U_{v2} is 0.1 kV. Thus,

$$\frac{U_{v2}}{V_2} = 0.0050 \quad (12.11)$$

12.5 Particle Concentration

12.5.1 Particle concentration of aluminum particle

The aluminum concentration $C_{m,al}$ is calculated by dividing the mass of the aluminum by the volume of the test section. That is,

$$C_{m,al} = \frac{m_{al}}{V_{cyl}} \quad (12.12)$$

where, V_{cyl} is the volume of the cylinder. Thus,

$$C_{m,al} = \frac{4m_{al}}{\pi D^2 H} \quad (12.13)$$

where, D is the diameter of the test section and H is the plate separation distance of the test section.

The propagation of error equation for coal is

$$\frac{U_{c,al}}{C_{m,al}}^2 = \frac{U_{m,al}}{m_{al}}^2 + 4\frac{U_D}{D}^2 + \frac{U_H}{H}^2 \quad (12.14)$$

The uncertainty of the weight of aluminum powder $U_{m,al}$ is the sum of the uncertainties of the measuring the mass of aluminum powder U_{m1} , and due to the error of the particles sticking to the walls of the test section U_{m2} . U_{m1} is the resolution of the scale (Torsion balance Model EA-1AP), which is equal to 0.0001 gram, and U_{m2} can be obtained from the error analysis of the powders sticking to the walls. The amount of aluminum powers sticking to the walls at the time of suspension is measured experimentally for various particle sizes and concentrations, and found out to be about $\pm 4\%$ of the total amount of the aluminum particles are sticking to the walls. For the case that aluminum particle of 0.005 grams are tested for the experiment,

$$U_{m,al} = 0.0001 + (0.04)(0.005) = 0.0003 \quad (12.15)$$

Thus, the uncertainty of the particle mass is,

$$\frac{U_{m,al}}{m_{al}} = 0.06 \quad (12.16)$$

The uncertainties of the test section diameter and plate separation distance are the resolution of the measure which is a caliper in this case.

$$U_D = 0.01\text{cm} \quad (12.17)$$

$$U_H = 0.01\text{cm} \quad (12.18)$$

Thus,

$$\frac{U_D}{D} = 0.0007 \quad (12.19)$$

The plate separation distance of 2.0 cm is chosen;

$$\frac{U_H}{H} = 0.005 \quad (12.20)$$

Thus,

$$\frac{U_{c,al}}{C_{m,al}}^2 = 0.06^2 + 4 \times 0.0007^2 + 0.005^2 \quad (12.21)$$

Thus,

$$\frac{U_{c,al}}{C_{m,al}} = 0.060 \quad (12.22)$$

12.5.2 Particle concentration of coal particles

In case of coal particles, the particle concentration is measured by the ration of the intensity of the laser scattering light using the Beer-Lambert's law.

$$\frac{I_o}{I} = \exp(-\epsilon A n l) \quad (12.23)$$

The expression for the particle concentration can be calculated from the above equation as follows.

$$C_{m,coal} = \frac{2\rho_p d_p}{3el} \ln\left(\frac{I_0}{I}\right) \quad (12.24)$$

The equation of propagation of error is,

$$\left(\frac{U_{C,coal}}{C_{m,coal}}\right)^2 \simeq \frac{U_d^2}{d_p} + \frac{U_I^2}{I} \quad (12.25)$$

The uncertainty of the particle size is obtained in previous section.

$$\frac{U_d}{d_p} = 0.044 \quad (12.26)$$

The uncertainty of the intensity of the light is the resolution of the laser power meter or a oscilloscope scale. Thus, the uncertainty of the intensity of the light is chosen to be 0.005. For $I = 0.1$ mW,

$$\frac{U_I}{I} = 0.05 \quad (12.27)$$

Finally the uncertainty of the particle concentration is,

$$\frac{U_{m,coal}}{C_{m,coal}} = 0.067 \quad (12.28)$$

In the average of aluminum and coal particles,

$$\frac{UC'_m}{C'_m} = 0.063 \quad (12.29)$$

12.6 Quenching Distance

Finally, the quenching distance d_q , which is a dependent variable in this research is a function of the previous independent variables.

$$d_q = f(d_p, V, C'_m, C') \quad (12.30)$$

Thus, the uncertainty is,

$$\left(\frac{U_{dq}}{dq}\right)^2 \simeq \left(\frac{U_d}{dp}\right)^2 + \left(\frac{U_v}{V}\right)^2 + \left(\frac{U_c}{C}\right)^2 + \left(\frac{U_{cm}}{C_m}\right)^2 \quad (12.31)$$

$$\left(\frac{U_{dq}}{dq}\right)^2 \simeq 0.0667^2 + 0.005^2 + 0.009^2 + 0.063^2 \quad (12.32)$$

$$\left(\frac{U_{dq}}{dq}\right)^2 \simeq 0.008524 \quad (12.33)$$

Thus, the uncertainty of the quenching distance is,

$$\frac{U_{dq}}{dq} = 0.0923 \quad (12.34)$$

13 APPENDIX B: THEORETICAL ANALYSIS OF QUENCHING

To date, many theories of flame quenching have been proposed. They all fall into one of two classes; either they begin with an arbitrary assumption concerning the conditions required for flame propagation, or they begin by solving the conservation of energy equation including heat losses. The two types of theories are discussed in this chapter.

13.1 Energy Conservation Method

A differential equation for energy conservation in flames with the effect of heat loss is solved. A radiation heat loss in addition to conduction heat loss is included in this model (Arpaci and Tabaczynski [1982, 1984]). The analysis is made on the flame quenching of powdered fuels in parallel plates.

13.1.1 Radiative heat flux

The thin gas and thick gas limits of the one-dimensional radiation flux near a wall are, respectively,

$$\frac{dq^r}{dx} = 2\kappa_p[2(E_b - E_{b\infty}) - \epsilon_w(E_{bw} - E_{b\infty})e^{-x\sqrt{3\kappa_p/\beta_r}}] \quad (13.1)$$

and,

$$q^r = -\frac{4}{3\beta_r} \left[1 - \left(1 - \frac{\epsilon_w}{2} e^{-x\sqrt{3\kappa_p\beta_r}} \right) \right] \frac{dE_b}{dx} \quad (13.2)$$

where, x is a distance normal to the wall, E_b is the blackbody emissive power, subscripts w and ∞ denotes the wall and far from wall, κ_p is the Plank mean of the absorption coefficient, and ϵ_w is the emissivity of the wall.

In the limit, the exponential term goes to 1. Thus, on the wall the foregoing radiation fluxes reduce to,

$$\frac{dq^r}{dx} = 4\kappa_p \left(1 - \frac{\epsilon_w}{2} (E_b - E_{b\infty}) \right) \quad (13.3)$$

for thin gas, and

$$q^r = \frac{\epsilon_w}{2} \left(-\frac{4}{3\beta_r} \frac{dE_b}{dx} \right) \quad (13.4)$$

for thick gas. On dimensional groups, the above equations take the following form;

$$q^r \sim \eta\tau \left(1 - \frac{\epsilon_w}{2} \right) 4\Delta E_b, \tau \rightarrow 0 \quad (13.5)$$

$$q^r \sim \eta(1 - \omega) \frac{\epsilon_w}{2} \frac{4\Delta E_b}{3\tau}, \tau \rightarrow \infty \quad (13.6)$$

where, ω is the Rosseland albedo of single scattering, η is the weighted non-grayness, and τ is the optical thickness. The above two equations show the radiative fluxes for thin gas and thick gas as τ goes to zero and infinity, respectively.

Thus, the radiative heat flux for an arbitrary optical thickness is,

$$q^r \sim \frac{4\eta\tau(1 - \epsilon_w/2)}{2} \Delta E_b (1 + 3\tau^2) (2/\epsilon_w - 1) / (1 - \omega) \quad (13.7)$$

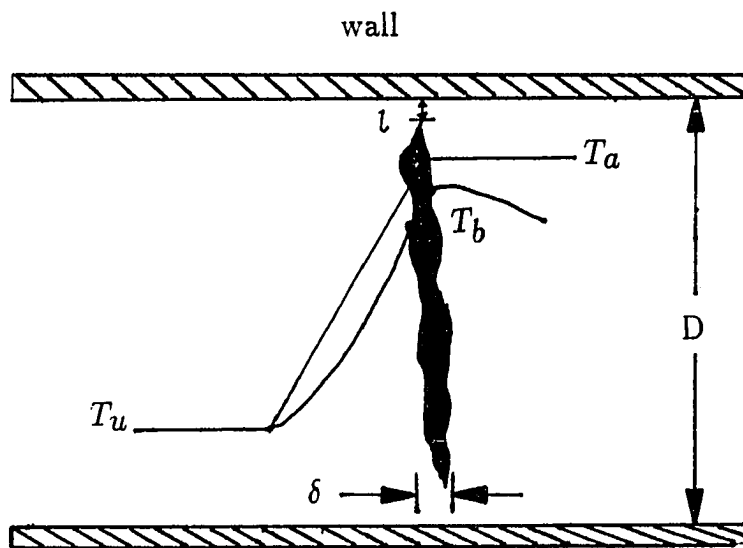


Figure 13.1: Schematics of flame quenching in parallel plates

13.1.2 Flame quenching

Figure 13.1 shows the schematics of the system for a flame that propagates between the parallel plates. A coordinate system is selected so that a flame is stationary, that is, the walls are moving with a flame. Downstream of the flame, in the burned zone, the mixtures are moving at a speed different than the wall so that somewhere in the flame a boundary layer begins to grow. Also, the walls are assumed to be at the same temperature as the unburned mixture temperature, T_u , so that a thermal boundary layer grows.

The characteristic length over which the flame loses heat is assumed to be the dead space of thickness l . The dead space thickness is assumed to be quite small compared to the quenching distance.

In the ideal case of an adiabatic flame propagation,

$$\rho S_u^0 (C_p T_u + Q) - \rho S_u^0 C_p T_a = 0 \quad (13.8)$$

where, S_u^0 is a adiabatic burning velocity, Q is a heat of reaction, and T_a is a adiabatic flame temperature. The adiabatic temperature is calculated readily from the above equation.

$$T_a = T_u + Q/C_p \quad (13.9)$$

In the actual case involving heat losses by conduction and radiation, the flame temperature falls below the adiabatic flame temperature. In this case the energy equation is,

$$(\rho S_u (C_p T_u + Q) - \rho S_u C_p T_b)(D - 2l)W - (q^c + q^r)2W\delta = 0 \quad (13.10)$$

where, D is the plate separation distance, and W is the width of the plate. Using the assumption that the dead space thickness l is much smaller than the plate separation distance D , the above equation reduces to;

$$(\rho S_u (C_p T_u + Q) - \rho S_u C_p T_b) D - 2\delta(q^c + q^r) = 0 \quad (13.11)$$

The above equation can be expressed in terms of adiabatic flame temperature using the relationship obtained in the previous equation.

$$\rho S_u C_p (T_a - T_b) D - 2\delta(q^c + q^r) = 0 \quad (13.12)$$

The Arrhenius relation between the burning velocity and temperature is used.

$$\frac{S_u}{S_u^0} = \exp\left[-\frac{E}{2R}\left(\frac{1}{T_b} - \frac{1}{T_a}\right)\right] \quad (13.13)$$

Substituting the above Arrhenius relation into the energy equation,

$$\rho S_u^0 C_p (T_a - T_b) D \exp\left[-\frac{E}{2R}\left(\frac{1}{T_b} - \frac{1}{T_a}\right)\right] \simeq -2\delta(q^c + q^r) \quad (13.14)$$

the conductive heat loss is expressed as follows.

$$q^c = \lambda \frac{T_b - T_u}{l} \quad (13.15)$$

Using the expression for the radiative heat flux obtained in the previous section and noting that $E_b = \sigma T^4$, the above energy equation can be expressed as follows:

$$\begin{aligned} \rho S_u^0 C_p (T_a - T_b) D \exp\left[-\frac{E}{2R}\left(\frac{1}{T_b} - \frac{1}{T_a}\right)\right] \simeq 2\delta\left[\lambda \frac{T_b - T_u}{l} + \right. \\ \left. \frac{4\eta\tau(1 - \epsilon_w/2)}{2} \sigma (T_b^4 - T_u^4) / [(1 + 3\tau^2)(2/\epsilon_w - 1)/(1 - \omega)]\right] \end{aligned} \quad (13.16)$$

Arranging the above equation,

$$\rho S_u^0 C_p \left(\frac{T_a - T_b}{T_b - T_u} \right) D \exp \left[- \frac{E}{2RT_a} \left(\frac{T_a}{T_b - 1} \right) \right] \simeq 2\delta \left[\frac{\lambda}{l} + \frac{4\eta\tau(1 - \epsilon_w/2)}{2} \right. \\ \left. \sigma(1 + 3\tau^2)(2/\epsilon_w - 1)/(1 - \omega) \left(\frac{T_b^4 - T_u^4}{T_b - T_u} \right) \right] \quad (13.17)$$

Introducing the following dimensionless parameters,

$$\theta_u = \frac{T_u}{T_a} \quad (13.18)$$

$$\theta_b = \frac{T_b}{T_a} \quad (13.19)$$

$$B_b^0 = \frac{4\sigma T_a^4}{\rho S_u^0 C_p T_a} \quad (13.20)$$

$$P_b = \frac{4\sigma T_b^4}{\lambda(T_b/D)} \quad (13.21)$$

$$R_w = \frac{\eta\tau(1 - \epsilon_w/2)}{2} B_b^0 (1 + 3\tau^2)(2/\epsilon_w - 1)/(1 - \omega) \quad (13.22)$$

$$P_e = \frac{\rho S_u^0 C_p T_a}{\lambda T_a/D} \quad (13.23)$$

where, θ_u and θ_b are dimensionless temperatures, B_b^0 is a adiabatic flame Boltzmann number, P_b is a burned gas Plank number, R_w is a radiation number, and P_e is a Peclet number. Substituting the above dimensional groups into the energy equation and arranging, the following equation is obtained.

$$\frac{1 - \theta_b}{\theta_b - \theta_u} \exp \left[- \frac{E}{2RT_a} \left(1 - \frac{1}{\theta_b} \right) \right] = 2 \frac{\delta}{l} \left[\frac{1}{P_e} + \frac{l}{D} R_w \frac{\theta_b^4 - \theta_u^4}{\theta_b - \theta_u} \right] \quad (13.24)$$

When there is no radiative heat losses, the following relation is obtained by setting $R_w = 0$.

$$P_e = 2 \frac{\delta}{l} \frac{\theta_b - \theta_u}{1 - \theta_b} \exp \left[- \frac{E}{2RT_a} \left(1 - \frac{1}{\theta_b} \right) \right] \quad (13.25)$$

The minimum quenching distance can be calculated from the condition;

$$\frac{\partial}{\partial \theta_b}(Pe) = 0 \quad (13.26)$$

13.2 Ignition Criteria Method

Ballal [1980] described a model of ignition and flame quenching. Central to his model is the assumption that the initiation of spark discharge between the electrodes create a small, roughly spherical volume of gas, the temperature of which is sufficiently high enough to ensure a chemical reaction of powdered fuels with a diffusing oxygen.

Ballal [1983a, b] modified the above model by removing the restriction of infinitely fast reactions and allowing a finite time for the surface reactions of fuels or the gas phase reactions of powdered fuels such as aluminum, coal to proceed. Also, for the coal particle, passage of the spark leads to its complete devolatilization and swelling. The surface reaction of the porous char particles with the diffusing oxygen yields carbon monoxide, CO. Upon its release from the particle surface and pores, the gas phase CO and combustible volatiles burn with the counter-diffusing oxygen to produce CO₂ and other products.

Finally, the radiative heat loss from fuel particles composing the spark kernel is calculated in addition to the conduction heat loss from kernel surface.

13.2.1 Mass transfer number

Spalding [1956] and Kanury [1975] defined a mass transfer number for droplets and solid fuels. For solid particles that their reaction proceeds on the surface of the

particle, such as coal, the mass transfer number B is,

$$B = q_{st} \quad (13.27)$$

where q_{st} is a stoichiometric fuel to air ratio.

For the solid particles whose reaction with oxygen proceeds in the vapor phase, such as aluminum, the mass transfer number is,

$$B = \frac{q_{st}H + C_{p,g}(T_g - T_b)}{L + C_{p,f}(T_b - T_s)} \quad (13.28)$$

where, H is the heat of combustion, $C_{p,g}$ and $C_{p,f}$ are the specific heats of gas and solid respectively, T_g is the temperature of gas, T_b is the boiling temperature of solid particle, and T_s is the surface temperature of a solid particle.

13.2.2 Criterion for successful ignition

The criterion for successful ignition is that the time required for evaporation (or evolution) and burning must be less than or equal to the time required for the cold surrounding mixture to quench the spark kernel, that is,

$$t_q \geq t_e + t_c \quad (13.29)$$

where, t_q is quench time, t_e is evaporation or evolution time, and t_c is chemical reaction time.

If $t_q \leq t_e + t_c$, then the size of the spark kernel is smaller than its quench diameter, or its rate of heat generation is lower than the rate of heat loss from its surface, and no ignition is possible. On the contrary, if $t_q \geq t_e + t_c$, the kernel is capable of generating heat in excess of that required to meet its heat losses. Therefore,

its size and ignition energy requirements can both be reduced to a level such that the criterion specified by the above equation is satisfied. Further, the simple addition of t_e and t_c in the above equation implies that these effects are sequential.

The definition of each of the term are defined as follows.

$t_q = (\text{Heat Capacity of the Spark Kernel}) / (\text{Average Rate of Heat Loss by Convection and Radiation})$

$t_e = (\text{Mass of Fuel within the Spark Kernel}) / (\text{Average Rate of Fuel Evaporation (or Evolution)})$

$t_c = (\text{Quenching Distance}) / (\text{Laminar Burning Velocity})$

13.2.3 Quenching of powdered fuels

Each term are calculated mathematically according to the definitions of each term.

13.2.3.1 Quenching time Heat losses by conduction and radiation are, respectively,

$$Q_c = 1.33\pi d_q \Delta T_k \quad (13.30)$$

$$Q_r = n\pi(C_1 D_{32})^2 \epsilon \sigma T_p^4 \quad (13.31)$$

Thus, the quench time is,

$$t_q = \left[\frac{8\alpha}{d_q^2} + \frac{9qC_1^2 \epsilon \sigma T_p^4}{C_p \rho_f C_3^3 f D_{32} \Delta T_{st}} \right]^{-1} \quad (13.32)$$

where, D_{32} is a count mean diameter, D_{30} is a volume mean diameter, D_{20} is a surface area mean diameter, C_3 is equal to volume mean diameter divided by counter mean diameter, and f is a swelling factor.

13.2.3.2 Evolution (Evaporation) time The evaporation time of liquid mist consisting solely of liquid droplets and air are also valid for dust clouds except that the swelling factor, f , should be considered for coal particles.

$$t_e = \frac{C_3^3 \rho_f D_{32}^2}{8C_1 f^2 (k/C_p) \phi \ln(1+B)} \quad (13.33)$$

where, C_1 is a surface area mean diameter divided by counter mean diameter.

13.2.3.3 Chemical reaction time For quiescent mixtures, Ballal and Lefebvre [1980] proposed the chemical reaction time;

$$t_c = \frac{12.5\alpha}{S_u^2} \quad (13.34)$$

13.2.4 Quenching distance

The quenching distance can be found from the criterion described in previous section,

$$t_q = t_e + t_c \quad (13.35)$$

Solving the above equation after substituting the mathematical form of each term, the following expression for quenching distance can be obtained.

$$d_q = (8\alpha)^{1/2} \left[\left(\frac{C_3^3 \rho_f D_{32}^2}{8C_1 f^2 (k/C_p) \phi \ln(1+B)} + \frac{12.5\alpha}{S_u^2} \right)^{-1} - \frac{9qC_1^2 \epsilon \sigma T_p^4}{C_p \rho_f C_3^3 f D_{32} \Delta T_{st}} \right]^{-1/2} \quad (13.36)$$

The first term on the right-hand side of the above equation is the diffusion term, the second term is the chemical reaction term, and the last term is the radiation loss term.

The above formula provide a good physical insight into the effects of various key parameters, such as transfer number, particle concentration, particle size, burning velocity, and radiation losses on the quenching process. The above equation shows that the chemical reaction term becomes relatively important for low particle size, low equivalence ratio, and for fuels such as coal, which yields appreciable gaseous volatile matter upon rapid heating. Further, the radiation heat loss term becomes important as high dust concentration, fine particle size, high particle emissivity.

Also, the above equation embody all the three terms that are generally known to affect the combustion of fuel particles or dust clouds. Therefore, depending on the relative magnitude of each term, the ignition and the quenching process will either become diffusion controlled or kinetic controlled, or even controlled by radiation heat loss from fuel particles. For example, when the particle size is small, and the emissivity of fuel particles is high, both the chemical reaction and the radiation term dominate over the diffusion term and vice versa.

14 APPENDIX C: EXPERIMENTAL DATA

Table 14.1: Quenching distance vs. methane concentration in air, $P = 1 \text{ atm.}$,
 $T = \text{room temperature}$

quenching distance mm	methane concentration % vol.	flame propagation (Yes/No)
10.000	2.718	No
10.000	4.895	Yes
10.000	4.009	No
10.000	5.125	Yes
10.000	4.584	No
10.000	5.521	Yes
10.000	12.820	No
10.000	6.379	Yes
10.000	13.560	No
10.000	7.146	Yes
10.000	13.968	No
10.000	5.125	Yes
10.000	16.564	No
10.000	9.646	Yes
6.000	2.718	No
10.000	11.917	Yes
6.000	4.009	No
10.000	12.333	Yes
6.000	4.895	No
6.000	5.590	Yes
6.000	5.125	No
6.000	6.379	Yes
6.000	5.521	No
6.000	9.646	Yes
6.000	12.333	No
6.000	10.448	Yes
6.000	12.954	No
6.000	10.917	Yes
3.800	4.009	No
6.000	11.458	Yes
3.800	5.950	No

Table 14.2: Quenching distance vs. methane concentration in air, $P = 1 \text{ atm.}$,
 $T = \text{room temperature}$

quenching distance mm	methane concentration % vol.	flame propagation (Yes/No)
6.000	11.917	Yes
3.800	6.379	No
3.800	7.146	Yes
3.800	11.458	No
3.800	9.646	Yes
3.800	13.968	No
3.800	9.974	Yes
2.700	4.009	No
3.800	10.448	Yes
2.700	5.950	No
3.800	10.917	Yes
2.700	6.379	No
2.700	8.725	Yes
2.700	7.146	No
2.700	9.646	Yes
2.700	7.942	No
2.700	9.091	Yes
2.700	7.236	No
2.700	9.551	Yes
2.700	8.291	No
2.700	9.923	Yes
2.700	8.692	No
2.400	8.724	Yes
2.700	10.298	No
2.400	9.091	Yes
2.700	10.714	No
2.400	9.551	Yes
2.000	4.009	No
2.400	9.923	Yes
2.000	5.950	No
2.000	7.942	No

Table 14.3: Quenching distance vs. methane concentration in air, $P = 1 \text{ atm.}$,
 $T = \text{room temperature}$

quenching distance mm	methane concentration % vol.	flame propagation (Yes/No)
2.000	8.291	No
2.000	8.692	No
2.000	9.091	No
2.000	9.923	No
2.000	10.298	No
2.000	10.714	No
2.400	5.950	No
2.400	8.291	No
2.400	8.692	No
2.400	10.298	No
2.400	10.714	No
2.000	5.950	No
2.000	7.942	No
2.000	8.291	No
2.000	8.692	No
2.000	9.091	No
2.000	9.923	No
2.000	10.298	No
2.000	10.714	No
2.400	5.950	No
2.400	8.291	No
2.400	8.692	No
2.400	10.298	No
2.400	10.714	No

Table 14.4: Quenching distance vs. particle concentration for a 10 – 15 μ m aluminum particle

quenching distance mm	particle concentration g/m^3	flame propagation (Yes/No)
18.000	57.050	No
18.000	100.030	Yes
18.000	74.290	No
18.000	141.720	Yes
18.000	88.450	No
18.000	114.050	Yes
18.000	89.530	No
18.000	214.650	Yes
15.000	127.950	No
15.000	184.050	Yes
15.000	147.860	No
15.000	212.370	Yes
15.000	175.650	No
15.000	380.690	Yes
10.000	174.790	No
10.000	244.100	Yes
10.000	220.750	No
10.000	261.430	Yes
7.000	176.800	No
10.000	271.220	Yes
7.000	214.630	No
10.000	824.970	Yes
5.000	245.810	No
7.000	260.100	Yes
5.000	290.020	No
7.000	343.770	Yes
5.000	327.150	No
7.000	525.370	Yes
4.000	738.690	No
5.000	358.980	Yes
4.000	828.660	No

Table 14.5: Quenching distance vs. particle concentration for a 10 – 15 μ m aluminum particle

quenching distance mm	particle concentration g/m^3	flame propagation (Yes/No)
5.000	436.790	Yes
4.000	931.250	No
5.000	502.220	Yes
4.000	1533.670	No
5.000	1513.740	Yes
4.000	1797.000	No
5.000	1612.770	Yes
3.000	649.720	No
5.000	2396.170	Yes
3.000	953.620	No
5.000	3200.780	Yes
3.000	1032.210	No
4.000	973.340	Yes
3.000	1294.200	No
4.000	1449.490	Yes
3.000	1493.300	No
4.000	660.560	Yes
3.000	1681.930	No
3.000	707.360	Yes
3.000	2101.110	No
3.000	704.860	Yes

Table 14.6: Quenching distance vs. particle concentration for a 15 – 20 μ m aluminum particle

quenching distance mm	particle concentration g/m^3	flame propagation (Yes/No)
18.000	125.070	No
18.000	279.510	Yes
18.000	115.740	No
18.000	204.750	Yes
18.000	120.580	No
18.000	156.050	Yes
18.000	129.090	No
18.000	141.010	Yes
15.000	236.590	No
15.000	305.750	Yes
15.000	191.460	No
15.000	268.110	Yes
15.000	239.920	No
15.000	378.940	Yes
15.000	192.720	No
10.000	424.920	Yes
15.000	252.290	No
10.000	482.930	Yes
10.000	373.680	No
10.000	1020.100	Yes
10.000	417.380	No
10.000	1231.800	Yes
7.000	389.770	No
7.000	590.220	Yes
7.000	530.830	No
7.000	1079.280	Yes
7.000	558.670	No
7.000	1191.570	Yes
7.000	1225.910	No
7.000	1271.380	Yes
6.000	581.370	No

Table 14.7: Quenching distance vs. particle concentration for a 15 – 20 μ m aluminum particle

quenching distance mm	particle concentration g/m^3	flame propagation (Yes/No)
6.000	757.160	Yes
6.000	694.380	No
6.000	833.760	Yes
6.000	1025.300	No
6.000	977.670	Yes
18.000	93.000	No
18.000	105.760	No
6.000	1067.530	No
5.000	666.860	No
5.000	751.210	No
5.000	851.480	No
5.000	1029.730	No
5.000	1311.440	No
5.000	1588.370	No
18.000	93.000	No
18.000	105.760	No
6.000	1067.530	No
5.000	666.860	No
5.000	751.210	No
5.000	851.480	No
5.000	1029.730	No
5.000	1311.440	No
5.000	1588.370	No

Table 14.8: Quenching distance vs. particle concentration for a 20 – 25 μ m aluminum particle

quenching distance mm	particle concentration g/m^3	flame propagation (Yes/No)
18.000	217.500	No
18.000	231.050	Yes
18.000	195.050	No
18.000	248.540	Yes
18.000	205.350	No
18.000	290.370	Yes
18.000	210.430	No
18.000	357.850	Yes
15.000	339.840	No
15.000	373.610	Yes
15.000	348.300	No
15.000	392.420	Yes
15.000	318.560	No
15.000	470.590	Yes
15.000	258.900	No
12.000	635.380	Yes
12.000	570.060	No
12.000	664.120	Yes
12.000	613.430	No
12.000	708.530	Yes
10.000	586.260	No
10.000	702.260	Yes
10.000	635.800	No
10.000	813.540	Yes
10.000	665.270	No
10.000	1120.540	Yes
10.000	687.840	No
10.000	1380.690	Yes
10.000	1425.210	No
7.000	1142.070	Yes
10.000	1695.460	No

Table 14.9: Quenching distance vs. particle concentration for a 20 – 25 μ m aluminum particle

quenching distance mm	particle concentration g/m^3	flame propagation (Yes/No)
7.000	1182.380	Yes
10.000	1981.880	No
7.000	1242.390	Yes
7.000	678.970	No
7.000	818.710	No
7.000	1060.560	No
7.000	1125.050	No
7.000	1254.930	No
7.000	1200.290	No
7.000	1372.270	No
6.000	960.380	No
6.000	1059.970	No
6.000	1141.800	No
6.000	1214.220	No
6.000	1248.080	No
6.000	1299.810	No
6.000	1371.290	No
6.000	1423.960	No
7.000	678.970	No
7.000	818.710	No
7.000	1125.050	No
7.000	1254.930	No
7.000	1200.290	No
7.000	1372.270	No
6.000	960.380	No
6.000	1059.970	No
6.000	1141.800	No
6.000	1214.220	No
6.000	1248.080	No
6.000	1299.810	No
6.000	1371.290	No
6.000	1423.960	No

Table 14.10: Quenching distance vs. particle concentration for a 25 – 30 μ m aluminum particle

quenching distance mm	particle concentration g/m^3	flame propagation (Yes/No)
20.000	309.080	No
20.000	487.400	Yes
20.000	301.430	No
20.000	402.590	Yes
20.000	250.450	No
20.000	380.020	Yes
20.000	273.060	No
20.000	345.670	Yes
20.000	231.570	No
20.000	321.630	Yes
18.000	429.110	No
18.000	598.060	Yes
18.000	533.610	No
18.000	609.550	Yes
18.000	568.450	No
18.000	850.950	Yes
18.000	591.790	No
18.000	874.640	Yes
15.000	749.910	No
15.000	854.000	Yes
15.000	764.130	No
15.000	870.720	Yes
15.000	824.740	No
15.000	888.280	Yes
15.000	843.550	No
12.000	1321.440	Yes
12.000	940.530	No
12.000	1417.580	Yes
12.000	1235.230	No
10.000	1950.650	Yes
12.000	1278.070	No

Table 14.11: Quenching distance vs. particle concentration for a 25 – 30 μ m aluminum particle

quenching distance mm	particle concentration g/m^3	flame propagation (Yes/No)
10.000	2213.380	Yes
12.000	1301.060	No
10.000	2356.340	Yes
10.000	1358.750	No
10.000	2373.890	Yes
10.000	1074.080	No
10.000	2419.660	Yes
10.000	1655.960	No
9.000	2131.860	Yes
10.000	1750.640	No
9.000	2200.840	Yes
10.000	2472.330	No
9.000	2384.060	Yes
9.000	1913.800	No
7.000	2435.430	Yes
9.000	2099.820	No
9.000	2399.390	No
9.000	2653.680	No
9.000	2686.430	No
8.000	2181.240	No
8.000	2216.510	No
8.000	2271.370	No
8.000	2383.450	No
8.000	2477.510	No
8.000	2580.180	No
8.000	2909.370	No
7.000	2029.930	No
7.000	2320.950	No
7.000	2675.670	No
7.000	3077.140	No

Table 14.12: Quenching distance vs. particle concentration for a 25 – 30 μ m aluminum particle

quenching distance mm	particle concentration g/m^3	flame propagation (Yes/No)
9.000	2099.820	No
9.000	2399.390	No
9.000	2653.680	No
9.000	2686.430	No
8.000	2181.240	No
8.000	2216.510	No
8.000	2271.370	No
8.000	2383.450	No
8.000	2477.510	No
8.000	2580.180	No
8.000	2909.370	No
7.000	2029.930	No
7.000	2320.950	No
7.000	2675.670	No
7.000	3077.140	No

Table 14.13: Quenching distance vs. particle concentration for a 30 – 38 μ m spherical aluminum particle

quenching distance mm	particle concentration g/m^3	flame propagation (Yes/No)
20.000	543.600	No
20.000	704.510	Yes
20.000	527.400	No
20.000	617.070	Yes
20.000	499.570	No
20.000	586.490	Yes
20.000	454.750	No
20.000	564.530	Yes
18.000	833.880	No
18.000	1056.480	Yes
18.000	744.710	No
18.000	887.180	Yes
15.000	1206.380	No
18.000	859.660	Yes
15.000	1244.420	No
18.000	852.000	Yes
15.000	1285.810	No
18.000	844.330	Yes
12.000	1600.460	No
15.000	1306.290	Yes
12.000	1542.990	No
15.000	1347.670	Yes
12.000	1973.020	No
15.000	1509.440	Yes
12.000	2129.250	No
15.000	1295.000	Yes
12.000	2356.020	No
12.000	1723.780	Yes
12.000	2589.060	No
12.000	1775.510	Yes
12.000	2821.580	No

Table 14.14: Quenching distance vs. particle concentration for a 30 – 38 μ m spherical aluminum particle

quenching distance mm	particle concentration g/m^3	flame propagation (Yes/No)
12.000	1826.190	Yes
12.000	1689.290	No
12.000	2338.260	Yes
12.000	1921.810	No
12.000	1705.490	Yes
11.000	1448.980	No
12.000	1839.790	Yes
11.000	1761.920	No
12.000	1863.290	Yes
11.000	1837.730	No
11.000	1967.700	No
11.000	2061.750	No
11.000	1549.310	No
11.000	2350.750	No
11.000	1837.730	No
11.000	1967.700	No
11.000	2061.750	No
11.000	1549.310	No
11.000	2350.750	No

Table 14.15: Quenching distance vs. particle concentration for a 38 – 45 μ m spherical aluminum particle

quenching distance mm	particle concentration g/m^3	flame propagation (Yes/No)
22.000	759.050	No
22.000	845.300	Yes
22.000	723.570	No
22.000	890.490	Yes
22.000	712.500	No
22.000	964.710	Yes
22.000	806.860	No
22.000	819.040	Yes
20.000	975.970	No
20.000	985.070	Yes
20.000	827.680	No
20.000	1077.240	Yes
20.000	751.400	No
20.000	1169.050	Yes
20.000	936.470	No
18.000	1412.530	Yes
18.000	1262.050	No
18.000	1443.190	Yes
18.000	1321.620	No
18.000	1287.830	Yes
18.000	1305.240	No
15.000	1467.220	Yes
18.000	1267.270	No
15.000	1552.500	Yes
15.000	1244.840	No
15.000	1456.770	Yes
15.000	1352.690	No
15.000	1660.350	Yes
15.000	1398.250	No
14.000	1631.590	Yes
15.000	1427.510	No
15.000	1449.670	No
15.000	1808.740	No

Table 14.16: Quenching distance vs. particle concentration for a 38 – 45 μ m spherical aluminum particle

quenching distance mm	particle concentration g/m^3	flame propagation (Yes/No)
15.000	1740.600	No
15.000	1727.650	No
15.000	1695.880	No
14.000	1538.670	No
14.000	1493.650	No
14.000	1706.830	No
14.000	1675.480	No
14.000	1308.680	No
13.000	1453.720	No
13.000	1533.300	No
13.000	1582.500	No
13.000	1607.100	No
13.000	1648.090	No
13.000	1869.480	No
13.000	2043.600	No
15.000	1427.510	No
15.000	1449.670	No
15.000	1808.740	No
15.000	1740.600	No
15.000	1727.650	No
15.000	1695.880	No
14.000	1538.670	No
14.000	1493.650	No
14.000	1706.830	No
14.000	1675.480	No
14.000	1308.680	No
13.000	1453.720	No
13.000	1533.300	No
13.000	1582.500	No
13.000	1607.100	No
13.000	1648.090	No
13.000	1869.480	No
13.000	2043.600	No

Table 14.17: Quenching distance vs. particle concentration for a batch spherical aluminum particle

quenching distance mm	particle concentration g/m^3	flame propagation (Yes/No)
18.000	210.050	Yes
15.000	297.680	No
15.000	381.380	Yes
15.000	223.350	No
15.000	321.260	Yes
10.000	557.930	No
15.000	633.980	Yes
10.000	500.540	No
10.000	835.560	Yes
7.000	504.300	No
10.000	654.300	Yes
7.000	568.800	No
10.000	594.180	Yes
7.000	667.330	No
10.000	1609.090	Yes
7.000	729.130	No
7.000	876.030	Yes
7.000	765.860	No
7.000	802.580	Yes
7.000	1220.890	No
7.000	1022.040	Yes
7.000	1050.700	No
6.000	679.360	No
6.000	879.330	No
6.000	985.880	No
6.000	1093.450	No
6.000	1209.870	No
6.000	1358.710	No
6.000	1719.760	No
6.000	2842.680	No
7.000	1050.700	No

Table 14.18: Quenching distance vs. particle concentration for a batch spherical aluminum particle

quenching distance mm	particle concentration g/m^3	flame propagation (Yes/No)
18.000	164.680	No
18.000	289.400	Yes
18.000	175.370	No
18.000	249.380	Yes
18.000	197.560	No
6.000	679.360	No
6.000	879.330	No
6.000	985.880	No
6.000	1093.450	No
6.000	1209.870	No
6.000	1358.710	No
6.000	1719.760	No
6.000	2842.680	No

Table 14.19: Quenching distance vs. particle concentration for a 15 – 20 μ m irregular aluminum particle

quenching distance mm	particle concentration g/m^3	flame propagation (Yes/No)
15.000	205.430	No
15.000	226.520	Yes
15.000	178.810	No
15.000	277.750	Yes
15.000	141.040	No
15.000	695.640	Yes
10.000	227.350	No
15.000	368.160	Yes
10.000	271.350	No
10.000	304.760	Yes
5.000	516.370	No
10.000	370.770	Yes
5.000	475.700	No
10.000	651.980	Yes
5.000	381.970	No
5.000	694.980	Yes
5.000	968.120	No
5.000	557.040	Yes
5.000	1141.170	No
5.000	815.120	Yes
4.000	426.620	No
5.000	781.000	Yes
4.000	545.990	No
5.000	919.210	Yes
4.000	621.150	No
4.000	499.570	Yes
4.000	848.830	No
4.000	873.140	Yes
4.000	1080.930	No
4.000	956.200	No
4.000	990.690	No

Table 14.20: Quenching distance vs. particle concentration for a 15 – 20 μ m irregular aluminum particle

quenching distance mm	particle concentration g/m^3	flame propagation (Yes/No)
4.000	1214.850	No
4.000	867.590	No
4.000	1080.930	No
4.000	956.200	No
4.000	990.690	No
4.000	1214.850	No
4.000	867.590	No

Table 14.21: Quenching distance vs. particle concentration for a 25 – 30 μ m irregular aluminum particle

quenching distance mm	particle concentration g/m^3	flame propagation (Yes/No)
20.000	231.680	No
20.000	1136.470	Yes
20.000	286.230	No
20.000	424.490	Yes
20.000	297.830	No
20.000	320.090	Yes
15.000	188.110	No
20.000	305.360	Yes
15.000	278.810	No
15.000	749.910	Yes
15.000	305.570	No
15.000	585.220	Yes
10.000	408.340	No
15.000	374.540	Yes
10.000	348.820	No
15.000	323.540	Yes
7.000	511.570	No
10.000	559.770	Yes
7.000	1357.050	No
10.000	482.170	Yes
7.000	999.650	No
10.000	444.500	Yes
7.000	988.000	No
7.000	727.570	Yes
7.000	962.920	No
7.000	621.460	Yes
7.000	434.270	No
7.000	581.040	Yes
6.000	592.410	No
7.000	838.410	Yes
6.000	694.090	No

Table 14.22: Quenching distance vs. particle concentration for a 25 – 30 μ m irregular aluminum particle

quenching distance mm	particle concentration g/m^3	flame propagation (Yes/No)
7.000	923.510	Yes
6.000	837.040	No
6.000	739.780	Yes
6.000	884.190	No
6.000	1009.450	Yes
6.000	944.610	No
6.000	1102.300	Yes
6.000	1199.560	No
6.000	1035.980	No
6.000	978.510	No
5.000	520.440	No
5.000	656.070	No
5.000	822.300	No
5.000	1246.710	No
5.000	1338.670	No
5.000	1511.970	No
5.000	1642.830	No
6.000	1199.560	No
6.000	1035.980	No
6.000	978.510	No
5.000	520.440	No
5.000	656.070	No
5.000	822.300	No
5.000	1246.710	No
5.000	1338.670	No
5.000	1511.970	No
5.000	1642.830	No

Table 14.23: Quenching distance vs. particle concentration for a 30 – 38 μ m irregular aluminum particle

quenching distance mm	particle concentration g/m^3	flame propagation (Yes/No)
22.000	1062.230	No
22.000	1759.930	Yes
22.000	1438.440	No
22.000	1090.930	Yes
22.000	2095.950	No
22.000	1762.720	Yes
20.000	1043.470	No
20.000	1720.850	Yes
20.000	1587.710	No
20.000	1452.270	Yes
20.000	845.910	No
20.000	1234.290	Yes
20.000	1141.330	No
20.000	1308.200	Yes
20.000	1158.820	No
15.000	1515.710	Yes
20.000	1191.870	No
15.000	1660.350	Yes
15.000	1135.320	No
15.000	1620.340	Yes
22.000	1037.030	No
20.000	1084.050	No
15.000	1310.890	No
15.000	1396.190	No
15.000	1449.250	No
15.000	1491.050	No
15.000	1876.880	No
15.000	1744.370	No
15.000	1686.260	No
14.000	1035.240	No
14.000	1241.500	No

Table 14.24: Quenching distance vs. particle concentration for a 30 – 38 μ m irregular aluminum particle

quenching distance mm	particle concentration g/m^3	flame propagation (Yes/No)
14.000	1721.270	No
14.000	1439.910	No
14.000	1524.350	No
14.000	1915.680	No
14.000	1397.200	No
22.000	1037.030	No
20.000	1084.050	No
15.000	1310.890	No
15.000	1396.190	No
15.000	1449.250	No
15.000	1491.050	No
15.000	1876.880	No
15.000	1744.370	No
15.000	1686.260	No
14.000	1035.240	No
14.000	1241.500	No
14.000	1721.270	No
14.000	1439.910	No
14.000	1524.350	No
14.000	1915.680	No
14.000	1397.200	No

Table 14.25: Quenching distance vs. particle concentration for a 38 – 45 μ m irregular aluminum particle

quenching distance mm	particle concentration g/m^3	flame propagation (Yes/No)
20.000	1138.980	No
20.000	1415.590	No
20.000	1763.490	No
20.000	2344.740	No
20.000	1973.930	No
20.000	1658.810	No
15.000	770.100	No
15.000	1132.020	No
15.000	1316.740	No
15.000	1432.610	No
15.000	1537.570	No
15.000	1711.010	No
15.000	1884.820	No
18.000	864.080	No
18.000	1043.960	No
18.000	1248.000	No
18.000	1517.460	No
18.000	1002.430	No
25.000	917.350	No
25.000	1149.270	No
25.000	1235.780	No
25.000	1413.020	No
25.000	1721.470	No
25.000	1043.250	No
25.000	1671.040	No
25.000	813.800	No
25.000	1562.490	No

Table 14.26: Quenching distance vs. particle concentration for a batch irregular aluminum particle

quenching distance mm	particle concentration g/m^3	flame propagation (Yes/No)
15.000	320.670	Yes
15.000	145.360	No
15.000	283.530	Yes
10.000	163.580	No
15.000	236.960	Yes
10.000	144.830	No
15.000	222.230	Yes
10.000	178.250	No
15.000	555.920	Yes
7.000	208.420	No
15.000	192.160	Yes
7.000	192.120	No
10.000	418.220	Yes
7.000	160.290	No
10.000	285.590	Yes
5.000	340.290	No
10.000	236.080	Yes
5.000	1860.140	No
10.000	190.990	Yes
5.000	1799.150	No
7.000	449.680	Yes
4.000	749.290	No
7.000	349.890	Yes
4.000	355.140	No
7.000	298.100	Yes
4.000	1424.900	No
7.000	256.420	Yes
4.000	1268.150	No
7.000	233.680	Yes
4.000	300.690	No
5.000	809.920	Yes

Table 14.27: Quenching distance vs. particle concentration for a batch irregular aluminum particle

quenching distance mm	particle concentration g/m^3	flame propagation (Yes/No)
3.000	669.940	No
5.000	693.210	Yes
3.000	985.620	No
5.000	438.350	Yes
3.000	1585.410	No
5.000	370.000	Yes
3.000	1262.410	No
5.000	1443.410	Yes
3.000	1394.500	No
5.000	1754.760	Yes
3.000	1721.470	No
5.000	1705.260	Yes
3.000	1801.590	No
4.000	1163.120	Yes
3.000	1093.510	No
4.000	979.720	Yes
3.000	460.050	No
4.000	826.100	Yes
4.000	590.960	No
4.000	710.280	No
4.000	594.530	No
4.000	468.260	No
4.000	1214.850	No
3.000	1213.610	No
3.000	883.470	No
4.000	590.960	No
4.000	710.280	No
4.000	594.530	No
4.000	468.260	No
4.000	1214.850	No
3.000	1213.610	No
3.000	883.470	No

Table 14.28: Quenching distance vs. particle concentration for a 16.7 μ m Adaville No. 11 coal particle

quenching distance mm	particle concentration g/m^3	flame propagation (Yes/No)
25.000	154.380	No
25.000	162.350	Yes
25.000	149.470	No
25.000	212.470	Yes
20.000	194.350	No
20.000	205.670	Yes
20.000	187.250	No
20.000	210.380	Yes
20.000	183.210	No
20.000	220.390	Yes
20.000	175.320	No
20.000	229.570	Yes
20.000	160.320	No
20.000	269.080	Yes
15.000	236.450	No
15.000	247.210	Yes
15.000	226.590	No
15.000	256.120	Yes
15.000	204.900	No
15.000	276.820	Yes
15.000	354.380	No
15.000	343.890	Yes
15.000	369.700	No
15.000	328.500	Yes
15.000	378.490	No
15.000	300.760	Yes
15.000	187.470	No
15.000	302.350	Yes
11.000	277.570	No
11.000	300.040	Yes
11.000	265.680	No

Table 14.29: Quenching distance vs. particle concentration for a $16.7\mu\text{m}$ Adaville No. 11 coal particle

quenching distance mm	particle concentration g/m^3	flame propagation (Yes/No)
11.000	312.380	Yes
11.000	256.900	No
11.000	316.890	Yes
11.000	333.330	No
11.000	325.890	Yes
11.000	347.560	No
11.000	320.210	Yes
10.000	246.400	No
10.000	357.600	No
10.000	375.300	No
10.000	289.300	No
10.000	302.400	No
10.000	213.600	No

Table 14.30: Quenching distance vs. particle concentration for a 25.5 μ m Adaville No. 11 coal particle

quenching distance mm	particle concentration g/m^3	flame propagation (Yes/No)
30.000	195.800	No
30.000	207.480	Yes
30.000	189.210	No
30.000	220.470	Yes
25.000	214.670	No
25.000	222.580	Yes
25.000	208.570	No
25.000	238.080	Yes
25.000	195.340	No
25.000	268.600	Yes
20.000	219.780	No
20.000	228.600	Yes
20.000	204.350	No
20.000	237.900	Yes
20.000	199.450	No
20.000	278.900	Yes
17.000	258.690	No
17.000	267.560	Yes
17.000	245.670	No
17.000	278.320	Yes
17.000	220.780	No
17.000	301.350	Yes
17.000	483.560	No
17.000	480.070	Yes
17.000	497.580	No
17.000	451.560	Yes
17.000	517.580	No
17.000	412.460	Yes
14.000	297.600	No
14.000	308.220	Yes
14.000	279.900	No

Table 14.31: Quenching distance vs. particle concentration for a 25.5 μ m Adaville No. 11 coal particle

quenching distance mm	particle concentration g/m^3	flame propagation (Yes/No)
14.000	325.680	Yes
14.000	243.540	No
14.000	358.900	Yes
14.000	200.340	No
14.000	378.900	Yes
14.000	430.450	No
14.000	417.340	Yes
14.000	446.570	No
14.000	400.370	Yes
14.000	457.350	No
14.000	386.560	Yes
13.000	175.400	No
13.000	458.900	No
13.000	203.400	No
13.000	257.500	No
13.000	304.500	No
13.000	356.400	No
13.000	426.700	No
13.000	156.700	No

Table 14.32: Quenching distance vs. particle concentration for a 36.6 μm Adaville No. 11 coal particle

quenching distance mm	particle concentration g/m^3	flame propagation (Yes/No)
32.000	268.780	No
32.000	279.900	Yes
32.000	254.560	No
32.000	300.550	Yes
30.000	292.570	No
30.000	304.890	Yes
30.000	286.210	No
30.000	317.780	Yes
30.000	265.430	No
30.000	357.870	Yes
25.000	330.210	No
25.000	339.670	Yes
25.000	312.290	No
25.000	356.780	Yes
25.000	302.340	No
25.000	387.560	Yes
25.000	275.670	No
25.000	405.370	Yes
20.000	373.780	No
20.000	391.550	Yes
20.000	365.790	No
20.000	402.340	Yes
20.000	350.450	No
20.000	412.450	Yes
20.000	521.340	No
20.000	512.670	Yes
20.000	534.890	No
20.000	487.570	Yes
20.000	548.680	No
20.000	461.450	Yes
19.000	389.900	No

Table 14.33: Quenching distance vs. particle concentration for a 36.6 μ m Adaville No. 11 coal particle

quenching distance mm	particle concentration g/m^3	flame propagation (Yes/No)
19.000	400.000	Yes
19.000	374.670	No
19.000	412.560	Yes
19.000	357.890	No
19.000	422.870	Yes
19.000	468.780	No
19.000	458.790	Yes
19.000	482.320	No
19.000	446.870	Yes
19.000	499.450	No
19.000	427.680	Yes
18.000	346.300	No
18.000	506.700	No
18.000	517.400	No
18.000	364.300	No
18.000	436.300	No
18.000	476.100	No
18.000	304.100	No

Table 14.34: Quenching distance vs. particle concentration for a 16.7 μm Hanna No. 80 coal particle

quenching distance mm	particle concentration g/m^3	flame propagation (Yes/No)
20.000	130.300	No
20.000	138.900	Yes
20.000	125.400	No
20.000	153.700	Yes
15.000	145.600	No
15.000	154.700	Yes
15.000	137.800	No
15.000	165.700	Yes
15.000	126.800	No
15.000	187.600	Yes
13.000	173.200	No
13.000	182.500	Yes
13.000	164.600	No
13.000	196.700	Yes
13.000	147.500	No
13.000	236.900	Yes
10.000	235.800	No
10.000	250.400	Yes
10.000	221.300	No
10.000	257.800	Yes
10.000	196.500	No
10.000	281.400	Yes
10.000	339.500	No
10.000	332.400	Yes
10.000	354.300	No
10.000	321.500	Yes
10.000	368.500	No
10.000	300.600	Yes
9.000	264.300	No
9.000	273.700	Yes
9.000	253.200	No

Table 14.35: Quenching distance vs. particle concentration for a 16.7 μ m Hanna No. 80 coal particle

quenching distance mm	particle concentration g/m^3	flame propagation (Yes/No)
9.000	280.800	Yes
9.000	223.500	No
9.000	302.500	Yes
9.000	327.000	No
9.000	320.600	Yes
9.000	341.600	No
9.000	316.800	Yes
9.000	385.400	No
9.000	308.600	Yes
8.000	230.500	No
8.000	350.600	No
8.000	257.400	No
8.000	295.200	No
8.000	314.000	No
8.000	337.300	No
8.000	210.300	No

Table 14.36: Quenching distance vs. particle concentration for a 25.5 μ m Hanna No. 80 coal particle

quenching distance mm	particle concentration g/m^3	flame propagation (Yes/No)
25.000	162.400	No
25.000	173.500	Yes
25.000	157.400	No
25.000	186.500	Yes
20.000	178.500	No
20.000	188.700	Yes
20.000	163.600	No
20.000	198.700	Yes
20.000	156.300	No
20.000	231.600	Yes
15.000	203.400	No
15.000	213.600	Yes
15.000	197.500	No
15.000	224.600	Yes
15.000	175.700	No
15.000	248.700	Yes
15.000	162.500	No
15.000	284.300	Yes
12.000	247.500	No
12.000	258.700	Yes
12.000	235.800	No
12.000	267.500	Yes
12.000	217.400	No
12.000	283.600	Yes
12.000	194.300	No
12.000	295.100	Yes
12.000	373.200	No
12.000	362.900	Yes
12.000	386.700	No
12.000	337.900	Yes
12.000	395.700	No

Table 14.37: Quenching distance vs. particle concentration for a 25.5 μ m Hanna No. 80 coal particle

quenching distance mm	particle concentration g/m^3	flame propagation (Yes/No)
12.000	312.200	Yes
11.000	283.400	No
11.000	284.300	Yes
11.000	272.200	No
11.000	294.300	Yes
11.000	253.500	No
11.000	302.400	Yes
11.000	233.300	No
11.000	315.600	Yes
11.000	332.100	No
11.000	325.300	Yes
11.000	347.800	No
11.000	319.400	Yes
11.000	374.000	No
11.000	308.400	Yes
10.000	251.300	No
10.000	357.800	No
10.000	285.200	No
10.000	302.500	No
10.000	332.700	No
10.000	224.700	No
10.000	339.000	No

Table 14.38: Quenching distance vs. particle concentration for a $36.6\mu\text{m}$ Hanna No. 80 coal particle

quenching distance mm	particle concentration g/m^3	flame propagation (Yes/No)
30.000	224.600	No
30.000	231.500	Yes
30.000	213.600	No
30.000	257.600	Yes
25.000	240.300	No
25.000	250.400	Yes
25.000	231.500	No
25.000	267.400	Yes
25.000	219.600	No
25.000	289.600	Yes
20.000	265.400	No
20.000	273.600	Yes
20.000	258.500	No
20.000	283.600	Yes
20.000	243.400	No
20.000	287.500	Yes
17.000	302.400	No
17.000	312.400	Yes
17.000	294.600	No
17.000	326.700	Yes
17.000	275.600	No
17.000	346.800	Yes
17.000	426.500	No
17.000	416.800	Yes
17.000	440.300	No
17.000	400.200	Yes
17.000	452.400	No
17.000	379.700	Yes
15.000	342.400	No
15.000	350.400	Yes
15.000	333.600	No

Table 14.39: Quenching distance vs. particle concentration for a $36.6\mu\text{m}$ Hanna No. 80 coal particle

quenching distance mm	particle concentration g/m^3	flame propagation (Yes/No)
15.000	358.500	Yes
15.000	302.400	No
15.000	368.500	Yes
15.000	396.400	No
15.000	386.300	Yes
15.000	405.300	No
15.000	379.000	Yes
15.000	425.600	No
15.000	368.000	Yes
15.000	274.500	No
15.000	354.300	Yes
14.000	301.400	No
14.000	405.200	No
14.000	246.700	No
14.000	345.700	No
14.000	379.000	No
14.000	369.700	No

Table 14.40: Quenching distance vs. particle concentration for a 16.7 μ m Illinois No. 6 coal particle

quenching distance mm	particle concentration g/m^3	flame propagation (Yes/No)
25.000	170.200	No
25.000	181.200	Yes
25.000	165.400	No
25.000	190.300	Yes
20.000	194.300	No
20.000	204.200	Yes
20.000	189.300	No
20.000	211.300	Yes
20.000	182.300	No
20.000	220.500	Yes
20.000	169.300	No
20.000	256.400	Yes
15.000	231.400	No
15.000	240.800	Yes
15.000	224.300	No
15.000	250.300	Yes
15.000	203.400	No
15.000	286.400	Yes
15.000	182.500	No
15.000	301.500	Yes
14.000	301.300	No
14.000	309.400	Yes
14.000	283.500	No
14.000	321.500	Yes
14.000	253.500	No
14.000	331.500	Yes
14.000	203.400	No
14.000	313.500	Yes
14.000	358.400	No
14.000	349.500	Yes
14.000	373.400	No

Table 14.41: Quenching distance vs. particle concentration for a $16.7\mu\text{m}$ Illinois No. 6 coal particle

quenching distance mm	particle concentration g/m^3	flame propagation (Yes/No)
14.000	336.500	Yes
14.000	386.400	No
14.000	330.200	Yes
13.000	278.600	No
13.000	386.000	No
13.000	300.200	No
13.000	321.500	No
13.000	356.300	No
13.000	243.100	No
13.000	342.000	No

Table 14.42: Quenching distance vs. particle concentration for a 25.5 μ m Illinois No. 6 coal particle

quenching distance mm	particle concentration g/m^3	flame propagation (Yes/No)
30.000	225.600	No
30.000	235.700	Yes
30.000	215.400	No
30.000	253.700	Yes
25.000	253.600	No
25.000	264.300	Yes
25.000	246.500	No
25.000	270.300	Yes
25.000	236.500	No
25.000	297.500	Yes
20.000	304.600	No
20.000	316.400	Yes
20.000	296.400	No
20.000	326.400	Yes
20.000	276.400	No
20.000	374.600	Yes
20.000	510.400	No
20.000	503.600	Yes
20.000	517.500	No
20.000	492.400	Yes
20.000	523.400	No
20.000	472.100	Yes
20.000	242.500	No
20.000	331.400	Yes
17.000	353.500	No
17.000	363.200	Yes
17.000	342.500	No
17.000	374.200	Yes
17.000	324.300	No
17.000	390.200	Yes
17.000	295.300	No

Table 14.43: Quenching distance vs. particle concentration for a 25.5 μ m Illinois No. 6 coal particle

quenching distance mm	particle concentration g/m^3	flame propagation (Yes/No)
17.000	394.200	Yes
17.000	447.600	No
17.000	432.700	Yes
17.000	463.100	No
17.000	415.000	Yes
17.000	500.500	No
17.000	401.100	Yes
16.000	332.100	No
16.000	459.800	No
16.000	356.800	No
16.000	386.500	No
16.000	412.600	No
16.000	432.000	No
16.000	302.100	No

Table 14.44: Quenching distance vs. particle concentration for a 36.6 μ m Illinois No. 6 coal particle

quenching distance mm	particle concentration g/m^3	flame propagation (Yes/No)
32.000	303.400	No
32.000	311.200	Yes
32.000	289.600	No
32.000	324.800	Yes
32.000	267.400	No
32.000	365.900	Yes
30.000	321.000	No
30.000	330.300	Yes
30.000	314.500	No
30.000	339.700	Yes
30.000	299.400	No
30.000	376.400	Yes
25.000	357.500	No
25.000	366.400	Yes
25.000	339.700	No
25.000	380.300	Yes
25.000	301.300	No
25.000	395.400	Yes
25.000	520.300	No
25.000	500.400	Yes
25.000	527.500	No
25.000	491.400	Yes
25.000	542.400	No
25.000	469.700	Yes
25.000	276.500	No
25.000	402.100	Yes
23.000	393.200	No
23.000	402.100	Yes
23.000	381.400	No
23.000	415.300	Yes
23.000	363.200	No

Table 14.45: Quenching distance vs. particle concentration for a $36.6\mu\text{m}$ Illinois No. 6 coal particle

quenching distance mm	particle concentration g/m^3	flame propagation (Yes/No)
23.000	430.100	Yes
23.000	324.100	No
23.000	410.100	Yes
23.000	480.400	No
23.000	471.300	Yes
23.000	487.500	No
23.000	462.600	Yes
23.000	502.400	No
23.000	442.500	Yes
22.000	375.000	No
22.000	491.000	No
22.000	351.500	No
22.000	452.100	No
22.000	412.000	No
22.000	387.700	No

Table 14.46: Quenching distance vs. particle concentration for a 16.7 μ m Lower Kittaining coal particle

quenching distance mm	particle concentration g/m^3	flame propagation (Yes/No)
25.000	191.500	No
25.000	200.000	Yes
25.000	183.200	No
25.000	213.500	Yes
25.000	171.400	No
25.000	253.700	Yes
20.000	204.600	No
20.000	211.500	Yes
20.000	194.500	No
20.000	224.600	Yes
20.000	182.400	No
20.000	246.700	Yes
20.000	188.400	No
20.000	283.000	Yes
16.000	246.800	No
16.000	255.100	Yes
16.000	238.900	No
16.000	261.300	Yes
16.000	200.400	No
16.000	270.800	Yes
16.000	314.200	No
16.000	304.700	Yes
16.000	321.600	No
16.000	298.200	Yes
16.000	351.700	No
16.000	290.200	Yes
13.000	278.600	No
13.000	386.000	No
13.000	300.200	No
13.000	321.500	No
13.000	356.300	No
13.000	243.100	No
13.000	342.000	No

Table 14.47: Quenching distance vs. particle concentration for a 25.5 μ m Illinois No. 6 coal particle

quenching distance mm	particle concentration g/m^3	flame propagation (Yes/No)
30.000	225.600	No
30.000	235.700	Yes
30.000	215.400	No
30.000	253.700	Yes
25.000	253.600	No
25.000	264.300	Yes
25.000	246.500	No
25.000	270.300	Yes
25.000	236.500	No
25.000	297.500	Yes
20.000	304.600	No
20.000	316.400	Yes
20.000	296.400	No
20.000	326.400	Yes
20.000	276.400	No
20.000	374.600	Yes
20.000	510.400	No
20.000	503.600	Yes
20.000	517.500	No
20.000	492.400	Yes
20.000	523.400	No
20.000	472.100	Yes
20.000	242.500	No
20.000	331.400	Yes
17.000	353.500	No
17.000	363.200	Yes
17.000	342.500	No
17.000	374.200	Yes
17.000	324.300	No
17.000	390.200	Yes
17.000	295.300	No

Table 14.48: Quenching distance vs. particle concentration for a 25.5 μ m Illinois No. 6 coal particle

quenching distance mm	particle concentration g/m^3	flame propagation (Yes/No)
17.000	394.200	Yes
17.000	447.600	No
17.000	432.700	Yes
17.000	463.100	No
17.000	415.000	Yes
17.000	500.500	No
17.000	401.100	Yes
16.000	332.100	No
16.000	459.800	No
16.000	356.800	No
16.000	386.500	No
16.000	412.600	No
16.000	432.000	No
16.000	302.100	No

Table 14.49: Quenching distance vs. particle concentration for a 36.6 μ m Illinois No. 6 coal particle

quenching distance mm	particle concentration g/m^3	flame propagation (Yes/No)
32.000	303.400	No
32.000	311.200	Yes
32.000	289.600	No
32.000	324.800	Yes
32.000	267.400	No
32.000	365.900	Yes
30.000	321.000	No
30.000	330.300	Yes
30.000	314.500	No
30.000	339.700	Yes
30.000	299.400	No
30.000	376.400	Yes
25.000	357.500	No
25.000	366.400	Yes
25.000	339.700	No
25.000	380.300	Yes
25.000	301.300	No
25.000	395.400	Yes
25.000	520.300	No
25.000	500.400	Yes
25.000	527.500	No
25.000	491.400	Yes
25.000	542.400	No
25.000	469.700	Yes
25.000	276.500	No
25.000	402.100	Yes
23.000	393.200	No
23.000	402.100	Yes
23.000	381.400	No
23.000	415.300	Yes
23.000	363.200	No

Table 14.50: Quenching distance vs. particle concentration for a $36.6\mu\text{m}$ Illinois No. 6 coal particle

quenching distance mm	particle concentration g/m^3	flame propagation (Yes/No)
23.000	430.100	Yes
23.000	324.100	No
23.000	410.100	Yes
23.000	480.400	No
23.000	471.300	Yes
23.000	487.500	No
23.000	462.600	Yes
23.000	502.400	No
23.000	442.500	Yes
22.000	375.000	No
22.000	491.000	No
22.000	351.500	No
22.000	452.100	No
22.000	412.000	No
22.000	387.700	No

Table 14.51: Quenching distance vs. particle concentration for a 9.1 μ m Penn. Seam coal particle

quenching distance mm	particle concentration g/m^3	flame propagation (Yes/No)
20.000	145.270	No
20.000	151.580	Yes
20.000	141.460	No
20.000	155.690	Yes
20.000	115.790	No
20.000	160.040	Yes
20.000	109.480	No
20.000	188.640	Yes
15.000	170.230	No
15.000	178.310	Yes
15.000	163.440	No
15.000	185.200	Yes
15.000	142.800	No
15.000	199.500	Yes
15.000	126.350	No
15.000	243.570	Yes
13.000	212.460	No
13.000	225.480	Yes
13.000	203.870	No
13.000	231.900	Yes
13.000	187.550	No
13.000	240.750	Yes
13.000	165.390	No
13.000	271.490	Yes
10.000	259.470	No
10.000	279.580	Yes
10.000	251.770	No
10.000	286.400	Yes
10.000	244.050	No
10.000	310.470	Yes
10.000	331.670	No

Table 14.52: Quenching distance vs. particle concentration for a $9.1\mu\text{m}$ Penn. Seam coal particle

quenching distance mm	particle concentration g/m^3	flame propagation (Yes/No)
10.000	319.580	Yes
10.000	347.670	No
10.000	321.580	Yes
9.000	231.600	No
9.000	367.300	No
9.000	267.100	No
9.000	299.400	No
9.000	331.200	No
9.000	347.100	No

Table 14.53: Quenching distance vs. particle concentration for a 16.7 μ m Penn. Seam coal particle

quenching distance mm	particle concentration g/m^3	flame propagation (Yes/No)
30.000	167.450	No
30.000	174.970	Yes
30.000	160.470	No
30.000	179.490	Yes
30.000	147.210	No
30.000	201.100	Yes
25.000	176.360	No
25.000	182.500	Yes
25.000	173.220	No
25.000	186.700	Yes
25.000	162.140	No
25.000	197.950	Yes
25.000	125.330	No
25.000	221.520	Yes
20.000	199.530	No
20.000	206.160	Yes
20.000	195.520	No
20.000	214.370	Yes
20.000	191.040	No
20.000	220.060	Yes
20.000	152.750	No
20.000	251.680	Yes
20.000	136.720	No
20.000	277.210	Yes
15.000	243.680	No
15.000	247.600	Yes
15.000	228.050	No
15.000	254.390	Yes
15.000	204.750	No
15.000	278.070	Yes
15.000	376.780	No

Table 14.54: Quenching distance vs. particle concentration for a 16.7 μ m Penn. Seam coal particle

quenching distance mm	particle concentration g/m^3	flame propagation (Yes/No)
15.000	345.700	Yes
15.000	390.010	No
15.000	338.580	Yes
15.000	399.450	No
15.000	312.470	Yes
13.000	291.210	No
13.000	295.380	Yes
13.000	288.310	No
13.000	301.260	Yes
13.000	251.310	No
13.000	309.220	Yes
13.000	209.210	No
13.000	311.210	Yes
13.000	342.590	No
13.000	332.530	Yes
13.000	358.670	No
13.000	327.050	Yes
13.000	378.400	No
13.000	315.360	Yes
11.500	250.100	No
11.500	350.100	No
11.500	230.500	No
11.500	286.400	No
11.500	300.500	No
11.500	328.900	No
11.500	378.300	No

Table 14.55: Quenching distance vs. particle concentration for a 25.5 μ m Penn. Seam coal particle

quenching distance mm	particle concentration g/m ³	flame propagation (Yes/No)
30.000	205.480	No
30.000	219.900	Yes
30.000	200.120	No
30.000	227.470	Yes
25.000	213.340	No
25.000	221.600	Yes
25.000	208.480	No
25.000	236.700	Yes
25.000	201.350	No
25.000	251.580	Yes
20.000	222.800	No
20.000	231.490	Yes
20.000	215.690	No
20.000	243.490	Yes
20.000	206.790	No
20.000	289.090	Yes
16.000	254.780	No
16.000	264.380	Yes
16.000	243.580	No
16.000	273.800	Yes
16.000	225.750	No
16.000	280.290	Yes
16.000	512.490	No
16.000	491.000	Yes
16.000	527.600	No
16.000	465.800	Yes
16.000	544.300	No
16.000	401.580	Yes
15.000	309.900	No
15.000	318.400	Yes
15.000	298.210	No

Table 14.56: Quenching distance vs. particle concentration for a 25.5 μ m Penn. Seam coal particle

quenching distance mm	particle concentration g/m^3	flame propagation (Yes/No)
15.000	328.700	Yes
15.000	287.550	No
15.000	359.070	Yes
15.000	427.600	No
15.000	417.400	Yes
15.000	440.250	No
15.000	402.580	Yes
15.000	457.290	No
15.000	384.320	Yes
14.000	297.600	No
14.000	454.100	No
14.000	263.100	No
14.000	324.700	No
14.000	354.300	No
14.000	391.300	No
14.000	425.800	No

Table 14.57: Quenching distance vs. particle concentration for a 36.6 μ m Penn. Seam coal particle

quenching distance mm	particle concentration g/m^3	flame propagation (Yes/No)
32.000	271.360	No
32.000	281.300	Yes
32.000	263.380	No
32.000	289.600	Yes
32.000	255.180	No
32.000	310.280	Yes
30.000	288.680	No
30.000	297.140	Yes
30.000	280.240	No
30.000	310.200	Yes
30.000	255.900	No
30.000	322.350	Yes
30.000	268.470	No
30.000	358.500	Yes
25.000	318.580	No
25.000	328.570	Yes
25.000	304.570	No
25.000	335.680	Yes
25.000	300.280	No
25.000	358.590	Yes
25.000	269.790	No
25.000	405.380	Yes
20.000	360.570	No
20.000	369.900	Yes
20.000	354.370	No
20.000	376.500	Yes
20.000	304.210	No
20.000	396.500	Yes
20.000	268.490	No
20.000	419.040	Yes
20.000	512.050	No

Table 14.58: Quenching distance vs. particle concentration for a 36.6 μ m Penn. Seam coal particle

quenching distance mm	particle concentration g/m^3	flame propagation (Yes/No)
20.000	488.690	Yes
20.000	547.590	No
20.000	472.570	Yes
20.000	564.320	No
20.000	464.880	Yes
19.000	393.590	No
19.000	405.250	Yes
19.000	382.350	No
19.000	415.360	Yes
19.000	352.490	No
19.000	436.900	Yes
19.000	468.360	No
19.000	457.600	Yes
19.000	477.380	No
19.000	447.590	Yes
18.000	364.100	No
18.000	482.000	No
18.000	321.000	No
18.000	502.500	No
18.000	406.700	No
18.000	435.200	No
18.000	465.100	No
18.000	385.200	No